NMR spectroscopic measurements of diffusion in heart

Carsten Liess

Department of Biochemistry

The University of Oxford

Submitted to The University of Oxford in fulfilment of the requirements

for the degree of Doctor of Philosophy

Hertford College

Trinity Term 1999

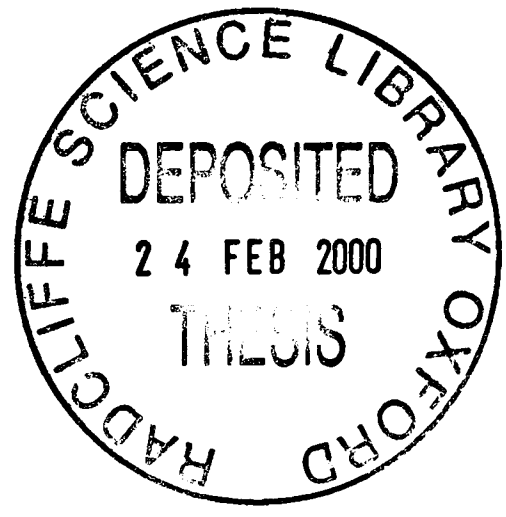

To my parents

Rejoice in the Lord always. I will say it again: Rejoice! Let your gentleness be evident to all. The Lord is near. Do not be anxious about anything, but in everything, by prayer and petition, with thanksgiving, present your requests to God. And the peace of God, which transcends all understanding, will guard your hearts and your minds in Christ Jesus.

from Paul's letter to the Philippians, 4: 4-7

Acknowledgements

I am very grateful to Dr. Kieran Clarke for supervision, continued encouragement and patience over the past few years. Thanks are also due to Prof. George Radda for initially taking on a Medical Physicist as a D.Phil. student, and to Prof. Peter Styles for helpful discussions. I am thankful to the EU and the BHF for financing my studies; it is a privilege to be able to study at Oxford and I hope I can repay their investment someday.

There are a number of people I would like to mention that have contributed to this work in one way or another. Justin Duckworth helped with the ^{31}P-NMR studies during many a late night on the spectrometer. I am indebted to Doug Befroy for his patient and skilful help with the perfused hearts; this also applies to Marilyn Mielke and Barney Jones. Hang in there guys, you're almost there! Paul Cassidy for designing, constructing and maintaining RF probes and other vital NMR equipment. Room 14, past and present, for great entertainment and stimulating discussions about Roman messenger bees, minibuses and genuine Italian pasta. I am also grateful to those people that work behind the scenes and usually go unnoticed. Yvonne^{2}, Carol Davey and the BSU staff need to be mentioned here.

Finally my love and thanks to Bruna Tamai for her support and wisdom in dealing with me throughout this time. May God bless you and be with you always.

NMR spectroscopic measurements of diffusion in heart

Carsten Liess

Hertford College, The University of Oxford

D.Phil., Trinity Term 1999

Abstract

A decrease in the apparent diffusion coefficient (ADC) of water is becoming an important tool for the detection of acute and chronic brain disorders, yet it is not known whether changes in myocardial ADCs hold similar potential. Consequently, this work determined whether the ADCs of water or intracellular metabolites could be used to show ischaemia or cell swelling in the isolated rat heart.

A modified STEAM pulse sequence was designed to measure the ADCs of the ^{1}H-NMR detectable metabolites, taurine and creatine, with 4 min time resolution in a 3 mm myocardial slice. Experiments included the measurement of: a) metabolite diffusion coefficients and diffusion tensors in solutions, and ADCs and diffusion tensors in the isolated, KCl-arrested rat heart; b) taurine and creatine content during 32 min total, global ischaemia in the isolated rat heart; c) metabolite and water ADCs before, during and after ischaemia; and d) changes in average cardiomyocyte diameter during perfusion and ischaemia using the taurine ADC measurements.

At a diffusion time of 50 ms, the myocardial ADCs were 1.06×10^{-3} mm^2/s for water, 0.29×10^{-3} mm^2/s for taurine and 0.26×10^{-3} mm^2/s for creatine. Neither taurine nor creatine was lost from the heart during ischaemia, making either suitable for ischaemic diffusion measurements. Contrary to changes in the brain, myocardial water and taurine ADCs remained constant during ischaemia; however, the total creatine ADC increased by 35% which was shown to result from hydrolysis of PCr to creatine. Using the taurine ADC measurements at diffusion times between 50 ms and 1510 ms, the average myocyte diameter was calculated to be 40 μm during perfusion and 27 μm by the end of ischaemia. The decrease in myocyte diameter indicates that the buffer perfused heart is highly oedematous. This is the first time that: 1) metabolite ADCs have been measured in isolated heart, and 2) NMR spectroscopy has been used to determine the myocyte diameter. Thus ADC changes may not have potential for detecting ischaemia in the heart, although the measurement of myocyte diameter using taurine ADCs could indicate myocardial oedema.

Table of Contents

Chapter 2

Chapter 3

Chapter 4

LOCALISED ^{1}H-NMR SPECTROSCOPY OF THE PERFUSED RAT HEART: DEVELOPMENT OF EXPERIMENTAL METHODS FOR THE MEASUREMENT OF METABOLITE DIFFUSION COEFFICIENTS 72

Chapter 5

Chapter 7

Chapter 8

Chapter 9

Appendices

Figures

Chapter 1

Chapter 2

Chapter 3

Chapter 5

Chapter 6

Chapter 7

Chapter 8

Appendices

Tables

Abbreviations

$\langle x \rangle$	Average diffusion distance
$\vec{g}$	Gradient pattern in a STEAM pulse sequence
$f(\vec{g}, D)$	Diffusion mediated signal loss
$\langle (\vec{r} - \vec{r}_0)^2 \rangle$	Squared average diffusion distance
Δ	Diffusion time
δ	Duration of diffusion gradient; chemical shift
γ	Proton gyromagnetic ratio (= 2.675197×10^8 rad s^{-1} T^{-1})
τ	TE/2
η	Viscosity
$O(D_0 \cdot t_{dif})$	Higher order terms for the calculation of time dependent diffusion coefficient
$\nabla \mathbf{C}$	Vectorial concentration gradient
$\partial C / \partial \vec{r}$	Concentration gradient
[...]	Concentration
$[...]^T$	Transposed vector
[^{14}C]-inulin	Radioactively labelled inulin
[^{3}H]-H_2O	Tritiated water
^{1}H	Proton
^{31}P	Phosphorus
Å	Angstrom
A_{ATP}	Resonance area of ATP
Acet	Acetate peak in ^{1}H spectrum

Acq.	Acquisition
ADC	Apparent diffusion coefficient
ADC(x), ADC(y), ADC(z)	Spatial components of the ADC
$ADC_{cyto}/ADC_{solution}$	Ratio of ADC values in cytoplasm and solution
A_{DMMP}	Resonance area of DMMP
ADP	Adenosine diphosphate
AMP	Adenosine monophosphate
A_{MPA}	Resonance area of MPA
ANOVA	Analysis of variance
A_{PPA}	Resonance area of PPA
ATP	Adenosine triphosphate
b	**b**-matrix
b	Scalar b-value
b_{ij}	**b**-matrix components; i,j = x,y,z
C	Crusher gradients during TM
Car	Carnitine
CHESS	Chemical shift selective
Cho	Choline-containing compounds
Cho/Car/Tau	^{1}H peak consisting of choline-containing compounds, carnitine and taurine
CoA	Coenzyme A
Cr_t	Total creatine peak in a ^{1}H spectrum
CSF	Cerebrospinal fluid

d	Average cardiomyocyte diameter
D	Diffusion tensor
D	Scalar self-diffusion coefficient
$d\varphi$	Net phase change of diffusing spins
$d\varphi_1$	Phase shift of spins at position x_1
$d\varphi_2$	Phase shift of spins at position x_2
D'	Mutual diffusion coefficient
D_0	Free diffusion coefficient
DC	Diffusion coefficient
D_{ex}	Diffusion coefficient of water in the extracellular compartment
D_{ij}	Diffusion tensor components; i,j = x,y,z
D_{in}	Diffusion coefficient of water in the intracellular compartment
DMMP	Dimethyl methylphosphonate
d_{normal}	Average *in vivo* cardiomyocyte diameter
$d_{swollen}$	Average cardiomyocyte diameter during perfusion
D_x, D_y, D_z	Spatial components of diffusion coefficient
ECG	Electrocardiogram
EDTA	Ethylenediaminetetra-acetic acid
$\vec{f}$	$\vec{F}(t)$ function at TE/2
$\vec{F}(t)$	Integrated $\vec{G}(t)$ function
f_{ex}	Volume fraction of extracellular water
FID	Free induction decay
f_{in}	Volume fraction of intracellular water

FOV	Field of view
FRAP	Fluorescence recovery after photo bleaching
FT	Fourier transformation
fwhm	Full-width at half-maximum
G	Diffusion and spoiler gradients during τ period
$\vec{G}(t)$	Gradient time function
G	Strength of diffusion gradient
Glu/Gln	Glutamine/glutamate peak in ^{1}H spectrum
$G_x(t)$, $G_y(t)$, $G_z(t)$	Spatial components of gradient time function
H	Heaviside function
HPLC	High-pressure liquid chromatography
$\vec{J}$, $\boldsymbol{J}$	Solute flow per unit cross-sectional area
k	Constant relating peak area to amount of substance
k_B	Boltzmann constant (= 1.380662×10^{-23} J/K)
KCl	Potassium chloride
kHz	kilo Hertz
k_{isch}	Rate constant of signal increase during ischaemic period
k_{reperf}	Rate constant of signal decay during reperfusion period
LAD	Left anterior descending
LDH	Lactate dehydrogenase
MPA	Methylphosphonic acid
NAA	N-acetyl aspartate
NAD^+	Nicotine adenine dinucleotide, oxidised

NADH	Nicotine adenine dinucleotide, reduced
NMR	Nuclear magnetic resonance
P	Probability
p	Significance
PCr	Phosphocreatine
PCr/Cr	Ratio of PCr to creatine concentrations
PGSE	Pulsed-gradient spin-echo
pH	Negative logarithmic proton concentration
pH_i	Intracellular pH
P_i	Intracellular phosphate
PPA	Phenyl phosphonate
ppm	Parts per million
Pyr	Pyruvate peak in ^1H spectrum
$\vec{r}$	Final position of diffusing molecule
$\vec{r}_0$	Original position of diffusing molecule
R^2	Squared regression coefficient
RF	Radiofrequency
R_H	Hydrodynamic radius
S	NMR signal of spin system
S/V	Surface-to-volume ratio
S_0	Equilibrium magnetisation of spin system
$S_{0,isch}$	Detected NMR signal at the end of the ischaemic period
$S_{0,norm}$	Detected NMR signal during perfusion period
$S_{0,R}$	Detected signal in a fully relaxed STEAM sequence
SEM	Standard error of the mean

SGP	Short-gradient pulse
$S_{isch}(t)$	Detected NMR signal during ischaemic period
SNR	Signal-to-noise ratio
$S_{reperf}(t)$	Detected NMR signal during reperfusion period
STEAM	Stimulated echo acquisition mode
T	Absolute temperature
T_1	Longitudinal relaxation time
T_2	Transverse relaxation time
Tau	Taurine peak in ^1H spectrum
TCA	Tricarboxylic acid
t_{dif}	Diffusion time
TE	Echo time
TG	Triglyceride peak in ^1H spectrum
TM	Mixing time
TR	Repetition time
V_{extra}	Extracellular water volume
V_{intra}	Intracellular water volume
V_i	Intracellular compartment
V_o	Extracellular compartment
V_{total}	Total water volume
WEFT	Water-eliminated Fourier transform
x	ppm position of P_i peak relative to PCr peak position in a ^{31}P-NMR spectrum

Chapter 1

Introduction: NMR diffusion measurement in biological systems

1.1. The measurement of diffusion

The mobility of intracellular molecules, such as PCr or ATP, is crucial for many biochemical processes in the cell (Clegg 1984; Le Bihan 1991; Wallimann et al. 1992). Most importantly, the rate of energy metabolism is limited by the availability of substrates, and the transport of substrates from the site of production to the site of utilisation must proceed at rates sufficient for the cell to maintain normal function. The mobility of molecules in cells can be measured using 'probe' molecules, similar to radioactive tracers, that reside exclusively in the intracellular space. Furthermore, if the probe molecules carry protons and are present in sufficient amounts, their mobility may be measured using NMR techniques. Typical ^{1}H-containing molecules fulfilling these conditions in the heart are small organic molecules such as creatine or taurine. Such molecules can be tagged and their mobility monitored using a modified spin-echo pulse sequence. The measurement of the mobility or the amount of diffusion, can, in principle, yield two types of information. Firstly, 'free' diffusion can be measured by selecting a short diffusion time, such that the molecules 'travel' a distance that is small compared to the cell size. This will show the properties of the immediate intracellular environment, such as viscosity and temperature. Secondly, a long diffusion time will allow molecules to travel a distance comparable to, or longer than, the dimensions of the cell. During this time, interactions with cell organelles or the cell wall takes place, and the mobility of the molecules depends on their immediate environment and on structural barriers further away. This process is commonly referred to as 'restricted diffusion'.

In this chapter the theory of diffusion is given with methods for quantification of diffusion coefficients and tensors using NMR techniques. The use of restricted diffusion for the measurement of the cell size is described.

1.2. The diffusion process

When a liquid is heated, the energy added increases the internal kinetic energy, leading to increased rates of particle motion. Apart from macroscopic convection and convection-like phenomena caused by thermal or density gradients in the system, molecular motion can be distinguished into internal molecular motion (rotation about bonds and vibrations) and translational (or lateral) diffusion of molecules and aggregates (Stilbs 1987). Translational diffusion can be distinguished further, depending on the state of the system. *In a non-equilibrium system*, displaying a macroscopic concentration gradient such as a two-component system of solvent/solute layered upon pure solvent, the *mutual* diffusion coefficient characterises the relaxation of the concentration gradients in the system according to Fick's Law:

$$\vec{J} = -D'\left(\frac{\partial C}{\partial \vec{r}}\right) \tag{1.1}$$

where $\partial C/\partial \vec{r}$ represents the solute concentration gradient, D' is the mutual diffusion coefficient and $\vec{J}$ is the flow of solute molecules per unit cross sectional area (Agutter et al. 1995; Le Bihan 1991; Nicholson and Phillips 1981). The once sharp boundary becomes blurred until the concentration difference disappears and a single homogeneous solution remains.

Under *equilibrium conditions*, in which the concentration of the species is uniform and stable, no macroscopic evolution can be seen. However, motion is present on a molecular level which, in an equilibrium system, is referred to as *self*-diffusion. This is also known as Brownian motion and can be defined as the net result of the thermal motion-induced random-walk process experienced by particles or molecules in solution. Fick's Law

cannot describe self-diffusion because the system is in equilibrium and other approaches must be used to measure Brownian motion. One approach is to artificially create a concentration gradient using a radioactive tracer similar to the solution under investigation and to monitor the tracer concentration according to Fick's Law (Le Bihan 1995). The obvious disadvantage is that this method cannot be used in humans, although it has been used in experimental animal models (Le Bihan 1991). Another approach to describe self-diffusion is to monitor the random molecular walk on a macroscopic, statistical scale. The probability P of finding a molecule, originally at a position $\vec{r}_0$, at a position $\vec{r}$ after a time t_{dif}, is given by a Gaussian distribution:

$$P(\vec{r},\vec{r}_0,t_{dif}) = \left(\frac{1}{4\pi D t_{dif}}\right)^{3/2} \exp\left\{-\frac{(\vec{r}-\vec{r}_0)^2}{4Dt_{dif}}\right\} \tag{1.2}$$

where D is the self-diffusion coefficient. From this probability distribution, the average distance a molecule travels within the time t_{dif} can be calculated. The average displacement of all molecules in all three directions is zero, owing to the fact that the system is in equilibrium, but the mean square displacement, the average distance travelled by a single molecule, is given by the Einstein relation:

$$\left\langle (\vec{r}-\vec{r}_0)^2 \right\rangle = 6Dt_{dif} \tag{1.3}$$

in which the angular brackets symbolise a time average. With one-dimensional motion, this equation becomes:

$$\left\langle \left(\vec{r} - \vec{r}_0\right)^2 \right\rangle = 2Dt_{dif} \tag{1.4}$$

The diffusion coefficient relates diffusion distance with time, and depends on properties of the system and the diffusing molecule. It is given by the Stokes-Einstein relation:

$$D = \frac{k_B T}{6\pi\eta R_H} \tag{1.5}$$

where k_B is the Boltzmann constant, T the absolute temperature, η the viscosity of the medium, and R_H is the hydrodynamic radius of the diffusing species (Einstein 1906).

1.3. Diffusion measurements with NMR methods

1.3.1. Non-NMR *vs.* NMR methods

Diffusion coefficients can be measured using a variety of techniques. The classical method is to use radioactive tracers, and displacements in the mm-range can be observed (Caillé and Hinke 1974). Spatially resolved methods may be used such as infrared spectroscopy or Raleigh scattering, giving μm-resolution; neutron scattering is a powerful method giving Å-resolution. However, these techniques are not suitable for *in vivo* studies. NMR methods, on the other hand, are completely non-invasive, no tracer substance needs to be introduced to the system, and no experimental apparatus other than the magnet system is needed. In addition, the diffusion measurement can be combined with almost all NMR pulse sequences, allowing for diffusion measurements by imaging or spectroscopic methods. Because the range of NMR-measured displacements is a few μm to tens of μm, it is close to cellular dimensions, making it a useful tool for biological

investigations.

1.3.2. The pulsed-gradient spin-echo (PGSE) pulse sequence

A commonly used NMR method to measure diffusion is to apply pulsed field gradients to impart position-dependent phase changes on the diffusing molecules. The principle is illustrated by the Stejskal-Tanner pulsed-gradient spin-echo (PGSE) pulse sequence (Fig. 1.1) (Stejskal 1965; Stejskal and Tanner 1965).

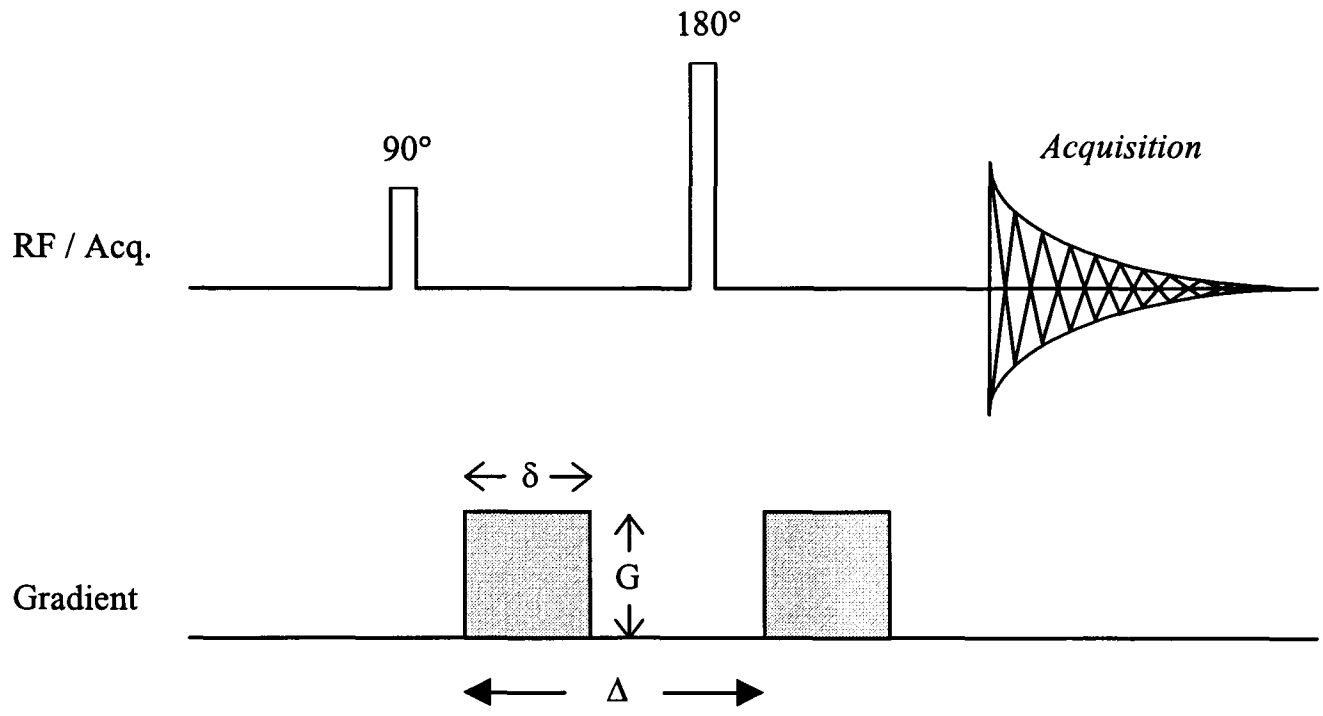

Fig. 1.1: The Stejskal-Tanner pulsed-gradient spin-echo (PGSE) pulse sequence to quantify diffusion. It is a spin-echo sequence with the 180° RF pulse sandwiched between a pair of identical gradient pulses with a duration δ, a strength G and a time Δ apart. The first one dephases and the second one rephases the magnetisation. Movement, such as Brownian motion, between the application of the gradient pulses leads to incomplete rephasing and associated signal loss proportional to the amount of diffusion.

The sequence is a basic spin-echo sequence with an additional gradient pulse on either side of the 180° RF pulse. The function of these gradient pulses is to 'label' the diffusing spins, which then act as endogenous tracers. In the above sequence, G is the strength of the applied diffusion gradients, δ their duration and Δ the time between the onset of the two gradient pulses. Assuming a single spin initially, the action of the first gradient is to impart a phase shift on the spin, which is dependent on its position. Suppose the gradient is applied along the x-direction, then the phase shift of the spin at position x_1 is given by

$$d\varphi_1 = \gamma \int_0^{\delta} G x_1 \mathrm{d}t = \gamma G \delta x_1 \tag{1.6}$$

where γ is the gyromagnetic ratio; it is assumed that the spin remains at x_1 during the application of the gradient pulse. The 180° RF pulse transforms the phase shift into $-d\varphi_1$. The second gradient pulse, applied at a time Δ after the first gradient pulse, 'unwinds' the spin:

$$d\varphi_2 = \gamma \int_{\Delta}^{\Delta+\delta} G x_2 \mathrm{d}t = \gamma G \delta x_2 \tag{1.7}$$

where x_2 is the position of the spin during the application of the second gradient pulse. The net phase difference the spin has experienced is:

$$d\varphi = d\varphi_1 - d\varphi_2 = \gamma G \delta \left(x_1 - x_2 \right) \tag{1.8}$$

Static spins ($x_1 = x_2$) do not experience a net phase shift, but moving spins ($x_1 \neq x_2$) do.

The net phase shift, and therefore the obtained signal, is proportional to the distance diffused.

In order to derive the diffusion-mediated signal attenuation of a spin system, the summation over all diffusing spins *j* has to be calculated. The magnetisation of a spin system is given by:

$$S = S_0 \sum_j \exp\{i\, d\varphi_j\} \tag{1.9}$$

The signal attenuation S/S_0 can be derived using the probability distribution (see eq 1.2), and integrating over the complete distance:

$$S/S_0 = \int\int \exp\{i\gamma G\delta (x_1 - x_2)\} P(x_1) P(x_2, x_1, t_{dif})\, dx_1 dx_2 \tag{1.10}$$

By definition, the integral of the initial probability of finding a molecule at position x_1 over the whole distance is unity:

$$\int P(x_1, t_{dif})\, dx_1 = \int P(x_1)\, dx_1 \equiv 1 \tag{1.11}$$

Using the probability distribution from eq 1.2, one obtains for the remaining integral

$$S/S_0 = \exp\{-(\gamma G\delta)^2 \Delta D\} \tag{1.12}$$

Thus, the diffusion-mediated signal loss depends on the diffusion coefficient and on the gradient parameters. It should be noted that this approach is oversimplified in that

diffusion might not be negligible during the gradient pulses and there might be other gradient pulses in the pulse sequence, leading to additional diffusion-mediated signal attenuation. The mathematically correct form for the signal attenuation can be derived by solving the Bloch equations, with additional terms for diffusion, the "Bloch-Torrey" equations (Le Bihan 1991; Torrey 1956). The general solution for diffusion-mediated signal attenuation is:

$$S/S_0 = \exp\left\{-D\left(\gamma^2 \int_0^{TE}\left(\int_0^{t'} G(t')\,dt''\right)^2 dt'\right)\right\} \tag{1.13}$$

A factor was introduced to characterise the sensitivity of a pulse sequence to diffusion, the "*b*-value" (Le Bihan et al. 1986):

$$b = \left(\gamma^2 \int_0^{TE}\left(\int_0^{t'} G(t')\,dt''\right)^2 dt'\right) \tag{1.14}$$

leading to:

$$S/S_0 = \exp\{-bD\} \tag{1.15}$$

In the PGSE sequence, the *b*-value may be calculated (Le Bihan 1991) as:

$$b = \gamma^2 G^2 \delta^2 \left(\Delta - \delta/3\right) \tag{1.16}$$

The diffusion coefficient can be calculated from NMR experiments in which the *b*-value is varied. A linear regression of the natural logarithm of the signal attenuation as a function of the *b*-value (see eq 1.15) yields a graph of slope $-D$ and intercept with the abscissa being the signal intensity S_0, in the absence of diffusion gradients. The *b*-value can be varied by changing the strength or the timing of the diffusion gradients. The latter is a correct method for an infinite system, but for a system of finite dimensions, such as cells, restriction effects due to the cell walls or other cellular components influence the diffusion path. Hence it is generally advisable to vary the strength rather than the timing of the diffusion gradients.

1.4. The diffusion coefficient

Diffusion coefficients of molecules in liquid systems at room temperature range from about 10^{-3} for small molecules in non-viscous solutions to 10^{-6} mm^2/s for large polymers in solutions (Stilbs 1987); for example, water at room temperature has a diffusion coefficient of 2.2×10^{-3} mm^2/s (Mills 1973). In the human body, diffusion coefficients for small molecules or water range from 0.1×10^{-3} mm^2/s in brain white matter to 3.0×10^{-3} mm^2/s in body fluids such as cerebrospinal fluid (CSF) (Kwong et al. 1991; van der Toorn et al. 1996a). For a molecule with a diffusion coefficient of 10^{-3} mm^2/s, the average diffusion distance during a typical diffusion time of 20 ms is around 6 μm (eq 1.4).

According to eq 1.15, the higher the *b*-value the smaller the diffusion coefficient that can be measured. High *b*-values are achieved either by choosing strong gradients or, once at their maximum, by extending the timing. As is evident from Fig. 1.1, this lengthens the echo time with a consequent signal loss due to increased T_2 relaxation. Hence, in a PGSE sequence, the T_2 of the diffusing substance becomes the limiting factor when measuring

small diffusion coefficients. Excessively rapid transverse spin relaxation makes diffusion measurements difficult or even impossible. As will be discussed later, a diffusion-weighted stimulated echo-based sequence may circumvent this problem.

1.5. Practical aspects of diffusion measurement

The shape of an ideally rectangular gradient pulse is modified by the finite rise time of the gradients which alters the form of the gradient to a ramped pulse, and changes the *b*-value. However, this is negligible as the area and the amplitude of the gradient are the same (Price and Kuchel 1991; Stejskal and Tanner 1965). The positioning of the diffusion gradients within the pulse sequence can be altered. For example, the unipolar gradient pair on either side of the 180° pulse in the PGSE sequence (see Fig. 1.1) can be turned into a single bipolar pattern (a positive followed immediately by a negative gradient or vice versa) on one side of the 180° pulse. This pattern can provide short diffusion times, but reduces the *b*-value because Δ is shortened (see eq 1.12).

The quality of the magnet system and the gradient hardware in particular are crucial for accurate diffusion measurements. As the diffusion coefficient is derived from a number of measurements, system stability is essential. The calibration of the gradients should be checked by carrying out a spectroscopic diffusion experiment on a water sample at known temperature and comparing the obtained diffusion coefficient with published values. It is also good practice to allow the gradient set to warm up before the experiment to ensure constant output. Eddy currents, which are induced in the cryostat by switching a magnetic field gradient, change the gradient form, thus changing the *b*-value and leading to errors in the estimation of diffusion coefficients. Thus eddy currents should be minimised, preferably by using actively-shielded gradient coils (Mansfield and Chapman 1986).

1.6. The 'apparent diffusion coefficient' (ADC)

1.6.1. Diffusion in biological systems

The above equations assume that diffusion takes place in an 'infinite system', that there are no physical restrictions, and that the longer the diffusing molecule travels, the further away it has travelled from its origin. This 'free diffusion' is a process encountered in solutions. Biological systems differ from an 'infinite' system, being heterogeneous with multiple compartments. Barriers, such as the cell walls or organelles, limit the paths of diffusion, or, if permeable, can slow down the diffusion process. Adsorption and desorption processes or specific binding can also slow the diffusion process (Agutter et al. 1995). In such systems, the probability distribution deviates from a Gaussian function, and eqs 1.2-1.4 no longer apply. To estimate the diffusion coefficient in a biological system, the system must be geometrically modelled for the probability distribution (eq 1.2). However, such an approach is difficult as the structure of the system is generally not sufficiently well known and geometric models can be complex. Probability distribution calculations have been performed on systems that are easy to model, such as equally spaced mica stacks or spherical yeast cells (Tanner and Stejskal 1968). Nonetheless it is useful to measure diffusion coefficients in biological systems using the NMR methods described above, assuming a Gaussian probability distribution. Because the diffusion coefficient is influenced by the properties of the biological system and by the experimental parameters, such as pulse sequence timing, it is commonly referred to as the '*apparent diffusion coefficient*' (ADC).

1.6.2. *In vivo* ADC *vs. in vitro* diffusion coefficient

Metabolite ADCs are lower *in vivo* than *in vitro* at the same temperature (Le Bihan 1991; Merboldt et al. 1993; van der Toorn et al. 1996a), due to the increased viscosity of the cell cytosol (Luby-Phelps 1994; Luby-Phelps et al. 1987), which decreases the diffusion coefficient according to the Stokes-Einstein relation (eq 1.5). In addition, diffusing molecules encounter a number of barriers such as cell walls, organelles and macromolecules, which force them onto tortuous pathways, also reducing their mobility (Le Bihan 1991; Norris and Niendorf 1995; van der Toorn et al. 1996a). The molecule might be contained in a specific organelle in the cell which leads to a high degree of motional restriction with a consequent decrease of its diffusion coefficient.

Molecules in different cell types have a variety of ADC values. The ADC of creatine in muscle is twice as high as in brain, which has been attributed to the cytoplasm in muscle being less tortuous than in brain (Hansen 1971; Nicolay et al. 1995). However, ADC differences cannot simply be attributed to variations in cytosolic viscosities and cellular organelle densities because other factors, such as cell size and pulse sequence parameters, also influence the ADC.

1.7. Anisotropic diffusion and the diffusion tensor

NMR imaging studies in animals (Moseley et al. 1990a) and humans (Kwong et al. 1991) have shown that the diffusion coefficient of water in brain white matter depends on the direction along which the diffusion gradient is applied. In general, the diffusion coefficient with diffusion gradients applied perpendicular to the neuron fibre axis is about 2/3 of those measured with diffusion gradients applied parallel to the fibre axis. Thus, in an *in vivo* system, the diffusion coefficient depends on structural features of the tissue; in

other words the diffusion coefficient is not a scalar quantity but exhibits a directional dependence, a phenomenon commonly referred to as 'anisotropic diffusion'.

Measurements of diffusion anisotropy are useful in the investigation of structural changes in the cellular environment; for example, in stroke the change of the degree of anisotropy of the brain fibre organisation is diagnostically useful (Carano et al. 1998; Jones et al. 1998b; Miranda et al. 1998; Pattany et al. 1997; Werring et al. 1998). Diffusion was found to be anisotropic in other tissues such skeletal muscle (Cleveland et al. 1976; Tanner 1979) and heart (Edelman et al. 1994; Garrido et al. 1994) - an indication of microstructural features (Basser 1995). Furthermore, diffusional anisotropy was also observed in spectroscopic metabolite diffusion studies (in this case, NAA) of cat brain (Nicolay et al. 1995).

Thus, the dependence of diffusion on the direction would turn the diffusion coefficient into a vector; however, there are interactions in orthogonal directions, which require the diffusion process to be represented by a *tensor*. To illustrate this, consider a molecule diffusing along the axis of a bundle of muscle fibres (Fig. 1.2).

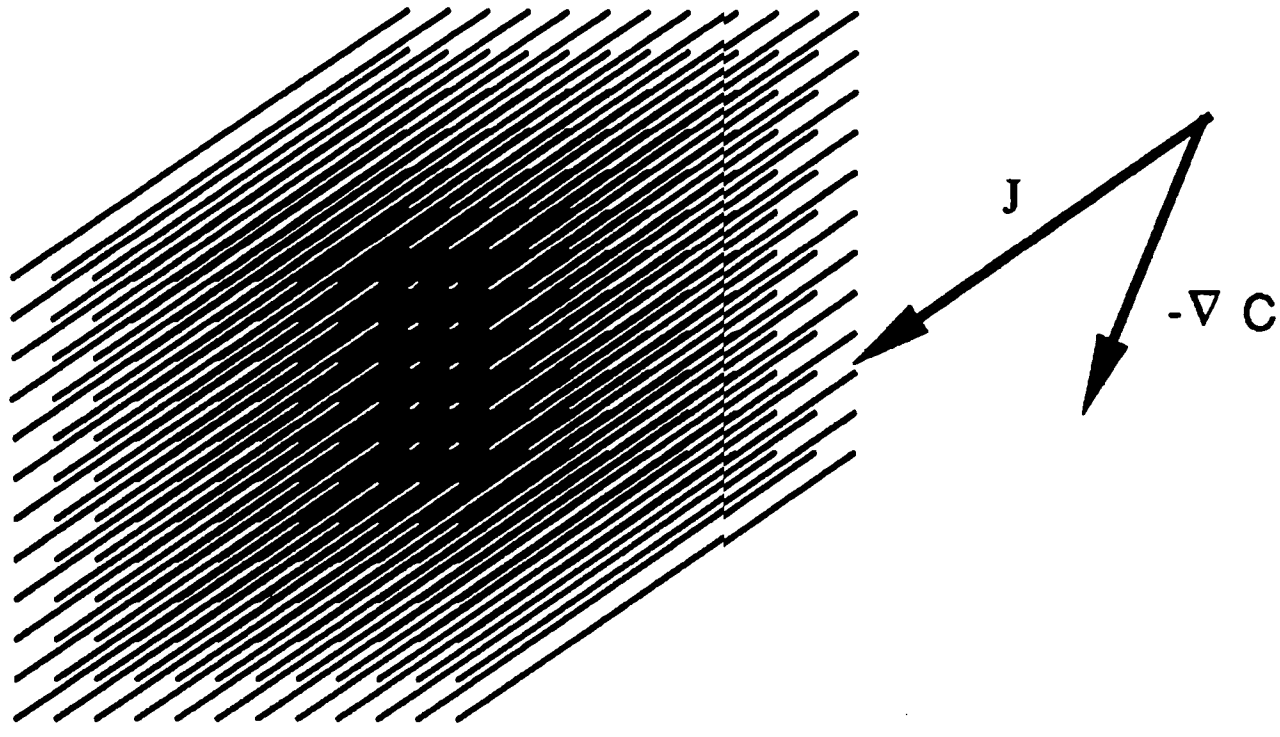

*Fig. 1.2: Representative diagram of the tensorial diffusion of a molecule in a bundle of muscle fibres. The concentration gradient -∇C is not necessarily parallel to the flux direction, **J**. Hence the diffusion process must be described by a 3x3 tensor.*

The path of the molecule is predetermined by its surrounding structure, such that it is forced to travel in the direction of the muscle fibre. However, the concentration gradient will not necessarily point in that direction. Thus eq 1.1 is no longer valid because the particle flux direction and the direction of the concentration gradient are no longer parallel. Instead, it needs to be modified by turning the scalar diffusion coefficient into a matrix (a 3x3 tensor), accounting for possible cross terms:

$$\vec{J} = -\mathbf{D}\begin{pmatrix} \partial C/\partial x \\ \partial C/\partial y \\ \partial C/\partial z \end{pmatrix} \quad \text{where} \quad \mathbf{D} = \begin{pmatrix} D_{xx} & D_{yx} & D_{zx} \\ D_{xy} & D_{yy} & D_{zy} \\ D_{xz} & D_{yz} & D_{zz} \end{pmatrix} \qquad (1.17a+b)$$

Diagonal elements of the diffusion tensor scale fluxes and concentration gradients in the same direction, whereas off-diagonal elements couple fluxes and concentration gradients in orthogonal directions. All elements of the symmetric diffusion tensor must be known in order to characterise a system adequately (Basser et al. 1994b).

1.8. The b-matrix

1.8.1. Dependence of the *b*-value on the direction of the applied gradients

In section 1.3.2. the scalar *b*-value was calculated from eq 1.16. This equation was derived for a simple spectroscopic spin-echo sequence with diffusion gradients applied in one direction of the gradient system. Often the diffusion measurements are combined with imaging or localised spectroscopic pulse sequences, and a number of other gradients, such as slice-selection or read-out gradients, are applied in addition to the diffusion gradients. The dephasing and rephasing of spins caused by such gradients has to be taken into account, a precaution often neglected. This has two important consequences: First, as the *b*-value depends on the gradient switching pattern along each axis, it will not necessarily be identical for each direction. In addition, not only do gradients interact along the same axis, as is the case in the basic PGSE sequence, but also along orthogonal axes. In other words, the scalar *b*-value is no longer appropriate to describe the relation between signal attenuation and diffusion coefficient, and must be replaced by a **b**-matrix. The **b**-matrix consists of diagonal elements describing interactions of gradients applied along the same axis, and off-diagonal elements describing interactions between gradients applied in perpendicular directions.

1.8.2. Calculation of the b-matrix

The calculation of the **b**-matrix is, in principle, similar to the calculation of the scalar *b*-value in that the switching pattern of all gradients in the pulse sequence must be considered. Such calculations were performed early in the history of NMR diffusion measurements (Stejskal 1965), but were ignored until recently due to the complexity of the calculations and the necessity for longer experiments (see below). A gradient timing function may be defined as:

$$\vec{G}(t) := \begin{pmatrix} G_x(t) \\ G_y(t) \\ G_z(t) \end{pmatrix} \tag{1.18}$$

which includes all gradients along all three gradient axes, such that this function defines the complete gradient switching pattern of the pulse sequence. It is convenient to define the time integral over the gradient switching function:

$$\vec{F}(t) := \int_0^t \vec{G}(t')dt' \tag{1.19}$$

similar to defining the gradient area with δ and G in eq 1.13. The **b**-matrix may be defined as:

$$\mathbf{b} = \gamma^2 \int_0^{TE} \left[\vec{F}(t') - 2H\left(t' - \frac{TE}{2}\right)\vec{f} \right] * \left[\vec{F}(t') - 2H\left(t' - \frac{TE}{2}\right)\vec{f} \right]^T dt' \tag{1.20}$$

where H(t') is the unit Heaviside function, TE is the echo time, $[...]^T$ is a transposed

vector and:

$$\vec{f} := \vec{F}\left(TE/2\right) \tag{1.21}$$

(Basser et al. 1994a; Basser et al. 1994b; Mattiello et al. 1994). When the gradient strength is changed, such as in scalar diffusion coefficient measurements, the **b**-matrix needs to be re-calculated.

1.8.3. b-matrix *vs.* scalar *b*-value

Under certain circumstances it is justifiable to calculate the scalar *b*-value instead of the full **b**-matrix for an imaging or spectroscopic sequence in which other gradients are present. This can be done when gradients, other than the diffusion gradients, have a negligible effect on the signal attenuation, for example when slice-selection or read-out gradients are small compared to the diffusion gradients and are immediately re- or prefocused. However, if diffusion gradients are comparable in strength to other gradients applied in the pulse sequence, cross terms are considerable, and neglecting them can lead to serious errors in the estimation of the ADC (Mattiello et al. 1994; Neeman et al. 1990).

1.9. The diffusion tensor

The diffusion-mediated signal attenuation is given by the dot-product of the **b**-matrix and the diffusion tensor (Basser et al. 1994a):

$$\ln\left(\frac{S}{S_0}\right) = -\sum_{i=1}^{3}\sum_{j=1}^{3} b_{ij} D_{ij} = -\mathbf{b}\cdot\mathbf{D} \tag{1.22}$$

Because of the symmetry of **b** and **D**, this expression expands to

$$\ln\left(\frac{S}{S_0}\right) = -\left[b_{xx}D_{xx} + b_{yy}D_{yy} + b_{zz}D_{zz} + 2b_{xy}D_{xy} + 2b_{xz}D_{xz} + 2b_{yz}D_{yz}\right] \qquad (1.23)$$

Six variables have to be determined in order to obtain the complete diffusion tensor, which leads to longer measurement times, the major reason that diffusion tensor measurements are not routinely implemented in the clinical environment.

The diffusion tensor is measured not by varying the gradient strength, as is the case when measuring the scalar diffusion coefficient, but by varying the gradient orientation in order to probe for diffusion in different directions. The basic measurement involves seven experiments, one in which S_0 is measured (see eq 1.22) and six in which the signal attenuation is measured depending on the direction of the diffusion gradients. A typical form for these latter measurements is to apply diffusion gradients in a non-collinear fashion, for example according to the pattern (0,0,1), (0,1,0), (1,0,0), (0,√½,√½), (√½,0,√½), (√½,√½,0) where each 'vector' represents the unit diffusion gradient strength applied in x-, y-, and z-direction. These different gradient patterns lead to six different **b**-matrices; in each of the six experiments the signal attenuation is recorded. Together with the S_0 measurement this yields six equations with six unknowns – the diffusion tensor elements. Such a system can be solved by matrix inversion.

The basic measurement is carried out with a fixed strength of the diffusion gradient (the 'basic diffusion gradient strength'), and only the orientation of the diffusion gradient is changed. In order to increase the accuracy, the experiment might be repeated a number of times using different basic strengths. The diffusion tensor is then obtained using multivariate linear regression (Basser et al. 1992; Basser et al. 1994a). However, it has

been demonstrated recently that a measurement with only one basic diffusion gradient strength can provide sufficient accuracy, provided the imaging gradients do not contribute more than 1% to the total **b**-matrix value (Basser and Pierpaoli 1998).

1.10. Applications of diffusion tensor measurements

After preliminary studies of fibre direction in muscle (Basser and Le Bihan 1992), Basser and co-workers developed diffusion tensor imaging and spectroscopy, making available the quantification of diffusion in three dimensions (Basser et al. 1992). This allowed the mapping of the structure surrounding diffusing molecules, such as water or intracellular metabolites (van Gelderen et al. 1994b). Today fibre orientation and structural anisotropy have been mapped using NMR imaging techniques in various organs, such as the brain (Basser and Pierpaoli 1996; Coremans et al. 1994) or the heart (Garrido et al. 1994; Tseng et al. 1997). However, the diffusion tensor is useful in *in vivo* studies of tissue only when the diffusion time is long enough to 'sense' any directional differences in mobility. On the other hand, in an isotropic medium or with an average diffusion distance much shorter than cellular dimensions, the diffusion tensor should have identical values for the diagonal elements and zero off-diagonal elements.

1.11. Restricted diffusion

Woessner was the first to realise that the ADC depended on the diffusion time in a colloidal system because of colloid particles restricting the motion of the diffusing species (Woessner 1963). The geometry of a compartment influences the ADC of diffusing molecules at long diffusion times, and by measuring the ADC at long diffusion times, it is possible to derive some information about the structure of the compartment.

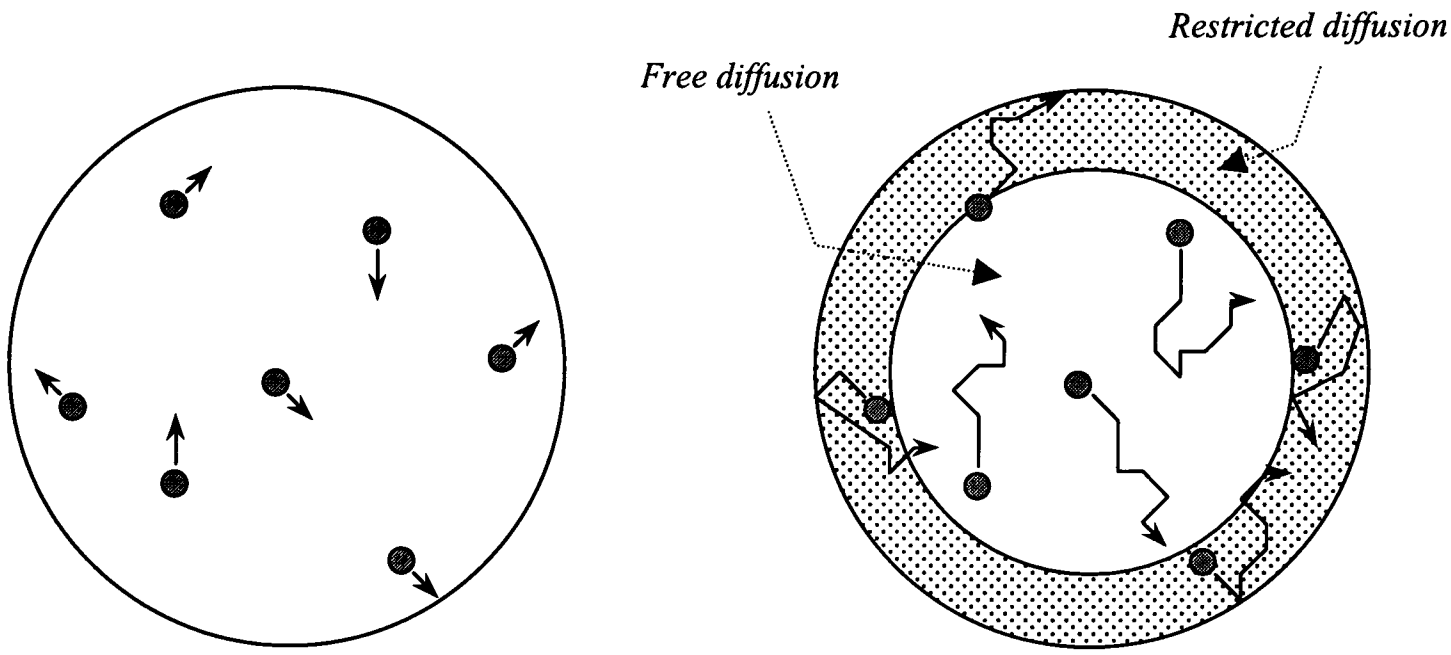

(a) Short diffusion time

(b) Medium diffusion time

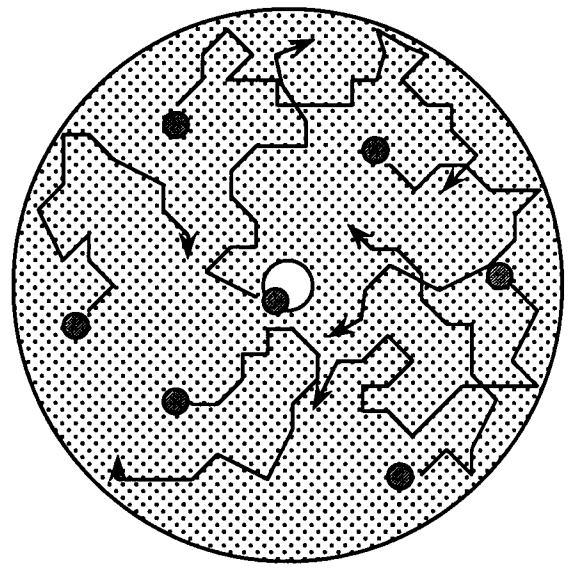

(c) Long diffusion time

Fig. 1.3: Schematic illustration of how the duration of the diffusion time affects the ADC. (a): Free diffusion; very few molecules reach the cell wall and are repelled by it. (b): Medium diffusion time. Molecules within the shaded area can reach, and be repelled by the cell wall, hence shortening their diffusion path. Molecules in the centre of the sphere cannot reach the cell wall within the given diffusion time. Therefore the observed ADC is a mixture of the 'free' and the restricted diffusion process with a consequent reduction in the ADC compared to (a). At long diffusion times (c), almost all molecules encounter the cell wall with a concomitant further reduction in the measured ADC. Eventually, at infinitely long diffusion times the measured ADC will depend only on the size of the sphere, not on the physico-chemical properties of the diffusing species and the solvent.

At very short diffusion times the average distance travelled, $\sqrt{\langle x^2 \rangle}$, of each solute molecule is extremely small. Consequently, only minute amounts of molecules can reach the cell wall and be repelled by it; hence the diffusion process can be assumed to be 'free' (see Fig. 1.3*a*), and the equation

$$\sqrt{\langle x^2 \rangle} = \sqrt{2 \cdot ADC \cdot t_{dif}} \tag{1.24}$$

for the average travelled distance is valid. However, cells contain a large number of organelles such as mitochondria and myofibrils, structural barriers that influence the path of the diffusing molecules. Under such circumstances diffusion is not free, but it is *hindered*. In fact, diffusion times in the order of picoseconds are required to avoid significant contribution from any possible barriers.

Upon increasing the diffusion time, the diffusion process of the solute molecules in and around the centre of the sphere is still unrestricted, hence their movement is reflected by true Brownian movement and is not influenced by the confining walls of the compartment. However, molecules which started their journey further away from the centre are likely to encounter, and subsequently be repelled by, the compartment wall (Fig. 1.3*b*). Such molecules have travelled a shorter distance from their origin of movement and consequently their diffusion coefficient is reduced compared to the freely diffusing molecules. In other words, the more molecules that encounter the compartment wall, the smaller the ADC.

Increasing the diffusion time further increases the probability for the solute molecules to encounter the cell wall, thus leading to a decrease in the ADC until all molecules are likely to hit, and be repelled by it (Fig. 1.3*c*). Hence, at an infinitely long diffusion time,

the ADC no longer depends on parameters such as temperature or viscosity (see Stokes-Einstein equation, eq 1.5), but on the geometric borders of the compartment in which the diffusion process takes place.

Following the above argument, the ADC decreases with increasing diffusion time until it reaches an asymptotic minimum value (Fig. 1.4). The smallest diffusion time realisable in the NMR experiment is still too long to observe 'free' diffusion inside cells.

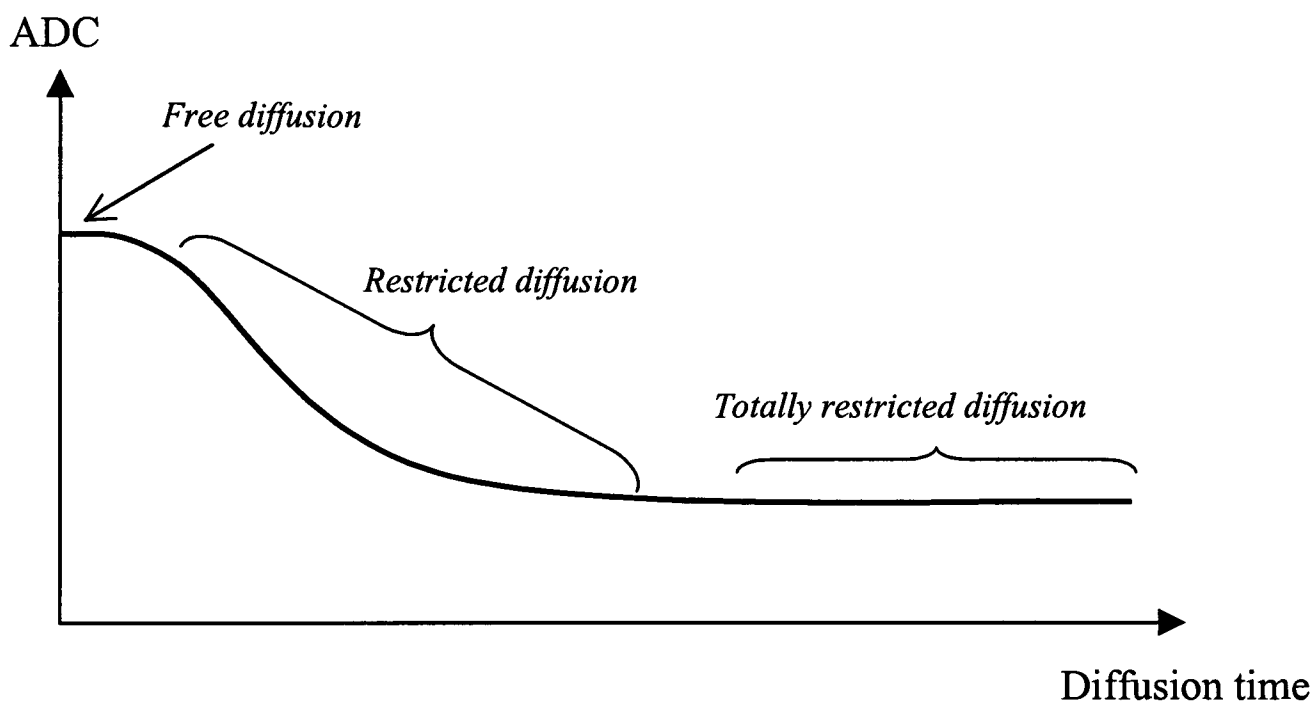

Fig. 1.4: The ADC at different diffusion times. The 'free diffusion' zone cannot be detected using NMR methods. During the 'restricted diffusion' period more molecules encounter the cell wall until diffusion becomes totally restricted and determined solely by the dimension of the compartment.

Although these arguments illustrate the principle of the ADC dependence on the diffusion time in a closed system, the situation is more complicated in biological systems, such as muscle fibres or heart. Cells are generally not spherical but tend to be cylindrical (Nash et

al. 1979; Powell et al. 1978; van Gelderen et al. 1994b), and are oriented in various directions (Edelman et al. 1994; Garrido et al. 1994; Scollan et al. 1998; Tseng et al. 1997). However, the basic principle of free diffusion, restricted and totally restricted diffusion as a function of the diffusion time is valid, and the ADC of diffusing substances in an enclosed space, such as intracellular metabolites, can be described by a graph similar to that in Fig. 1.4.

1.12. Determination of the cell size from restricted diffusion measurements

Only a few groups have investigated how the restriction due to confining geometries, such as cell walls, influence the ADC. Models for the calculation of signal attenuation for diffusion in parallel planes, spheres and cylinders generally rely on the "short-gradient-pulse" (SGP) approximation (Balinov et al. 1993; Callaghan 1995; Murday and Cotts 1968; Söderman and Jönsson 1995). It requires that there is no diffusion occurring during the application of the diffusion gradient pulse of duration δ, and that the product $\delta \cdot G$ (where G is the strength of the diffusion gradient) is finite, while $\delta \rightarrow 0$ and $G \rightarrow \infty$ (Callaghan 1995; Söderman and Jönsson 1995). These models start from basic principles of calculating the three-dimensional probability distribution with boundary conditions for the respective geometries. The results of such calculations are formidable equations for the signal attenuation due to restricted diffusion, containing eigenvalue systems and sums over spherical or cylindrical Bessel functions (Callaghan 1995; Söderman and Jönsson 1995; Stejskal 1965; Tanner 1978; Tanner and Stejskal 1968). Consequently, almost all investigators let $\Delta \rightarrow \infty$ and assume $D(t_{dif} = \infty) \rightarrow 0$ (Murday and Cotts 1968; Stejskal 1965; Tanner and Stejskal 1968); these are conditions that do not necessarily apply to NMR experiments in which relaxation times are finite.

A more general approach, independent of the geometry of the compartment, has been proposed in order to determine the ADC of molecules enclosed in a compartment as a function of the diffusion time (Mitra and Sen 1992; Mitra et al. 1992). In this approach, the diffusion propagator for a molecule confined to a pore volume was calculated and Green's function was assumed near the walls of the (impermeant) compartment to specify the boundary conditions. The final formula for the time-dependent diffusion coefficient, $D(t_{dif})$, was:

$$\frac{D(t_{dif})}{D_0} = 1 - \frac{4}{9\sqrt{\pi}} \cdot \frac{S}{V} \sqrt{D_0 \cdot t_{dif}} + O(D_0 \cdot t_{dif}) \qquad (1.25)$$

where D_0 is the 'free' diffusion coefficient, S/V is the surface-to-volume ratio of the pore space, t_{dif} is the diffusion time and $O(D_0 \cdot t_{dif})$ are higher order terms (Mitra and Sen 1992; Mitra et al. 1992). This will be referred to as the "Mitra model".

Latour and co-workers (1993) adopted this model and showed that the above equation applies to biological cell systems with S/V = 6/d, where d is the apparent cell diameter. They applied eq 1.25 in an onion and demonstrated that the higher order terms in $D_0 \cdot t_{dif}$ are negligible (Latour et al. 1993). This model has also been used for the estimation of restricted diffusion in goldfish skeletal muscle (Kinsey et al. 1999).

1.13. Application of the Mitra model to the cardiomyocyte

The ratio of the length to the diameter of the rat ventricular cardiomyocyte is about 5:1 (Boyett and Kirby 1989; Nash et al. 1979; Powell et al. 1978). With this and the assumption of cylindrical geometry of cardiomyocytes, the surface-to-volume ratio is $S/V = 4.4/d$. Hence, for the application of the Mitra model to cardiomyocytes with cylindrical

geometry, eq 1.25 becomes

$$\frac{D(t_{dif})}{D_0} = 1 - \frac{17.6}{9\sqrt{\pi}} \cdot \frac{1}{d} \sqrt{D_0 \cdot t_{dif}} \qquad (1.26)$$

Plotting $D(t_{dif})$ as a function of $\sqrt{t_{dif}}$ yields the average diameter, d, of the cardiomyocytes as well as the 'free' diffusion value, D_0.

1.14. Summary

The non-invasive measurement of the ADC can show the structure and pathology of biological tissue, providing information on the physico-chemical properties of the environment of the diffusing substance and yielding estimates for the motion hindrance and average cell size. The diffusion tensor can reveal fibre organisation in an organ, requiring the calculation of the **b**-matrix rather than the scalar *b*-value.

The aim of the work in this thesis was to develop and apply NMR methods to measure the ADCs of water and of intracellular metabolites in the rat heart during perfusion, ischaemia and reperfusion to determine whether swelling occurred during ischaemia, and whether changes in the ADC can be used as an indicator of ischaemic damage. In Chapter 2, changes in the energetics and cell volumes of perfused rat hearts during ischaemia were measured using ^{31}P NMR spectroscopy and phosphonate space markers. In Chapters 3 and 4 a localised ^{1}H spectroscopic pulse sequence was developed and tested on solutions and in perfused rat hearts. The work in Chapter 5 demonstrated pitfalls when measuring metabolite ADCs during the transition from perfusion to ischaemia and from ischaemia to reperfusion in the isolated rat heart. A comparison between the diffusion tensor and the scalar ADC of metabolites was made. Furthermore, it was determined whether the

perfused heart released taurine or creatine during ischaemia to prevent cell swelling. In Chapter 6 the ADCs of taurine and creatine were monitored during perfusion, total global ischaemia and reperfusion to investigate whether the metabolite ADCs may indicate ischaemic damage. In Chapter 7 these measurements were extended to estimate the average diameter of the ventricular cardiomyocyte. The work in Chapter 8 determined whether the water ADC was an indicator of ischaemic damage in the rat heart.

Chapter 2

Changes in intra- and extracellular volumes in the whole isolated rat heart during ischaemia measured using ^{31}P-NMR spectroscopy

Abstract

The aims of the work in this chapter were to quantify the total, intracellular and extracellular water volumes of the KCl-arrested, isolated rat heart during perfusion and 32 min of low-flow ischaemia. This was done using phosphonate space markers detected with ^{31}P-NMR spectroscopy, which also gave information about cardiac energetics. Two extremes of injury during low-flow ischaemia were used to give differences in the extent of cell swelling. To produce least injury, hearts were provided with 11 mM glucose and 1 mM Na-pyruvate, and to maximise injury, hearts were provided with no substrates. Water volumes were determined using dimethyl methylphosphonate and phenylphosphonate markers in the buffer that gave a measure of the total and the extracellular water spaces, respectively. The volume of all spaces in both the substrate-free and the substrate-perfused hearts decreased at the start of low-flow ischaemia as a consequence of the drop in the perfusion pressure. In substrate-free hearts this decrease was significantly greater and more prolonged, due to the onset of contracture. No cell swelling during the ischaemic period could be detected in either of the two groups of hearts. By the end of ischaemia, substrate-perfused hearts had slightly reduced levels of high-energy phosphates, but the substrate-free hearts had no remaining ATP or PCr. In conclusion, the presence of substrates exerted a protective effect during ischaemia by preserving the ATP content and preventing the loss of the extracellular water volume. The lack in the detection of significant cell swelling might be either because there was no cell swelling or because any swelling was below the sensitivity of the method.

2.1. Introduction

The high permeability of cell membranes to water makes cells vulnerable to any osmotic imbalance, and therefore to volume changes. When the number of osmolytes inside a cell is different from the number of osmolytes outside the cell, water is transported in the direction of the osmotic gradient because it is in thermodynamic equilibrium across the cell wall. However, even without osmotic stress, all cells face the problem of volume homeostasis, because the cytoplasm is richer in charged, impermeant macromolecules than is the extracellular fluid (Lang et al. 1993; Parker 1993). This establishes a 'natural' osmotic gradient into the cell which, if unopposed, would cause cell swelling. Most cells can maintain their intracellular water content by constantly reversing water entry into the cell, which requires energy to maintain the function of the ion pumps in the sarcolemma (Kirk 1997; Lang et al. 1993; Parker 1993; Sarkadi and Parker 1991; Strange 1994; Vandenberg et al. 1996). If these energy requirements can no longer be met, for instance during severe ischaemia, cell swelling should occur (Jennings et al. 1975; Kirk 1997).

In order to investigate cell volume changes and regulatory mechanisms in isolated cells, an osmotic gradient is deliberately applied by varying the osmolarity of the extracellular medium. Most of the studies investigating cell swelling in cardiomyocytes use patch-clamp techniques in conjunction with light microscopy (Drewnowska and Baumgarten 1991; Tseng 1992; Vandenberg et al. 1994). However, there may be a difference between cell swelling in anisosmotically stressed isolated cardiomyocytes and in the whole heart under ischaemic conditions. During myocardial ischaemia, there are two processes that may be responsible for an increase in intracellular osmolarity. Firstly, under anaerobic conditions, molecules such as glycogen and ATP are broken down to smaller metabolic products, such as lactate and P_i, respectively. In addition, the Na^+ pump in the sarcolemma may be inhibited, preventing extrusion of Na^+ ions (Cross et al. 1995b;

Ingwall et al. 1996; Wright et al. 1995). The increase in the Na^+ concentration and the number of small molecules inside the cell raises the intracellular osmolarity. This could lead to an influx of water and eventually, if unopposed, to cell swelling. Evidence for this has come from Tranum-Jensen and co-workers (Tranum-Jensen et al. 1981), who used a home-built osmometer implanted into the ventricular myocardium of isolated porcine hearts to show that the intracellular osmolarity increased by 11% after 45 min of total global ischaemia at 37°C. In addition, wet- to dry-weight ratios, a measure of the total tissue water volume, increased by 16.5%.

In severely ischaemic myocardium, the swelling that will occur acutely is a function of the cell's ability to maintain volume, by supplying sufficient energy for the sarcolemmal ion pumps, and the amount of extracellular fluid available to move across the sarcolemma for swelling (Jennings et al. 1975). Little or no swelling has been found to occur in mildly ischaemic tissue (Jennings et al. 1975; Tranum-Jensen et al. 1981; Vandenberg et al. 1996), suggesting that ion pumps are still active. Consequently, it has been hypothesised that the degree of cell swelling corresponds to the severity of the ischaemia (Jennings et al. 1975; Powers et al. 1984; Sarkadi and Parker 1991). Hence cell volume changes during ischaemia could serve as an indicator for the degree of damage.

Myocardial cell volumes have been measured using various techniques. The most common is morphometric analysis using electron or light microscopy (Drewnowska and Baumgarten 1991; Powell et al. 1978; Roos 1986; Schwartz et al. 1973). However this method is prone to artefacts because of the effect of the fixation process on cell volume (Powell et al. 1978; Tranum-Jensen et al. 1981). Another method uses radiolabeled substances specific to the respective water spaces; for instance, tritiated water, $[^3H]$-H_2O, can be used as a total water marker and $[^{14}C]$-inulin as an extracellular marker. However, these methods result in the termination of the experiment, making time course studies

laborious and expensive. In addition, the use of radiolabeled substances assumes that the concentration of the marker in the extracellular space is the same as that in the buffer; but this assumption is not correct during total global ischaemia, as water may move across the cell membrane without the radiolabeled marker. Hence, residual buffer flow is required with methods using specific markers. It has been demonstrated by Clarke and colleagues (Clarke et al. 1994; Cross et al. 1995a), that the total, intra- and extracellular water space can be monitored continuously in isolated rat hearts during perfusion and low-flow ischaemia using phosphonate markers together with ^{31}P-NMR spectroscopy. These markers distribute selectively in the total and the extracellular space and resonate away from the metabolite peaks in ^{31}P-NMR spectra. Thus, the continuous and simultaneous measurement of cellular volumes and cardiac energetics is possible within a single spectrum and with good time resolution.

Therefore the aim of the work in this chapter was to monitor cell volumes in the whole perfused rat heart during perfusion and low-flow ischaemia, and to simultaneously measure changes in the concentrations of high-energy phosphates. It was to be determined whether the severity of the ischaemic insult altered the amount of cell swelling. Hence two extremes of ischaemia were studied; in the first group, hearts were perfused with substrates and in the second group without substrates. The intracellular and extracellular water spaces were quantified using ^{31}P-NMR spectroscopy and specific phosphonate space markers, with a standard positioned next to the heart to allow absolute quantification.

2.2. Theory: Determination of metabolite concentrations and water spaces

The use of an external reference, such as methylphosphonic acid (MPA), next to the perfused heart allows the absolute quantification of metabolite concentrations in the heart.

For instance, the intracellular ATP concentration is given by

$$[ATP](mM) = \frac{A_{ATP}}{A_{MPA}} \cdot \frac{MPA(\mu mol)}{V_{intra}(ml)} \qquad (2.1)$$

where A refers to the integrated area of the respective peak in the ^{31}P-NMR spectrum, $MPA\ (\mu mol)$ is the amount of MPA used as the external standard and $V_{intra}\ (ml)$ is the intracellular volume (Clarke et al. 1994).

The intracellular volume can be quantified using phosphonate markers in the perfusion buffer, which exhibit resonances in phosphorus spectra and are specific to the total and the extracellular water spaces. Such substances are dimethyl methylphosphonate (DMMP) for the total water space, and phenylphosphonic acid (PPA) for the extracellular water space (Barry et al. 1993; Clarke et al. 1990; Clarke et al. 1993; Kirk and Kuchel 1985). It has been shown that these markers are non-cytotoxic, resonate away from the endogenous high energy phosphates and the inorganic phosphate (P_i) peak and give clear, easily quantifiable ^{31}P-NMR signals (Nedelec et al. 1991; Saunders et al. 1990). The peak area of the resonance of the total water space marker, DMMP, is proportional to the amount of DMMP, which can be expressed as its concentration, *[DMMP]*, multiplied by the total water volume, $V_{total}\ (ml)$:

$$A_{DMMP} = k \cdot DMMP(\mu mol) = k \cdot [DMMP](\mu mol/ml) \cdot V_{total}(ml) \qquad (2.2)$$

Similarly, the area of the resonance of the external standard, MPA, is proportional to its amount:

$$A_{MPA} = k \cdot MPA(\mu mol) \tag{2.3}$$

Combining eqs 2.2 and 2.3, the total water volume can be calculated:

$$\frac{A_{MPA}}{A_{DMMP}} = \frac{MPA(\mu mol)}{[DMMP](\mu mol/ml) \cdot V_{total}(ml)} \tag{2.4}$$

Rearranging gives:

$$V_{total}(ml) = \frac{A_{DMMP}}{A_{MPA}} \cdot \frac{MPA(\mu mol)}{[DMMP](\mu mol/ml)} \tag{2.5}$$

Similarly the extracellular water volume can be obtained from the area of the PPA resonance, relative to the area of the MPA resonance:

$$V_{extra}(ml) = \frac{A_{PPA}}{A_{MPA}} \cdot \frac{MPA(\mu mol)}{[PPA](\mu mol/ml)} \tag{2.6}$$

The intracellular volume is then calculated as the difference between the total and the extracellular water volume:

$$V_{intra}(ml) = V_{total}(ml) - V_{extra}(ml) \tag{2.7}$$

In order to convert the intracellular volume into cytosolic volume, a correction factor of 1.3 needs to be applied to eq 2.1 (Gard et al. 1985), as 28-32% of a rat ventricular cardiomyocyte volume is occupied by mitochondria (Barth et al. 1992; Schaper et al.

1985). Furthermore, if partially saturated spectra are acquired, the peak areas must be corrected for saturation effects.

2.3. Methods

2.3.1. Heart perfusion

Hearts from male Wistar rats with a mean body weight of 390 ± 8 g (n = 8) were used to determine total, extracellular and intracellular water volumes and the cytosolic PCr, ATP and P_i concentrations. After intraperitoneal injection of sodium pentobarbitone (75 mg/kg body weight), hearts were rapidly excised through a median sternotomy and arrested in ice-cold Krebs-Henseleit buffer (for buffer composition, see Appendix A). Excess tissue was removed and the hearts cannulated, via the ascending aorta, for perfusion by the Langendorff method using Krebs-Henseleit buffer. During the experiment the hearts were arrested by switching the buffer line to Krebs-Henseleit buffer containing 20 mM KCl ('KCl-arrest') to match the conditions employed in later studies. The buffers were aerated with 95% O_2 : 5% CO_2 to give a working pH of 7.4 at 37°C. Hearts were perfused at a constant pressure of 100 mmHg, corresponding to the average systolic blood pressure of the rat *in vivo* (Baker et al. 1980). The pulmonary artery was cut to prevent venous pressure built-up, and intraventricular pressure development was prevented by insertion of an apical drain into the left ventricle. A cut was made across the left atrium to reveal the mitral valve. This enabled a water-filled latex balloon, attached via polyethylene tubing to a Gould pressure transducer, to be inserted into the left ventricle via the valve and inflated sufficiently to give an end diastolic pressure of 3-4 mmHg. Left ventricular pressure and heart rate were monitored using the Gould pressure transducer and recorder. Hearts were then inserted into a 20 mm NMR tube; coronary effluent was pumped from

the tube via an outlet above the heart, and the buffer was not recirculated.

2.3.2. Buffers

Two different buffers were used in order to produce two extremes of ischaemic damage; hearts were perfused without substrates (n = 4), or with 11 mM glucose and 1 mM Na-pyruvate (n = 4). The phosphonate markers, DMMP, a marker for the total water space, and PPA, a marker for the extracellular water space, were added to the buffer at concentrations of 10 mM and 5 mM, respectively. Phosphonate-free buffer was used to wash around the hearts, by pumping to the bottom of the NMR tube at 35 ml/min to reduce the contribution of the surrounding bath to about 20% of the DMMP resonance area and to prevent changes in coil loading during ischaemia (Nedelec et al. 1992). A sealed capillary containing 10 μmoles (20 μl of a 500 mM solution) MPA was positioned next to the heart as an external reference.

2.3.3. Hardware and pulse sequence

All experiments were performed using an 89 mm vertical bore 9.4T Oxford magnet (Oxford Instruments Ltd., Oxford, England), interfaced to a Bruker AM-400 spectrometer (Bruker Analytik GmbH, Karlsruhe, Germany). A 24 mm inner diameter Helmholtz coil (Morris Instruments Inc., Ontario, Canada) was used for RF transmission and signal detection. Hearts were contained entirely in the NMR-sensitive volume of the coil. A temperature control unit was attached to the probe connected to an air heating system, keeping the bore temperature at 37°C.

A ^{31}P pulse-collect sequence was used and 4k data points were acquired with a sweepwidth of 16 kHz to give a spectral range of 100 ppm, sufficient to observe peaks from the phosphonate markers and the high-energy phosphate compounds. Fully relaxed

spectra were acquired with a repetition time, TR, of 30 s, and 64 averages, giving a total acquisition time of 32 min. Partially saturated spectra were collected using a TR of 2.15 s, a flip angle of 60° and 104 averages, giving a total acquisition time of 4 min per spectrum.

2.3.4. Experimental protocol

After mounting on the perfusion cannula, hearts were allowed to equilibrate for 20 min, after which one fully relaxed and one partially saturated spectrum were acquired. Hearts were then motion-arrested by switching the buffer flow to the high-KCl Krebs-Henseleit reservoir. After 15 min equilibration, a second partially saturated spectrum was acquired, followed by a 32 min period of low-flow ischaemia at a flow rate of 0.5 ml/min (n = 8), during which eight partially saturated spectra were acquired.

2.3.5. Data processing and analysis

All FIDs were zero-filled once and a 20 Hz line broadening was applied prior to FT. Peaks were fitted to a Lorenzian line shape and the area obtained from peak integration using the NMR1 software package (NMRi, Syracuse, New York). Metabolite concentrations and water spaces were calculated using eq 2.1 and eqs 2.5-2.7.

2.4. Results

2.4.1. ^{31}P-NMR spectra during perfusion

Fig. 2.1 shows a typical fully relaxed ^{31}P-NMR spectrum acquired from a perfused rat heart in the absence of substrates. The right hand side of the spectrum, from 10 ppm to -36 ppm, consists of peaks from PCr, ATP and P_i. The left hand side consists of peaks

from the total water marker DMMP at 41.5 ppm, the MPA standard at 33.5 ppm and the extracellular water marker PPA at 14.8 ppm.

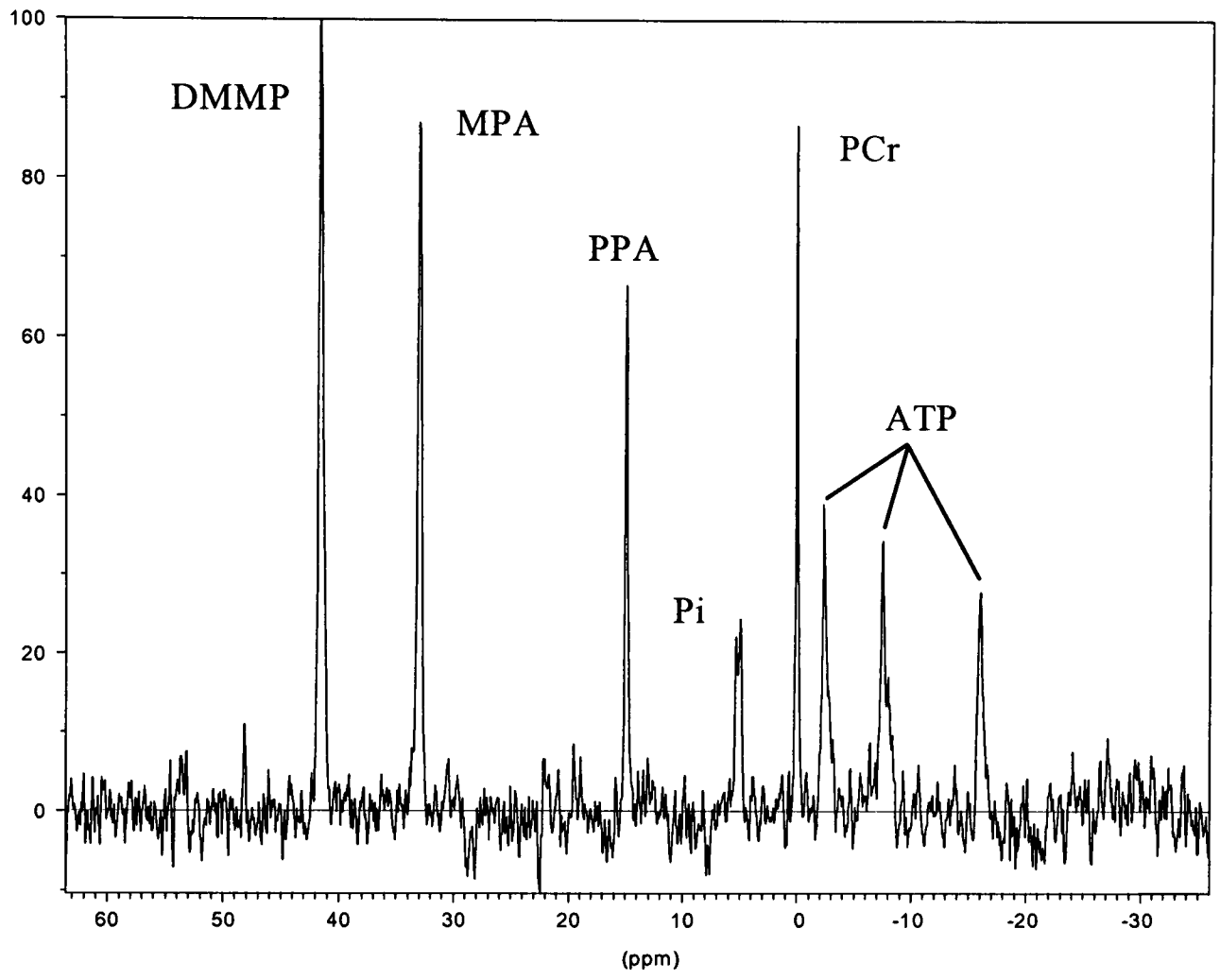

Fig. 2.1: Typical ^{31}P NMR spectrum of a perfused rat heart showing the peaks of the total water marker, DMMP, the extracellular water marker, PPA, the external standard, MPA, and the high energy phosphates, PCr and ATP, and P_i.

The changes in the cytosolic concentration of high energy phosphates and P_i during the ischaemic period in hearts perfused with or without substrates is shown in Fig. 2.2. The initial PCr and ATP concentrations were higher in hearts perfused with substrates. In both cases the PCr, ATP and P_i concentrations were constant during the first 4 min of ischaemia. Hearts perfused without substrates exhibited a continuous decline in the PCr

and ATP concentration throughout the ischaemic period with a concomitant increase in the P_i levels. By the end of the ischaemic period there was no detectable ATP or PCr, and P_i had reached a concentration of around 28 mM. In hearts perfused with substrates, the PCr concentration declined initially to 36% of control to remain constant after 16 min of low-flow ischaemia. The ATP concentration remained constant throughout ischaemia, and the decreased PCr was mirrored by the increased P_i levels.

(a)

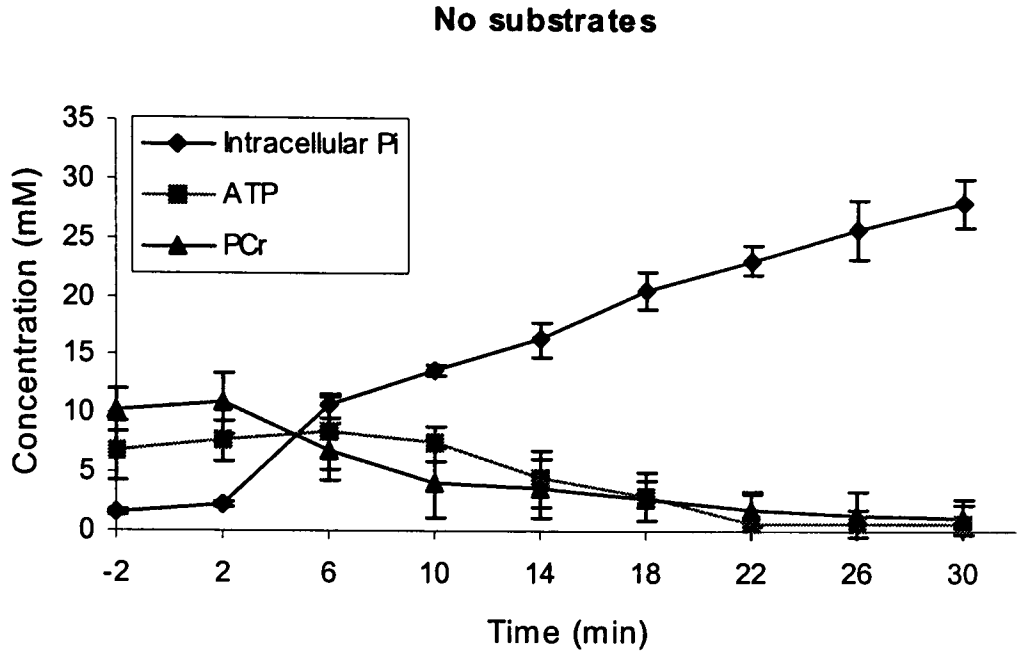

(b)

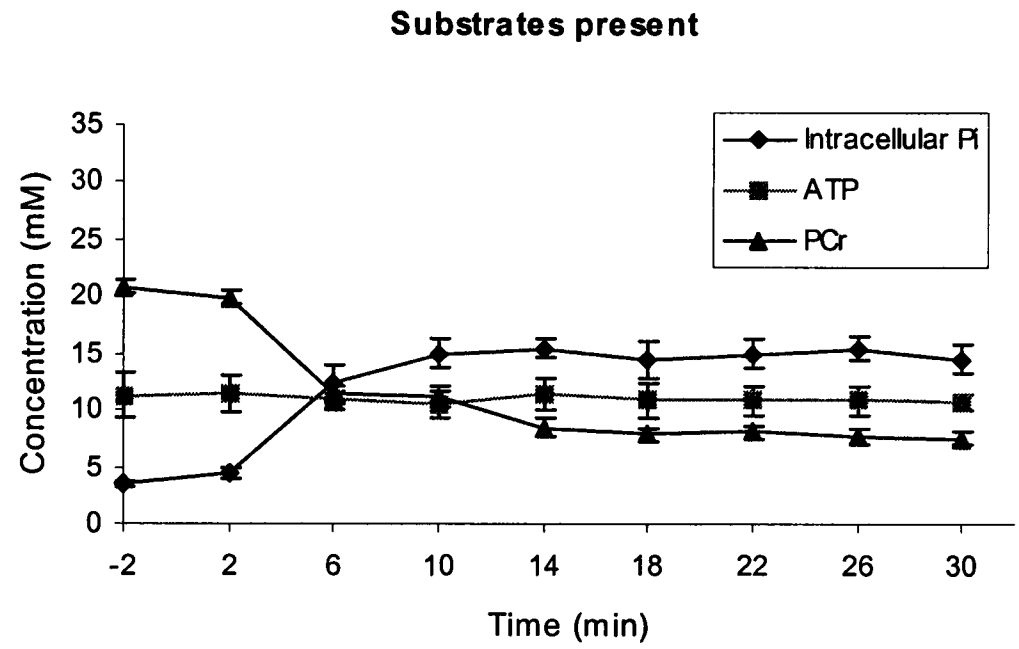

Fig. 2.2: Changes in ATP, PCr and P_i concentrations during 32 min of 0.5 ml/min low-flow ischaemia in the absence (a) and presence (b) of substrates. Note that the ATP and PCr concentration declined to zero in the absence of substrates, but remained constant when substrates were present.

(a)

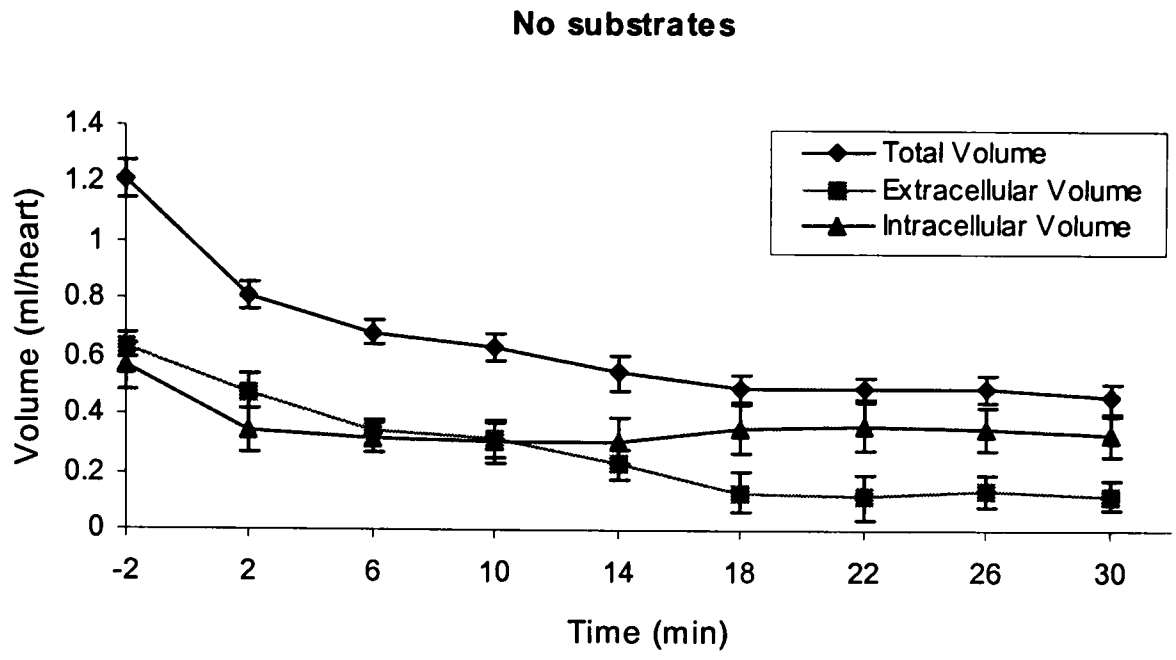

(b)

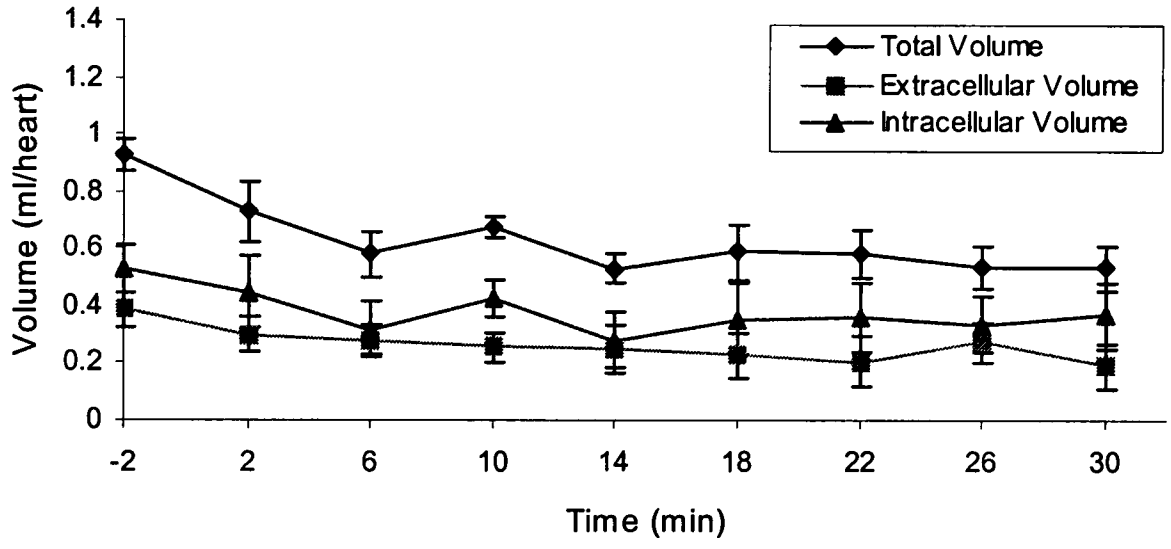

Fig. 2.3: Changes in the total, extracellular and intracellular water space volume during 0.5 ml/min low-flow ischaemia in hearts perfused without (a) and with substrates (b).

The severity of ischaemia made no difference to the changes in the water volumes, in that there was a continuous decrease of all water spaces to a constant value, reached after 6 min in hearts perfused with substrates, and after 18 min in substrate-free hearts (Fig. 2.3). In the latter group the decline was significantly more pronounced, due to different total and extracellular water volumes at the beginning of the ischaemic period (see Table 2.1).

Table 2.1: Comparison of total, extracellular and intracellular water volumes during control perfusion and at the end of the ischaemic period. The pre-ischaemic total and extracellular water volumes were different in hearts perfused with and without substrates, but their final values were identical. Data are means ± SEM from all hearts (n = 4). p-values were obtained by means of 1-way ANOVA.

		No substrates Volume (ml/heart)	Substrates present Volume (ml/heart)	Significance *p*
Total water	*Pre-ischaemia*	1.21 ± 0.06	0.93 ± 0.06	0.008
	End ischaemia	0.47 ± 0.05	0.54 ± 0.08	0.43
Extrac. water	*Pre-ischaemia*	0.64 ± 0.05	0.39 ± 0.06	0.008
	End ischaemia	0.13 ± 0.05	0.19 ± 0.08	0.44
Intrac. water	*Pre-ischaemia*	0.57 ± 0.08	0.53 ± 0.08	0.68
	End ischaemia	0.33 ± 0.07	0.37 ± 0.11	0.98

The total water volume decreased by 61%, from 1.21 ± 0.06 ml/heart during control to 0.47 ± 0.05 ml/heart at the end of ischaemia, significantly more (p = 0.005; 2-way ANOVA) than the decrease of 42% from 0.93 ± 0.06 ml/heart to 0.54 ± 0.08 ml/heart in substrate-perfused hearts. The final values were not significantly different (p = 0.43; 1-way ANOVA). Similarly the extracellular volume decreased by 80% from 0.64 ± 0.05 ml/heart to 0.13 ± 0.05 ml/heart in substrate-free hearts, significantly more (p = 0.02; 2-way ANOVA) compared to a decrease by 51% from 0.39 ± 0.06 ml/heart to 0.19 ± 0.08 ml/heart in substrate-perfused hearts. Again the final values were not significantly different. In both cases the volume of the intracellular space reached a constant value after less than 6 min, which was 0.33 ± 0.07 ml/heart in substrate-free hearts and 0.37 ± 0.11 ml/heart in substrate-perfused hearts (p = 0.98), respectively.

In substrate-free hearts contracture occurred after 12 min of low-flow ischaemia, shown by an increase in the diastolic pressure (Cross et al. 1995b) from 4 mmHg to around 60 mmHg within 8 min, after which it remained constant. Hearts perfused with substrates did not go into contracture (data not shown).

2.5. Discussion

2.5.1. High-energy phosphates

The changes in the high-energy phosphates in the absence of substrates was similar to that reported by others in the perfused low-flow ischaemic rat heart (Cross et al. 1995b). The PCr declined first, gradually followed by a drop in the ATP content, and eventual loss of both compounds after 32 min of low-flow ischaemia. There was a concomitant rise in the P_i, from the hydrolysis of PCr and ATP. The initial concentrations were somewhat lower than those reported in the literature (Cross et al. 1995b), because the hearts were perfused in the absence of substrates during the equilibration period.

The hearts perfused with the glucose-pyruvate containing buffer showed a high initial PCr concentration of 21 mM, which has been observed by others (From et al. 1986; From et al. 1990; Saks et al. 1994; Zweier and Jacobus 1987). Hearts suffered only minor ischaemic damage in the presence of substrates, indicated by the partial PCr loss and the constant ATP concentration during ischaemia. Also, hearts did not go into contracture. However, Cross and co-workers (Cross et al. 1995b) found a decrease in the ATP content of about 38% at the end of a 32 min period of low-flow ischaemia in the glucose-perfused rat heart. The difference can be explained with the protective effect of the KCl-arrest (Drewnowska et al. 1991; Flaherty et al. 1982; Nishiki et al. 1978). The effects of high KCl content in the perfusion buffer might also explain why the high-energy phosphate

levels remained at control levels during the first 2 min of ischaemia. Others have reported immediate changes in PCr after the onset of ischaemia, but their hearts were not KCl-arrested (Clarke et al. 1993; Cross et al. 1995b).

2.5.2. Water space volumes

The values detected for the intracellular water volumes during perfusion of around 0.55 ± 0.08 ml/heart, compare favourably with 0.56 ± 0.03 ml/heart and 0.52 ± 0.05 ml/heart previously determined (Clarke et al. 1994; Cross et al. 1995a). The total, extracellular and intracellular volume decreased upon the induction of low-flow ischaemia in hearts perfused with or without substrates. This was due to the loss of the perfusion pressure which caused the collapse of the vasculature and heart chambers with a consequent shrinking of the hearts (Clarke et al. 1993). During this period, water was lost from the heart by bulk flow and diffusion. Because it is in thermodynamic equilibrium across the sarcolemma, the intracellular volume also declined in conjunction with the decrease in the extracellular volume. After the initial perfusion pressure-related changes in cell volumes, there was no cell swelling detected in either group of hearts.

In the substrate-free hearts the initial total and extracellular water volumes were larger than in substrate-perfused hearts; this caused the volume decrease to be more pronounced compared to the substrate-perfused hearts. In substrate-free hearts the total and extracellular volumes remained constant after 20 min of low-flow ischaemia, which coincided with the end of the contracture. This agrees with experiments in which hearts perfused with glucose did not go into contracture during low-flow ischaemia, but glucose-free hearts did (Cross et al. 1995b). Furthermore, in that study the onset of contracture in substrate-free hearts started at around 6 min, which was 6 min earlier than in KCl-arrested substrate-free hearts, demonstrating the protective effect of KCl-arrest.

The total and extracellular water volumes altered with the perfusion conditions, such as temperature and perfusion pressure, and with the flow rate of the bath around the heart. This may explain why the initial total and extracellular water volumes were different in the two groups of hearts, as experiments were performed on different days. It might also explain why Clarke and co-workers, who used total global ischaemia, found a higher decrease (83%) of the extracellular water space, from 1.45 ml/g to 0.25 ml/g (Clarke et al. 1993). Conversely, Cross and colleagues found a smaller decrease of 36% in low-flow ischaemic glucose-perfused hearts, from 1.10 ml/heart to 0.70 ml/heart (Cross et al. 1995a).

2.5.3. Changes in high-energy phosphates and cell volumes

Hearts perfused with substrates had a mild degree of ischaemia with changes in cell volumes and metabolite levels present only during the first 8-12 min after the onset of ischaemia, suggesting that hearts reached a steady state. Hearts perfused in the absence of substrates showed a more severe degree of ischaemia, because of the onset of contracture and complete loss of high energy phosphates by the end of ischaemia. Also, changes in cell volumes were more prolonged in substrate-free hearts, reaching a constant level after about 20 min of low-flow ischaemia. However, the P_i concentration was still rising by the end of the ischaemic period due to continuation of ATP hydrolysis. This suggests that the volume changes cannot be used as an indicator for the severity of the ischaemic damage, as has been suggested by others (Jennings et al. 1975; Powers et al. 1984; Sarkadi and Parker 1991).

2.5.4. The sensitivity of the method

The extracellular space in this experiment consisted of interstitial, vascular and ventricular water, and of water in the balloon and the bath surrounding the heart. The total water space consisted of all the above plus the water in the intracellular space. The subtraction of the extracellular from the total water space yielded the intracellular space. Thus, errors in the measurement of both the total and the extracellular water volumes will translate into errors for the intracellular water volume. For instance, during perfusion the intracellular water content was 0.53 ± 0.08 ml/heart where the error was ± 15%. This figure can be considered to represent the sensitivity of the method. However, as the severity of the ischaemia was mild due to the protective effects of KCl-arrest with residual flow, cell swelling was probably absent.

Although the phosphonate marker method provided good time resolution it cannot be applied in total global ischaemia (see section 2.1.), and would not be sensitive to small (< ~ 15%) cell volume changes. These limitations were circumvented in Chapter 7, where the average ventricular cardiomyocyte diameter was measured during perfusion and total global ischaemia. The method was based on the measurement of the apparent diffusion coefficient of the endogenous taurine molecules at different diffusion times.

2.6. Conclusion

Changes in high-energy phosphate compound concentrations, and the degree of ischaemic injury, were dependent on the availability of substrates in the perfusion buffer. Glucose and pyruvate were protective during low-flow ischaemia, as was KCl-arrest. The intracellular water volume, measured during low-flow ischaemia, did not change during either a mild or a more severe ischaemic insult. This was either because of a lack of

sensitivity in the method, or because the ischaemia was not severe enough to cause cell swelling. Hearts shrank at the start of ischaemia due to the drop in perfusion pressure and the decreased oedema. The intracellular water volume agreed well with current literature figures.

Chapter 3

Method development for the measurement of diffusion coefficients and tensors

Abstract

The aim of the work in this chapter was to ensure that the NMR hardware and software would allow diffusion measurements on perfused rat hearts in later work. Experiments included: (a) The measurement of the water diffusion coefficient using a pulsed-gradient spin-echo (PGSE) pulse sequence, giving a value of $(1.93 \pm 0.01) \times 10^{-3}$ mm^2/s at 18°C, in good agreement with published values. (b) The development of a slice-selective STEAM pulse sequence to measure the water and metabolite diffusion coefficients in solution. It was found that the new sequence provided good signal-to-noise ratio and water suppression in ^1H metabolite spectra. Typical measurement times to obtain the diffusion coefficient of metabolites, such as physiologic concentrations of creatine and taurine, were around 4 min. The measured water diffusion coefficient of $(1.94 \pm 0.01) \times 10^{-3}$ mm^2/s was identical to that obtained with the PGSE sequence, whereas metabolite diffusion coefficients of $0.74\text{-}0.93 \times 10^{-3}$ mm^2/s were comparable with published values. (c) The modification of the slice-selective STEAM sequence to allow measurement of the water and the metabolite diffusion tensor. After correcting for temperature differences, the diagonal elements of the water and the metabolite diffusion tensors were found to be identical to the water diffusion coefficients obtained with the PGSE sequence, and to the metabolite diffusion coefficients obtained with the scalar STEAM sequence, respectively. It was concluded that the NMR hardware and software performed adequately for the measurement of diffusion coefficients and tensors in the perfused rat heart.

3.1. Introduction

In order for an NMR pulse sequence to be used to measure diffusion in the whole perfused rat heart, it should allow incorporation of short (tens of ms) and long (hundreds of ms to seconds) diffusion times to study the immediate environment of the diffusing substance and restricted diffusion caused by cell boundaries. Clearly, a sequence in which the magnetisation is in the transverse plane throughout the experiment is not a good choice, because of substantial signal loss due to T_2 relaxation. Instead, a STEAM (*st*imulated *e*cho *a*cquisition *m*ode) sequence can be used in which the magnetisation is stored in the longitudinal plane during the diffusion period, such that it relaxes with T_1 rather than T_2 (Frahm et al. 1985; Haase et al. 1986; Merboldt et al. 1985). As $T_2 << T_1$ in tissue, the STEAM pulse sequence should produce sufficient signal-to-noise (SNR), even at long diffusion times. Another advantage of the STEAM sequence is that it can localise to a predefined volume, such as the ventricles in the perfused rat heart, with the exclusion of the atria (Opie 1998; Schaper et al. 1985). As any movement would introduce large errors when determining the ADC, beating hearts can be motion-arrested by perfusing them with buffer containing a high KCl concentration (Fieno and Judd 1998; Hsu et al. 1998; Scollan et al. 1998).

The aim of the work in this chapter was to develop and test a slice-selective STEAM pulse sequence to measure diffusion coefficients and tensors in water or metabolite solutions for later studies of the mobility of small molecules in the cytoplasm of the isolated rat heart (see Chapters 4-8).

3.2. General methods

All experiments described in the remainder of this thesis used a vertical 400 MHz Oxford magnet (Oxford Instruments Ltd., Oxford, England) with a room-temperature bore of 89 mm, interfaced to a Varian Unity INOVA spectrometer (Varian Ltd., Palo Alto, CA, USA). An actively-shielded gradient set with an inner diameter of 40 mm (type GCS 73/40/50G, Fraunhofer-Institute Biomedical Engineering [FhG IBMT], St. Ingbert, Germany), was connected to three gradient amplifiers (type L700, Highland Technology Inc., San Francisco, CA, USA). The complete gradient system was capable of delivering 20 G/cm on all three axes. A homebuilt temperature-controlled probe was used in all experiments; a 20 mm outer diameter NMR tube fitted snugly into an etched double-sided Helmholtz coil, which was tuned to 400 MHz. The magnet bore temperature was measured in the beginning and the end of the experiment.

Statistical significance was tested using analysis of variance (ANOVA) tests, and a value of $p < 0.05$ was considered significant. Diffusion coefficients were obtained from best fits of semi-logarithmic signal attenuation as a function of the b-value. Preliminary experiments showed that RF stability was well within the manufacturer's specification of < 1% amplitude variation over 20 ^{1}H-spectra (Varian 1995). The eddy current behaviour was characterised and a 1 ms delay was found to be sufficient to achieve complete recovery for each of the gradient axes (data not shown).

3.3. Scalar PGSE experiment on water

3.3.1. Introduction

The aim of this experiment was to check the gradient calibration by measuring the diffusion coefficient of water along the three gradient axes, using a slice-selective PGSE sequence (Chapter 1).

3.3.2. Methods

A 20 mm NMR tube was filled with distilled water and inserted into the NMR probe. A slice-selective PGSE sequence was used with the slice-selection gradient applied in the z-direction and immediately refocused to minimise any additional diffusion effects. The selected slice was 3 mm thick, and a 4 ms 5-lobed sinc-shaped RF pulse was used for both the 90° and 180° RF pulses. Typical shim values for the selected slice were around 5-8 Hz at full-width half-maximum (fwhm) of the water peak. The repetition time, TR, was set to 3 s, the echo time, TE, was 110 ms, sweepwidth 4 kHz, and 8k data points were sampled. Diffusion coefficients were measured separately in all three directions; diffusion gradients were arrayed from 1 G/cm to 16 G/cm in 16 steps, yielding *b*-values from 9-2385 s/mm^2 in x- and y-direction, and 9-2376 s/mm^2 in z-direction. The slight difference in *b*-values was due to the presence of the slice-selection gradient and refocusing gradient along the z-axis. The duration of the diffusion gradients, δ, was 5 ms with a separation, Δ, of 50 ms. These parameters were chosen in order to match the slice-selective STEAM sequence (see later).

Each experiment was repeated five times, with eight scans averaged for each gradient strength. The *b*-values were calculated according to eq 1.14, using the Mathematica programme (Wolfram Research Inc., Illinois, USA; see Appendix B). Free induction

decays (FIDs) were line-broadened by 2 Hz and zero-filled once prior to Fourier Transformation (FT).

3.3.3. Results

The signal attenuation of the water peak in ^{1}H spectra with increasing gradient strength at 18°C is shown in Fig. 3.1.

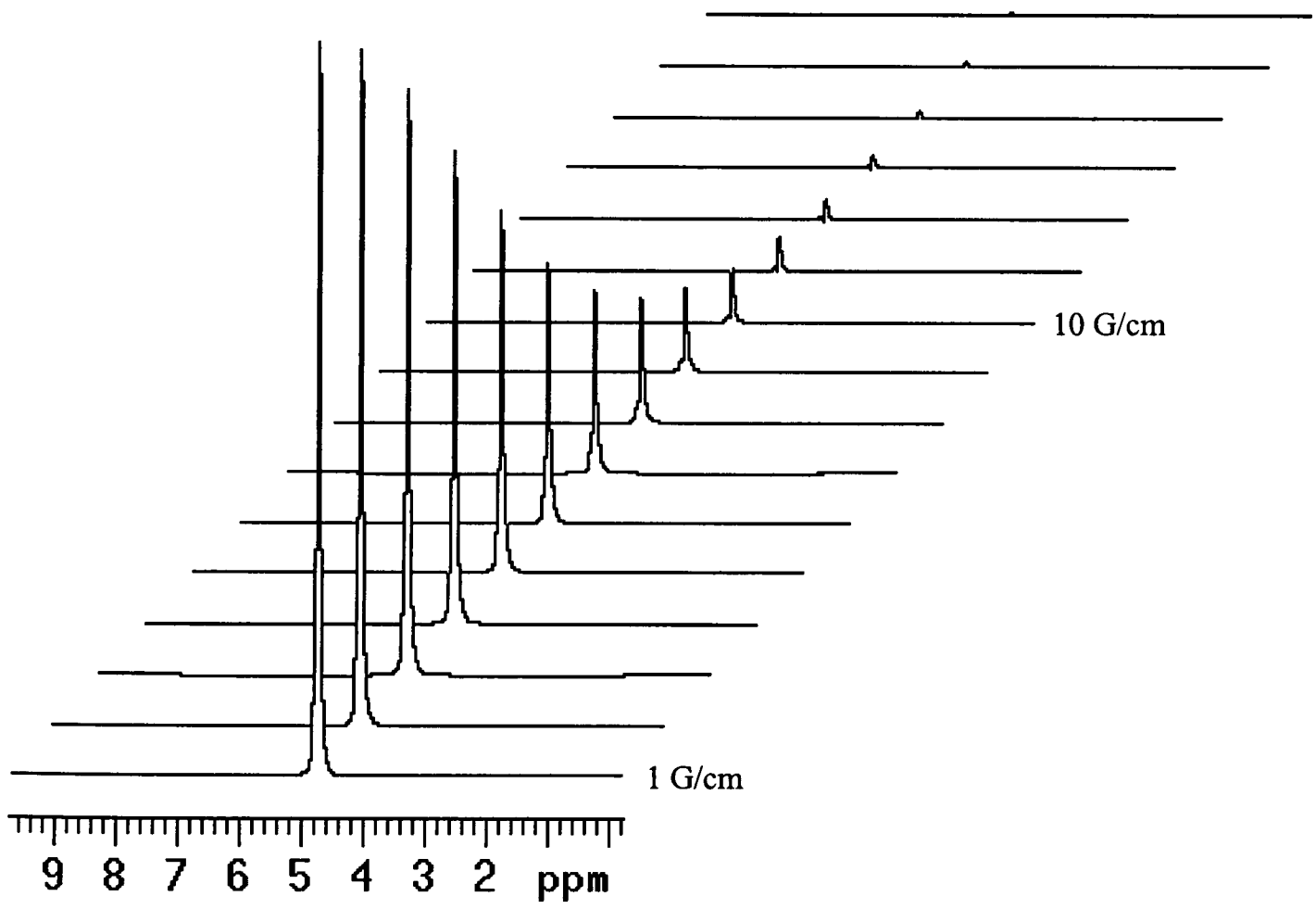

Fig. 3.1: ^{1}H spectra of water showing signal attenuation as a function of the gradient strength in x-direction.

The natural logarithm of the signal was plotted as a function of the *b*-value, and the slope of the best fit through the data points gave the diffusion coefficient (Fig. 3.2).

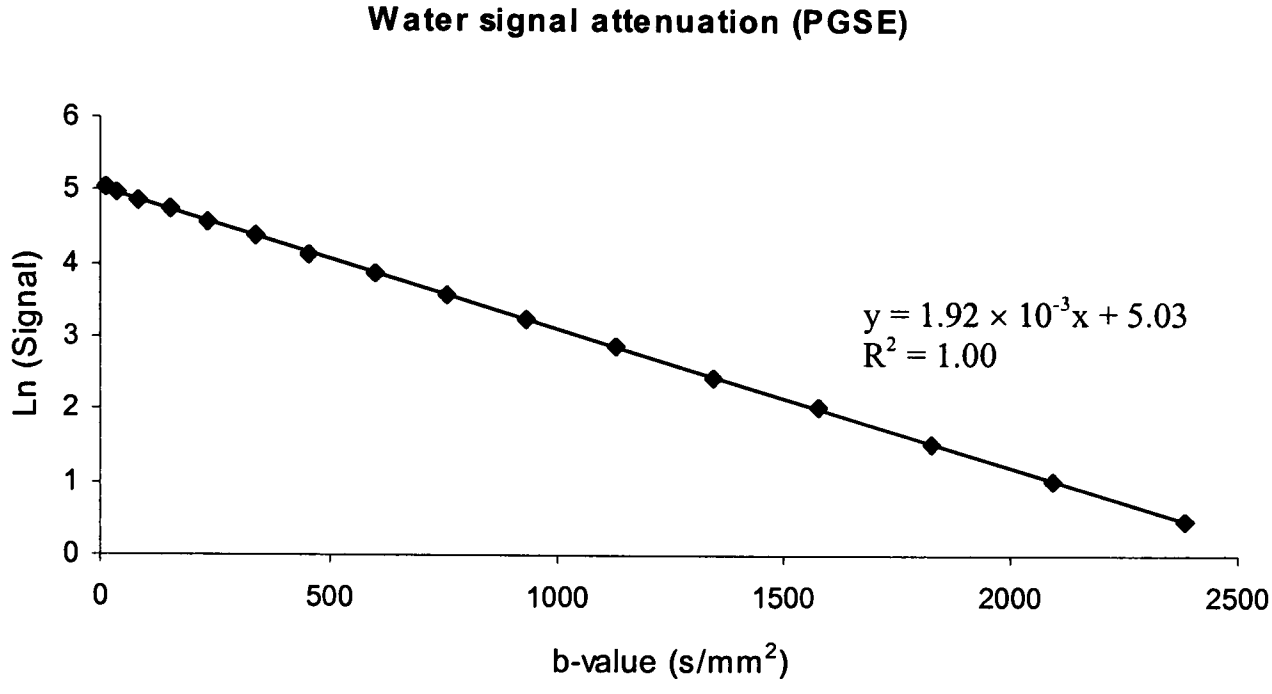

Fig. 3.2: Semi-logarithmic plot of the water signal intensity as a function of the b-value; the raw data were taken from Fig. 3.1.

Table 3.1 lists the values of the water diffusion coefficient in the three directions. All fits had $R^2 > 0.998$ and the values listed were not significantly different from each other.

Table 3.1: Water diffusion coefficients along the three gradient axes acquired at 18°C. Data are means ± SEMs (n = 5).

	D_x	D_y	D_z
Water diffusion coefficient (10^{-3} mm^2/s)	1.93 ± 0.01	1.92 ± 0.01	1.93 ± 0.01

3.3.4. Discussion

The water diffusion coefficients were 1.93×10^{-3} mm^2/s and identical in the three directions with an error of ± 0.5%, which compares favourably with other studies reporting errors of ± 1-2% (Callaghan et al. 1980; Harris et al. 1978). In addition, the measured diffusion coefficients agreed with the interpolated literature value for the water diffusion coefficient at 18.0°C, which was 1.93×10^{-3} mm^2/s (Mills 1973). Hence it can be concluded that the gradient calibration was accurate.

3.4. Diffusion measurements in solutions with a slice-selective STEAM sequence

3.4.1. Introduction

The aim of this experiment was to develop a slice-selective STEAM pulse sequence to be used to determine diffusion coefficients of water and ^{1}H-detectable metabolites in the perfused rat heart (Chapters 4-8). Water suppression schemes were incorporated into the sequence and the sensitivity in the detection of metabolites at physiologic concentrations was evaluated. The diffusion coefficients of water, creatine, taurine and choline were measured in solution.

3.4.2. Theory: The slice-selective STEAM pulse sequence

The simplest way to measure diffusion by NMR is to use a PGSE sequence in which two gradient pulses, separated by the time Δ, are incorporated into a basic spin-echo sequence and the signal attenuation measured as a function of the *b*-value. This basic concept can

be applied to many NMR pulse sequences in imaging and spectroscopy. A well-known example is the diffusion-weighted variant of a spin-echo imaging sequence (MacFall et al. 1991; Neeman et al. 1990). The diffusion-weighted variant of a slice-selective STEAM sequence was used in almost all of the experiments in this thesis (Fig. 3.3).

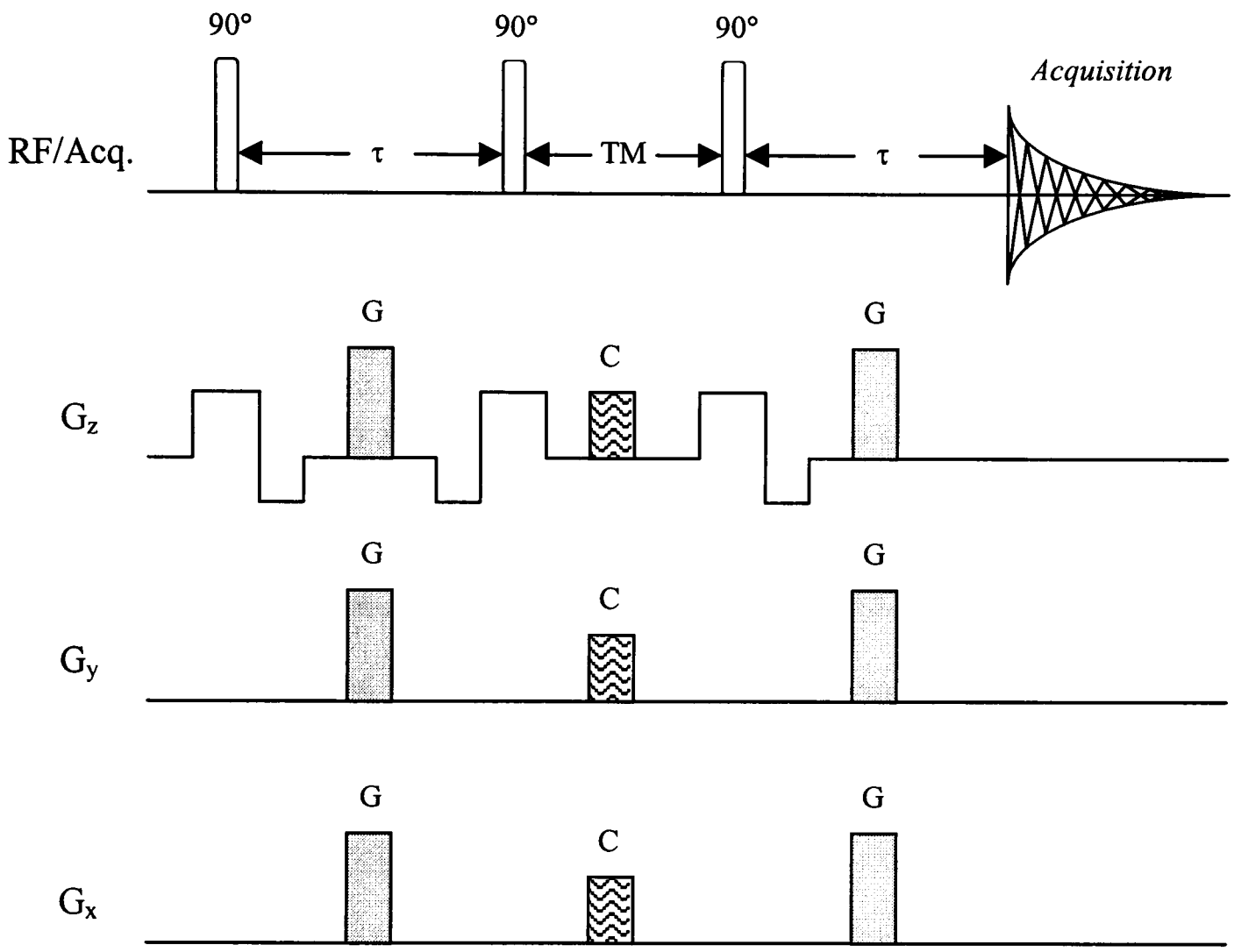

Fig. 3.3: Slice-selective STEAM pulse sequence. The diffusion gradients (G) were applied along a single gradient direction. Crusher gradients (C) during the TM period destroyed unwanted coherences. Note the immediate re- and prefocusing of the slice-selection gradients along the z-direction (timing and gradient amplitudes not to scale).

This sequence consisted of three 1 ms sinc-RF pulses (bandwidth, 6000 Hz), the slice selection and refocusing gradients, and the necessary spoiler gradients during the TM and the two τ periods. During the latter intervals, these gradients also acted as diffusion gradients (similar to the PGSE sequence) and were applied in one direction only in order to minimise unwanted diffusion weighting and cross terms (Basser et al. 1994a; Hsu and Mori 1995; Mattiello et al. 1994). During the TM interval, crusher gradients (2 ms long, -3 G/cm) were applied in all three directions simultaneously to destroy unwanted coherences.

Because all three slice-selection gradients were applied along the z-direction, the pulse sequence localised to an axial slice. The main reason for this modification from the standard voxel-selective STEAM spectroscopy sequence was to increase the SNR per unit time. STEAM sequences are particularly useful when measuring ADCs at long diffusion times in tissues, in which the T_1 relaxation time is usually much longer than the T_2 relaxation time (Bottomley et al. 1984). In a PGSE sequence, choosing a long diffusion time leads to a prolonged echo time and hence considerable signal loss due to increased T_2 relaxation. However, in a STEAM sequence the diffusion time can be increased by lengthening the TM interval (whilst keeping the echo time constant), during which magnetisation is stored longitudinally and therefore relaxes with T_1 rather than T_2, leading to less relaxation-mediated signal loss.

In order to make the slice-selective STEAM sequence insensitive to gradient cross terms, it was designed in such a way as to minimise the diffusion-mediated signal loss from any slice-selection and refocusing gradients. This was achieved by immediately refocusing or prefocusing the slice-selection gradients such that only the diffusion gradients during the two τ periods would introduce significant diffusion-mediated signal loss (Le Bihan 1995). It was ensured that the diffusion gradients were of sufficient strength (0.5 G/cm) to satisfy

the STEAM condition of completely dephased magnetisation before the application of the second 90° RF pulse (Hahn 1950). In addition, care was taken to ensure that the crusher gradients during the TM period did not refocus the diffusion gradients applied during the τ period.

3.4.3. Methods

3.4.3.1. General

The samples used in this experiment were (a) double distilled water, and (b) a solution containing physiologic concentrations (in mM) of taurine (30), creatine (15), choline (5), glutamate (5), glutamine (5) and aspartate (9) in a 20 mm NMR tube (Sato et al. 1995). The slice-selective STEAM sequence (Fig. 3.3) was used to measure (a), the water diffusion coefficient along the three gradient axes and (b), the metabolite diffusion coefficient along the x-axis. The following parameters were used in both experiments: TR of 3 s, TE of 20 ms, TM of 40 ms, sweepwidth 4 kHz, 8k data points. Diffusion gradients were 5 ms long and separated by Δ = TM + 10 ms = 50 ms. The *b*-values were calculated using eq 1.14, which was computed using the Mathematica programme (see Appendix B). FIDs were zero-filled once and line-broadened by 2 Hz. Typical water linewidths were in the order of 6 Hz at full-width half-maximum (fwhm). Each diffusion coefficient measurement was repeated five times.

3.4.3.2. Non water-suppressed STEAM

The diffusion coefficient of distilled water was measured separately in three gradient directions with the strength of the diffusion gradient arrayed in 16 steps from 1 G/cm to 16 G/cm, corresponding to a *b*-value range from 9-2384 s/mm^2 (x- and y-direction) and 9-

2375 s/mm^2 (z-direction). Eight scans were averaged at each gradient strength.

3.4.3.3. Water-suppressed STEAM

The slice-selective STEAM sequence was modified to include water suppression using a WEFT inversion recovery scheme ('*w*ater-*e*liminated *F*ourier *T*ransformation'; (Patt and Sykes 1972)) prior to the sequence, and a three-pulse CHESS (*che*mical *s*hift *s*elective; (Matthaei et al. 1986)) scheme during the TM period. The WEFT inversion pulse was a 60 ms adiabatic 180° sech-shaped RF pulse whereas the CHESS pattern consisted of three 8 ms Gaussian pulses, each followed by a pair of spoiler gradients, applied along two gradient axes. The length of the water suppression pulses was chosen so as to obtain a suppression width of 200 Hz (≡ 0.5 ppm) at fwhm at the water peak frequency of 4.77 ppm. This delivered adequate water suppression and did not reduce metabolite peaks close to the water resonance, such as creatine at 3.95 ppm.

The TM period had a minimum duration of 40 ms because it had to accommodate spoiler gradients for unwanted coherences as well as the three-pulse CHESS pattern. In addition, the minimum repetition time increased to 2.1 s because of the WEFT suppression scheme in the beginning of the sequence. After adjusting the 90° STEAM RF pulses and shimming on the slice, the chemical shift offset artefact was accounted for and the slice moved to the creatine position at 3.03 ppm, upfield by 1.75 ppm (≡ 700 Hz). Afterwards the inversion time for the WEFT sequence (typically around 1 s at a TR of 3 s) and the 90° RF pulse gain for the CHESS pattern were adjusted individually to give optimum water suppression.

Sixteen averages were acquired for each scan. In order to match experimental conditions to those employed later in the perfused heart, diffusion gradients were applied in the x-direction, and only five *b*-values were used, ranging from 27 s/mm^2 to 1350 s/mm^2.

Metabolite diffusion coefficients could then be sampled with a time resolution of 4 min. After 2 Hz line-broadening and single zero-filling of FIDs, spectral peak heights of creatine, taurine, and choline were measured.

3.4.4. Results

3.4.4.1. Non water-suppressed STEAM

The magnet bore temperature was 18.0°C in the beginning, and 18.2°C at the end of the experiment; this did not cause the individual diffusion coefficients to increase over time. The increase from 18.0°C to 18.2°C would have accounted for a change of less than 0.01 mm^2/s (Mills 1973), so it can be assumed that the 0.2°C change in the magnet bore temperature did not affect the water diffusion coefficient.

A typical set of water spectra acquired at increasing *b*-values is shown in Fig. 3.4. The diffusion gradient was applied in the x-direction.

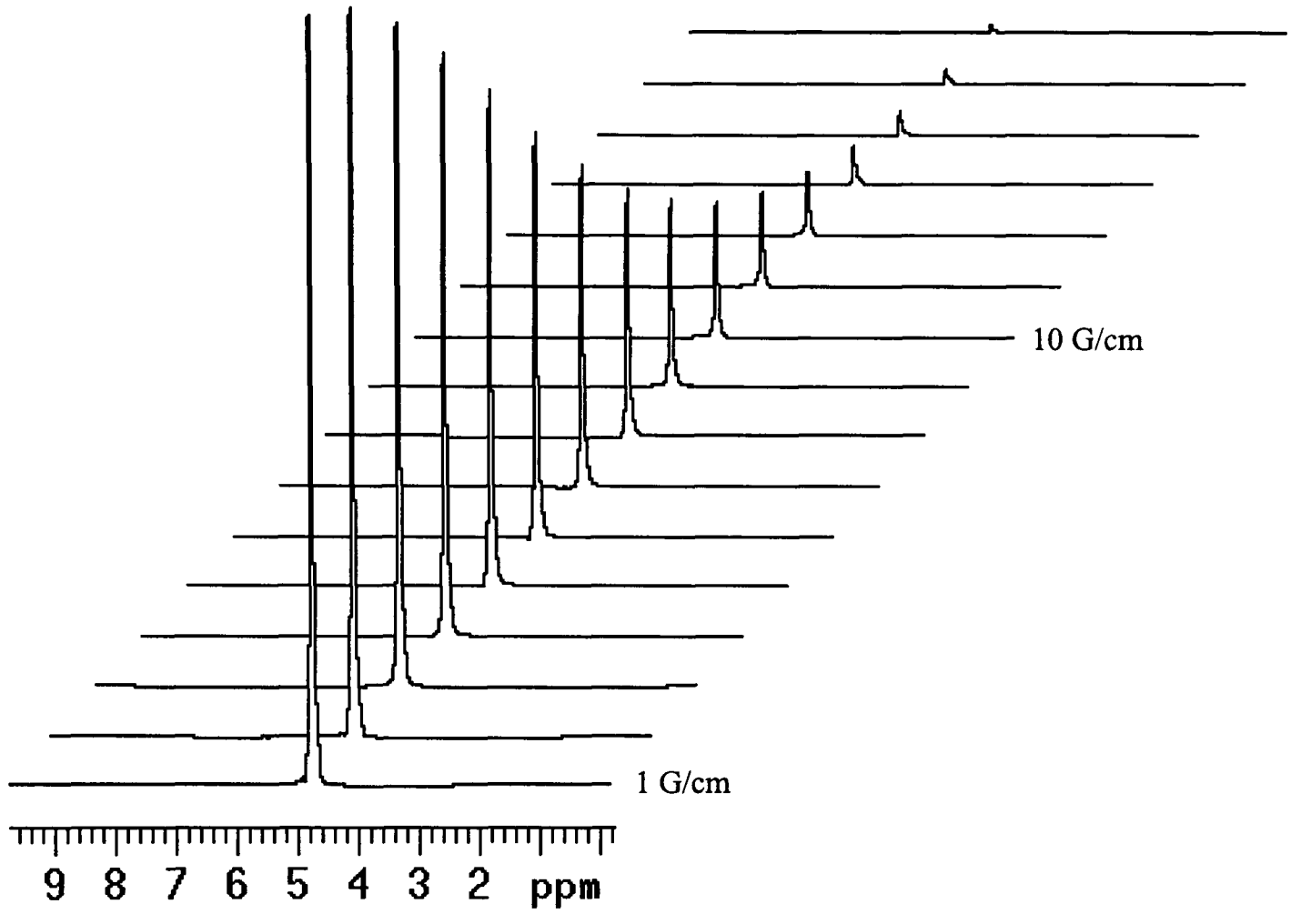

Fig. 3.4: Representative stacked plot of the water peak with increasing b-values from 9-2384 s/mm^2. The diffusion gradient was applied in the x-direction.

Fig. 3.5 displays the corresponding semi-logarithmic signal amplitude plotted as a function of the *b*-value.

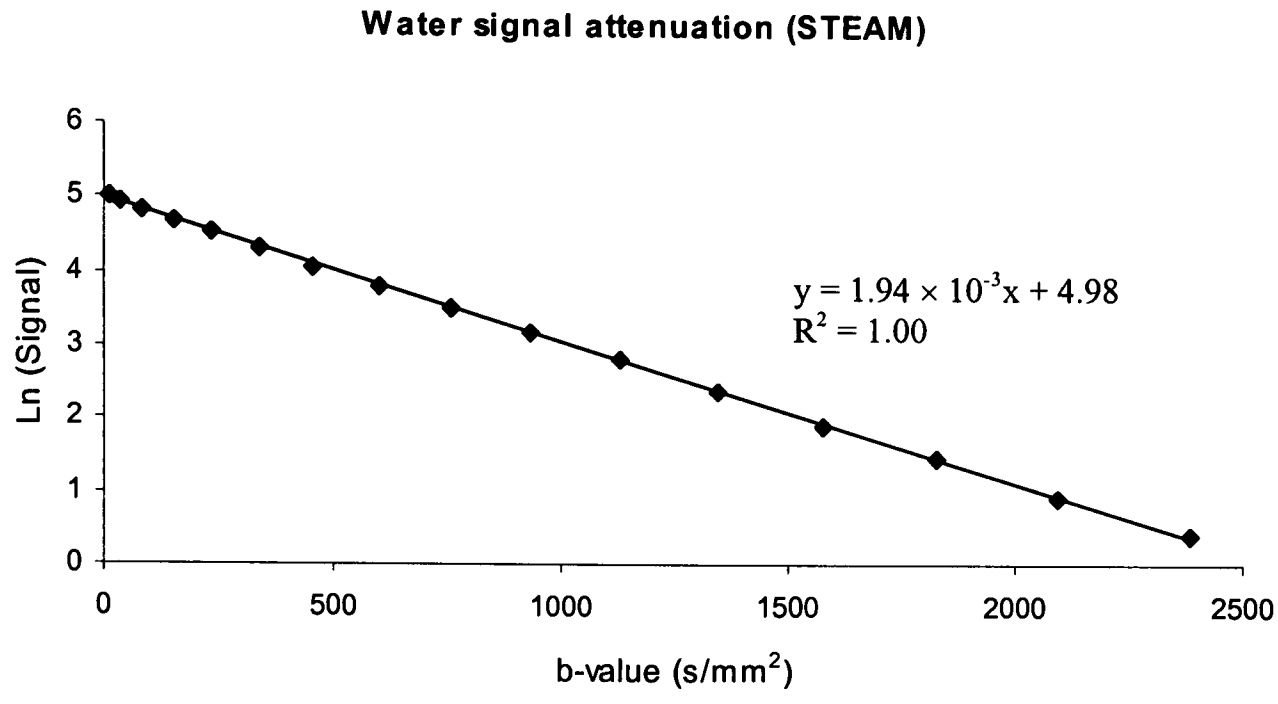

Fig. 3.5: Semi-logarithmic plot of the signal amplitude as a function of the applied b-value. In general, fits gave $R^2 > 0.998$. The data were taken from Fig. 3.4.

The water diffusion coefficients in the three gradient directions are listed in Table 3.2.

Table 3.2: Water diffusion coefficients acquired at 18.1°C in x-, y-, and z-direction using the STEAM pulse sequence. Data are means ± SEMs (n = 5).

	D_x	D_y	D_z
Water diffusion coefficient (10^{-3} mm^2/s)	1.93 ± 0.00	1.94 ± 0.01	1.94 ± 0.01

None of the values were significantly different, nor were they different from those obtained in the PGSE experiment (Table 3.1).

3.4.4.2. Water-suppressed STEAM

The temperature remained constant throughout the experiment at 21.5°C. A typical ^{1}H spectrum acquired from the metabolite solution is shown in Fig. 3.6. The area from 2.6-5 ppm contains peaks from creatine, choline, taurine, glutamine/glutamate (Gln/Glu) and aspartate. The water resonance was well suppressed.

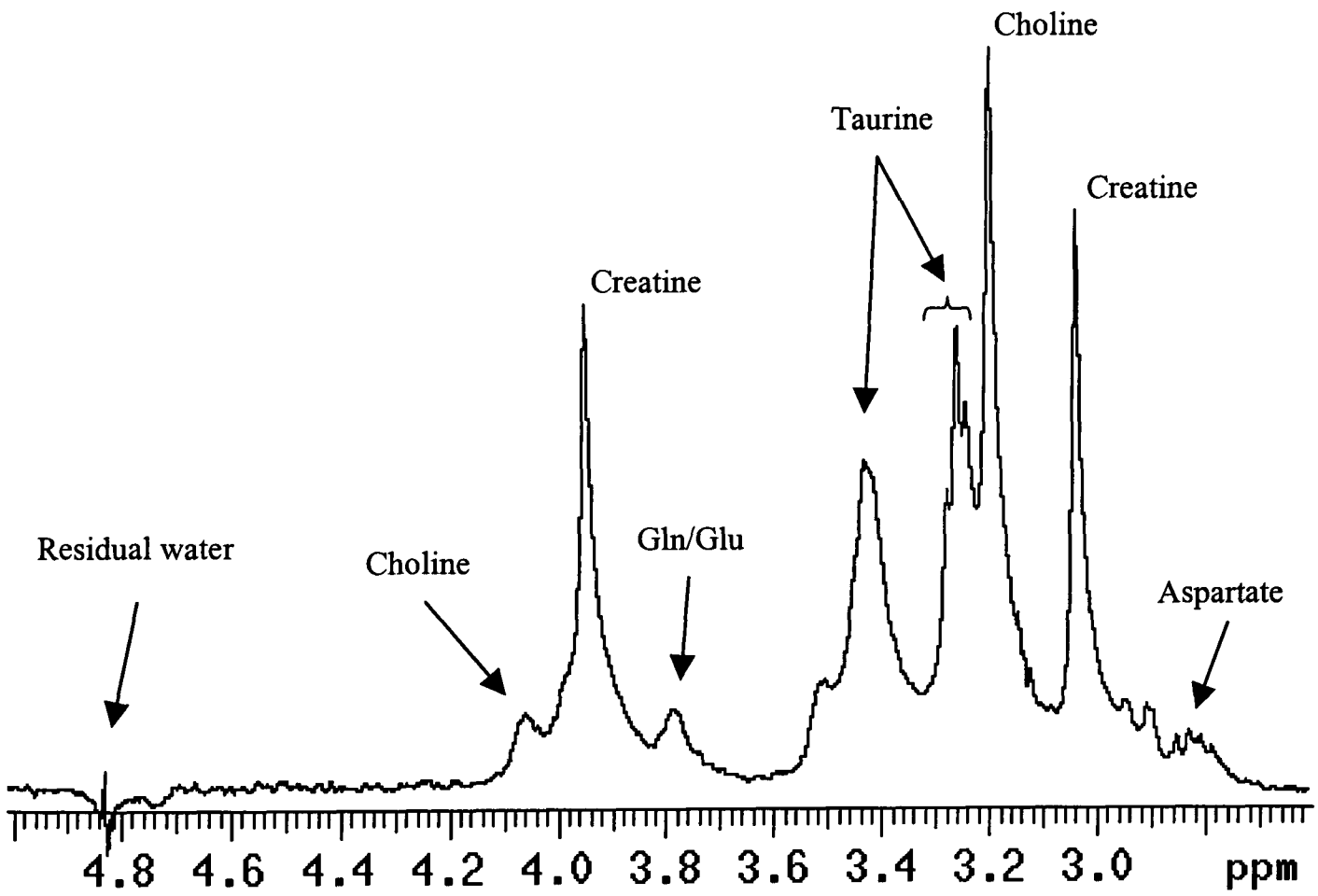

Fig. 3.6: Typical ^{1}H spectrum of a solution of creatine, choline, taurine, glutamine, glutamate and aspartate acquired using the water-suppressed slice-selective STEAM sequence. The water was well suppressed and metabolites in physiologic concentrations were easily detected within 0.8 min. Gln/Glu: glutamine and glutamate.

Typical semi-logarithmic plots of signal amplitude *vs.* *b*-value for the two creatine peaks (3.95 ppm and 3.03 ppm), the two taurine peaks (3.43 ppm and 3.26 ppm) and the choline

peak (3.20 ppm) are shown in Fig. 3.7. In general, fits gave $R^2 > 0.995$.

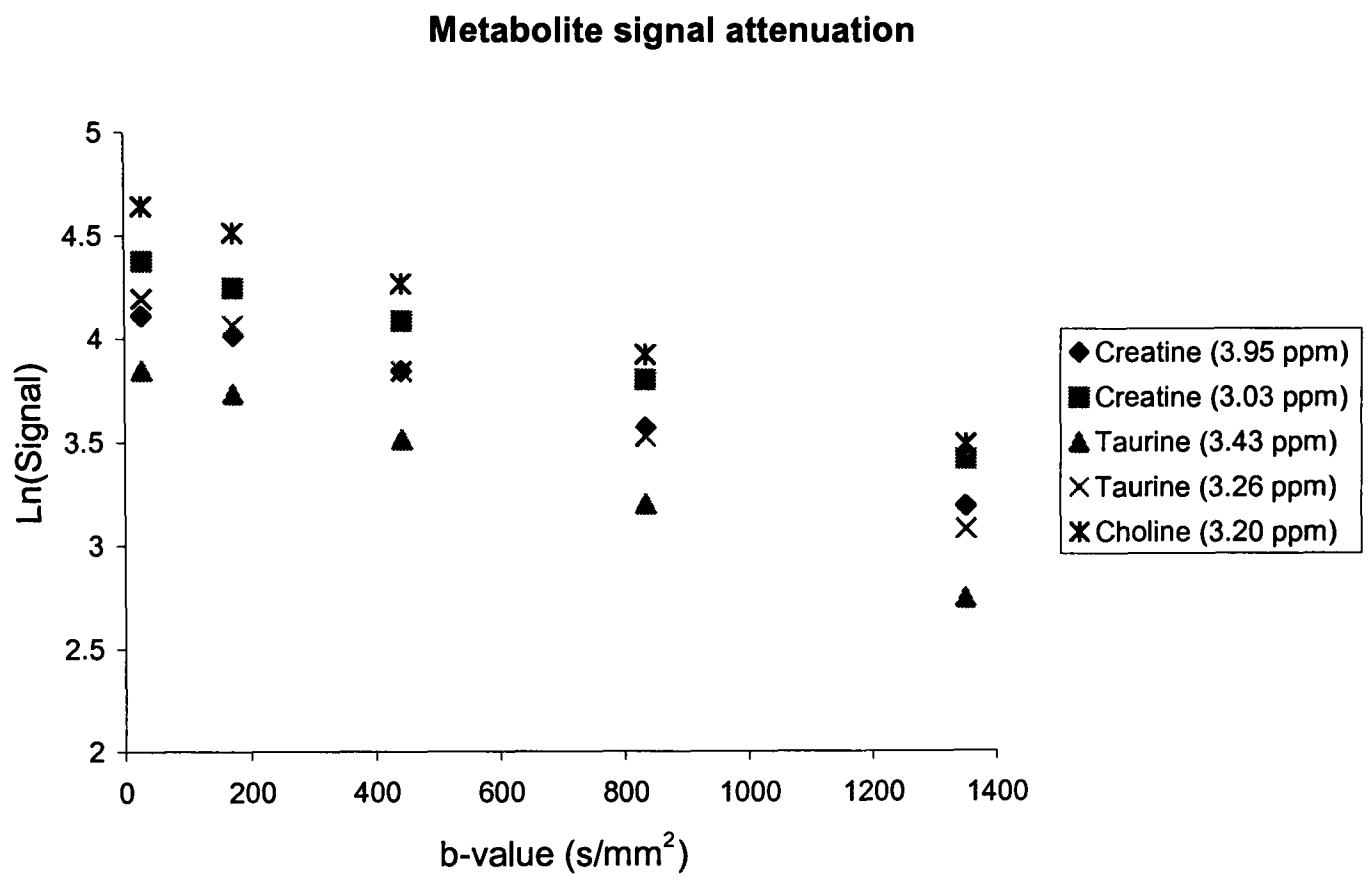

Fig. 3.7: Semi-logarithmic plot of the signal intensities of the detected metabolite peaks as a function of the b-value. Linear fits were not shown for clarity.

The diffusion coefficient of creatine was $(0.74 \pm 0.02) \times 10^{-3}$ mm^2/s, significantly lower than that of taurine at $(0.89 \pm 0.04) \times 10^{-3}$ mm^2/s and choline at $(0.93 \pm 0.01) \times 10^{-3}$ mm^2/s (Table 3.3).

Table 3.3: Measured diffusion coefficients for the two creatine peaks, the two taurine peaks and the choline peak. The diffusion coefficient of creatine was significantly different from taurine and choline (: $p < 0.05$).*

	Chemical shift (ppm)	Diffusion coefficient (10^{-3} mm^2/s)
Creatine	3.95	$0.74 \pm 0.01^*$
Creatine	3.03	$0.74 \pm 0.02^*$
Taurine	3.43	0.88 ± 0.01
Taurine	3.26	0.89 ± 0.01
Choline	3.20	0.93 ± 0.01

3.4.5. Discussion

The values obtained for the water diffusion coefficients compare favourably with published values (Mills 1973), and those obtained using the PGSE sequence, with small errors of ± 0.3%. Therefore it was concluded that the slice-selective STEAM sequence was properly designed to measure the water diffusion coefficient.

Diffusion coefficients calculated for the two creatine peaks, the two taurine peaks and the choline peak agreed well with published values (van der Toorn et al. 1996a). The diffusion coefficient for creatine was 16% lower than for taurine and 20% lower than for choline, which may be attributed to the larger hydrodynamic radius of creatine. Hence it can be concluded that the water-suppressed STEAM sequence allowed the reproducible measurement of diffusion coefficients of metabolites at physiologic concentrations. This experiment was later to reveal whether the chosen timing parameters of the slice-selective STEAM sequence were appropriate to obtain spectra with good SNR, and whether five *b*-

values were sufficient to quantify the diffusion of intracellular metabolites in the perfused rat heart.

3.5. Water and metabolite diffusion tensors of solutions

3.5.1. Introduction

As heart tissue has a variety of fibre orientations (Edelman et al. 1994; Garrido et al. 1994; Reese et al. 1995), the ADC might be anisotropic, and the diffusion tensor rather than the scalar diffusion coefficient should be determined (see Chapter 1). The aim of this preliminary experiment was to measure the diffusion tensor of water and metabolites in solutions, using the slice-selective STEAM sequence. The same method, together with the calculation of **b**-matrices, was applied later to the isolated rat heart (Chapter 5).

3.5.2. Methods

The diffusion tensors of (a), water and (b), metabolites in a solution containing (in mM) taurine (30), creatine (15), choline (5), glutamate (5), glutamine (5) and aspartate (9) were measured. The slice-selective STEAM sequence was used, with and without water suppression, as described above. TE was 20 ms, TM 40 ms, TR 3 s, and 16 averages were acquired for each diffusion gradient strength.

Six non-collinear diffusion gradient 'vectors' were applied with a basic diffusion gradient strength of 11 G/cm ($\sqrt{½} \equiv 7.78$ G/cm). The sampling pattern was identical to that in Chapter 1. The equilibrium magnetisation, S_0, was measured with a scalar diffusion experiment using the same pulse sequence and arraying the diffusion gradient in the x-direction from 1-13 G/cm in five steps of 3 G/cm. The value for S_0 was obtained from the

abscissa intercept of the graph displaying the best linear fit through the semi-logarithmic signal amplitude as a function of the applied *b*-value. A single experiment to determine the diffusion tensor took about 9 min and was repeated five times.

FIDs were zero-filled once and line-broadened by 2 Hz prior to FT. The **b**-matrices, and the water, creatine, taurine and choline diffusion tensors were calculated using the Mathematica programme. According to eq 1.22, the signal amplitudes obtained from the six diffusion gradient vectors, together with the measured equilibrium magnetisation S_0, generated a system of six linear equations with six unknowns (the elements of the diffusion tensor). This system was solved by matrix inversion.

3.5.3. Results

Three typical **b**-matrices calculated for the slice-selective STEAM sequence with a basic diffusion gradient strength of 11 G/cm are displayed in Fig. 3.8. Gradients were applied in x-, y-, and z-direction, thus the gradient vectors were (1,0,0), (0,1,0) and (0,0,1), respectively.

$$\mathbf{b}(1,0,0) = \begin{pmatrix} 1049.94 & 0 & 2.60565 \\ 0 & 0 & 0 \\ 2.60565 & 0 & 0.155923 \end{pmatrix}$$

$$\mathbf{b}(0,1,0) = \begin{pmatrix} 0 & 0 & 0 \\ 0 & 1049.94 & 2.60565 \\ 0 & 2.60565 & 0.155923 \end{pmatrix}$$

$$\mathbf{b}(0,0,1) = \begin{pmatrix} 0 & 0 & 0 \\ 0 & 0 & 0 \\ 0 & 0 & 1044.88 \end{pmatrix}$$

*Fig. 3.8: **b**-matrices calculated for the slice-selective STEAM sequence with a basic diffusion gradient strength of 11 G/cm, applied in x-, y-, and z-directions.*

The diagonal component was highest for each **b**-matrix, and the matrices were symmetric. The b_{zz} component in the first two matrices originated from the application of the slice-selection and refocusing gradients along the z-direction. The b_{zz} component was lower in the last matrix compared to its diagonal counterpart in the first two matrices because of the slice-selection and refocusing gradients. It was the only non-zero component in the matrix as there were no gradients applied along the x- or the y-direction. The non-zero off-diagonal elements, giving an indication of the cross-terms between gradients applied in different directions, were small because the selected spectroscopy slice was immediately re- or prefocused, respectively.

During the experiments the temperature was constant at 20.5°C. All elements of the water and metabolite diffusion tensor are listed in Table 3.4. The diagonal components of the diffusion tensors were the same ($p > 0.05$) and the off-diagonal elements were close to zero.

Table 3.4: The diffusion tensor components for water, taurine, creatine and choline. Diagonal elements of each metabolite were identical, off-diagonal elements were close to zero. All values are expressed in units of 10^{-3} mm^2/s and are means ± SEM (n = 5).

	Diffusion Tensor Component					
Substance	D_{xx}	D_{yy}	D_{zz}	D_{xy}	D_{yz}	D_{xz}
Water (4.77 ppm)	2.07 ± 0.00	2.07 ± 0.00	2.06 ± 0.00	0.01 ± 0.00	0.01 ± 0.00	-0.03 ± 0.00
Creatine (3.95 ppm)	0.72 ± 0.02	0.71 ± 0.01	0.69 ± 0.05	-0.00 ± 0.01	-0.02 ± 0.02	-0.01 ± 0.01
Creatine (3.03 ppm)	0.72 ± 0.04	0.71 ± 0.01	0.74 ± 0.02	0.00 ± 0.02	-0.01 ± 0.02	-0.03 ± 0.01
Taurine (3.43 ppm)	0.89 ± 0.04	0.86 ± 0.01	0.86 ± 0.02	-0.01 ± 0.01	0.00 ± 0.03	-0.02 ± 0.01
Taurine (3.26 ppm)	0.88 ± 0.02	0.87 ± 0.00	0.89 ± 0.04	0.01 ± 0.01	-0.02 ± 0.02	-0.01 ± 0.01
Choline (3.20 ppm)	0.89 ± 0.01	0.90 ± 0.00	0.90 ± 0.01	0.01 ± 0.00	0.02 ± 0.01	-0.00 ± 0.00

3.5.4. Discussion

With 'free' diffusion, the molecular movement is not restricted by any barriers such as membranes, hence a single molecule would diffuse in all directions with equal probability. In such a case the diagonal elements of the diffusion tensor would be identical, and, as no structures force the diffusing molecule along a path (such as in muscle tissue along the fibre axis), all cross terms of the diffusion tensor would be zero. This was observed in this experiment, for the water and the metabolites. Furthermore, the diagonal elements of the diffusion tensor did not differ from the scalar diffusion coefficients acquired using the slice-selective STEAM sequence, after applying correction

factors of 0.937 for water and 1.025 for metabolites to account for the difference in temperatures (Mills 1973) (data not shown).

The errors in the diffusion tensor measurements were larger than in the scalar diffusion experiments, ranging from ± 0.2% for water up to ± 7.7% for creatine (3.95 ppm) with an average of ± 2.3%. This is because the value of the diffusion coefficient was derived with the scalar STEAM sequence from 16 experimental values, whereas the diffusion tensor was calculated using only seven values. In addition, each element of the tensor was from a single measurement, thus increasing the uncertainty in the estimation of the diffusion tensor.

The accuracy of the diffusion tensor estimation could be improved by repeating the experiment at several basic diffusion gradient strengths and obtaining the diffusion tensor through a multivariate linear regression analysis (Basser et al. 1992; Basser et al. 1994a). However, because time resolution was important, especially when monitoring dynamic changes, only one basic diffusion gradient strength (11 G/cm) was used here and in the perfused rat heart (Chapter 5). Basser and co-workers reported good agreement between use of one *vs.* several basic diffusion gradient strengths, provided all non-diffusion gradients contribute less than 1% to the total **b**-matrix value (Basser and Pierpaoli 1998). This condition was fulfilled by the slice-selective STEAM sequence.

It can be concluded that the water and metabolite diffusion tensors were measured with good accuracy and that diagonal components agreed well with previously acquired scalar diffusion coefficients. Accuracy could be improved by sampling the signal attenuation not only in different directions but also at different basic diffusion gradient strengths. However this would have led to prohibitive measuring times for use in the perfused heart.

3.6. Conclusion

The gradient hardware was found to give reproducible measurements of the scalar diffusion coefficients and the diffusion tensors of water and metabolites in solutions. The newly designed slice-selective STEAM sequence provided good sensitivity for physiological concentrations of metabolite samples. Diffusion coefficients could be measured accurately with a time resolution of 4 min using five *b*-values. The diffusion tensor agreed with the scalar diffusion coefficient, displaying no anisotropy or significant off-diagonal terms, but with an increase in the experimental error due to the reduced number of measurements.

Chapter 4

Localised ^{1}H-NMR spectroscopy of the perfused rat heart: Development of experimental methods for the measurement of metabolite diffusion coefficients

Abstract

There are important differences between the NMR properties of living tissue and those of solutions which require the NMR pulse sequence parameters to be set appropriately. In addition, tissue NMR measurements are more variable because movement artefacts occur, even if an animal is restrained or a perfused heart is KCl-arrested. The aim of the work in this chapter was to establish the best experimental conditions for, and the reproducibility of, measurements of ^1H NMR-detectable metabolite ADCs in the perfused, KCl-arrested rat heart. In all experiments, the water-suppressed slice-selective STEAM pulse sequence (see above) was used. The composition of the perfusion buffer was checked for ^1H resonances occurring at frequencies similar to those of the heart metabolites. As glucose had resonances between 3 and 4 ppm, substrates chosen were 5 mM Na-acetate, 1.8 mM Na-pyruvate and 0.2 mM Na-lactate. The T_1 values of ^1H NMR-detectable cardiac metabolites were measured to be 5.4 ± 0.9 s for taurine at 3.43 ppm, 2.7 ± 0.4 s for total creatine at 3.95 ppm, 2.8 ± 0.5 s for total creatine at 3.03 ppm, and 5.1 ± 0.8 s for the mixed peak of choline-containing compounds, carnitine and taurine at 3.26 ppm. These T_1 values were sufficiently long to provide good SNR for ADC measurements at diffusion times as long as 1.5 s. The reproducibility of the intracellular metabolite ADCs was 4-5% of the mean, well within current literature values of 2-20%. In conclusion, these experiments demonstrated that the ADC measurement of intracellular ^1H NMR-detectable metabolites was reproducible in the KCl-arrested rat heart perfused with a glucose-free buffer containing acetate, pyruvate and lactate as substrates.

4.1. ^{1}H-NMR analysis of the perfusion buffer

4.1.1. Introduction

In order to measure metabolite ADCs in the perfused rat heart using the slice-selective STEAM sequence, one should be aware that the selected spectroscopy slice contains not only heart tissue, but buffer in the interstitial spaces, the ventricles and around the outside of the heart. Errors in the interpretation of the spectrum may arise from components in the buffer which have peaks with the same resonance frequency as metabolites in the heart, leading to an overestimation of heart metabolite ADCs because of the faster diffusion of the buffer components. The detected metabolite peaks in unlocalised ^{1}H spectra of the whole, glucose-perfused rat heart include total creatine at 3.03 and 3.95 ppm, taurine at 3.43 ppm, and a mixture of choline-containing compounds, carnitine and taurine at 3.26 ppm (Ugurbil et al. 1984; Unitt et al. 1992). The concentrations of these ^{1}H-detectable metabolites are, total creatine, 30 mM (Madden et al. 1993; Saks et al. 1994), taurine, 30-40 mM (Huxtable 1992), choline-containing compounds, 1.3 mM (Lochner and de Villiers 1989), and carnitine, 2-3 mM (Schwartz et al. 1973; Shug et al. 1978; Whitmer et al. 1978). The aim of this experiment was to determine those substrates that did not resonate at the frequency of heart metabolites, between 3 and 4 ppm, yet maintain the heart in a viable state.

4.1.2. Methods

4.1.2.1. STEAM spectroscopy of solutions

^{1}H spectra were acquired using the water-suppressed slice-selective STEAM sequence with a TE of 20 ms, TM of 40 ms, TR of 3 s and 32 scans. The following solutions, made up with double-distilled water, were investigated: a) 50 mM glucose, b) 20 mM Na-

acetate, c) 20 mM Na-pyruvate, d) Krebs-Henseleit solution containing 20 mM KCl (see Appendix A) but no substrates, and e) Krebs-Henseleit solution containing 20 mM KCl and Na-acetate (5 mM), Na-pyruvate (1.8 mM) and Na-lactate (0.2 mM). Because spectra of KCl-arrested rat hearts were to be acquired in future experiments, the Krebs-Henseleit solution contained 20 mM KCl, as opposed to the normal 4.7 mM, with a lowered NaCl concentration to keep the buffer osmolarity at 300 mOsm. FIDs were zero-filled once and line-broadened by 2 Hz prior to FT.

4.1.2.2. STEAM spectroscopy of the KCl-arrested rat heart

Hearts from male Wistar rats with body weights of 302 g and 312 g (n = 2) were excised and perfused according to the methods described in Chapter 2. Functional recordings were not made using a latex balloon in the left ventricle, as this would have decreased spectral quality (K. Clarke, personal communication). The first heart was perfused with Krebs-Henseleit buffer containing 11 mM glucose during the initial equilibration period, and the second heart with Krebs-Henseleit buffer containing 5 mM acetate, 1.8 mM pyruvate and 0.2 mM lactate. For the remainder of the experiment, each buffer contained 20 mM KCl to arrest the hearts, with the same substrates.

After excision, hearts were perfused inside the magnet and allowed to equilibrate for 15 min during which the coronary flow rate was measured. The RF coil was tuned and matched, and hearts were shimmed on the ^1H FID using a simple pulse-collect sequence. Linewidths were 20-30 Hz at fwhm. After hearts were KCl-arrested, axial multi-slice spin-echo images were acquired to localise the spectroscopy slice for the STEAM experiments. Nine 2 mm thick slices were acquired, each with a field-of-view (FOV) of 25×25 mm^2, 128×128 matrix, 3 mm spacing between the centre of the slices, a TE of 50 ms to ensure sufficient contrast between the heart and the perfusate, and a TR of 1 s,

giving a total imaging time of 128 s. The centre slice corresponded to both the centre of the magnet and of the RF coil. For processing, no weighting functions or zero-filling were applied. The slice displaying the ventricle at its largest cross section was chosen for the spectroscopy acquisition.

The 90° RF pulse of the water-suppressed slice-selective STEAM sequence was adjusted to give maximum signal from the selected 3 mm slice, which was then shimmed to 10-15 Hz. In order to correct for the position-related off-resonance effect of the metabolites, the slice was shifted downfield by 696 Hz, corresponding to the 3.03 ppm methyl resonance of creatine (at 400 MHz). The inversion time for the WEFT, and the 90° Gaussian pulse for the CHESS water suppression schemes were adjusted. A control spectrum with 16 averages, a TE of 20 ms, TM of 40 ms and TR of 3 s was acquired. The acquisition parameters used were a sweepwidth of 4 kHz, 8k data points and 1 s acquisition time. FIDs were zero-filled once and line-broadened by 5 Hz prior to FT. The time from inserting the perfused hearts into the magnet till the end of the acquisition of the control spectrum was 35-40 min.

4.1.3. Results

4.1.3.1. STEAM spectra of solutions

The spectrum of the 50 mM glucose solution had resonances between 3 and 4 ppm (Fig. 4.1*a*), whereas spectra of the 20 mM Na-acetate and the 20 mM Na-pyruvate solutions (Fig. 4.1*b*,*c*) had peaks at 1.91 ppm (Na-acetate), and at 1.45 ppm and 2.32 ppm (Na-pyruvate).

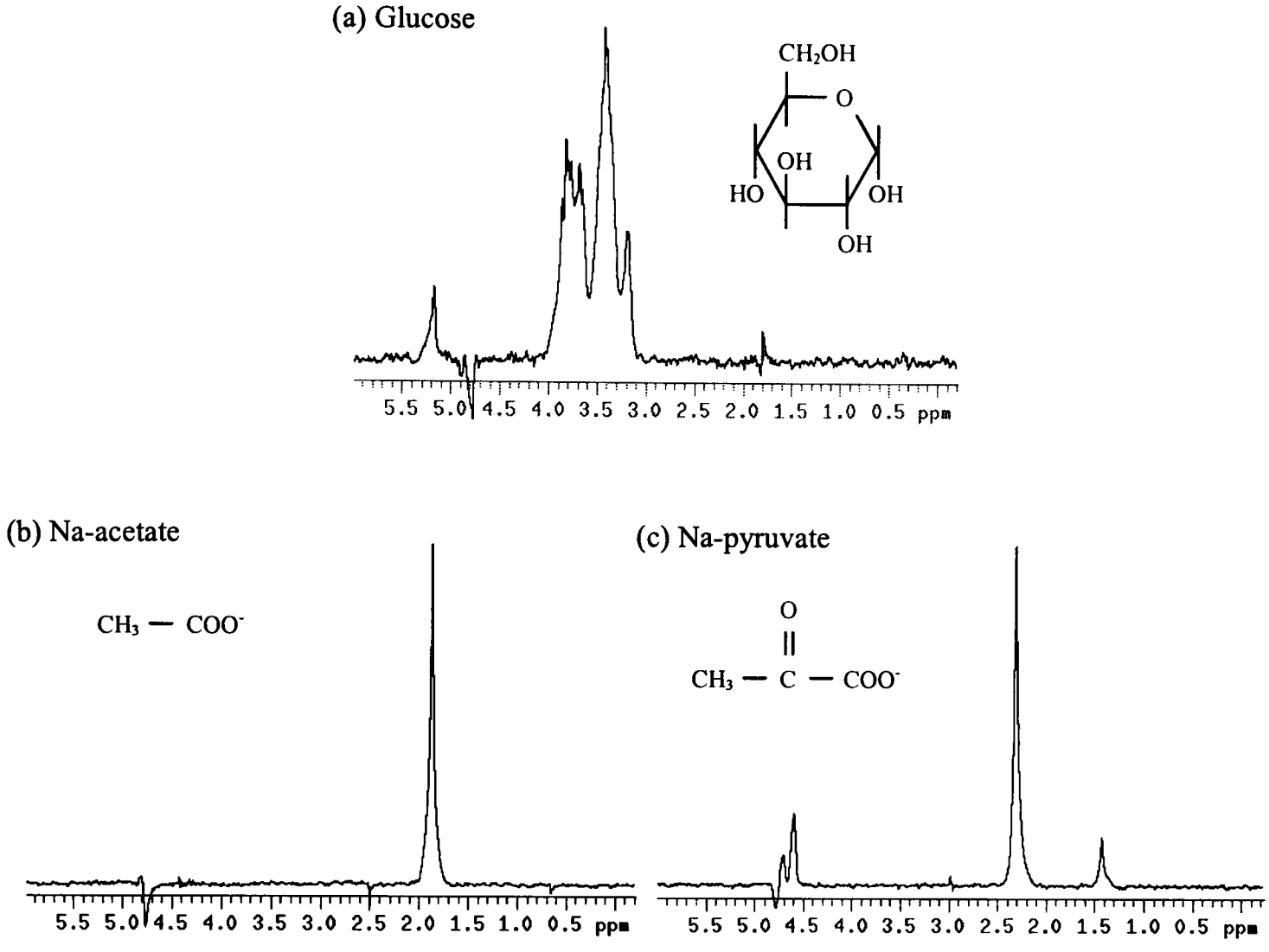

Fig. 4.1: Spectra and structures of substrates used to perfuse the isolated heart. Glucose (a) has resonances between 3 and 4 ppm, whereas Na-acetate (b) and Na-pyruvate (c) resonate at 1.91 ppm, and at 1.45 and 2.32 ppm, respectively. Spectra are not scaled equally.

In spectra of the Krebs-Henseleit buffer without substrates, peaks were visible at 2.55 and 3.12 ppm (Fig. 4.2*a*). These peaks were found to originate from the 0.5 mM Na_2-EDTA in the Krebs-Henseleit buffer. The same peaks were observed in spectra of the Krebs-Henseleit buffer containing 5 mM Na-acetate, 1.8 mM Na-pyruvate and 0.2 mM Na-lactate as substrates, which showed resonances at 1.91 ppm, 2.32 ppm and 1.30 ppm, respectively (Fig. 4.2*b*).

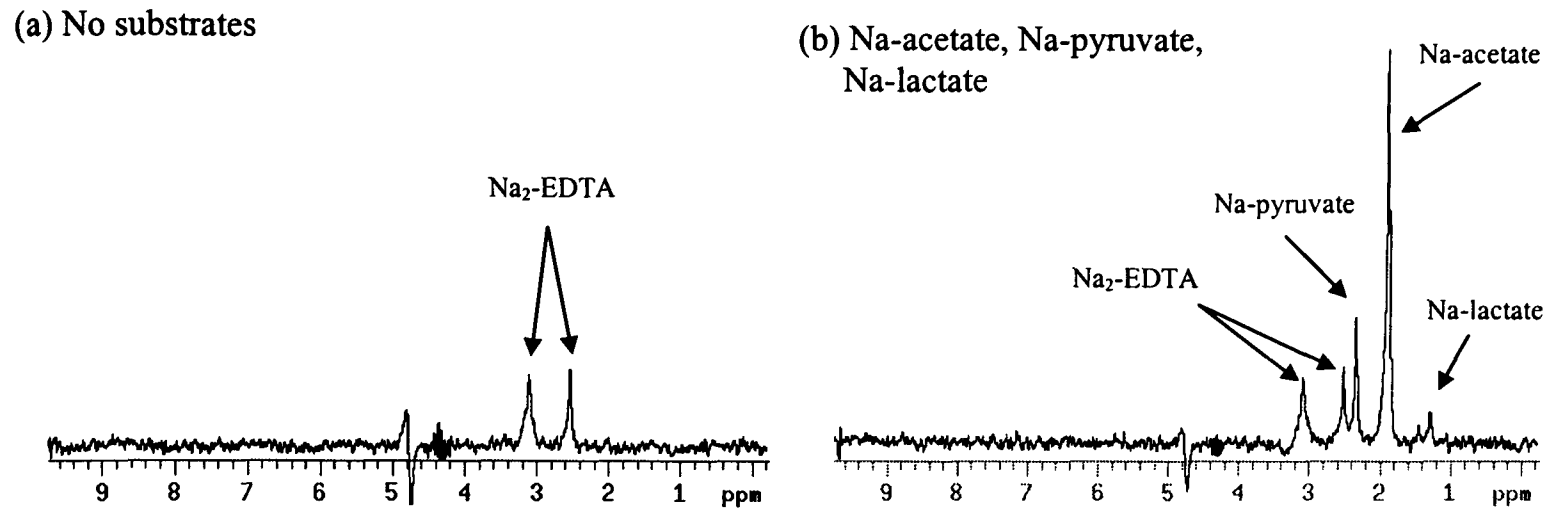

Fig. 4.2: Spectra of: (a), Krebs-Henseleit buffer without substrates, showing peaks at 2.55 ppm and 3.12 ppm and (b), Krebs-Henseleit buffer containing 5 mM Na-acetate, 1.8 mM Na-pyruvate and 0.2 mM Na-lactate. The peaks in (a) are from 0.5 mM Na_2-EDTA. Spectra are scaled equally.

4.1.3.2. Perfused heart experiments

Fig. 4.3 shows a typical example for the centre slice image of the multi-slice scout images of an isolated perfused rat heart. The left and right ventricles and their chambers are clearly seen.

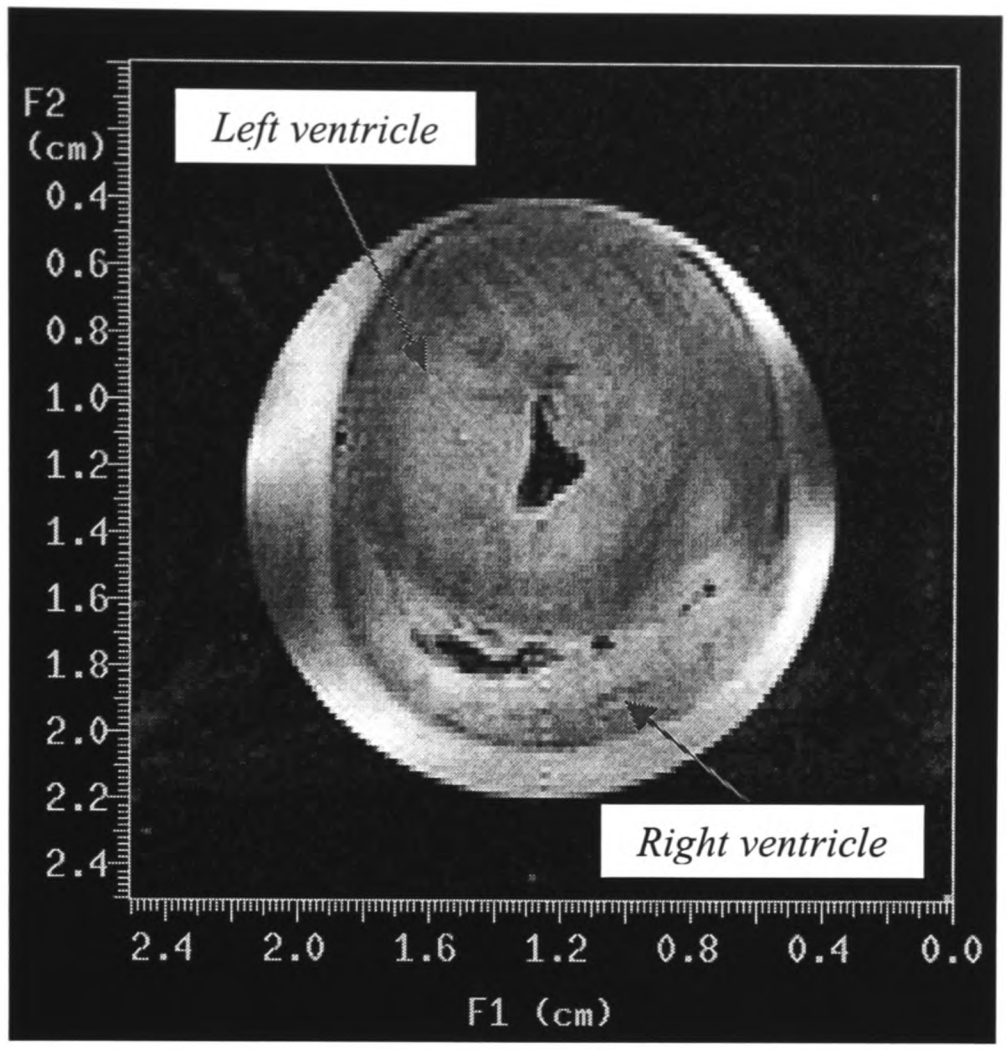

Fig. 4.3: Axial 128 × 128 spin-echo image of a perfused KCl-arrested rat heart from which spectroscopic data were acquired using the slice-selective STEAM pulse sequence. The image is the centre image of a set of multi-slice spin-echo images acquired with a TE of 50 ms and a TR of 1 s. Left and right ventricles and their respective chambers are clearly visible.

Resonance peaks from heart metabolites in the 3-4 ppm region were obscured in hearts perfused with Krebs-Henseleit buffer containing 11 mM glucose (Fig. 4.4*a*), but not so in hearts perfused with Krebs-Henseleit buffer containing 5 mM Na-acetate, 1.8 mM Na-pyruvate and 0.2 mM Na-lactate (Fig. 4.4*b*). Heart metabolites include total creatine at 3.95 ppm and 3.03 ppm, taurine at 3.43 ppm, a mixture of choline-containing compounds, carnitine and taurine (Cho/Car/Tau) at 3.26 ppm and triglycerides at 0.9 ppm and 1.3 ppm (Fig. 4.4*b*). Substrate peaks from Na-pyruvate at 2.32 ppm and Na-acetate at 1.91 ppm were also observed.

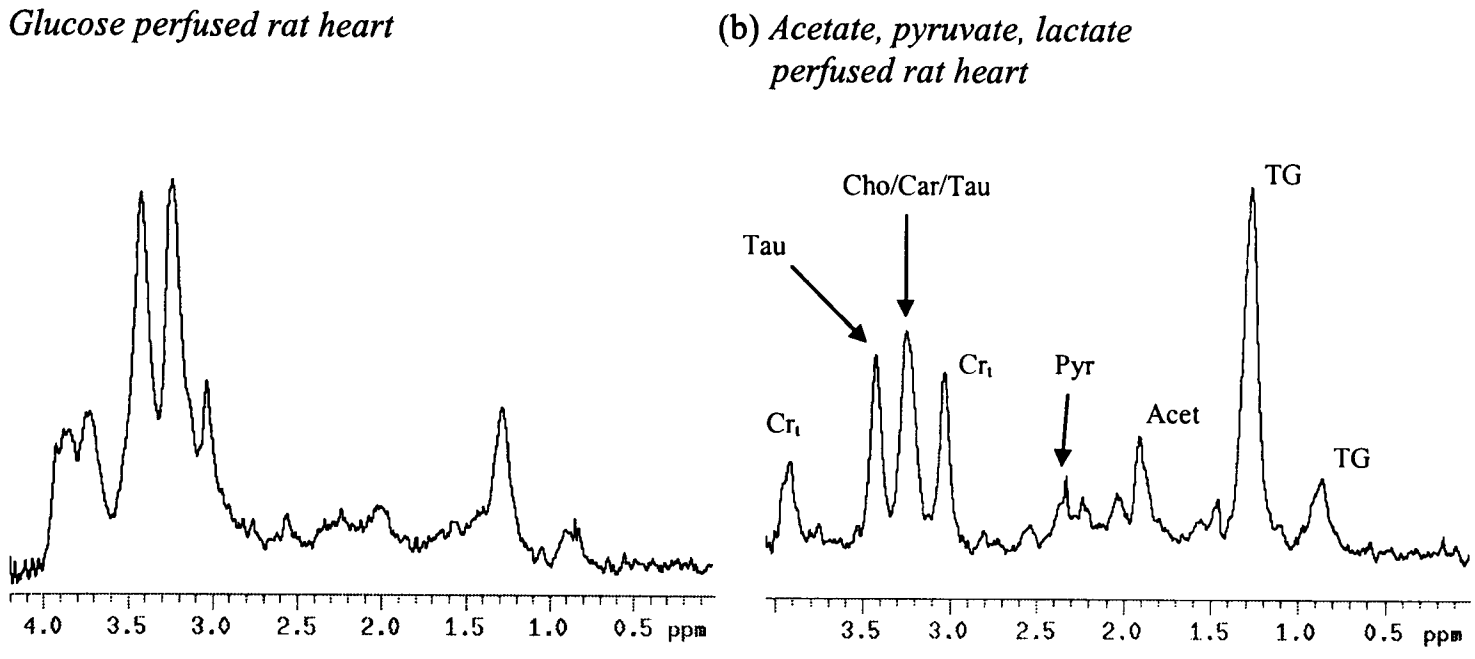

Fig. 4.4: Spectra of isolated rat hearts perfused with glucose (a), and acetate-pyruvate-lactate (b). Note the contamination of heart metabolite peaks by glucose in (a). Spectra are not scaled equally. Abbreviations are Cr_t, total creatine; Cho/Car/Tau, mixture of choline-containing compounds, carnitine and taurine; Pyr, Na-pyruvate; Acet, Na-acetate; TG, triglycerides.

In later studies on the perfused rat heart the total creatine peak at 3.03 ppm was analysed. Possible contamination of this peak might have arisen from the heavy-metal ion chelator Na_2-EDTA resonating at 3.12 ppm (Fig. 4.2*a*). However Na_2-EDTA had only a small influence on the peak height of the 3.03 ppm total creatine resonance; in Fig. 4.2*b* the peak height ratio for Na-acetate to the 3.12 ppm Na_2-EDTA peak was 5.6:1. In the acetate-pyruvate-lactate perfused heart spectrum (Fig. 4.4*b*), the ratio for the 3.03 ppm total creatine peak to the Na-acetate peak (1.91 ppm) height was 2:1. Combining these two, the height of the 3.12 ppm Na_2-EDTA peak would be 9% (1:11.2) of the 3.03 ppm total creatine peak. In fact, a simulation assuming Lorentzian line shapes, a 10% peak amplitude for the 3.12 ppm Na_2-EDTA peak compared to the total creatine peak, a creatine fwhm of 25 Hz (typically encountered in later perfused heart studies), an EDTA fwhm of 30 Hz and a peak position difference of 0.09 ppm (36 Hz) showed that the Na_2-

EDTA contributed less than 1.5% to the total creatine peak height.

4.1.4. Discussion

4.1.4.1. Substrate choice for heart perfusions

These experiments showed that glucose was not a suitable substrate for the isolated heart perfusions because it had resonances between 3 and 4 ppm, thereby obscuring heart metabolite peaks such as total creatine at 3.95 ppm and 3.03 ppm, and taurine at 3.43 ppm. Na-acetate, Na-pyruvate and Na-lactate were found to resonate away from the 3-4 ppm region. The only contamination originated from the Na_2-EDTA, with peaks at 2.55 and 3.12 ppm, but the contribution from the latter peak to the 3.03 ppm total creatine peak was negligible (< 1.5%). In addition, in later ADC studies of intracellular metabolites in the perfused rat heart, the 3.12 ppm Na_2-EDTA peak from the buffer was considerably more attenuated by diffusion processes than the 3.03 ppm total creatine peak.

4.1.4.2. Effect of acetate-pyruvate-lactate buffer on cardiac metabolism

Absence of glucose in the perfusion buffer would reduce glycolytic ATP production, which might then be derived from glycogen if needed. However, when measuring intracellular ADCs, the hearts were KCl-arrested and performed relatively little work, lessening the need for glycolytic ATP (Nishiki et al. 1978). Acetate feeds into the TCA cycle *via* acetyl CoA (Fig. 4.5), requiring the hydrolysis of one ATP. Pyruvate is converted into acetyl CoA to feed into the TCA cycle, whilst lactate is converted to pyruvate *via* the LDH reaction and provides a NAD^+/NADH ratio consistent with the redox potential of the cytosol. As the workload of the heart was low, sufficient ATP could be obtained from the TCA cycle, without provision of glucose.

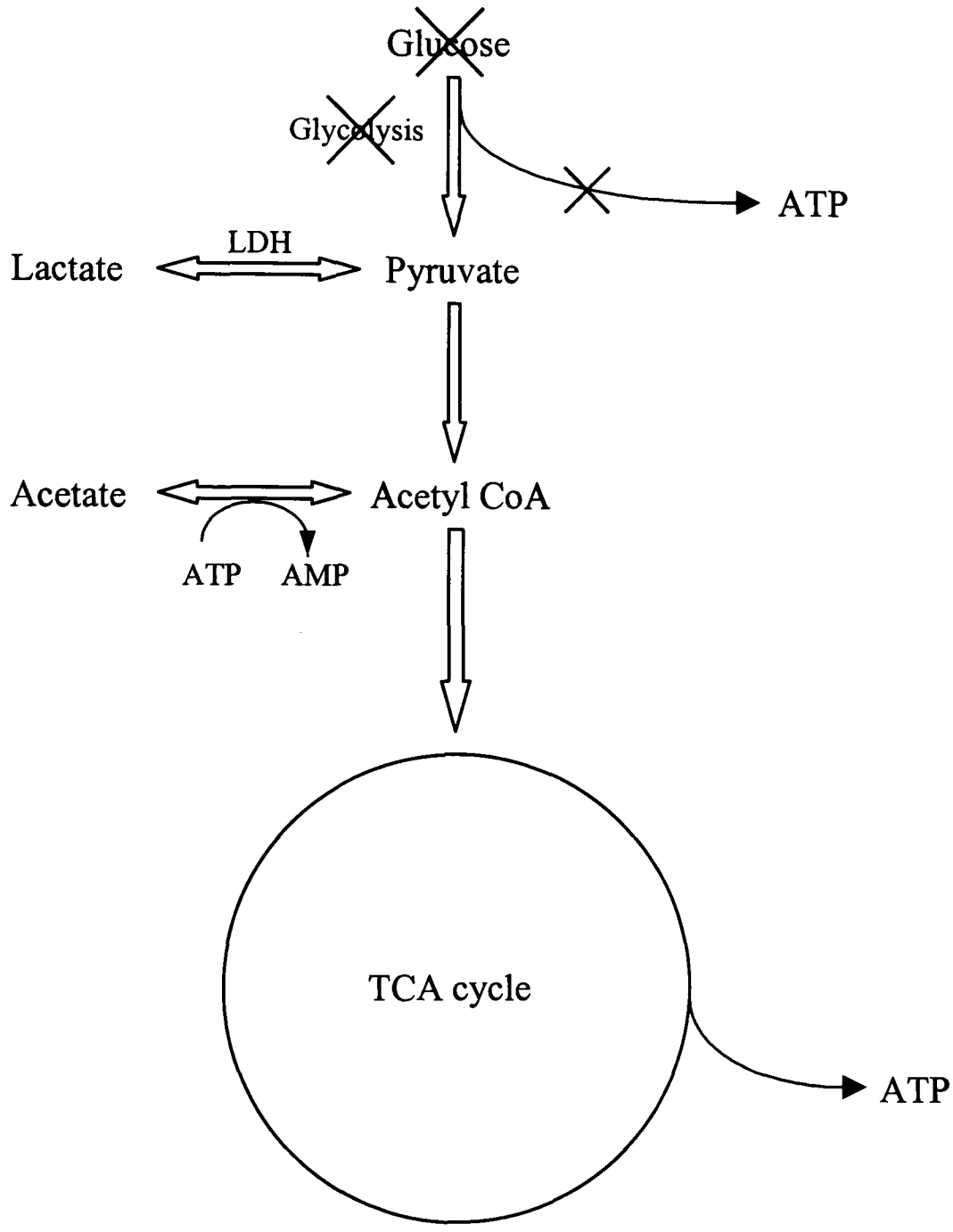

Fig. 4.5: The substrates lactate, pyruvate and acetate produce acetyl CoA which feeds into the TCA cycle. Glycolytic ATP, thought to be important for ion pumps in the sarcolemma, would be needed in small quantities only as hearts were KCl-arrested. The pyruvate/lactate ratio via the lactate dehydrogenase (LDH) reaction controls the NAD^+/NADH ratio, which, in turn, drives the acetyl CoA production.

In conclusion, because hearts were KCl-arrested, the choice of 5 mM Na-acetate, 1.8 mM Na-pyruvate and 0.2 mM Na-lactate as a substrate combination did not have any deleterious effects on the heart, so these substrates were used in the following perfused rat heart experiments.

4.2. Measurement of T_1 relaxation times of ^1H NMR-detectable heart metabolites

4.2.1. Introduction

In any NMR experiment it is important to set the acquisition parameters according to the NMR properties of the tissue. In a stimulated echo pulse sequence the magnetisation relaxes with T_2 during the first and second TE/2 period, and with T_1 during TM and between scans. In ADC measurements using STEAM-type sequences, the T_1 times are of particular importance as they are the limiting factor for the duration of the diffusion time. Although ^1H spectra have been acquired from the whole perfused rat heart (Ugurbil et al. 1984; Unitt et al. 1992), T_1 relaxation times of intracellular metabolites were not measured. Therefore, the aim of this experiment was to determine the T_1 relaxation times of total creatine, taurine and the mixture of choline-containing compounds, carnitine and taurine in the perfused rat heart using progressive saturation in the water-suppressed slice-selective STEAM sequence. It could then be estimated if the measured T_1 times were sufficient to provide good SNR for later heart studies performed at long TMs (Chapter 7).

4.2.2. Methods

4.2.2.1. Experimental

Hearts from male Wistar rats with a body weight of 337 ± 12 g (n = 5) were excised and perfused as above, with Krebs-Henseleit buffer containing 5 mM Na-acetate, 1.8 mM Na-pyruvate and 0.2 mM Na-lactate. The water-suppressed slice-selective STEAM sequence was used with a TE of 20 ms and a TM of 40 ms. The T_1 times of ^1H NMR-detectable intracellular heart metabolites were measured using a progressive saturation experiment in which the TR was varied in 19 non-equidistant steps from 1.2 s, the shortest possible

time for this pulse sequence, to 8 s. The order of the respective TR times was random. Sixteen averages were acquired for each TR. Including the time for the WEFT suppression scheme adjustments for each TR time, the experiment took about 110 min for each heart.

4.2.2.1. Spectral processing and data analysis

FIDs were zero-filled once and line-broadened by 5 Hz prior to FT. The signal intensities of the total creatine peaks at 3.03 ppm and 3.95 ppm, the taurine peak at 3.43 ppm, and the Cho/Car/Tau peak at 3.26 ppm were measured for each TR. The resulting plots of signal intensity as a function of the repetition time, *S(TR)*, were fitted to the equation:

$$S(TR) = S_{0,R}\left(1 - \exp\left\{-TR/T_1\right\}\right) \tag{4.1}$$

using the Origin program (Version 4.0, Microcal Software, Inc., Northampton, MA, USA). In this equation, $S_{0,R}$ contains terms for the equilibrium magnetisation, S_0, the T_1 and T_2 relaxation processes during the TE/2 and the TM periods, respectively, and the diffusion-mediated signal losses, and is given by the equation:

$$S_{0,R} = \frac{1}{2}S_0 \cdot \exp\left\{-\left(TE/T_2 + TM/T_1\right)\right\} \cdot \mathrm{f}(\vec{g}, D) \tag{4.2}$$

where the function $\mathrm{f}(\vec{g}, D)$ represents the diffusion-mediated signal loss depending on the gradient pattern, $\vec{g}$, of the pulse sequence and the diffusion coefficient, D (Sattin et al. 1985). As $S_{0,R}$ was constant when varying *TR*, curves could be fitted to eq 4.1.

4.2.3. Results

T_1 relaxation curves for the total creatine peaks at 3.03 ppm and 3.95 ppm, the taurine peak at 3.43 ppm, and the Cho/Car/Tau peak at 3.26 ppm for all five hearts are shown in Fig. 4.6. The signal amplitude at a TR of 8 s for each heart was normalised to the mean value from all hearts at that TR. The total creatine T_1 times were shorter than those of taurine and the Cho/Car/Tau mixture (Table 4.1).

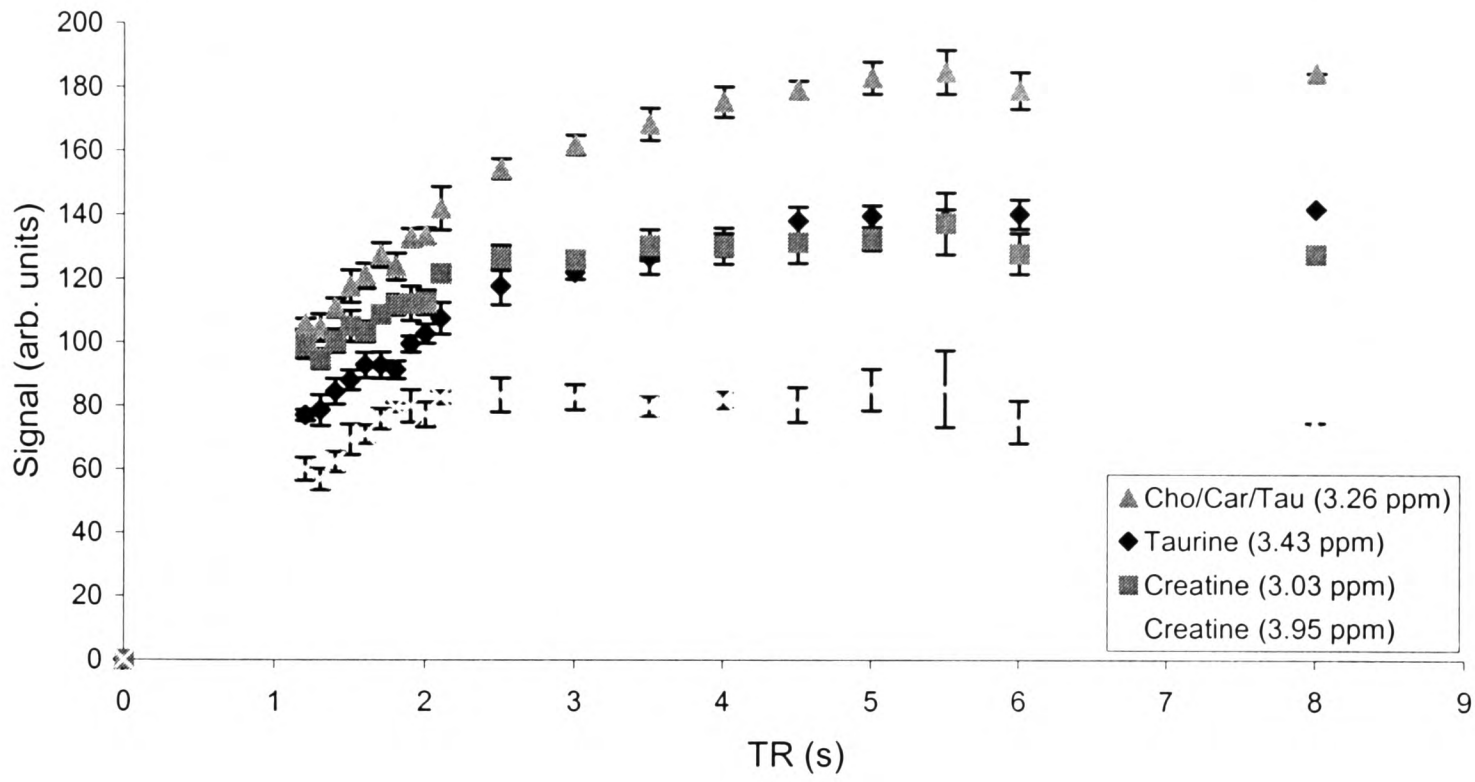

Fig. 4.6: Plot of metabolite signal intensities as a function of TR in all hearts. Signal amplitudes were normalised for each heart to the mean value of the last point at a TR of 8 s from all hearts; data represent the mean ± SEM (n = 5). The initial rate of change of the total creatine signal was largest, indicating the shortest T_1 relaxation time.

Table 4.1: T_1 relaxation times for total creatine, taurine, and the Cho/Car/Tau mixture in isolated perfused rat heart (n = 5). The total creatine T_1 times were significantly lower than those of the other metabolites.

	δ (ppm)	$T_1 \pm$ SEM (s)
Total Creatine	3.95	2.7 ± 0.4
Taurine	3.43	5.4 ± 0.9
Cho/Car/Tau	3.26	5.1 ± 0.8
Total Creatine	3.03	2.8 ± 0.5

Total creatine T_1 times were 2.7 s, significantly lower than those of taurine and the Cho/Car/Tau peaks. The T_1 times were sufficient to provide good SNR at long TM times for diffusion experiments. For instance, assuming the total creatine T_1 time of 2.7 s, a T_2 of 50 ms (Schneider et al. 1998), an ADC of 0.3×10^{-3} mm^2/s and a *b*-value of 8.7 s/mm^2, the $S/S_{0,R}$ with typical sequence parameters of TE of 20 ms, TM of 40 ms and TR of 3 s, would be 0.22. With a long TM of 1.5 s, as used in later heart studies, this ratio would be 0.13. Thus the signal loss due to T_1 relaxation during TM would be only 42%, making diffusion measurements at long TM feasible.

4.2.4. Discussion

The total creatine T_1 was about half that of the taurine and the Cho/Car/Tau peak, possibly because the structural differences of these molecules lead to a different relaxation behaviour. In addition, the total creatine peak contained contributions from both the PCr and the creatine, and PCr is larger than creatine (Fig. 4.7).

Taurine:

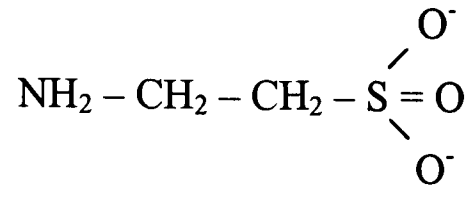

Creatine:

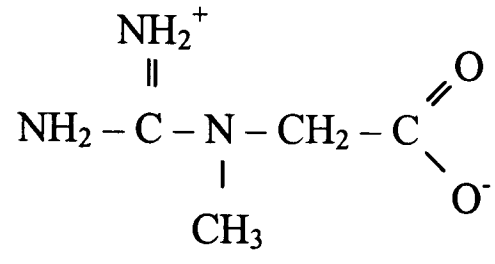

PCr:

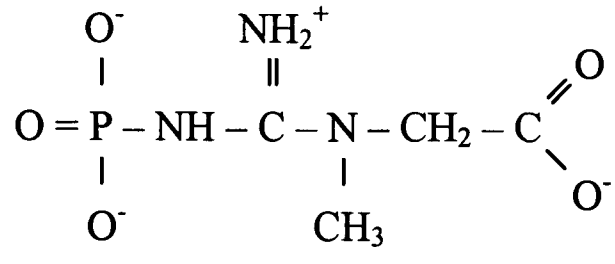

Fig. 4.7: Chemical structures of taurine, creatine and PCr, demonstrating that creatine and PCr have a longer principal chain and a more branched structure than taurine.

Spin-lattice relaxation is caused by randomly fluctuating local magnetic fields, which oscillate at the resonance frequency and induce transitions between spin states. A common source of time-dependent local fields is the dipolar interactions between nuclei within the same molecule. This interaction is anisotropic so that, as the molecule tumbles randomly in solution, the field experienced by one nucleus due to the dipole of a neighbouring nucleus varies randomly with time. For taurine, a less complex molecule than creatine and PCr (Clark 1997; Huxtable 1992), the component of the local field at the transition-inducing frequency would be weaker and spin-lattice relaxation slower.

The measured T_1s were long enough to provide sufficient SNR ratio at relatively long

TMs (and hence diffusion times) with the slice-selective STEAM sequence.

4.3. Reproducibility of intracellular metabolite ADC measurements

4.3.1. Introduction

It is important to estimate the reproducibility of spectroscopic NMR measurements in order to determine if spectral variations are a consequence of random instrumental fluctuations or due to biochemical changes in the sample. The reproducibility of *in vitro* ADC measurements, as performed in Chapter 3, revealed spectrometer and hardware instabilities, but *in vivo* ADC measurements can reveal instabilities in the sample, such as motion. In a KCl-arrested perfused rat heart, residual motion might influence the measured metabolite ADCs. Therefore, the aim of this experiment was to determine the reproducibility of ADC measurements of intracellular metabolites in the perfused KCl-arrested rat heart.

4.3.2. Methods

Hearts from male Wistar rats with a mean body weight of 343 ± 13 g (n = 5) were excised and perfused according to the methods described in Chapter 2. The water-suppressed slice-selective STEAM sequence was used with a TE of 20 ms, a TM of 40 ms and a TR of 3 s. ADCs were measured repeatedly in the x-direction using five gradient strengths from 1-13 G/cm in steps of 3 G/cm, corresponding to *b*-values from 8.7-1466 s/mm^2. This pattern was also used in later studies. Sixteen averages were acquired for each *b*-value, and each ADC measurement was repeated ten times for each of the five hearts. FIDs were zero-filled once and line-broadened by 5 Hz prior to FT. The ADC values were calculated

for the two total creatine peaks, taurine and the Cho/Car/Tau peak from a linear fit of the logarithmic signal intensities *vs.* the *b*-value.

4.3.3. Results

Fig. 4.8 shows five spectra from the perfused rat heart acquired with increasing *b*-values from 8.7 s/mm^2 to 1466 s/mm^2.

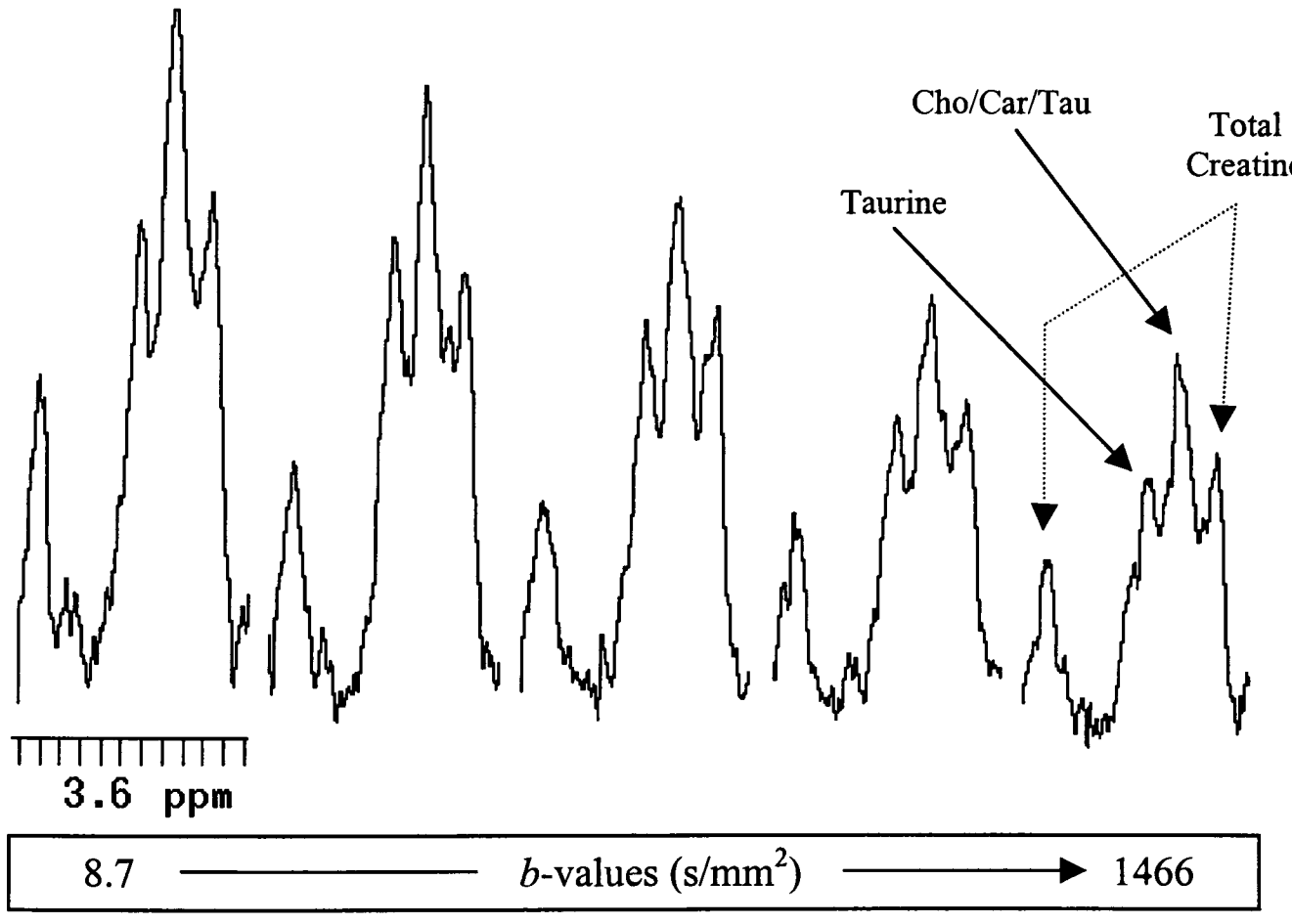

Fig. 4.8: Typical localised spectra from the perfused rat heart acquired with increasing b-values. Spectra displayed show the two total creatine peaks at 3.03 ppm and 3.95 ppm, the taurine peak at 3.43 ppm and the Cho/Car/Tau peak at 3.26 ppm. The left-hand spectrum was acquired with a b-value of 8.7 s/mm^2, the right-hand one with 1466 s/mm^2.

Plotting the logarithm of the signal amplitudes of the taurine, the Cho/Car/Tau and the 3.03 ppm total creatine peak as a function of the *b*-value gave a slope equivalent to the ADC for each metabolite. Fig. 4.9 illustrates the quality of the fits for these metabolites.

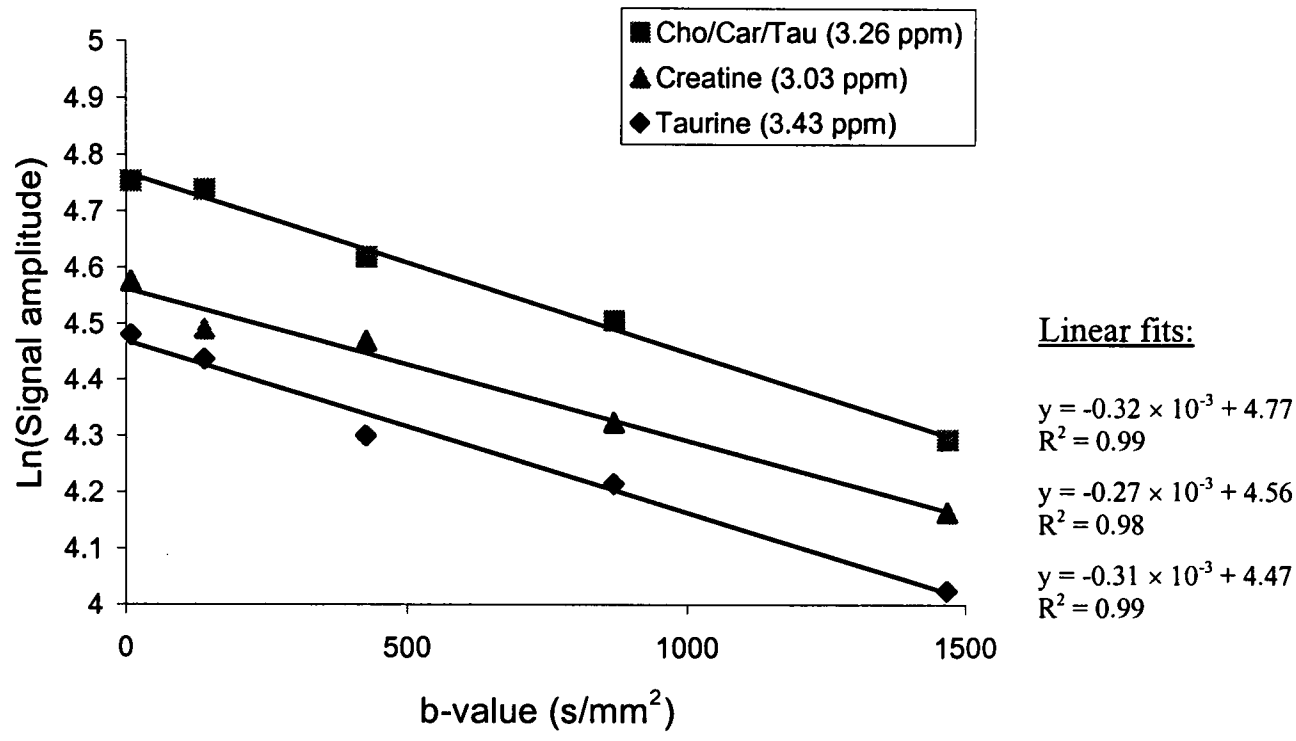

Fig. 4.9: Plot of the logarithmic signal amplitude vs. b-value for myocardial intracellular metabolites. The quality of the linear fits is shown by R^2 values ≥ 0.98.

For each heart, the ADC value of the metabolites was calculated from the mean of ten measurements. The mean values from the five hearts were then averaged and the SEM calculated. The mean ADC values of the detected metabolites are listed in Table 4.2.

Table 4.2: Heart metabolite ADCs showing that the error of the means range from 4-5%. All ADCs were significantly different from each other ($p < 0.005$). Data are means ± SEM ($n = 5$).

	δ (ppm)	ADC (10^{-3} mm^2/s)
Taurine	3.43	0.29 ± 0.01
Cho/Car/Tau	3.26	0.32 ± 0.01
Total creatine	3.03	0.26 ± 0.01

The total creatine peak at 3.95 ppm was not analysed due to fluctuations in later experiments, possibly caused by residual water. The ADC value of total creatine at 3.03 ppm was 0.26 × 10^{-3} mm^2/s, significantly lower than that of taurine at 0.29 × 10^{-3} mm^2/s ($p = 0.004$) and Cho/Car/Tau at 0.32 × 10^{-3} mm^2/s ($p = 0.0001$). Contributions from choline-containing compounds and carnitine to the peak at 3.26 ppm increased the ADC significantly ($p = 0.002$) from that of taurine alone. In addition, ADCs were a factor of about three lower than the diffusion coefficients measured in solutions (Chapter 3).

4.3.4. Discussion

4.3.4.1. Reproducibility

ADCs for taurine, total creatine and the Cho/Car/Tau peak were measured reproducibly in the perfused KCl-arrested rat heart with an error of 4-5% of the mean. This was well within the range of published standard errors of *in vivo* metabolite ADCs in rat brain, which range from 2-20% (Dreher and Leibfritz 1998; Merboldt et al. 1993; van der Toorn et al. 1996a). It was also close to the 1-2% obtained in Chapter 3 for solutions, suggesting

that any residual motion in the KCl-arrested rat heart did not influence the ADC measurements.

4.3.4.2. Heart metabolite ADCs

The ADC values obtained in the perfused rat heart were different for the different metabolites, suggesting that their diffusion paths may be different. Taurine is an inert molecule, present in the fluid-phase of the cytoplasm (Chapman et al. 1993), and should provide a good marker for intracellular diffusion without interference due to binding or other effects. The Cho/Car/Tau peak ADC represents a weighted average of ADC values arising from choline-containing compounds, carnitine and taurine. Compared to the taurine peak at 3.43 ppm, the 3.26 ppm peak had a larger ADC value, suggesting that choline-containing compounds and/or carnitine diffuse faster than taurine alone.

The total creatine peak at 3.03 ppm exhibited the smallest ADC value of the analysed intracellular metabolites. The explanation may be structure-based, in that the creatine compounds have a longer main chain with more extending branches compared to taurine (see Fig. 4.7; (Clark 1997; Huxtable 1992)). However, as the 3.03 ppm peak contains signal from creatine and phosphocreatine (PCr), the overall diffusion process will be slower because the 'average' molecular weight would be increased (see below).

4.3.4.3. Reduced metabolite ADC in the perfused heart compared to solution

The ADC values obtained from the perfused KCl-arrested rat heart are about three times lower than the diffusion coefficients obtained for the metabolite solutions in Chapter 3 (Table 4.3).

Table 4.3: Diffusion coefficients (DC) and ADCs of taurine and total creatine in solution and in perfused hearts, and the ratio of DC/ADC. Data are from this chapter and Chapter 3 and are the means ± SEM (n = 5). [a], data taken from (Dreher and Leibfritz 1998); [b], data represents PCr diffusion, taken from (de Graaf et al. 1998).

	DC solution (10^{-3} mm^2/s)	ADC heart (10^{-3} mm^2/s)	DC solution/ ADC heart	DC solution/ ADC brain[a]	DC solution/ ADC muscle[b]
Taurine	0.89 ± 0.01	0.29 ± 0.01	3.1 ± 0.1	3.9 ± 0.6	-
Creatine	0.74 ± 0.02	0.26 ± 0.01	2.8 ± 0.1	4.6 ± 0.2	1.4

This reflects the more restricted motion of these metabolites in the cytosol, which could be due to a higher cytosolic viscosity compared to that of water, hindered diffusion caused by cytoplasmic structures, binding, or compartmentation in the cardiomyocytes.

Increased cytosolic viscosity

According to the Stokes-Einstein relation (eq 1.5) the diffusion coefficient of probe molecules within a solution is proportional to the viscosity of that solution. Using picosecond polarisation microfluorimetry, some groups have shown that the fluid phase of the cytoplasm of various cell types is 1.2-1.4 times as viscous as water (Fushimi and Verkman 1991; Periasamy et al. 1992), or that it is similar to that of water (Luby-Phelps et al. 1993). Therefore the ADC of intracellular metabolites in the cell should only be 1.2-1.4 times smaller than their diffusion coefficient in solution. However, the intracellular metabolite ADCs in the perfused KCl-arrested rat heart were almost 3 times lower. It must therefore be concluded that either the cytosolic viscosity is higher in heart cells than in other cell types, or that another mechanism is responsible for the lower ADC.

Elastic collisions with cellular structures

Due to the tightly packed cytoplasm, intracellular molecules encounter a number of barriers by which they might be repelled with a consequent decrease in their ADC. It was found using fluorescence recovery after photobleaching (FRAP) that the translational motion of diffusing molecules in the cell cytosol of Swiss 3T3 cells was restricted 2.5-fold by elastic collisions with cellular structures (Kao et al. 1993). Diffusion hindrance due to tortuosity effects might therefore offer a possible explanation for the low metabolite ADC values observed in the perfused rat heart.

Binding effects

Diffusing molecules experiencing transient binding to macromolecules or intracellular structures in the cytoplasm have a lower ADC due to the reduced diffusion distance. The frequency of such binding effects depends on the type of probe molecule, and has mainly been observed for large proteins (Gershon et al. 1985). However, taurine diffuses freely in the cytosol of heart cells, is metabolised extremely slowly, and is not incorporated into proteins (Chapman et al. 1993; Crass and Lombardini 1978; Huxtable 1992; Nakada and Kwee 1991), making binding effects an unlikely explanation for the lower ADC in heart.

Compartmentation

Diffusing substances experience considerable restriction effects when confined to a small compartment, leading to a reduced ADC. However, taurine is resident only in the aqueous compartment of the cytoplasm (Huxtable 1992; Nakada and Kwee 1991) and would therefore diffuse freely. Creatine moves in and out of mitochondria, which could account for the lower ADC compared to that of taurine.

4.3.4.4. The total creatine ADC and a PCr/creatine transport system

The movement of a diffusing substance is slower in tissue than in solution due to the increased intracellular viscosity and/or movement restrictions in the cytoplasm. For taurine, the lower ADC is probably due to elastic collisions with cellular structures. The degree of these interactions can be expressed by the ratio of the ADC in solution to that in heart (Table 4.3), which can be taken as a measure for the inertness of the diffusing substance in the cytosol. Molecules that are not inert show reduced movement through the cytoplasm and will have a higher diffusion coefficient/ADC ratio. Inert molecules such as taurine should display the smallest possible ratios.

From Table 4.3 it seems that taurine and creatine display the same inertness in the cytoplasm of the heart cells. However, total creatine exists in the cytoplasm as PCr and creatine, and because they are in fast exchange, the measured ADC of the total creatine represents a combination of the PCr ADC and the creatine ADC, weighted by their relative concentrations. Hence, since PCr has a hydrodynamic radius 34% larger than that of creatine (Chapter 6), the total creatine ADC in heart should be reduced, resulting in a diffusion coefficient/ADC ratio that should be higher than that of taurine. However, this was not the case. This indicates that the diffusion of the total creatine in the cytosol occurs faster than that for inert molecules, suggesting that there might exist a transport system for the creatine/PCr system in addition to Brownian diffusion, which allows faster transport of PCr and/or creatine between the mitochondria and the myofibrils. This hypothesis is supported by publications reporting PCr ADC in muscle and brain tissue to be high, similar to that of PCr in solution (de Graaf et al. 1998; Moonen et al. 1990; Nakada et al. 1994). It was recently suggested that there exists a chain of creatine kinase reactions from the mitochondrion to the myofibril which could increase the rate of transport between these two sites (Saks et al. 1994).

4.3.4.5. *In vivo* ADCs in other tissues

Brain

Rat brain metabolites, detected with localised ^1H NMR using similar diffusion times to that used here, have relatively low ADCs, ranging from 0.16 to 0.23 $\times$ 10^{-3} mm^2/s for the major brain metabolites NAA, choline-containing compounds, total creatine and taurine (Assaf and Cohen 1998; Dreher and Leibfritz 1998; Duong et al. 1998; van der Toorn et al. 1996a), with most of the values at the lower end of the range. These values are lower than those in the perfused KCl-arrested rat heart. Since the probe molecules were the same in the brain and the heart, the observed difference can only be due to different intracellular environments. It might be that the cytosol in brain cells has an inherently higher viscosity than that in cardiomyocytes. In addition, because of their smaller size compared to cardiomyocytes (Nash et al. 1979; Stanisz et al. 1997), and the presence of dendrites and axons of neuronal and glial cell bodies with small dimensions (small compared to the average diffusion path length), the diffusion path of intracellular metabolites in the rat brain is likely to be more restricted, as suggested by others (Nicolay et al. 1995). Alternatively, the oedematous nature of the heart perfusion (Clarke et al. 1994) might allow more motional freedom for diffusing molecules. These factors should lead to a higher diffusion coefficient/ADC ratio in brain, as shown in Table 4.3.

Skeletal muscle

Skeletal muscle tissue, on the other hand, generally exhibits higher metabolite ADC values than heart, as shown in the rat hind leg muscle at similar diffusion times (de Graaf et al. 1998; Moonen et al. 1990). This suggests structural differences, perhaps involving decreased viscosity of the skeletal muscle cells compared to that of cardiomyocytes.

Restriction effects due to cell walls affected their measurements only slightly as diffusion distances were short compared to the average skeletal muscle cell length of 44 μm (Moonen et al. 1990). Alternatively, the cardiomyocyte might be more tightly packed with myofibrils, leading to increased movement obstruction for small molecules in the cytosol. However, the studies on skeletal muscle mentioned above investigated the diffusion of PCr in muscle; as discussed before, the diffusion of PCr and/or creatine might be increased by a transport system, which could explain the high ADC and low diffusion coefficient/ADC ratios (Table 4.3).

4.3.5. Conclusion

ADCs of total creatine, taurine and a mixture of choline-containing compounds, carnitine and taurine were measured with good reproducibility in the perfused KCl-arrested rat heart. Movement of these metabolites was slowed down in the cytosol of cardiomyocytes either due to increased viscosity, and/or elastic collisions of the diffusing molecules with intracellular components. Different ADC values for brain, skeletal muscle and heart indicated that the intracellular environment of these cells may be different. The ADC of the inert taurine molecules described the diffusion pathway in the heart cytosol with no interference due to binding effects; however the total creatine ADC was larger than expected, suggesting a transport system in addition to Brownian diffusion between sites of energy production and utilisation.

4.4. Conclusion

In this chapter, the composition of the perfusion buffer was checked for peaks that could contaminate spectra from the heart, leading to the use of a substrate combination of Na-acetate, Na-pyruvate and Na-lactate for heart perfusion buffers. Longitudinal relaxation times of heart metabolites were found to be sufficient for the measurement of the ADC at long diffusion times. Reproducibility experiments showed that the ADCs of intracellular heart metabolites could be measured accurately to within 4-5%. The ADCs of the intracellular ^{1}H-NMR detectable metabolites, taurine, total creatine and a mixture of choline-containing compounds, carnitine and taurine in the perfused KCl-arrested rat were significantly different from each other at 0.29, 0.26 and 0.32 $\times$ 10^{-3} mm^2/s, respectively.

Chapter 5

Effects of fibre orientation and morphologic changes during ischaemia and reperfusion on metabolite ADCs in the isolated rat heart

Abstract

In the previous chapter, the experimental parameters for ADC measurements in the perfused rat heart with the water-suppressed slice-selective STEAM sequence were established. With this sequence, data acquisition is restricted to a slice from the perfused heart, affecting the measurement of intracellular metabolite ADCs in two ways. First, should cardiac muscle fibres exhibit directionality, diffusion would be anisotropic and the diffusion tensor rather than the scalar ADC should be measured. However, the selected spectroscopy slice may contain fibres having a variety of directions; in this case, the directionality may average out, and it would be sufficient to measure the more time-efficient scalar ADC instead of the diffusion tensor. Second, with the cessation of buffer flow and the decreased perfusion pressure, hearts become less oedematous and shrink to a size more like that seen *in vivo*. This increases the number of myocytes in the selected spectroscopy slice, giving an apparent reduction in the measured ADC. Similarly, hearts swell during reperfusion, causing an apparent increase in the ADC.

The aims of the work in this chapter were to measure the diffusion tensor of ^{1}H NMR-detectable intracellular heart metabolites, and, in a separate experiment, to monitor the signal of these metabolites during perfusion, total global ischaemia and reperfusion. Diffusion tensor studies of the perfused rat heart revealed that, on a macroscopic scale, diffusion was isotropic in the spectroscopy slice, permitting the scalar ADC to be measured instead of the diffusion tensor. Signal amplitudes in ^{1}H spectra were sensitive to swelling and shrinking of the heart, substantially affecting ADCs during the transition periods from perfusion to ischaemia and from ischaemia to reperfusion. While taurine solely reflected this morphologic effect, the total creatine peak was modulated by an additional, probably compartment-related effect during ischaemia. The signal behaviours of both the taurine and the total creatine peaks were used to correct ADC measurements

in later studies.

5.1. Scalar ADC or diffusion tensor: Anisotropy effects in the perfused rat heart

5.1.1. Introduction

In this work, the method of choice to measure the ADCs of intracellular metabolites in the perfused rat heart is the water-suppressed slice-selective STEAM sequence as described in Chapter 3. It selects a 3 mm slice from which the ADCs are obtained with diffusion gradients applied in a single direction. If the selected volume has oriented fibres, the ADC measurement is biased towards this orientation relative to the direction of the applied diffusion gradient. Consequently diffusion would be anisotropic and the diffusion tensor would have to be measured with a minimum time resolution of 9 min (see Chapter 3). However, should the heart have a multitude of fibre orientations (Garrido et al. 1994; Scollan et al. 1998; Tseng et al. 1997), the measured ADC, representing an average from all orientations, would be isotropic for the selected slice. It would then be sufficient to measure the scalar ADC, with a smaller error and measurement times of only 4 min (see Chapter 4). This would improve the time resolution, thereby allowing ADC changes to be monitored during dynamic metabolic events, such as ischaemia or reperfusion.

The aim of this experiment was to investigate whether structural features of the perfused, KCl-arrested rat heart forced the diffusion of metabolites in a preferred direction within the selected spectroscopy slice. Diffusion tensors of the heart metabolites taurine, total creatine, and a mixture of choline-containing compounds, carnitine and taurine were measured and compared to their scalar ADCs acquired in x-, y-, and z-direction. The

water-suppressed slice-selective STEAM sequence was used with short (40 ms) and long (800 ms) TMs to vary the sensitivity of the diffusion process to anisotropy effects.

5.1.2. Methods

5.1.2.1. General

Hearts from male Wistar rats with a body weight of 310 ± 8 g (n = 4) were excised and perfused as described above. Care was taken to cannulate each heart in the same orientation, with the centre of the left atrium facing the x-direction of the magnet to minimise variation between hearts in the directional ADC and diffusion tensor measurements. Hearts were perfused with Krebs-Henseleit buffer for the first 15 min and KCl-arrested for the remaining 85-90 min of the protocol. The water-suppressed slice-selective STEAM sequence was used to measure the scalar and tensorial ADCs at a short TM of 40 ms and at a long TM of 800 ms. The TR was 3 s, the TE was 20 ms, and 16 scans were averaged for each *b*-value. FIDs were zero-filled once and line-broadened by 5 Hz prior to FT, and peak heights of the 3.03 ppm total creatine resonance, the Cho/Car/Tau resonance at 3.26 ppm, and the 3.43 ppm taurine peak were measured. All *b*-values, **b**-matrices and diffusion tensors were calculated using the Mathematica program.

5.1.2.2. Scalar ADC measurements

Scalar ADCs were measured in the x-, y-, and z-directions using eight *b*-values with gradient strengths from 1 to 15 G/cm in 2 G/cm steps for the TM = 40 ms measurement (corresponding to a *b*-value range of 9-1952 s/mm^2 for the x- and y-direction, and 8-1945 s/mm^2 for the z-direction), and 0.5-4 G/cm in 0.5 G/cm steps for the TM = 800 ms

experiment (*b*-value range, 37-2344 s/mm^2 and 37-2342 s/mm^2, respectively). ADC and S_0 values were obtained from semi-logarithmic fits of signal amplitude *vs.* *b*-value. The S_0 values were recorded for use in the following diffusion tensor experiments.

5.1.2.3. Diffusion tensor measurements

Diffusion tensors of heart metabolites were measured using the diffusion gradient pattern described in Chapter 3, with a basic diffusion gradient strength of 11 G/cm for the short TM experiment, and 3.52 G/cm for the long TM experiment, respectively. For the calculation of the diffusion tensor, S_0 values were taken as the mean of the three S_0 values obtained from the scalar ADC measurements.

5.1.3. Results

5.1.3.1. Scalar ADC measurements

Representative semi-logarithmic signal attenuation graphs of the Cho/Car/Tau peak in x-, y-, and z-direction are given in Fig. 5.1. The data were acquired with the short TM of 40 ms.

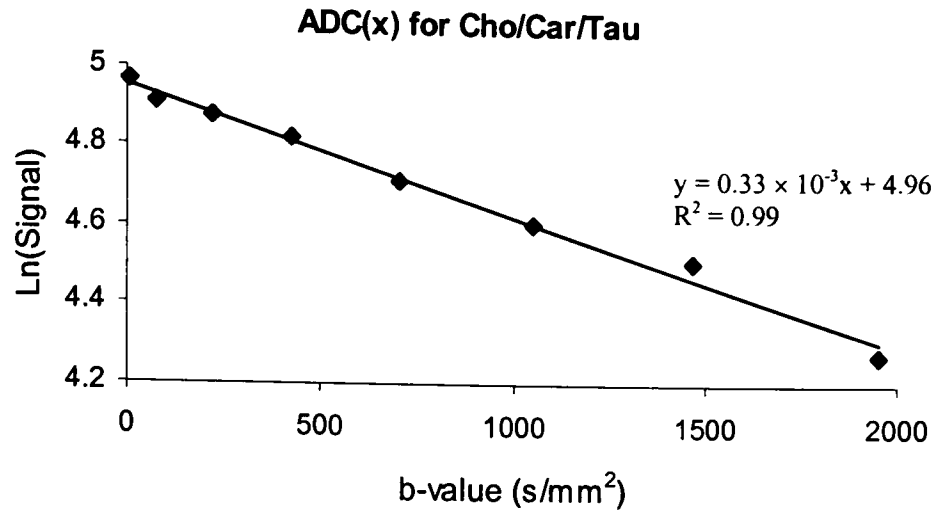

Fig. 5.1: Representative semi-logarithmic plots of the Cho/Car/Tau signal as a function of the b-value. Graphs are from a single heart displaying the best fit for diffusion data acquired in x-, y-, and z-direction. There was no difference between measurements in the three directions, and fits were good with $R^2 = 0.99$.

The ADCs from all hearts for the taurine, the Cho/Car/Tau and the total creatine peak at 3.03 ppm were the same in the different directions, with average ADCs of 0.29, 0.32 and 0.27×10^{-3} mm^2/s, respectively (Table 5.1). Fits generally had an $R^2 > 0.95$.

Table 5.1: Scalar ADCs for taurine, the Cho/Car/Tau mixture and total creatine in the x-, y-, and z-direction measured using the short TM of 40 ms. ADCs were not significantly different in the three directions. Data are means ± SEM for all hearts (n = 4).

	Taurine (10^{-3} mm^2/s)	Cho/Car/Tau (10^{-3} mm^2/s)	Total creatine (10^{-3} mm^2/s)
x-direction	0.30 ± 0.02	0.33 ± 0.02	0.28 ± 0.02
y-direction	0.29 ± 0.01	0.32 ± 0.02	0.26 ± 0.01
z-direction	0.29 ± 0.01	0.30 ± 0.02	0.27 ± 0.02

The ADC values for the respective metabolite peaks in x-, y-, and z-direction acquired with a TM of 800 ms are listed in Table 5.2. Again, the values were not significantly different from each other with respect to direction, but were smaller than those acquired with a TM of 40 ms. Errors were slightly larger than in the short TM experiment, presumably due to the reduced SNR at longer TM times.

Table 5.2: Scalar ADC values of the taurine, Cho/Car/Tau and the total creatine peak, acquired at a TM of 800 ms in x-, y-, and z-direction. ADCs did not differ significantly with direction. Data are means ± SEM (n = 4).

	Taurine (10^{-3} mm^2/s)	Cho/Car/Tau (10^{-3} mm^2/s)	Total creatine (10^{-3} mm^2/s)
x-direction	0.18 ± 0.02	0.19 ± 0.02	0.15 ± 0.03
y-direction	0.18 ± 0.02	0.20 ± 0.02	0.16 ± 0.03
z-direction	0.18 ± 0.03	0.21 ± 0.03	0.15 ± 0.02

5.1.3.2. Diffusion tensor measurements

The diagonal elements of the diffusion tensor (D_{xx}, D_{yy} and D_{zz}), acquired at a TM of 40 ms for taurine, Cho/Car/Tau and total creatine were close to the respective ADC values (Table 5.1), and were not significantly different from each other. The off-diagonal elements (D_{xy}, D_{yz} and D_{xz}) were close to zero (Table 5.3).

Table 5.3: Diffusion tensor elements for taurine, the Cho/Car/Tau peak and total creatine acquired with a TM of 40 ms. Diagonal elements were not significantly different from each other; off-diagonal elements were close to zero. Data are means ± SEM (n = 4).

	Taurine (10^{-3} mm^2/s)	Cho/Car/Tau (10^{-3} mm^2/s)	Total creatine (10^{-3} mm^2/s)
D_{xx}	0.29 ± 0.02	0.30 ± 0.03	0.28 ± 0.04
D_{yy}	0.31 ± 0.03	0.29 ± 0.03	0.32 ± 0.05
D_{zz}	0.27 ± 0.03	0.30 ± 0.03	0.25 ± 0.03
D_{xy}	0.03 ± 0.03	0.01 ± 0.02	0.03 ± 0.02
D_{yz}	0.01 ± 0.04	0.01 ± 0.03	-0.02 ± 0.03
D_{xz}	0.03 ± 0.03	0.03 ± 0.01	0.02 ± 0.01

The elements of the diffusion tensor of the various metabolites measured using a TM of 800 ms are listed in Table 5.4.

Table 5.4: Diffusion tensor elements of the detected metabolite peaks acquired using a TM of 800 ms. Diagonal elements resemble the ADC values acquired in the scalar diffusion experiment (Table 5.2); off-diagonal elements are close to zero. Data are means ± SEM (n = 4).

	Taurine (10^{-3} mm^2/s)	Cho/Car/Tau (10^{-3} mm^2/s)	Total creatine (10^{-3} mm^2/s)
D_{xx}	0.17 ± 0.04	0.22 ± 0.03	0.16 ± 0.03
D_{yy}	0.17 ± 0.06	0.24 ± 0.04	0.15 ± 0.04
D_{zz}	0.17 ± 0.04	0.21 ± 0.06	0.17 ± 0.05
D_{xy}	0.02 ± 0.03	0.01 ± 0.02	0.01 ± 0.02
D_{yz}	0.04 ± 0.05	0.04 ± 0.04	0.03 ± 0.04
D_{xz}	-0.00 ± 0.03	0.02 ± 0.01	0.01 ± 0.06

At the longer TM there were no significant differences between the scalar ADC values (Table 5.2) and the diagonal elements of the diffusion tensor. The diagonal diffusion tensor elements were shorter at the long TM than those at the short TM, and the off-diagonal elements were close to zero. Errors were increased compared to short TM measurements, ranging from 14-35% for the diagonal elements, probably due to the reduced SNR at long TM times and only one basic gradient strength being used to acquire the diffusion tensor.

5.1.4. Discussion and Conclusion

5.1.4.1. Sensitivity of the ADC measurements to fibre orientation

The shape of a rat cardiomyocyte is nearly cylindrical with a diameter around 25 μm and a length of around 110 μm (Drewnowska and Baumgarten 1991; Nash et al. 1979; Sorenson et al. 1985). With a measured ADC of 0.3×10^{-3} mm^2/s (Chapter 4) and diffusion times of 50 ms (corresponding to the short TM of 40 ms) and 810 ms (corresponding to the long TM of 800 ms), the average diffusion path lengths calculated from eq 1.4 were 5.5 μm and 22 μm, respectively. Hence for a TM of 40 ms not many diffusing molecules would experience restriction effects due to the sarcolemma as only few would have reached it. However, for a TM of 800 ms, the average diffusion path length was comparable to the average cardiomyocyte diameter, with a considerable number of molecules reaching the sarcolemma and being repelled, which was confirmed by the decreased ADC values compared to the short TM experiment. Therefore, the long TM measurement at 800 ms was considerably more sensitive to possible orientation effects in the myocardium.

5.1.4.2. Directional dependence of the ADC in the myocardium

The heart has a complicated fibre structure which allows it to pump blood efficiently (Chadwick 1982). With respect to the ventricular axis, the fibres are arranged in a helical fashion, for the most part circumferentially. There is a uniform transmural variation of the fibre pitch angle from -90° to +90° (Garrido et al. 1994; Tseng et al. 1997). Hence there would have been a variety of fibre orientations in the selected spectroscopy slice. However, at TMs of either 40 ms or 800 ms, no directional dependence of the ADC or differences in the diagonal diffusion tensor elements were detected, suggesting that

diffusion was isotropic on a macroscopic scale in the selected slice. Though diffusion might be anisotropic in single cardiomyocytes, particularly at long diffusion times, these effects were averaged out by the fact that the selected slice contained a multitude of fibre directions. Therefore it is justified to measure the scalar ADC value in either the x-, y-, or z-direction, thus increasing accuracy and time resolution.

5.2. Errors in the ADC measurements during ischaemia and reperfusion

5.2.1. Introduction

One of the aims of this project was to monitor the ADC of intracellular metabolites in the perfused, KCl-arrested rat heart during ischaemia and reperfusion. During total global ischaemia, a multitude of metabolic changes may occur that affect diffusion-related parameters, such as cytoplasmic viscosity or the degree of motion restriction by the cytoskeletal network (Jennings et al. 1986; Mastro et al. 1984; Steenbergen et al. 1985). However, ischaemia also leads to important morphologic changes. During perfusion, the heart is subjected to a perfusion pressure of 100 mmHg, making it oedematous because of the absence of osmolytes, such as albumin, in the crystalloid buffer. Once the buffer flow is turned off and ischaemia is induced, the perfusion pressure is reduced to zero and the heart shrinks (Clarke et al. 1993). Although this process does not alter NMR data acquisition from the whole heart, it may have a profound effect on the measurement of the intracellular metabolite ADC using the slice-selective STEAM sequence: The NMR signal is proportional to the number of myocytes in the selected slice, such that when the heart is ischaemic the signal increases in proportion to the degree of shrinkage and the increased number of cells. Similarly the signal decreases during reperfusion due to the

decreasing number of myocytes in the slice, with the heart swelling back to its original size. These signal changes would modulate the diffusion-mediated signal attenuation; for instance, upon induction of ischaemia, the progressive signal increase due to the increasing number of myocytes in the selected slice would weaken the diffusion-mediated signal attenuation, causing an underestimation of the ADC. Assuming a progressive 5% increase in signal for each of the five spectra used to calculate the ADC, simulations show that the ADC would be underestimated by around 40%; similarly a progressive 5% decrease would result in a 45% overestimation of the ADC (see Appendix C). This would prevent the measurement of ADC changes during early ischaemia and reperfusion, and artefact-free ADCs could only be obtained when the perfused heart has finished shrinking or swelling, with no changes in the number of myocytes in the selected slice. However, if the amount of shrinkage and swelling could be measured, it should be possible to correct for these effects.

The aim of this experiment was to measure the signal intensities of taurine, the Cho/Car/Tau peak and total creatine upon induction of ischaemia and reperfusion using the water-suppressed slice-selective STEAM sequence. The acquired data were used in later experiments to correct for shrinking- and swelling-induced ADC under- and overestimation during ischaemia and reperfusion, respectively. This data could also show whether or not the metabolites were released during the ischaemic period.

5.2.2. Methods

5.2.2.1. NMR experiments

Hearts from male Wistar rats with a mean body weight of 362 ± 22 g (n = 5) were excised and perfused according to the methods described in Chapter 2. The experimental protocol consisted of a control perfusion period with high-KCl buffer for 20 min, a 32 min total

global ischaemia period, and a 20 min reperfusion period. Total global ischaemia was induced by clamping off the buffer line to the heart, and reperfusion was initiated by releasing the clamp. Coronary flow rate was measured during perfusion and at 5 min intervals during reperfusion.

To illustrate heart volume changes during ischaemia, sagittal 128 × 128 FLASH images with a FOV of 40 × 25 mm^2, a slice thickness of 2 mm, a TR of 100 ms and a TE of 10 ms were acquired from the isolated heart during perfusion and at 3 min after induction of ischaemia. To monitor the heart metabolites during the protocol, the water-suppressed slice-selective STEAM sequence was used with a TR of 3 s, a TE of 20 ms, and a TM of 40 ms. A dephasing gradient of 1 G/cm was applied in the x-direction only during the two TE/2 periods, yielding a *b*-value of 9 s/mm^2. With 16 averages acquired for each scan, a time resolution of 0.8 min per spectrum was achieved. Thus, 25, 40, and 25 spectra were acquired during the perfusion, ischaemia and reperfusion, respectively.

5.2.2.2. Spectral processing and data analysis

All FIDs were zero-filled once and line-broadened by 5 Hz prior to FT. The peak heights of taurine (3.43 ppm), Cho/Car/Tau (3.26 ppm) and total creatine (3.03 ppm) were measured. In order to obtain shrinking and swelling rates from hearts, the signal intensities as a function of time were fitted to exponential equations. For simplicity it was assumed that the signal increase during ischaemia could be described by a first-order asymptotic exponential growth function,

$$S_{isch}(t) = S_{0,norm} + (S_{0,isch} - S_{0,norm}) \cdot (1 - \exp\{-k_{isch} \cdot t\}) \quad (5.1)$$

where $S_{isch}(t)$ represents the signal of a certain metabolite, $S_{0,norm}$ is the initial value prior

to ischaemia, $S_{0,isch}$ is its asymptotic value at the end of the ischaemic process, and k_{isch} is the rate of signal increase during the ischaemic shrinking process. The signal decay during reperfusion was assumed to be a decaying first-order exponential,

$$S_{reperf}(t) = S_{0,reperf} + (S_{0,isch} - S_{0,reperf}) \cdot \exp\{-k_{reperf} \cdot t\} \qquad (5.2)$$

where $S_{reperf}(t)$ is the signal time course during reperfusion, $S_{0,reperf}$ is its value at the end of the reperfusion period, and k_{reperf} represents the time constant during the swelling process.

5.2.2.3. HPLC experiment

Briefly, the result of the spectroscopy experiment indicated that taurine remained intracellularly during the ischaemia and reperfusion periods. In a separate experiment this was to be confirmed by using high-pressure liquid chromatography (HPLC) to test the effluent of rat hearts subjected to 32 min of low-flow ischaemia at a flow rate of 0.5 ml/min. Hearts from male Wistar rats with a mean body weight of 328 ± 16 g (n = 3) were perfused according to the methods described in Chapter 2. Samples of the effluent were collected from the apex of the heart, and the conditions of the equilibration period followed by KCl-arrest and low-flow ischaemia were matched to those employed in the NMR experiment. The total amount of released taurine during the perfusion and the ischaemic period was determined.

5.2.3. Results

5.2.3.1 NMR experiments

The buffer flow rate during perfusion was 19.4 ± 0.5 ml/min (n = 5), which was not significantly different from the flow rate during reperfusion. Two representative sagittal FLASH images from an isolated rat heart are shown in Fig. 5.2. The top image shows the heart during perfusion and the bottom image was acquired 3 min into total global ischaemia. Due to the cessation of the buffer flow the perfusion pressure dropped and the heart shrank (see distance between dashed lines in Fig. 5.2), thus increasing the number of cardiomyocytes in the selected spectroscopy slice.

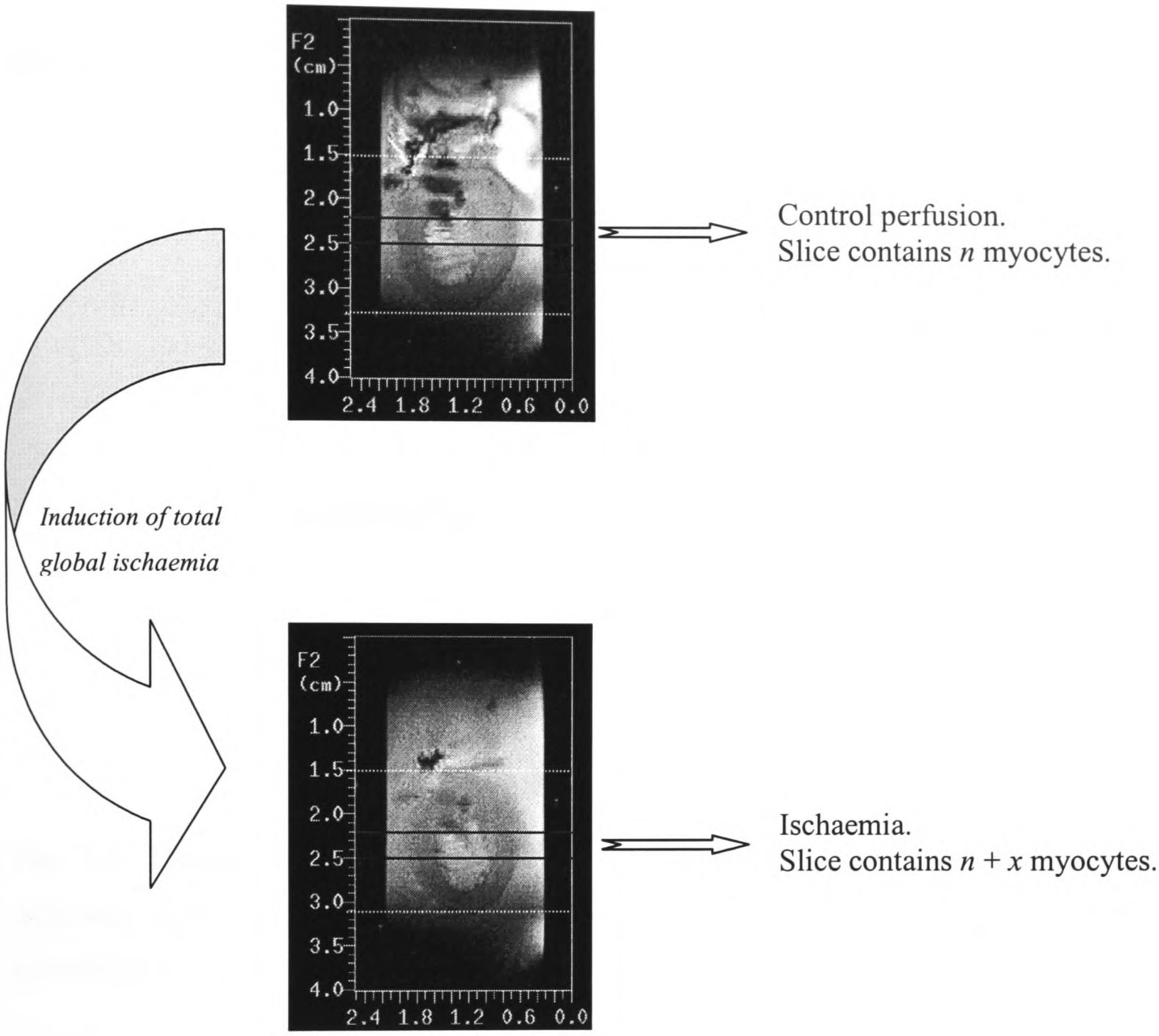

Fig. 5.2: Sagittal images of an isolated rat heart during control perfusion (top) and 3 min into ischaemia (bottom). Selecting a fixed 3 mm spectroscopy slice to monitor the ADC can lead to erroneous results because the number of myocytes in that slice changes with the perfusion state of the heart; here shrinkage of the heart, indicated by the dashed white lines, lead to an increase in cell number and consequently increased metabolite signal.

The average signal of the taurine peak (at 3.43 ppm) from all hearts during perfusion, total global ischaemia and reperfusion is shown in Fig. 5.3. The amplitude of the first point was normalised to 100 for each heart. There was a considerable signal increase just after induction of ischaemia, rising asymptotically to a value of around 128 at the end of

ischaemia. A sharp drop in the signal intensity was observed upon reperfusion, levelling out to the pre-ischaemic value after around 11 min.

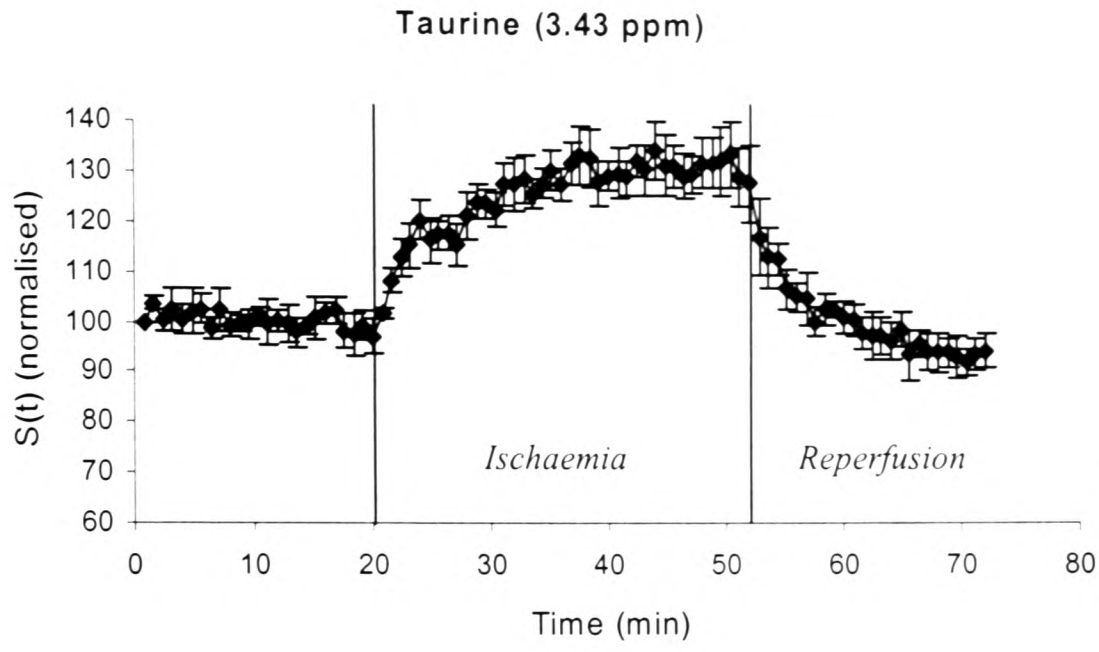

Fig. 5.3: Taurine signal S(t) of perfused rat hearts during perfusion, total global ischaemia and reperfusion. Data are means ± SEM (n = 5), with the first point normalised to a value of 100 for each heart.

Fig. 5.4 displays the Cho/Car/Tau peak signal intensity at 3.26 ppm as a function of time throughout the protocol. A similar pattern compared to that of the taurine peak was observed, with the signal increasing asymptotically to around 130 during the ischaemic period, followed by a sharp fall upon reperfusion.

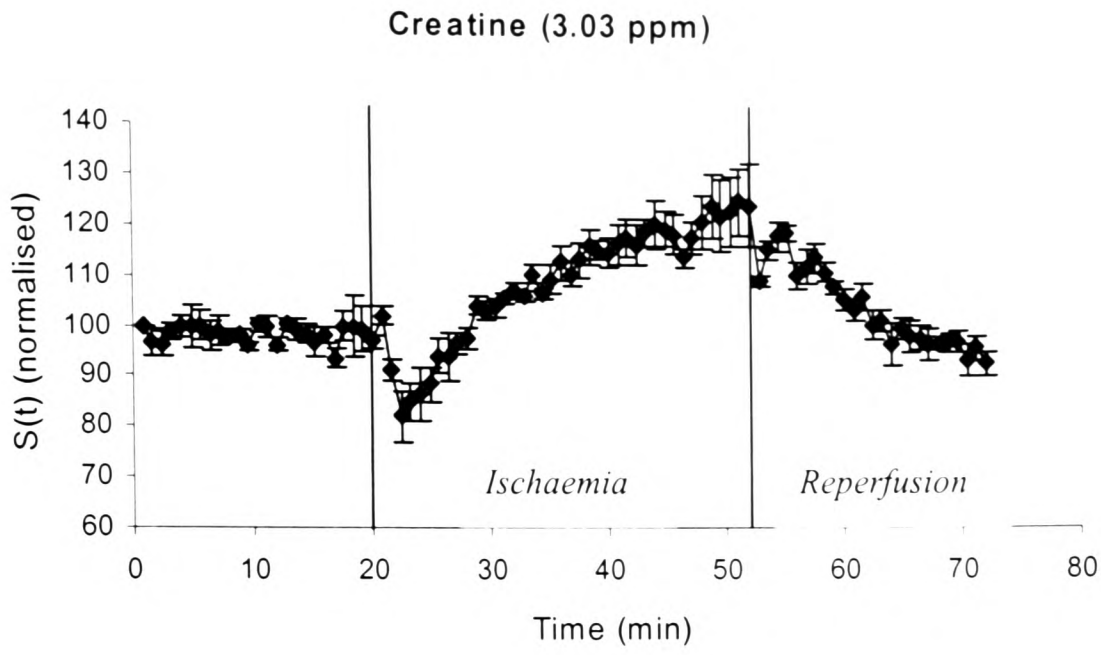

Fig. 5.4: Signal amplitude of the Cho/Car/Tau peak throughout the protocol. Note the similarity to the taurine signal (Fig. 5.3). Data are means ± SEM (n = 5), with the first point normalised to 100 for each heart.

In contrast, the total creatine peak at 3.03 ppm (Fig. 5.5) *fell* sharply to a value of about 80 upon induction of ischaemia and after about 2.4 min began to rise in an asymptotic fashion, similar to the rise in the taurine and Cho/Car/Tau signal. A maximum signal amplitude of 125 was reached more slowly than for the taurine and Cho/Car/Tau peaks. Furthermore, upon reperfusion the fall in the total creatine signal was not instantaneous but fluctuated for about 5.6 min, with a return to control values after 12 min.

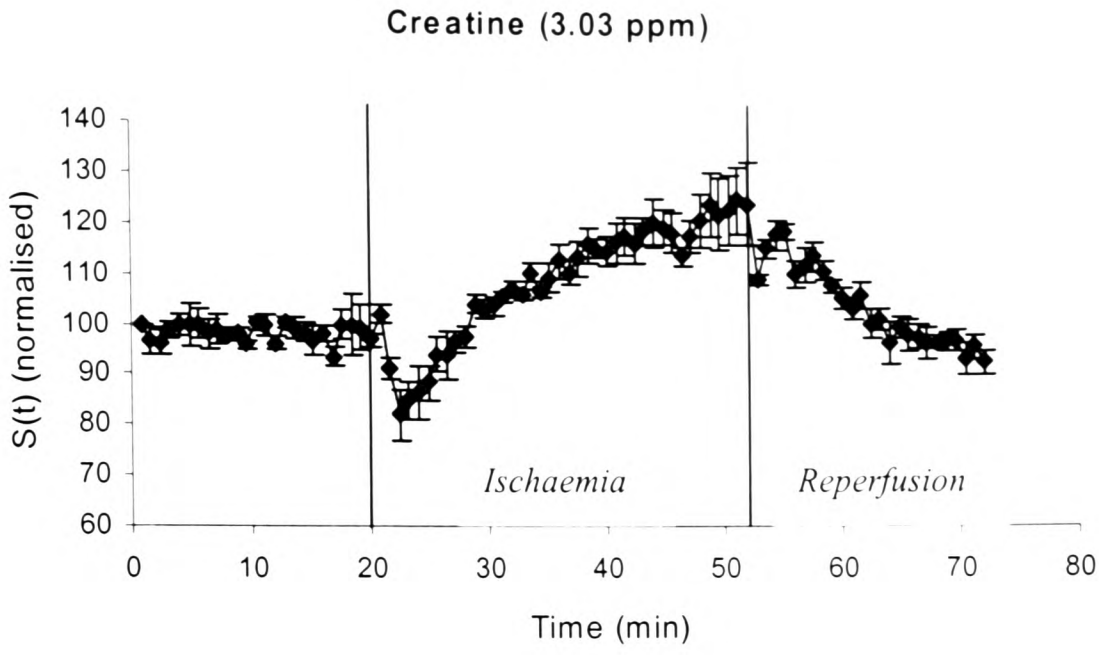

Fig. 5.5: Signal amplitude of the total creatine peak during the protocol. Note the initial sharp drop followed by a slower rise during ischaemia and a delayed return to control values during reperfusion. Data are means ± SEM (n = 5), with the first point normalised to 100 for each heart.

Using eq 5.1 and 5.2, the shrinking and swelling rates were calculated and listed in Table 5.5, together with the signal amplitudes during control perfusion, $S_{0,norm}$, at the end of ischaemia, $S_{0,isch}$, and at the end of reperfusion, $S_{0,reperf}$.

Table 5.5: Initial control ($S_{0,norm}$), end-ischaemia ($S_{0,isch}$) and end-reperfusion ($S_{0,reperf}$) signal values, and their respective shrinking and swelling rates for each of the metabolite peaks. Changes in the taurine and the Cho/Car/Tau peaks were similar but the total creatine behaved differently. Data shown are means ± SEM from all hearts (n = 5). [a]: Total creatine was fitted from the lowest point onwards during the ischaemic period. [*]: Significantly different from $S_{0,norm}$ of Cho/Car/Tau peak (p = 0.03). [†]: Significantly different from k_{isch} of taurine (p = 0.006) and Cho/Car/Tau (p = 0.01). [**]: Significantly different from k_{reperf} of Cho/Car/Tau (p = 0.02) and total creatine (p = 0.001). [††]: Significantly different from k_{isch} of Cho/Car/Tau (p = 0.008).

	Taurine (3.43 ppm)	Cho/Car/Tau (3.26 ppm)	Total creatine (3.03 ppm)
$S_{0,norm}$	97 ± 4	99 ± 2	97 ± 2
$S_{0,isch}$	128 ± 8	129 ± 6	124 ± 8
$S_{0,reperf}$	95 ± 3	92 ± 2[*]	96 ± 2
k_{isch} (min^{-1})	0.18 ± 0.02	0.16 ± 0.03	0.09 ± 0.02[a,†]
k_{reperf} (min^{-1})	0.22 ± 0.02[**]	0.30 ± 0.04[††]	0.05 ± 0.03

The taurine and the Cho/Car/Tau peak had similar increases in signal amplitudes during ischaemia and decreases during reperfusion. The rate of signal increase of the Cho/Car/Tau peak during reperfusion was slightly faster than its rate of decrease, and was also faster than the rate of signal increase of the taurine peak. The shrinkage rate of the total creatine signal during ischaemia was calculated from t = 2.4 min, when the signal had reached its minimum. The total creatine peak showed a slower rate of signal increase during ischaemia compared to the taurine and Cho/Car/Tau peak. It also appeared to take longer to return to the control signal levels upon reperfusion.

5.2.3.2. HPLC experiment

The total amount of taurine lost from the perfused heart was 0.75 ± 0.12 mM during control perfusion, and 0.55 ± 0.15 mM during 32 min low-flow ischaemia. Assuming a taurine concentration of 40 mM in the rat heart (Huxtable 1978; Huxtable 1992), this corresponds to losses of 1.9 ± 0.3% and 1.4 ± 0.4%, respectively.

5.2.4. Discussion

5.2.4.1. The observed changes in signal amplitude

A number of factors might contribute to the observed signal changes during ischaemia and reperfusion. They include changes in the available magnetisation, S_0, the metabolite's ADC, and its longitudinal and transverse relaxation times. This is reflected in the following equation, relating the signal intensity *S(t)* of the partially saturated STEAM sequence to S_0, the ADC, T_1 and T_2:

$$S(t) = \frac{1}{2} S_0 \exp\left\{-TE/T_2\right\} \exp\left\{-TM/T_1\right\} \cdot \left(1 - \exp\left\{-TR/T_1\right\}\right) \exp\{-b \cdot ADC\} \qquad (5.3)$$

This section discusses which of these four factors is most likely to be the cause of the signal changes.

The ADC

The ADC might change during ischaemia due to a change in the intracellular viscosity and/or the degree of hindrance in the cytoplasm (see, for instance, (Kao et al. 1993); for a detailed discussion see Chapter 4). However, the parameters for the water-suppressed

slice-selective STEAM sequence were chosen so as to yield minimum diffusion-related signal losses, with $b = 9$ s/mm^2, so that changes in the ADC would not significantly contribute to the change in signal amplitude.

Relaxation times

Assuming typical sequence parameters (TE of 20 ms, TM of 40 ms, TR of 3 s, $b = 9$ s/mm^2), T_1 relaxation times for taurine (5.39 s) and total creatine (2.83 s), and T_2 relaxation times for both metabolites of around 50 ms (Schneider et al. 1998), the effect of relaxation time changes on the observed signal can be estimated using eq 5.3. In order to obtain a 30% increase in signal, the T_2 would have to treble to around 145 ms within 16 min of ischaemia, which is roughly when the taurine signal amplitude reached its maximum value. Unfortunately there are no data in the literature on relaxation time measurements of intracellular heart metabolites, but it was shown in rat brain that metabolite T_2 times remained constant for at least 20 min of total global, or 3-6 h local ischaemia (Fujimori et al. 1998; van der Toorn et al. 1995). In addition, T_1 times would have to be reduced by 32% to 3.69 s for taurine and by 46% to 1.53 s for total creatine in order to achieve a 30% increase in the observed signal. Again, such changes are unlikely to have occurred within 16 min of ischaemia. T_1 relaxation times of the major brain metabolites remained constant during 3-6 h of focal cerebral ischaemia in the rat (van der Toorn et al. 1995). Thus changes in relaxation times are unlikely to have occurred during 16 min of ischaemia in the perfused rat heart. Similarly, the return of the signal to control values during reperfusion was even faster and would imply a reversal of the initial relaxation time changes. Again, this is quite unlikely within this short period.

Changes in the available magnetisation

Assuming that perfused hearts shrank by 30-40% during ischaemia (Liess et al. 1996), and that the dry weight/wet weight ratio decreased by about 40% (Clarke et al. 1994), a similar degree of signal increase was expected. This was observed for taurine, which is not metabolised (Crass and Lombardini 1978; Huxtable 1992), does not bind to proteins in the cytoplasm (Chapman et al. 1993; Suleiman et al. 1992), and is lost in negligible amounts from the ischaemic rat heart. Hence, from the exclusion of ADC and relaxation time related signal increases, and from the shrinking process during ischaemia, it can be concluded that the signal changes were due to shrinking and swelling of the perfused heart. Thus taurine is an ideal molecule to provide information about the extent of macroscopic shrinkage of the perfused rat heart during the ischaemic period. While this explanation is valid for inert molecules such as taurine, it cannot satisfy the observed signal changes of the total creatine peak, as will be discussed shortly.

5.2.4.2. Signal behaviour of taurine

The amplitude of the taurine signal at the end of control perfusion was not significantly different from that at the end of reperfusion, suggesting that, with the perfusion protocol employed here, taurine remained in the cells and did not act as an osmoregulator in the rat heart, as has been suggested by others (Leem et al. 1996; Thurston et al. 1981). This is supported by the HPLC data, demonstrating that only 1.4% of the total taurine content of the rat heart was released during ischaemia. A similar conclusion has been made by others (Chanin et al. 1956; Crass and Lombardini 1978; Huxtable 1978; Ugurbil et al. 1984). It has been shown in the isolated ischaemic guinea-pig heart that taurine was released in significant amounts only after the intracellular Na^+ concentration ($[Na^+]_i$) exceeded 20 mM (Chapman et al. 1993; Suleiman et al. 1992). Since there was hardly any

taurine released during the ischaemic period, it can be concluded that the $[Na^+]_i$ remained below 20 mM.

The change in the taurine signal amplitude during ischaemia appeared to exhibit a fast component in the beginning, attributed to the decrease in the perfusion pressure and the collapse of the vasculature, and a slower component due to loss of water; this has been observed before (Clarke et al. 1993).

5.2.4.3. Effect of observed signal changes on taurine ADC measurements

The observed signal changes during ischaemia and reperfusion have an effect on the measured ADC. As taurine is inert in the cytosol, the taurine data may be used to simulate the degree of ADC under- and overestimation during shrinking and swelling (Appendix D). Briefly, the simulation demonstrates that the ADC would be underestimated by around 23% at the beginning of the ischaemic period due to the shrinking process, and overestimated by 26% upon reperfusion due to the swelling process. This data can be used to correct ADCs obtained in later experiments for shrinking and swelling effects. Note that the above estimations do not apply for the total creatine, as it had a further underlying mechanism contributing to the observed signal changes (see below).

5.2.4.4. Signal behaviour of the Cho/Car/Tau peak

The Cho/Car/Tau signal appeared similar to that of taurine in terms of signal amplitudes and shrinking and swelling rates. However, the final value the Cho/Car/Tau signal reached at the end of the reperfusion period was significantly lower than during perfusion. Assuming that there was no difference in the relaxation times, the signal difference between the control and reperfusion period can be attributed to a reduction of the available magnetisation. Since the taurine content did not change significantly as

demonstrated in Fig. 5.3, the observed difference of the signal must be attributed to a signal reduction in either the choline-containing compounds or carnitine. The washout of such a compound during reperfusion might also explain the slightly higher rate of signal decay for Cho/Car/Tau compared to taurine. Although ischaemia affects choline metabolism in the heart by a subsequent redistribution in the amounts of the various choline-containing compounds (Choy et al. 1992; Rabkin 1993), the overall concentration of the choline-containing compounds of around 1.3 mM has been shown to remain constant (Choy et al. 1992; Lochner and de Villiers 1989). It was shown in the rat heart that the total carnitine pool of 2-3 mM was reduced by about 10% after 30 min of total global ischaemia (Idell-Wenger et al. 1978; Shug et al. 1978). Hence it might be speculated that the small signal reduction of the 3.26 ppm peak observed when comparing the perfusion period to the reperfusion period could be due to carnitine release. Measurement of the total carnitine content in the effluent should clarify this point.

5.2.4.5. Signal behaviour of the total creatine peak

There was no significant difference between the creatine signal amplitude at the end of control perfusion and reperfusion. This is in line with the findings of Kupriyanov and colleagues who, using HPLC, observed a constant total creatine pool in KCl-arrested pig hearts subjected to an ischaemic period of 45 min (Kupriyanov et al. 1995). The fact that the total creatine signal and the taurine signal returned to baseline values suggests that the sarcolemma remained intact during and after ischaemia.

The total creatine signal was modulated by another effect, in addition to the shrinking and swelling process, which caused the initial signal decrease upon induction of ischaemia and the delayed return to control values upon reperfusion. The following factors might be responsible for this behaviour. The 3.03 ppm total creatine peak is composed of PCr and

creatine, and during ischaemia the PCr is rapidly converted to creatine (see Chapter 2). Relaxation time changes might play a role in the observed signal decay; assuming that the PCr has a longer T_2 time constant than creatine, then once the PCr has been metabolised to creatine, the 3.03 ppm peak has the relaxation behaviour of creatine alone. This, being shorter, will lead to a decreased signal intensity. However, this cannot explain why the total creatine signal increases faster during ischaemia than the taurine signal, which, if the assumption is correct, would suggest that creatine was partly rephosphorylated during ischaemia. As shown in Chapter 2, this was not the case.

Hence the observed signal change must be due to changes in the available magnetisation. Because the total creatine concentration was constant throughout ischaemia, the decreased signal cannot be a consequence of creatine compounds leaving the cell, but must be due to a change in the NMR-visibility of these compounds. The PCr has been shown to be fully NMR-visible during ischaemia in the perfused rat heart (Garlick and Humphrey 1989; Humphrey and Garlick 1991; Takami et al. 1988), hence the observed changes must be related to the creatine signal. It is well known that chemical exchange of a free metabolite with its bound counterpart can lead to line broadening of the free metabolite peak, making it NMR-invisible (Garlick and Townsend 1992; Turner and Garlick 1984). Alternatively, part of the creatine might bind to macromolecules, thereby reducing its T_2 with a consequent decrease in NMR-visibility (Gadian 1996; Jeffrey et al. 1989).

Because of insufficient data, no rigid conclusions can be made concerning the origin of the decreased creatine signal. Whatever the reason may be, the only safe conclusion from the available experimental data is that creatine must exist in a bound and a free pool in the cytoplasm (Lee and Visscher 1961; Savabi 1988).

5.2.5. Conclusion

The observed signal changes in the taurine, the Cho/Car/Tau and the total creatine peak were due to changes in the available magnetisation. For the taurine peak this was caused purely by the shrinking and swelling process, whereas the Cho/Car/Tau peak displayed an additional signal loss, possibly due to the partial release of carnitine. The total creatine signal behaviour reflected the shrinking and swelling process, and a modulating effect, possibly related to the interaction of two creatine compartments during ischaemia. The obtained graphs of the signal behaviour were used to calculate the 'true' ADC values for these metabolites in later experiments, free from shrinking and swelling effects.

5.3. Final conclusion

The fibre orientation in the perfused rat heart did not affect the measurement of the diffusion process, whereas shrinking and swelling due to ischaemia and reperfusion did. It was found that it is sufficient to measure scalar ADC values instead of the time-consuming diffusion tensors, allowing dynamic changes of intracellular heart metabolites ADCs to be monitored with better time resolution. Changes in the available magnetisation due to shrinking and swelling effects can lead to substantial under- and overestimation of the ADC values. The signal behaviour of the taurine and the total creatine peak during ischaemia and reperfusion were recorded and served in later work to correct ADCs for shrinking and swelling effects.

Chapter 6

Intracellular metabolite ADCs in the isolated rat heart during perfusion, ischaemia and reperfusion

Abstract

The aim of the work in this chapter was to measure the ADCs of taurine and total creatine during perfusion, total global ischaemia and reperfusion in the isolated, KCl-arrested rat heart. Using the water-suppressed slice-selective STEAM sequence, the taurine ADC was found to remain constant during 28 min of total global ischaemia, while the total creatine ADC increased by 35% to return to control values upon reperfusion. For both metabolites the respective S_0 corrections, determined in Chapter 5, were performed. In order to assess the severity of the induced ischaemia, ^{31}P-NMR experiments were conducted with the aim to determine cardiac energetics and pH_i during 32 min of total global ischaemia in KCl-arrested rat hearts. In those hearts, PCr disappeared after 10 min and ATP gradually declined but was still detectable by the end of the ischaemic period, suggesting that the degree of ischaemia was not severe. In addition, from the ^{31}P-NMR spectroscopy experiments described in Chapter 2, it was known that there was little or no cell swelling. Thus, it can be hypothesised that the taurine ADC remained constant either because cells did not swell, or because cell swelling was accompanied by organelle swelling. Furthermore, the increase in the total creatine ADC could be explained by PCr hydrolysis to creatine during ischaemia and creatine rephosphorylation during reperfusion.

6.1. Introduction

Myocytes in a perfused or an *in vivo* heart undergo major structural alterations during and after an ischaemic incident. It has been hypothesised that they swell in response to the increase in intracellular osmolarity during ischaemia (Jennings et al. 1985; Steenbergen et al. 1985; Tranum-Jensen et al. 1981). For instance, the total water volume in perfused porcine hearts increased by 16.5% after 1 h of LAD coronary artery occlusion, with this increase probably equally distributed between intracellular and extracellular space (Tranum-Jensen et al. 1981). Others have demonstrated a similar level of swelling using specific radiolabeled total and extracellular space markers during low-flow ischaemia in the dog heart (Powers et al. 1984), or have inferred intracellular volume changes from the altered distribution of an extracellular marker during total global ischaemia in the rat heart (Knopf et al. 1990). Cardiomyocyte organelles also swell during ischaemia (Edoute et al. 1983; Greve and Grong 1991; Jennings et al. 1985; Murphy et al. 1987). For example, after 15 min of total global ischaemia in the rat heart, mitochondria were swollen with the cristae separated, and intra-myofibrillar spaces appeared with the occasional tearing of myofibrils (Edoute et al. 1983). After 25 min of total global ischaemia, mitochondria were severely swollen and occasionally ruptured, inter-myofibrillar oedema was present, but the sarcolemma was still intact. Following a 40 min period of total global ischaemia, subepicardial myocytes resumed their normal structure (Edoute et al. 1983). In severe ischaemia of over 60 min, disruption of the plasma membrane was observed, and subsarcolemmal blebs, a sign of irreversible ischaemic damage, formed (Greve et al. 1990; Steenbergen et al. 1985), with organelles appearing very severely swollen and often lysed (Edoute et al. 1983).

Such structural changes would alter the movement of small molecules in the cytosol of the cardiomyocytes. The swelling of the mitochondria and the fragmentation of other

organelles could cause intracellular motion to be more restricted. In addition, the breakdown of larger molecules, such as glycogen, could increase the cytosolic viscosity. Both occurrences would decrease the observed ADC, as shown in the ischaemic rat brain (van der Toorn et al. 1996a; Wick et al. 1995). On the other hand, cell swelling due to the accumulation of intracellular osmolytes (Steenbergen et al. 1985; Tranum-Jensen et al. 1981) would increase the mobility of small molecules in the cytosol. Furthermore, binding of the diffusing molecules to macromolecules or cellular organelles might change, causing either an increase (reduced binding) or a decrease (increased binding) in the ADC (Nilsson and Lindman 1983).

Thus, the aim of the work in this chapter was to measure the ADC of intracellular metabolites during perfusion, total global ischaemia and reperfusion in the isolated rat heart. A short diffusion time was chosen in order to probe the intracellular environment, with the effect of sarcolemmal membranes being small. With structural changes occurring during ischaemia, changes in the metabolite ADCs might be a sensitive measure of the severity of the ischaemic damage to the heart. The severity of the induced ischaemia during the ADC experiment was assessed in a second experiment by ^{31}P-NMR spectroscopy. Substrate-perfused hearts were KCl-arrested and subjected to 32 min of total global ischaemia and their energetics and pH_i monitored.

6.2. Methods

6.2.1. ADC measurements in perfused hearts

Hearts from male Wistar rats with a mean body weight of 355 ± 29 g (n = 4) were excised and perfused according to the methods described above. The protocol consisted of 10 min of perfusion, 28 min of total global ischaemia, and 15 min of reperfusion. The effluent

flow rate was measured during perfusion and at 5 min intervals during reperfusion. The water-suppressed slice-selective STEAM sequence was used with a TR of 2.1 s, a TM of 40 ms, and a TE of 20 ms. Five diffusion gradients from 1-13 G/cm in 3 G/cm steps were applied in the x-direction, corresponding to *b*-values from 9 s/mm^2 to 1466 s/mm^2. With 16 scans averaged for each *b*-value, a single ADC value could be measured within 2.8 min.

The ADCs of the taurine (3.43 ppm) and the total creatine peak (3.03 ppm) were calculated for each section of the protocol. Both compounds were shown to remain in the cell during prolonged ischaemia in the KCl-arrested heart (see Chapter 5). The necessary S_0 corrections for the taurine and the total creatine, to allow for effects caused by changes in the perfusion pressure during ischaemia and reperfusion, were taken directly from Chapter 5, Figs. 5.3 and 5.5. As discussed, these corrections eliminate artefacts from the change in the available magnetisation, and not changes in the ADC. Because different TRs were employed in the S_0 measurements, the time points were different and were corrected by factors obtained by interpolation from the S_0 data acquired in Chapter 5.

6.2.2. Solutions

It is known that the composition of the total creatine peak changes during ischaemia, in that PCr is hydrolysed to creatine. Assuming that the ADC of the total creatine is the sum of the ADCs of PCr and creatine, weighted by their relative concentrations, the loss of PCr during ischaemia would increase the ADC of the total creatine, as the 'effective' hydrodynamic radius (R_H) of the total creatine would be reduced. To obtain the R_H of PCr and creatine, a 30 mM PCr and a 30 mM creatine solution in double-distilled water were prepared and their diffusion coefficients measured using the water-suppressed slice-selective STEAM sequence with a TR of 3 s, a TM of 40 ms, a TE of 20 ms and 16

averages. Sixteen *b*-values were used with gradient strengths ranging from 1-16 G/cm in steps of 1 G/cm, being applied in the x-direction. Diffusion coefficients were obtained from semi-logarithmic plots of the signal intensities as a function of their respective *b*-values. Both creatine peaks at 3.95 ppm and at 3.03 ppm were analysed and the diffusion coefficient taken as the mean value of the diffusion coefficients of the two peaks. The experiment was repeated five times with the temperature recorded for each measurement. The hydrodynamic radii were calculated according to the Stokes-Einstein relation (eq 1.5). FIDs obtained from the phantom solutions and the perfused hearts were zero-filled once and line-broadened by 5 Hz prior to FT.

6.2.3. ^{31}P-NMR on perfused hearts

Hearts from male Wistar rats with a mean body weight of 376 ± 12 g (n = 4) were perfused according to the methods described in Chapter 2. After acquisition of a fully relaxed and a partially saturated ^{31}P control spectrum, hearts were subjected to 32 min of total global ischaemia. The buffer was a standard Krebs-Henseleit solution containing 11 mM glucose and 1 mM Na-pyruvate as substrates. A capillary containing 10 μmoles of MPA was positioned next to the heart as external reference. Data acquisition, FID processing and absolute quantification of metabolite concentrations was performed as above. The pH_i was measured from the chemical shift of the P_i peak relative to the PCr using the equation

$$pH_i = 6.72 + \log\left(\frac{x - 3.72}{5.72 - x}\right) \tag{6.1}$$

where x is the ppm position of the P_i peak in the ^{31}P spectrum (Clarke et al. 1993).

6.3. Results

6.3.1. ADC measurements in perfused hearts

The coronary flow rate was 19.0 ± 0.8 ml/min during the perfusion period, which was not significantly different after 15 min of reperfusion. Fig. 6.1*a* displays the 3-4 ppm region of spectra acquired from a single heart with five *b*-values during the perfusion period.

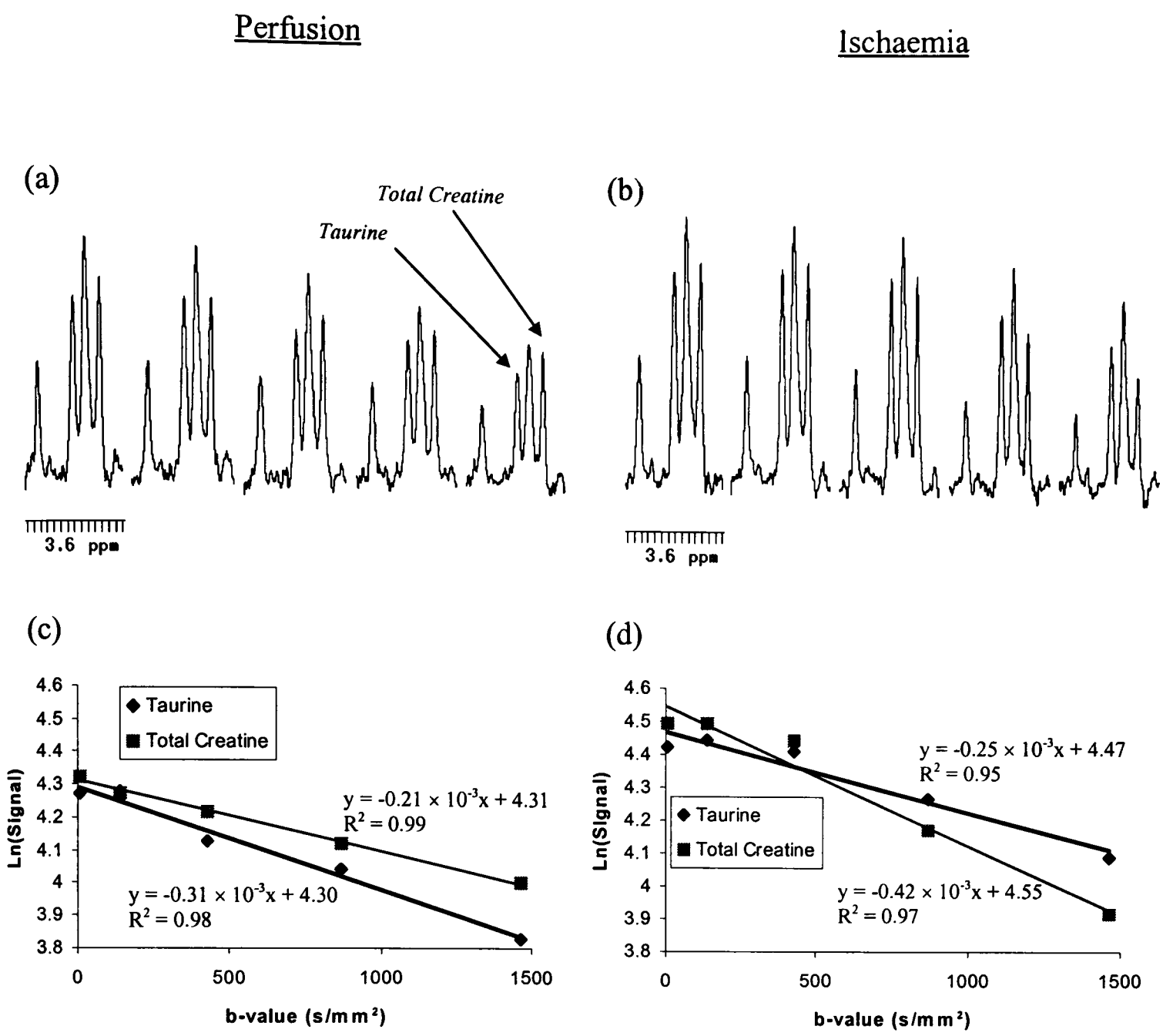

Fig. 6.1: (a) + (b), 3-4 ppm regions from five spectra acquired with b-values from 9 s/mm² (first spectrum) to 1466 s/mm² (last spectrum); (a), perfusion, (b), just after induction of ischaemia. (c) + (d), semi-logarithmic decay curves for the taurine (3.43 ppm) and the total creatine peaks (3.03 ppm) with their respective linear fits; (c), perfusion, (d) just after induction of ischaemia. Note the increase in the slope of the logarithmic total creatine signal decay.

The four peaks are from total creatine (3.95 ppm), taurine (3.43 ppm), Cho/Car/Tau (3.26 ppm) and the second total creatine peak at 3.03 ppm. Fig. 6.1*b* displays similar spectra acquired immediately after induction of ischaemia. The total creatine signal decayed more rapidly during ischaemia compared to the perfusion period (Fig. 6.1*b* *vs.* 6.1*a*). The semi-

logarithmic decay curves, and the best linear fits, for total creatine (3.03 ppm) and taurine (3.43 ppm) are shown in Fig. 6.1*c* and 6.1*d*. The decay rate of the total creatine peak doubled upon the induction of ischaemia whereas the taurine decay rate appeared to be less compared to perfusion. Note that these data are uncorrected for the effects caused by the changes in the perfusion pressure, and that the quality of the fits was reduced, presumably due to the S_0 changes occurring during the initial phase of ischaemia.

6.3.2. Taurine ADC

The S_0-corrected ADCs for taurine during the protocol are shown in Fig. 6.2. The correction values were obtained from the taurine data acquired in Chapter 5, and the uncorrected data are shown in Appendix E.

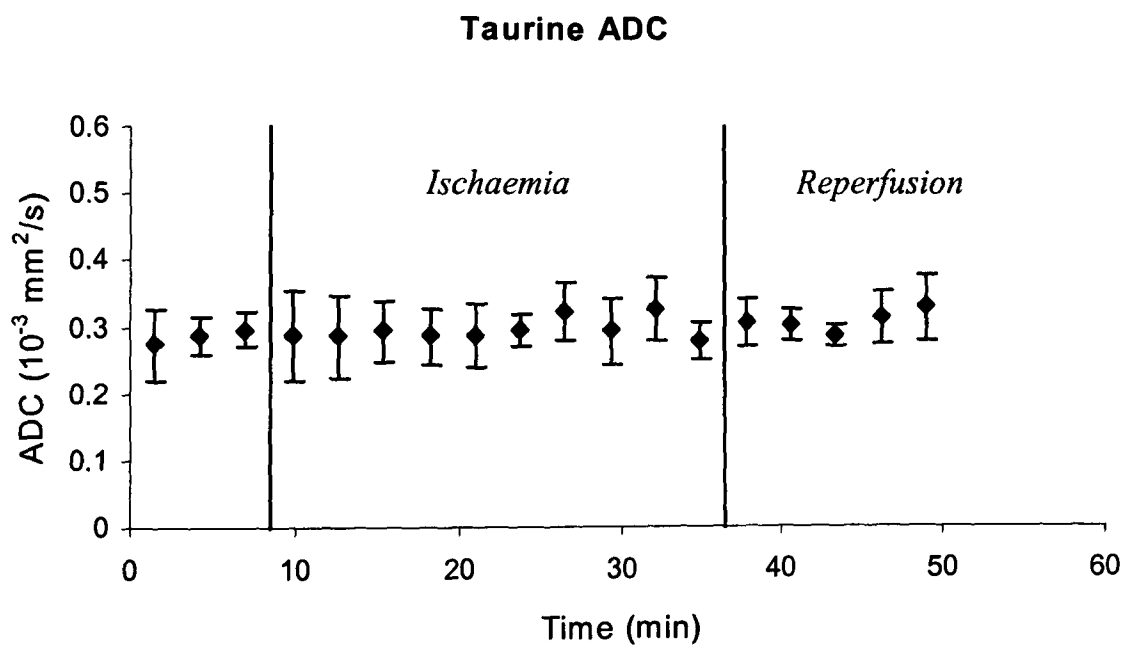

Fig. 6.2: The taurine ADC during perfusion, total global ischaemia and reperfusion, corrected for experimental artefacts in the ADC estimation caused by the increased signal due to less oedema with the loss of perfusion pressure in ischaemia, and the increased oedema due to restoration of perfusion pressure during reperfusion (obtained from Chapter 5).

There was no change in the taurine ADC throughout the protocol. During the perfusion period for all hearts it was $(0.29 \pm 0.01) \times 10^{-3}$ mm^2/s, and during ischaemia it was $(0.29 \pm 0.02) \times 10^{-3}$ mm^2/s. Similarly, the ischaemia ADC was not significantly different from the reperfusion ADC, which was $(0.31 \pm 0.02) \times 10^{-3}$ mm^2/s.

6.3.3. Total creatine ADC

The ADCs for the total creatine during the protocol after S_0 corrections are shown in Fig. 6.3 (see Appendix E for uncorrected data).

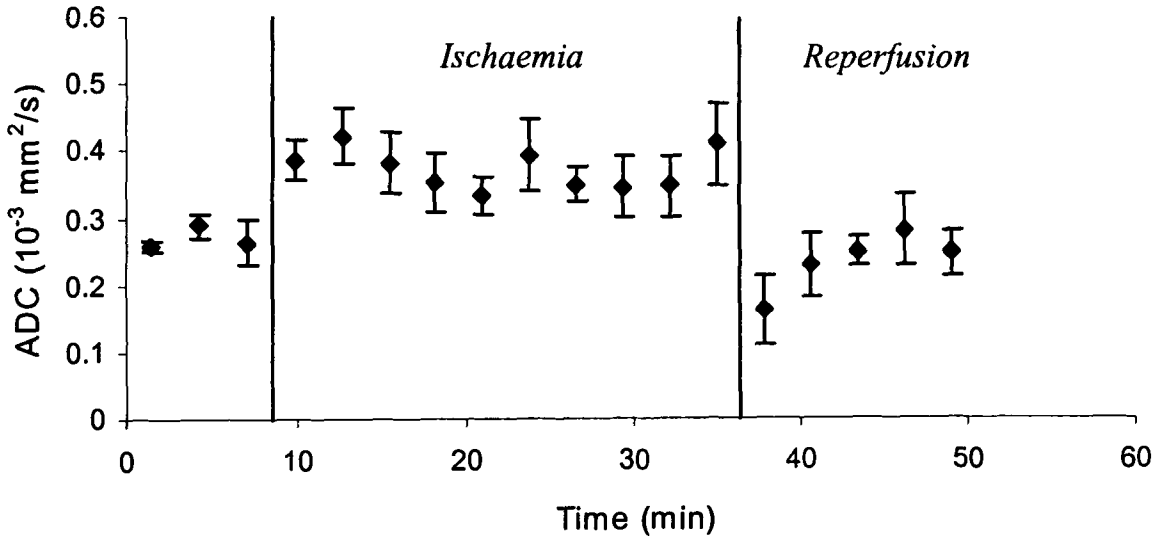

Fig. 6.3: Total creatine ADC during the protocol, corrected for the loss and reintroduction of oedema with the change in the perfusion pressure during ischaemia and reperfusion.

During perfusion the ADC of the total creatine was $(0.27 \pm 0.02) \times 10^{-3}$ mm^2/s, which increased significantly ($p = 0.0002$) during ischaemia by 35% to $(0.37 \pm 0.03) \times 10^{-3}$

mm^2/s. The total creatine ADC during reperfusion was $(0.26 \pm 0.02) \times 10^{-3}$ mm^2/s, which was significantly lower ($p = 0.0001$) than the total creatine ADC during ischaemia, but not different from that during perfusion. Hence, the total creatine ADC increased by 35 ± 9% during ischaemia.

6.3.4. PCr and creatine solutions

The ADCs of creatine and PCr in solution were obtained from 16 spectra acquired with increasing *b*-values corresponding to gradient strengths from 1-16 G/cm (Fig. 6.4*a* and 6.4*b*).

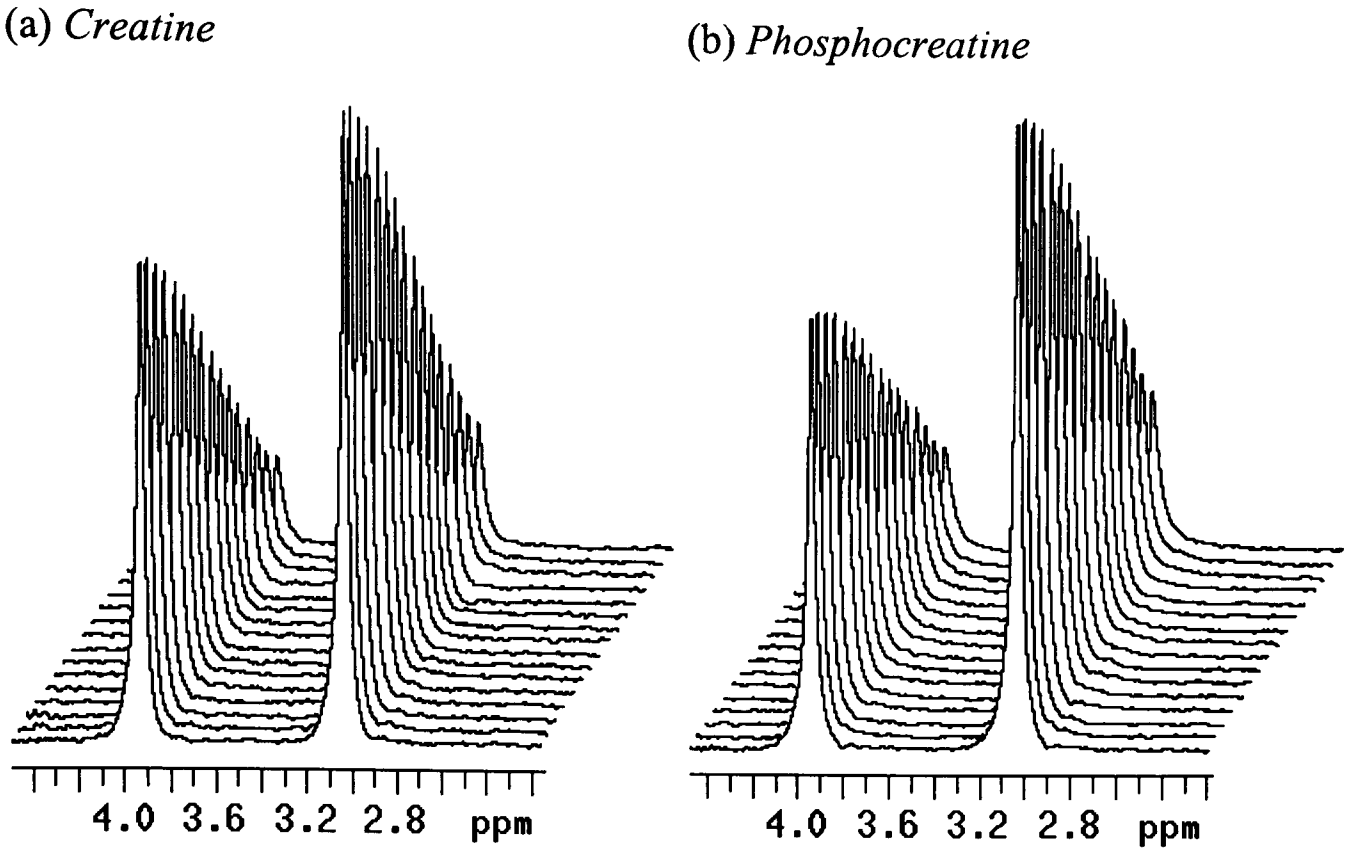

(c)

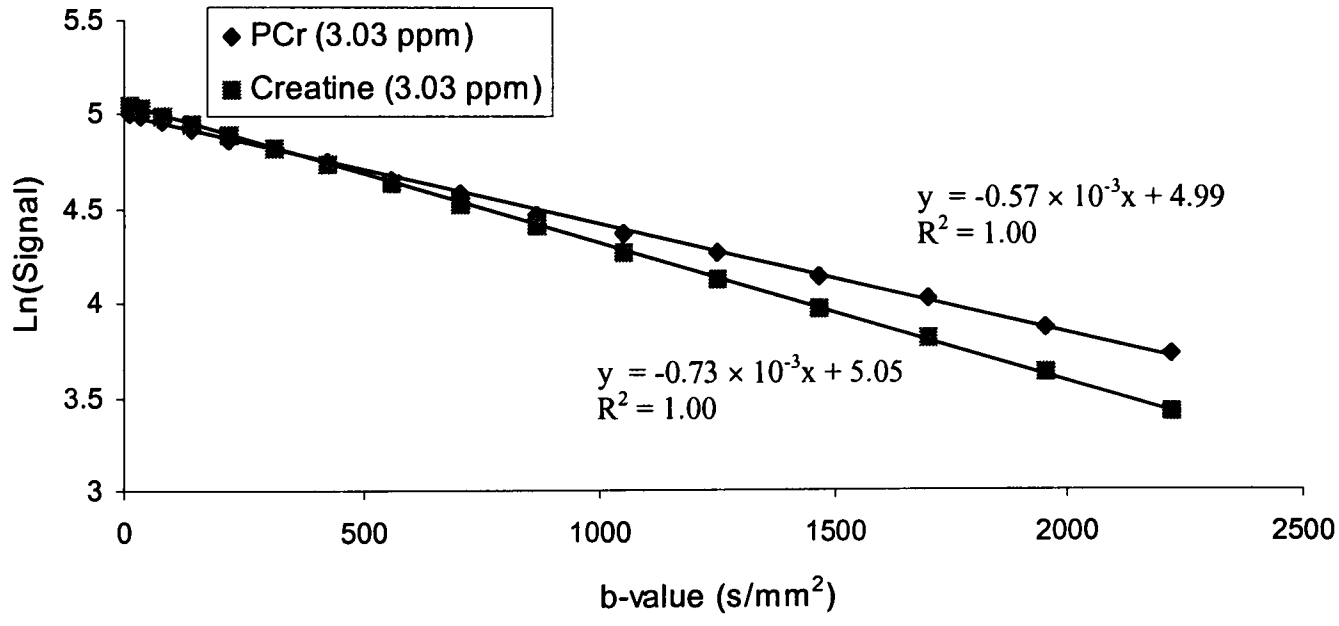

Fig. 6.4: Sixteen spectra acquired from 30 mM solutions of creatine (a) and PCr (b) with increasing b-values. The semi-logarithmic graph of the signal intensities as a function of the b-values in (c) demonstrates that creatine diffuses faster than PCr.

The PCr decayed at a 28% slower rate than creatine, more clearly seen in the semi-logarithmic plots and best linear fits in Fig. 6.4*c* for the two solutions. Using the Stokes-Einstein relation (eq 1.5), the hydrodynamic radii for creatine and PCr were calculated (Table 6.1), with the hydrodynamic radius of PCr being 34 ± 3% larger than that of creatine.

Table 6.1: Hydrodynamic radii of creatine and PCr in solution. Data are means ± SEM from n = 5 measurements.

	PCr	Creatine
Hydrodynamic radius, R_H (Å)	3.92 ± 0.09	2.92 ± 0.02

6.3.5. ^{31}P-NMR on perfused hearts

The absolute concentrations of PCr, ATP and P_i from all hearts during 32 min of total global ischaemia in the presence of substrates are shown in Fig. 6.5. The initial concentrations were not different from those measured in substrate-perfused low-flow ischaemia hearts (see Fig. 2.2*b*).

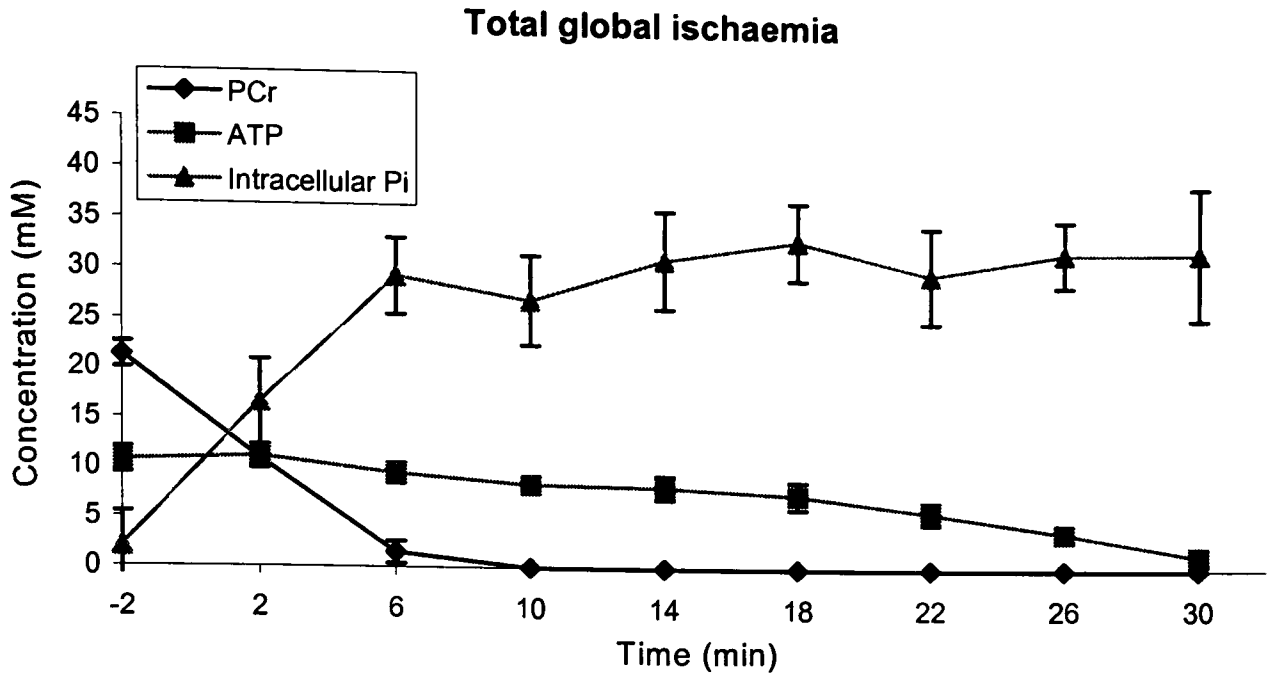

Fig. 6.5: PCr, ATP and Pi concentrations during 32 min of total global ischaemia of KCl-arrested, substrate-perfused hearts.

During total global ischaemia the PCr had disappeared after 10 min, and the ATP concentration gradually declined to 1.4 ± 0.9 mM by the end of ischaemia. The P_i concentration increased rapidly after the onset of ischaemia and reached a constant level after about 14 min.

The pH_i during the intervention is shown in Fig. 6.6. It remained constant for the first two minutes after the start of total global ischaemia, but then fell from 7.11 ± 0.09 to 5.90 ± 0.09 at the end of the ischaemic period.

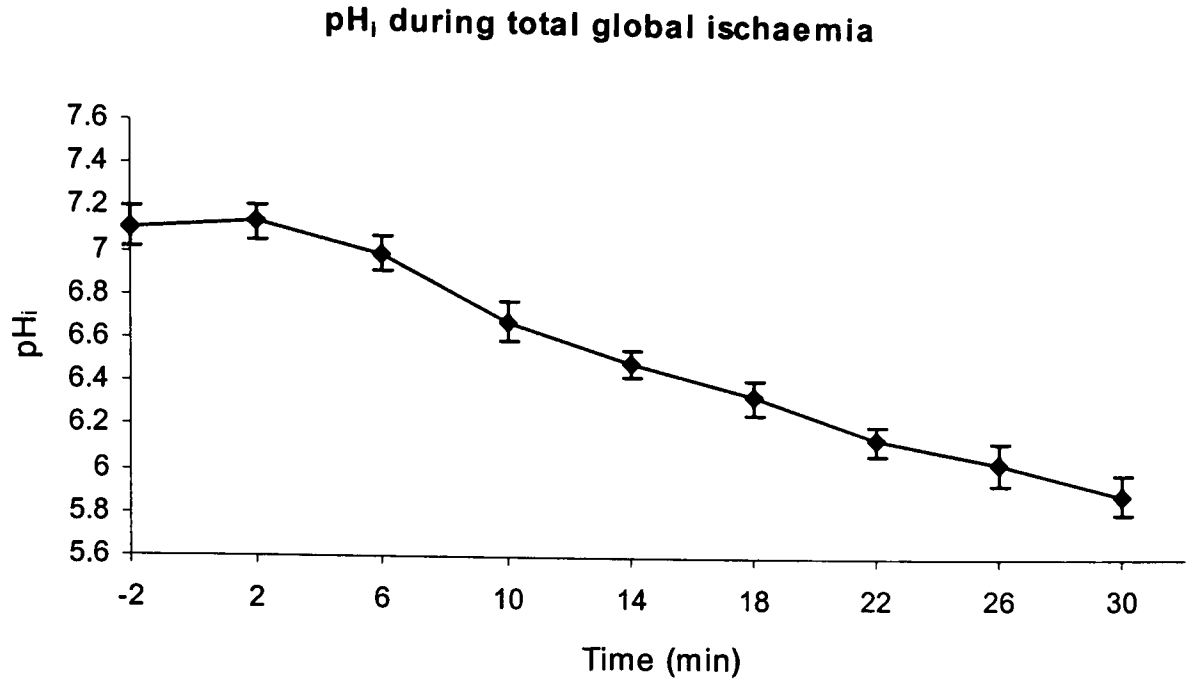

Fig. 6.6: Intracellular pH during 32 min of total global ischaemia in the KCl-arrested rat heart in the presence of substrates.

6.4. Discussion

6.4.1. Structural changes during ischaemia

Any ischaemia-induced structural changes in cardiomyocytes would alter the motional freedom of small, diffusing substances in the cytosol. A detailed study by Edoute and co-workers (Edoute et al. 1983) on structural changes in rat cardiomyocytes during ischaemia demonstrated that, during a 25 min period of total global ischaemia, moderate mitochondrial swelling and inter-myofibrillar spaces occurred, but the sarcolemma remained intact. These effects were fully reversible upon reperfusion. However, the severity of the ischaemic insult in the presented experiments was milder than that reported above (Edoute et al. 1983), because of the protective effect of KCl-arrest (Drewnowska et al. 1991; Flaherty et al. 1982; Nishiki et al. 1978). This was reflected in the present study by the fact that hearts started beating spontaneously after the 20 min

reperfusion period when perfused with standard Krebs-Henseleit solution (data not shown). Also, as demonstrated in Fig. 6.5, ATP was lost relatively slowly during ischaemia and was still detectable after 32 min of ischaemia. Based on the S_0 measurements in the previous chapter, there was no loss of intracellular taurine, thus it is unlikely that the intracellular Na^+ concentration rose above 20 mM (Suleiman and Chapman 1993). Furthermore, the total creatine peak recovered fully after 32 min of ischaemia, indicating that there was no sarcolemmal damage, with no leakage of creatine. Finally, coronary flow rates measured during the reperfusion period were not significantly different from control values. Thus, the severity of ischaemia was mild and cell swelling was probably absent.

6.4.2. Metabolite ADC changes during ischaemia

This is the first report of metabolite ADCs in the perfused heart. Most of the measurements of acute intracellular metabolite ADC changes under ischaemic and reperfusion conditions have been carried out in brain (Duong et al. 1998; Henriksen et al. 1995; Nicolay et al. 1995; van der Toorn et al. 1996a; Wick et al. 1995), where the ADC of intracellular metabolites such as total creatine, choline-containing compounds or NAA was shown to be decreased during acute ischaemia (Nicolay et al. 1995; van der Toorn et al. 1996a; Wick et al. 1995). For instance, van der Toorn and co-workers (van der Toorn et al. 1996a) reported a reduction in the total creatine and the NAA ADC in the ischaemic rat brain by 29% and 19%, respectively, which was tentatively attributed to a possible increase in hindrance due to dissociation of microtubules and fragmentation of other cellular components or macromolecules. Wick and colleagues (Wick et al. 1995) reported a decrease in the NAA ADC of 17% and a total creatine ADC decrease of 48% after 20 min of global forebrain ischaemia in the rat. They suggested that the reason for the

decreased ADC might be due to 'changes in the cytosolic and/or subcellular viscosities caused by yet unknown derangement at microstructural levels'.

From these experiments, it was surprising that the taurine ADC in perfused hearts did not change, and that the creatine ADC *increased* during the ischaemic period.

6.4.3. Taurine ADC

6.4.3.1. Cell size change due to ischaemia

The constancy of the taurine ADC during ischaemia and reperfusion might be explained by either no cell swelling or swelling of organelles and cells to the same extent. Greve and Grong (Greve and Grong 1991) found that, after 40 min of LAD coronary artery occlusion in the cat, the fractional volume of mitochondria was increased, that of myofibrils decreased, and the cytoplasmic volume fraction remained constant. Furthermore, in his review on cell volume regulation, Parker (Parker 1993) stated that cells are not defending their volume but their concentration of cytosolic macromolecules, which could be achieved by keeping a constant cytosolic volume. Hence, if cellular and organellar swelling processes occurred during ischaemia, then the cellular swelling must have been balanced by the organellar swelling to yield a constant intracellular environment (and therefore a constant ADC) for the diffusing taurine molecules. However, because the ischaemic insult was mild, it was unlikely that cell swelling and/or organellar swelling took place. Thus the taurine ADC would remain constant as the environment of the diffusing taurine molecules did not change.

Another factor that might contribute to possible ADC changes could be changes in the intracellular viscosity during ischaemia (Wick et al. 1995). However, the intracellular viscosity hardly changes in various osmotically stressed, shrunken and swollen mammalian cells (Mastro et al. 1984; Mastro and Keith 1984). Thus, the constancy of the

taurine ADC suggests that the ischaemia insult was milder in heart compared to the brain, where a decrease in the metabolite ADC was observed.

6.4.3.2. Cell size changes due to reduced perfusion pressure

When ischaemia was induced, the perfusion pressure dropped to zero and the heart and the cardiomyocytes shrank (Chapter 5). This decreased the average distance between intracellular diffusion barriers (for instance between cell organelles) and hence increased the degree of motional hindrance. Consequently the taurine ADC should be decreased in the shrunken cells compared to the swollen cells. One possible explanation as to why this was not observed is that the diffusion time was short and only few interactions with the sarcolemmal membranes occurred (see Chapter 7), making the measurement insensitive to cell volume changes. The surplus water during the oedematous perfusion period accumulated predominantly in cell organelles and the cytosol. When ischaemia was induced by the cessation of the perfusion pressure, water would leave the organelles and the cell. For a small molecule diffusing exclusively in the cytosol (as is the case for taurine), the amount of hindrance in both cases would be roughly identical, as the volume ratio of the total intracellular space to the organellar space remained constant. This hypothesis is supported by the findings of Greve and Grong (Greve and Grong 1991) who reported a constant cytoplasmic volume fraction during ischaemia whilst mitochondria were swollen considerably.

6.4.4. R_H of PCr and creatine

The hydrodynamic radius of creatine was found to be 2.92 ± 0.02 Å. The R_H of PCr was 3.92 ± 0.09 Å, in good agreement with literature values of 3.6 Å (Arrio-Dupont et al. 1996; Yoshizaki et al. 1990). Although creatine has roughly half the molecular weight of

PCr (131.1 *vs.* 255.1), their radii do not scale with their molecular weights, probably because the PCr molecule consists of a creatine molecule to which a polar phosphorus head group is attached on one side (see Fig. 4.7). Because there is no isotropic volume increase when attaching this phosphorus group, the hydration layers around the PCr molecule probably form an ellipsoid; they will also be more prominent around the phosphorus group. In that sense, R_H represents an 'average hydrodynamic radius', where 'average' refers to a space-averaged quantity. These physico-chemical characteristics for both the PCr and the creatine molecule apply in phantom solutions and cells; hence the ADCs of PCr and creatine were expected to be different in tissue (see below).

6.4.5. Total creatine ADC

The total creatine ADC of $(0.27 \pm 0.02) \times 10^{-3}$ mm^2/s increased by 35% during the ischaemic period, and returned to control values during reperfusion. This cannot be due to structural alterations in the intracellular space of the cardiomyocytes reducing the motional hindrance, because the taurine ADC should also have decreased. Therefore the ADC increase must have arisen from changes to the creatine molecule itself.

During the perfusion period the total creatine peak consists of PCr and creatine, whereas, during ischaemia, the PCr is hydrolysed to creatine, which has a smaller hydrodynamic radius. Hence, according to the Stokes-Einstein relation (eq 1.5), the diffusion coefficient of the total creatine should increase. The expected change in the ADC of the total creatine can be calculated, assuming that the ADC of the total creatine is given as a linear combination of the creatine and the PCr ADC weighed by their relative concentrations; in other words, fast exchange between PCr and creatine is assumed. The PCr to creatine ratio in the KCl-arrested perfused rat heart was 2.3 ± 0.2 (Chapter 2), and the ratio of their hydrodynamic radii was 1.34 ± 0.03. The total hydrolysis of PCr would account for an

ADC increase of around 22 ± 2% (Appendix F), significantly less than the observed increase in the total creatine ADC of 35 ± 9% (Fig. 6.3). However, the PCr/creatine ratio obtained for hearts in Chapter 2 was based on perfusions in which glucose and pyruvate were used as substrates. It is well known that PCr and creatine concentrations in the perfused heart depend on the type of substrate used; for instance, pyruvate and glucose perfusions increase the PCr concentration by 30% (Saks et al. 1994; Zweier and Jacobus 1987), or by 40% with acetate (Matthews et al. 1982). Assuming that the PCr concentration increased by 30% from 21 mM to 27 mM and creatine decreased to 3 mM, the ratio of PCr/creatine would be 9:1. This would lead to an ADC increase of 30 ± 3%, not significantly different from the observed change of 35 ± 9%. Hence it can be concluded that the conversion of PCr to creatine is probably responsible for the observed increase in the total creatine ADC. An obvious way to support this hypothesis would be to use different PCr/creatine ratios, for instance by altering the substrate composition, and measuring the ADC change from perfusion to ischaemia. As demonstrated in Appendix F, the maximum theoretical increase in the ADC for PCr/Cr $\rightarrow \infty$ is given by the ratio of the hydrodynamic radii of PCr to creatine, which was 1.34 ± 0.03.

As the ADC increase can be explained by the conversion of PCr to creatine during ischaemia, so the undershoot of the total creatine ADC during the reperfusion period could be explained with the PCr overshoot observed by others during the early phase of reperfusion (Cross et al. 1995a; Flaherty et al. 1982; Sako et al. 1988).

6.5. Conclusion

A 35% increase in the ADC of the total creatine during total global ischaemia in the perfused KCl-arrested rat heart could be attributed to the complete hydrolysis of PCr to creatine. During ischaemia there was no change in the taurine ADC, presumably due to either no cell swelling or simultaneous organellar and cellular swelling, with no change in the cytosolic volume. Hearts were only mildly affected by the ischaemic insult, as ATP was still detectable at the end of a 32 min period of total global ischaemia.

Chapter 7

Measurement of the myocyte diameter in the isolated rat heart during perfusion and ischaemia

Abstract

The aim of this work was to use the ADC of taurine to determine the ventricular myocyte diameter in the KCl-arrested rat heart during perfusion and total global ischaemia. Using the water-suppressed slice-selective STEAM sequence, the ADC of endogenous intracellular taurine molecules was measured over a range of diffusion times from 50 ms to 1510 ms, to determine the restriction caused by the cell membranes. The average cardiomyocyte diameter was calculated using an established model for restricted diffusion. The taurine ADC was also measured during ischaemia using a single TM of 800 ms and the average cell diameter was calculated. The taurine ADC was found to decrease as a function of the diffusion time, indicating restricted diffusion caused by sarcolemmal membranes. The average ventricular cardiomyocyte diameter was estimated to be 40 ± 6 μm for the perfused, and 27 ± 5 μm for the ischaemic heart. The taurine ADC did not vary with perfusion pressures between 50-100 mmHg. It can be concluded that myocytes were swollen during perfusion of the heart and that the swelling was abolished by the removal of 100 mmHg perfusion pressure. The measurement of the cell diameter indicated that there were no changes in cell volume, either because cell swelling had not occurred or the method of measurement lacked sensitivity.

7.1. Introduction

Cells regulate their volume in response to a change in osmotic pressure across the sarcolemma. However, if the volume regulating process is not fast enough to extrude the surplus water from the cell, swelling and damage may occur. It has been suggested that the extent of cell swelling is correlated to the severity of the ischaemic insult (Jennings et al. 1975; Powers et al. 1984; Sarkadi and Parker 1991), making cell volume a possible indicator of the degree of the ischaemic damage.

One method to measure cell volume is to use ^{31}P NMR together with phosphonate markers specific to the extracellular and the total water volume, from which the intracellular space can be calculated (see Chapter 2). Although changes in volume could be measured with good time resolution, this method used exogenous substances in the perfusate and lacked sensitivity in the perfused rat heart. The aim of this work was to determine whether the average ventricular myocyte diameter can be estimated in the KCl-arrested perfused rat heart by measuring the ADC of cytosolic taurine molecules at various diffusion times, thereby measuring restriction and allowing cell size to be calculated (see Chapter 1). Because this method is time consuming and cannot monitor dynamic changes, such as alterations in cell volume during ischaemia, the taurine ADC was measured continuously during perfusion, total global ischaemia and reperfusion, in order to estimate cell volume changes during ischaemia. A relatively long diffusion time of 800 ms was chosen to make the measurement more sensitive to restriction effects.

7.2. Methods

7.2.1. General

Hearts from male Wistar rats with a mean body weight of 330 ± 13 g (n = 13) were excised and perfused according to the methods described in Chapter 2. Coronary flow was monitored throughout each experiment. The water-suppressed slice-selective STEAM sequence was used with a TE of 20 ms and TMs and TRs described below. The ADC of the intracellular taurine signal was measured by a linear best fit of the semi-logarithmic signal attenuation as a function of the *b*-value. Diffusion gradients were applied along the x-direction. All FIDs were line-broadened by 5 Hz and zero-filled once prior to FT.

7.2.2. Cell size measurement during perfusion

Hearts from rats with a mean body weight of 361 ± 20 g (n = 5) were used for the measurement of the average cardiomyocyte diameter during perfusion, with hearts being KCl-arrested throughout the experiment. The water-suppressed slice-selective STEAM sequence was used with a TR of 4 s, and 17 TMs ranging from 40 ms to 1500 ms. As demonstrated in Chapter 4, the T_1 of taurine was sufficiently long to obtain adequate signal, even at a TM of 1500 ms. Five *b*-values were used with the strength of the diffusion gradients adjusted such to yield similar *b*-values at each TM time, generally ranging from 9 s/mm^2 to 1466 s/mm^2. However, at longer TM times the gradient strength required to obtain a *b*-value of 9 s/mm^2 was below that necessary to dephase the signal completely before the application of the second RF pulse (Hahn 1950). Hence, for TM times ≥ 600 ms, the minimum gradient strength applied was always 0.5 G/cm. With 24 averages acquired for each spectrum, the total acquisition time for each heart was around

135 min. The resulting ADC values as a function of the diffusion times were analysed according to the Mitra model described in Chapter 1, yielding an average diameter for the cardiomyocytes in the selected spectroscopy slice.

7.2.3. Cell size estimation during ischaemia

Hearts from rats with a mean body weight of 329 ± 18 g (n = 4) were used to monitor the ADC of taurine during 20 min perfusion, 32 min total global ischaemia, and 20 min reperfusion. The water-suppressed slice-selective STEAM sequence was used with a TM of 800 ms to increase the sensitivity of the taurine ADC to restriction effects. The TR was 3 s and 16 averages were acquired for each spectrum. Five *b*-values were used, ranging from 37 s/mm^2 to 1408 s/mm^2. During the intervention 5, 8 and 5 ADC values were acquired during perfusion, ischaemia and reperfusion, respectively.

As shown in Chapter 5, S_0 changes caused by a drop of the perfusion pressure during the ischaemic period and the effects of increased perfusion pressure during reperfusion cause artefacts in the ADC estimation. Because the S_0 changes were due to a change in the number of spins present in the selected slice, and not due to changes in the relaxation parameters or the ADC, the same S_0 correction could be applied here.

The average cell size during ischaemia was then estimated from the final ADC value acquired at the end of the ischaemic period using the Mitra model, as described above. However, during ischaemia cardiomyocytes shrank to about 61% of their perfused volume (see Chapter 2). Assuming that cells are swollen only radially (Roos 1986), the length to the diameter ratio is reduced to 3.9:1, and the surface-to-volume ratio is $S/V = 4.5/d$. Hence for the perfused rat heart, eq 1.26 was modified to

$$\frac{D(t_{dif})}{D_0} = 1 - \frac{18}{9\sqrt{\pi}} \cdot \frac{1}{d} \sqrt{D_0 \cdot t_{dif}} \qquad (7.1)$$

7.2.4. Dependence of the taurine ADC on perfusion pressure

7.2.4.1. Heart perfusions

In order to investigate if the observed reduction of the taurine ADC during ischaemia was due to the shrinkage induced by the cessation of buffer flow (and consequently the perfusion pressure), hearts from rats with a mean body weight of 293 ± 21 g (n = 4) were used to monitor the taurine ADC as a function of the perfusion pressure. Hearts were KCl-arrested throughout the experiment and the buffer flow rate was measured. Buffer was delivered to the heart *via* a calibrated peristaltic pump which allowed a controlled flow rate and hence perfusion pressure. The flow rate was reduced in steps of 10% of the original coronary flow, corresponding to a 10 mmHg drop of the perfusion pressure, to 50% of the initial coronary flow rate at 50 mmHg. Following a 10 min equilibration period, the taurine ADC was measured, and an axial FLASH image was acquired to monitor macroscopic shrinking of the perfused heart. The perfusion pressure was not reduced below 50 mmHg to prevent underperfusion of the heart (Clarke and Willis 1987).

7.2.4.2. NMR data acquisition

FLASH images were acquired with a 128 × 128 matrix, a field of view of 2.5 × 2.5 cm^2, 2 mm slice thickness, a TE of 15 ms and a TR of 100 ms. The water-suppressed slice-selective STEAM sequence was used with a TR of 3 s and a TM of 800 ms. Thirty-two averages were acquired and seven *b*-values were applied ranging from 147 s/mm^2 to 2344

s/mm^2. The acquisition times were 12.8 s for a single FLASH image and 11.2 min for the ADC measurement. Hence each pressure setting was applied for about 22 min, and the total time for all six pressure settings from 100 mmHg down to 50 mmHg was 132 min. The measurement protocol for the complete experiment is illustrated in Fig. 7.1.

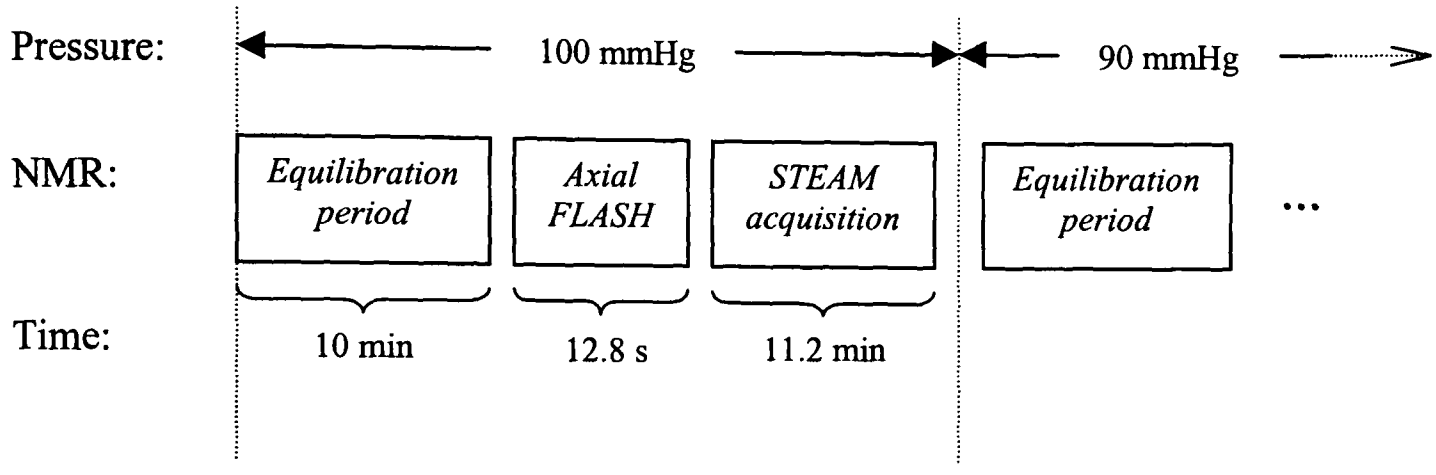

Fig. 7.1: Schematic of the experimental protocol for the perfusion pressure experiment. The equilibration period provided sufficient time for the heart to adjust to the new perfusion pressure. After the FLASH image was acquired and the taurine ADC obtained, the pressure was reduced by 10 mmHg and the measurement repeated.

7.3. Results

7.3.1. Cell size measurement during perfusion

The average coronary flow rate was stable throughout the KCl-arrest period at 19.8 ± 0.6 ml/min. Fig. 7.2 shows the 3-4 ppm region of two sets of increasingly diffusion-attenuated spectra obtained from the same heart at TMs of 40 ms *(a)* and 1500 ms *(b)*.

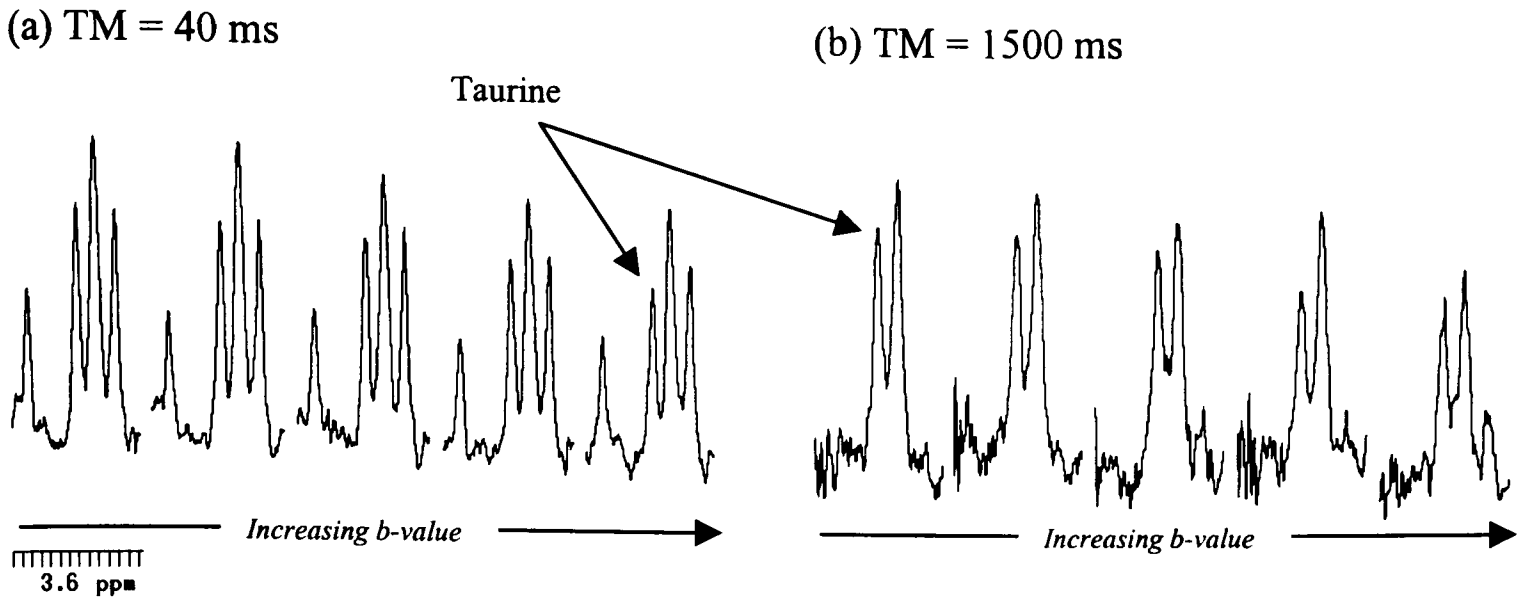

Fig. 7.2: Representative diffusion-attenuated spectra acquired with TMs of 40 ms (a) and 1500 ms (b). Spectra are not scaled equally.

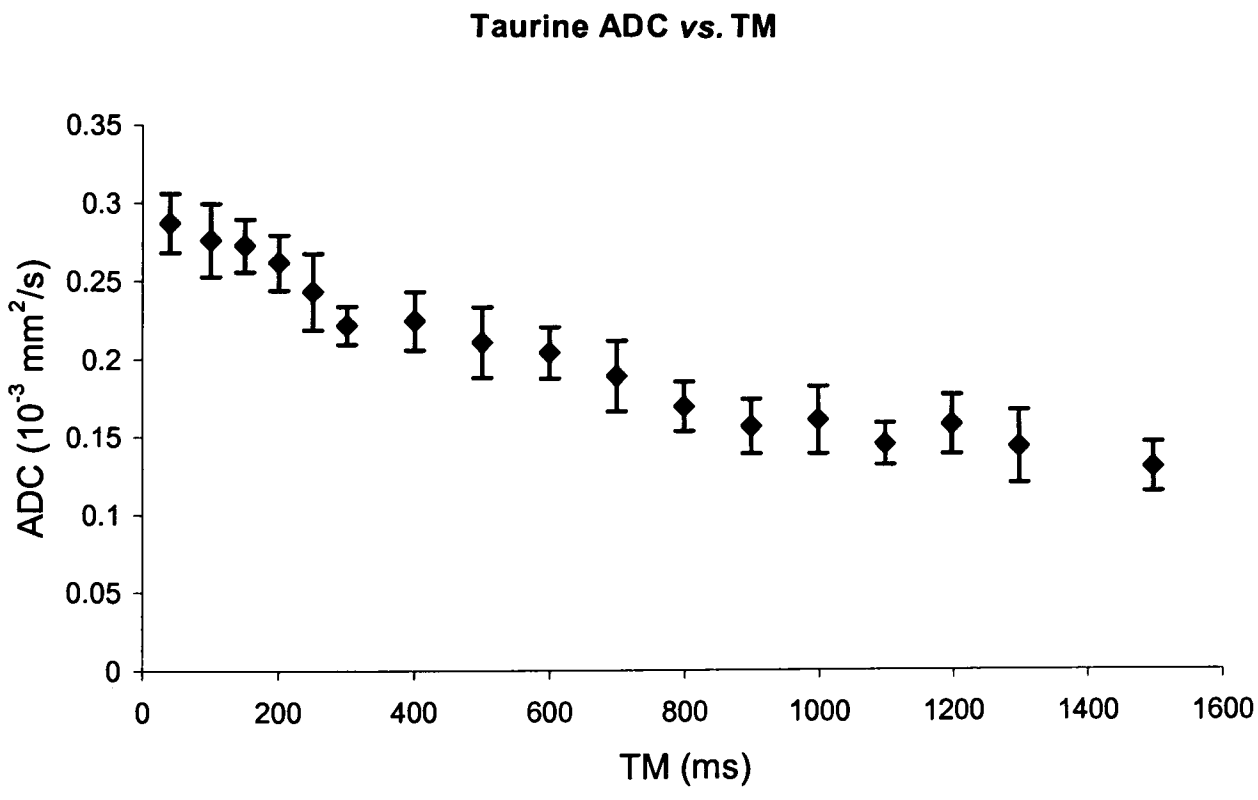

Fig. 7.3: Taurine ADC as a function of TM showing a decrease in the ADC with increasing diffusion times, which suggests restriction effects. The final value of the taurine ADC at a TM of 1500 ms was about half that at a TM of 40 ms.

The taurine ADC from all hearts at different TMs decreased steadily until it appeared to plateau at a TM of around 1200 ms (Fig. 7.3). The ADC results were plotted with respect to the square root of the diffusion time (Fig. 7.4).

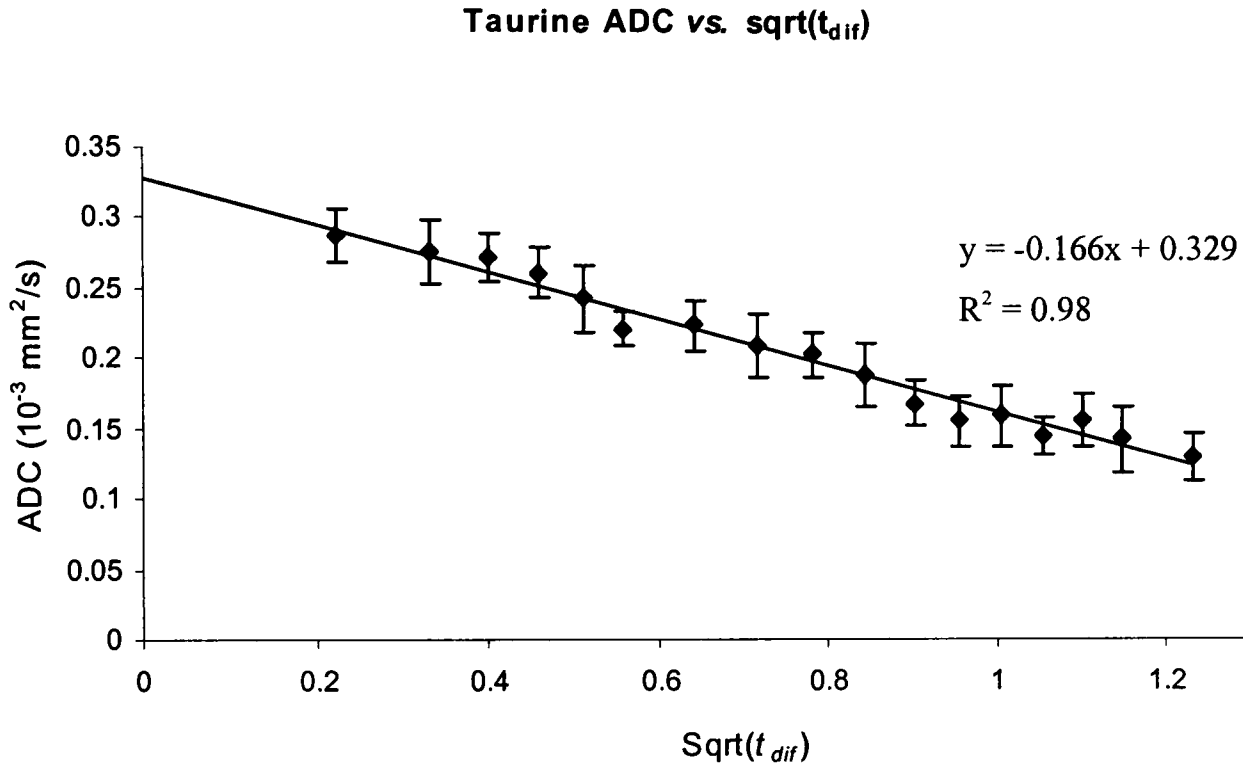

Fig. 7.4: ADC of taurine as a function of the square root of the diffusion time, t_{dif}. The data were fitted using a linear regression, with an R^2 of 0.98. According to the Mitra model, the slope of the fitted regression curve can be used to calculate the average diameter of the myocytes, whereas the abscissa intercept is equivalent to the 'free' diffusion ADC, D_0 (see Chapter 1).

The slope of the linear best fit was -0.166 ± 0.01 mm^2/s$^{3/2}$, and the intercept on the abscissa was $D_0 = (0.33 \pm 0.01) \times 10^{-3}$ mm^2/s. Using these data in eq 1.26, the average diameter, d, of the cardiomyocytes was calculated to be 40 ± 6 μm.

7.3.2. Cell size estimation during ischaemia

The coronary flow rate during the perfusion period was 20.8 ± 1.6 ml/min, and did not differ during reperfusion, suggesting that hearts were not severely damaged. This is supported by the fact that hearts started beating spontaneously when perfused with standard Krebs-Henseleit buffer after the reperfusion period (data not shown). The mean taurine ADCs acquired at a TM of 800 ms during perfusion, total global ischaemia and reperfusion are shown in Fig. 7.5. S_0 corrections due to the change in the perfusion pressure (Chapter 5) were applied to the data.

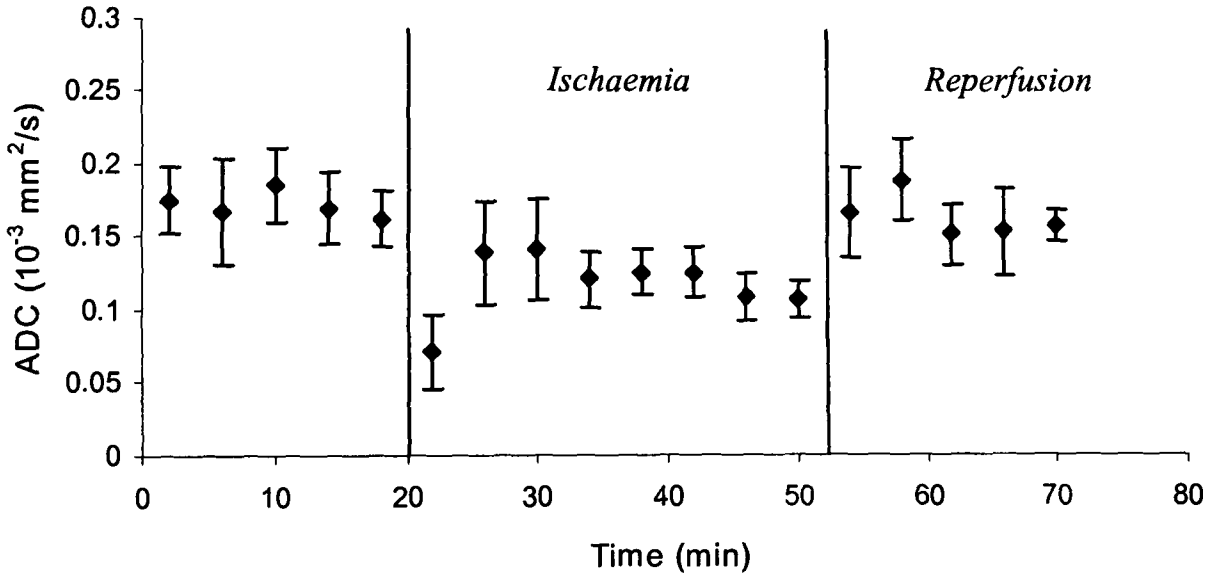

Fig. 7.5: Taurine ADC acquired during perfusion, 32 min of total global ischaemia and reperfusion. The measurement was made sensitive to restriction effects by using a TM of 800 ms.

The average value of the taurine ADC acquired at a TM of 800 ms during the perfusion period was $(0.17 \pm 0.01) \times 10^{-3}$ mm^2/s (Fig. 7.5; Table 7.1), which is identical to the value of $(0.17 \pm 0.02) \times 10^{-3}$ mm^2/s obtained in the previous experiment using the same TM

(Fig. 7.3). The taurine ADC was decreased during the ischaemic period, with the final value at 30 min of ischaemia being $(0.11 \pm 0.01) \times 10^{-3}$ mm^2/s, significantly different ($p < 0.05$) from the lowest values in the control and reperfusion periods, which were $(0.16 \pm 0.02) \times 10^{-3}$ mm^2/s and $(0.15 \pm 0.02) \times 10^{-3}$ mm^2/s, respectively. Averaging the measurements during the protocol (first point in ischaemia omitted) showed a 29% decrease in the taurine ADC ($p < 0.01$) during ischaemia, which recovered during reperfusion (see Table 7.1).

*Table 7.1: Average taurine ADCs during perfusion, ischaemia and reperfusion. Data represent means ± SEM for all hearts (n = 4). *: Significantly different from control and reperfusion (p < 0.01).*

	Taurine ADC (10^{-3} mm^2/s)
Control	0.17 ± 0.01
Ischaemia	0.12 ± 0.01*
Reperfusion	0.16 ± 0.01

In order to estimate the average cardiomyocyte diameter during ischaemia, a plot of the taurine ADC *vs.* the square root of the diffusion time similar to that in Fig. 7.4 was produced. However, because of the 132 min required to obtain the data only two taurine ADC values were used, both acquired at 30 min of ischaemia. The first value of $(0.28 \pm 0.03) \times 10^{-3}$ mm^2/s was measured with a TM of 40 ms (Chapter 6, Fig. 6.2). The second value of $(0.11 \pm 0.03) \times 10^{-3}$ mm^2/s was measured with a TM of 800 ms (Fig. 7.5). The

plot of the two data points is shown in Fig. 7.6. Using eq 7.1, the slope of the line gave an average cardiomyocyte diameter of 27 ± 5 μm.

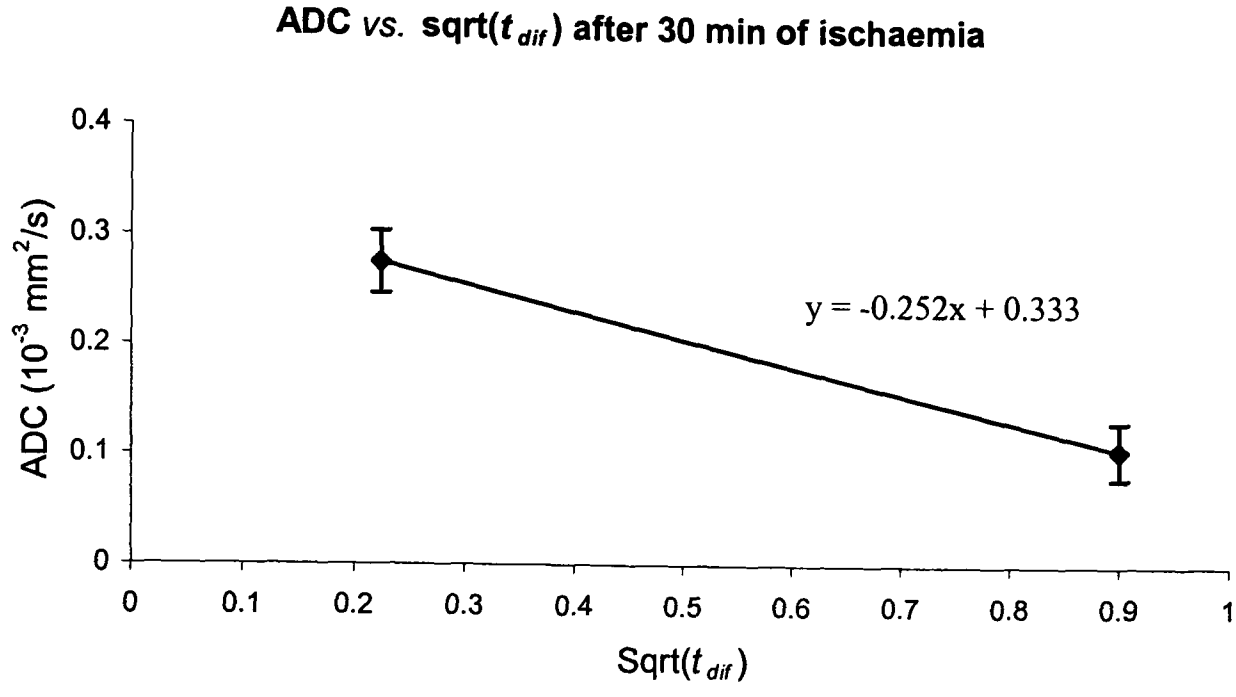

Fig. 7.6: Plot of the taurine ADC at 30 min of ischaemia as a function of the square root of the diffusion time, t_{dif}. Data points were taken from Chapter 6 (Fig. 6.2) and here (Fig. 7.5) The slope of the line through the points gives the average cardiomyocyte diameter.

7.3.3. Dependence of taurine ADC on perfusion pressure

The coronary flow rate was 18.6 ± 0.8 ml/min. Fig. 7.7 shows two axial FLASH images acquired from the same heart at perfusion pressures of 100 mmHg and 50 mmHg. Drawing manual regions of interest, hearts were found to have a 4 ± 1% smaller cross-sectional area at 50 mmHg compared to 100 mmHg. However, ADCs measured at 100 mmHg and at 50 mmHg were not significantly different (Fig. 7.8).

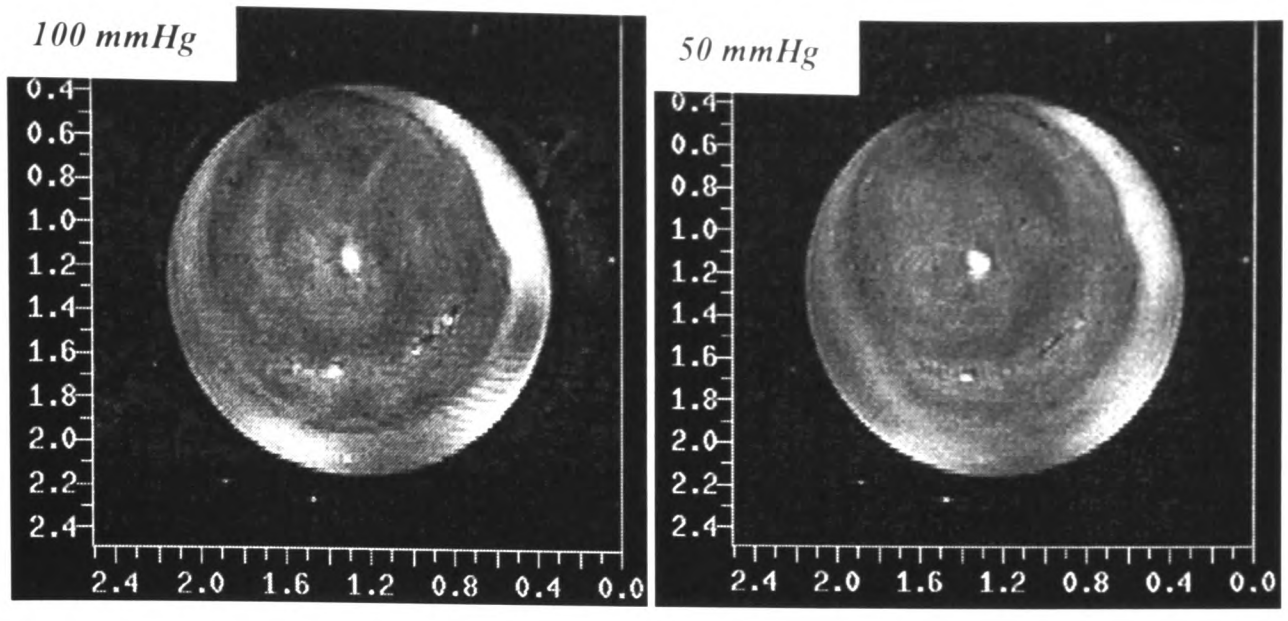

Fig. 7.7: Axial FLASH images acquired of an isolated rat heart at perfusion pressures of 100 mmHg (left) and 50 mmHg (right).

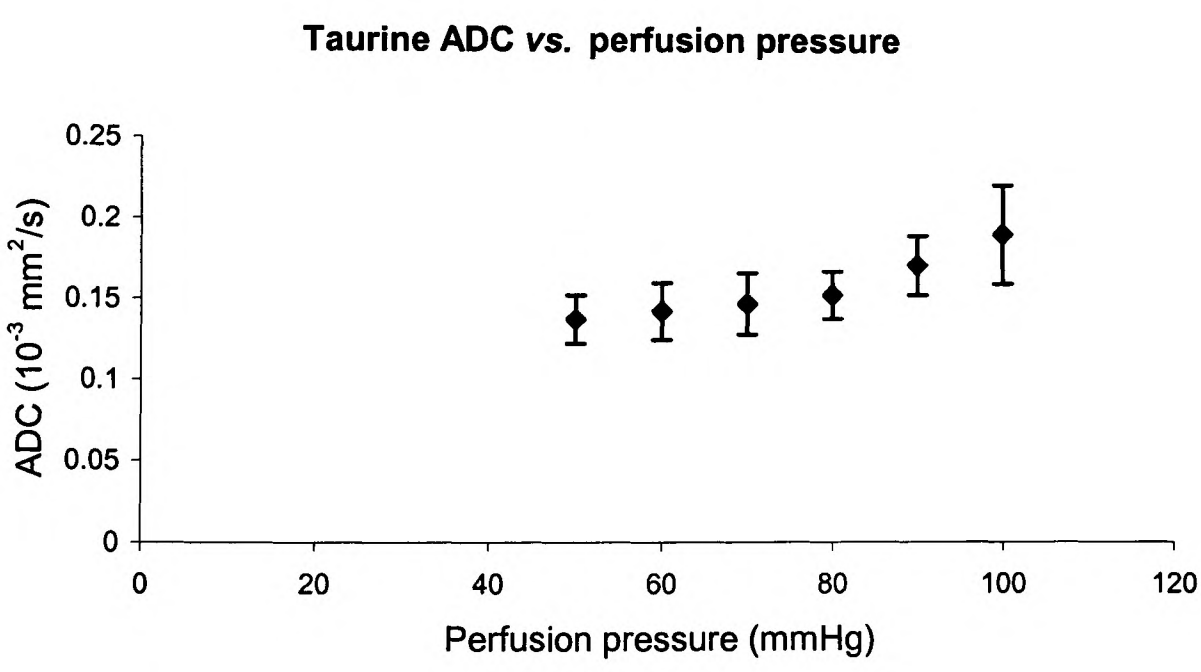

Fig. 7.8: The taurine ADC of taurine acquired at a TM of 800 ms as a function of the perfusion pressure. The ADC at 50 mmHg was not significantly different to that at 100 mmHg.

7.4 Discussion

This is the first report on the non-destructive measurement of the average myocyte diameter in a perfused and ischaemic heart using NMR diffusion measurements. It was based on the model suggested by Mitra and co-workers (1992; see Chapter 1), which was applied to the taurine ADC. The plot of the ADC *vs.* the square root of the diffusion time was linear with an R^2 of 0.98 and gave an average myocyte diameter of 40 ± 6 μm. By the end of 32 min ischaemia, the taurine ADC had decreased, giving an average cardiomyocyte diameter of 27 ± 5 μm. The taurine ADC at a TM of 800 ms did not change with the perfusion pressure when measured between 50 and 100 mmHg.

7.4.1. Cell size measurement during perfusion

7.4.1.1. Taurine ADC as a function of the diffusion time

Restricted diffusion effects have been demonstrated using NMR in various biological systems; for instance in yeast cells and other plant tissue (Latour et al. 1993; Tanner and Stejskal 1968), in rabbit (van Gelderen et al. 1994b), and goldfish (Kinsey et al. 1999) skeletal muscle. The plot of the taurine ADC as a function of the mixing time (Fig. 7.3) was similar to simulations of restricted diffusion (Tanner 1978). The decrease in the taurine ADC with increasing diffusion times suggests that restriction increased the longer the taurine molecules were allowed to diffuse. At TM times ≥ 1200 ms the ADC appeared to plateau. These observed restriction effects could be due to interactions with

a) the myofilament lattice

b) subcellular membranes

c) the sarcolemma

hence influencing the motion of the taurine molecules in the cytosol. First, the taurine

molecules interact with the myofilament lattice which consists of actin and myosin (Opie 1998; Schaper et al. 1989). Simulations using typical values for the filament radius and the distance between adjacent filaments revealed that the ADC of diffusing PCr molecules had reached a constant value at diffusion times of less than 0.3 ms (Kinsey et al. 1999). In other words, for diffusion times longer than 0.3 ms, these interactions can be treated as if they induced an increase in the bulk viscosity. Second, taurine molecules interact with subcellular membranes such as those of mitochondria and sarcoplasmic reticula. It was demonstrated experimentally in goldfish skeletal muscle that diffusion restriction due to these organelles caused the PCr ADC to reach a constant value at diffusion times of around 100 ms (Kinsey et al. 1999). Because their cells were large (around 100 μm in diameter) compared to the average diffusion distance, effects from the sarcolemma were negligible. Hence for diffusion times in excess of 100 ms the effects of subcellular membranes may also be treated as an increase the bulk viscosity. It is quite likely that this constant ADC value might be reached at even smaller diffusion times in cardiomyocytes because of the tighter packing of the cytoplasm (Opie 1998). Thus it may be concluded that the observed restriction effects were due to the sarcolemma of the cardiomyocytes, with the first point at a TM of 40 ms possibly containing contributions from subcellular membranes.

7.4.1.2. Estimation of the average myocyte diameter

The model to estimate a compartment size using ADCs as a function of the diffusion time has been proposed by Mitra and colleagues (Mitra and Sen 1992; Mitra et al. 1992). The linear relationship between the measured ADC and the square root of the diffusion time has been demonstrated in onion (Latour et al. 1993) and gold fish skeletal muscle (Kinsey et al. 1999). Here, in the perfused rat heart, the ADC as a function of the square root of

the diffusion time was linear with an R^2 of 0.98, supporting Mitra's model (1992). However, this model has limited applicability for ADC measurements at extremely short and long diffusion times, respectively. For instance, the intercept with the abscissa indicates a 'free' diffusion value of around 0.33×10^{-3} mm^2/s (Fig. 7.4), significantly higher than the value of $(0.29 \pm 0.01) \times 10^{-3}$ mm^2/s in the experiments in Chapter 4. As discussed in Chapter 1, free diffusion at very short diffusion times is independent of TM, hence the plot of the ADC *vs.* TM should display a constant ADC. It is clear that the graph of ADC as a function of $\sqrt{t_{dif}}$ would then deviate from linearity and the 'free' diffusion coefficient, D_0, obtained from the abscissa intercept would be overestimated. Similarly, at long diffusion times the ADC would be independent of the diffusion time, which again would lead to a deviation from linearity of the graph. However, for the range of diffusion times used here, the ADC *vs.* $\sqrt{t_{dif}}$ graph was linear; hence it can be concluded that Mitra's model was applicable to the diffusion process of the intracellular taurine molecules in the perfused KCl-arrested rat heart.

The average cardiomyocyte diameter was found to be 40 ± 6 μm. This is larger than literature values of single isolated rat cardiomyocytes; Powell and co-workers have reported an average diameter of 17 ± 5 μm (Powell et al. 1978) using electron microscopy, while others, using light microscopy, found a value of 27 ± 1 μm (Boyett and Kirby 1989; Nash et al. 1979). However, the hearts in the current experiments were perfused with crystalloid buffer and were highly oedematous (Clarke et al. 1993; Knopf et al. 1990; Polimeni and Buraczewski 1988). Hence the average cardiomyocyte diameter reflects the swollen state of the perfused heart, not the '*in vivo*' diameter.

Nevertheless, it is possible to estimate the '*in vivo*' average cardiomyocyte diameter using data from earlier experiments. Assuming that the myocyte volume returns to '*in vivo*' values on loss of perfusion pressure, and that they swell radially but not longitudinally

(Drewnowska et al. 1991; Roos 1986), an average '*in vivo*' cardiomyocyte diameter can be estimated from the volume data obtained using phosphonate markers and ^{31}P NMR in Chapter 2. There the intracellular volume decreased to around 61% of its oedematous volume when the buffer flow was clamped off. As the volume of a cylinder is linearly related to its squared diameter, the diameter of the '*in vivo*' cells, d_{normal}, can be calculated from the diameter of the swollen cells, $d_{swollen}$, by

$$d_{normal} = \sqrt{0.61} \cdot d_{swollen} \qquad (7.2)$$

Using 40 ± 6 μm as the value for $d_{swollen}$, the final myocyte diameter would be 31 ± 6 μm. This value agrees well with 27 ± 1 μm (Boyett and Kirby 1989; Nash et al. 1979), but not with 17 ± 5 μm (Powell et al. 1978). As the latter value was obtained using electron microscopy, the myocytes were contracted due to the fixation procedure (Powell et al. 1978). Hence it can be concluded that cardiomyocytes were swollen by around 30% during the perfusion with crystalloid buffer.

7.4.2. Cell size estimation during ischaemia

The value obtained for the average cardiomyocyte diameter of 27 ± 5 μm is identical to the value of 27 ± 1 μm reported in the literature (Boyett and Kirby 1989; Nash et al. 1979), and it compared favourably to the value of 31 ± 6 μm obtained in the previous experiment. When measuring the taurine ADC at short diffusion times (Chapter 6), it was suggested that (a) diffusion was almost free, and (b) that cell swelling and organellar swelling either occur to the same degree or did not occur at all. Here, at long TM times, the diffusion process was no longer free, and the measurements were more sensitive to

restriction effects caused by the sarcolemma of the cardiomyocytes. Because cells shrank upon the induction of ischaemia (due to the cessation of the perfusion pressure), restriction increased, resulting in a decrease of the ADC to about 72% of its pre-ischaemic value.

7.4.3. Taurine ADC as a function of the perfusion pressure

In the FLASH images it was shown that the reduction of the perfusion pressure from 100 mmHg to 50 mmHg caused only a 4% decrease of the cross-sectional area of the heart. This is in good agreement with the 3% decrease observed in the perfused KCl-arrested guinea-pig heart (Arnold et al. 1968). As water equilibrates rapidly across cell membranes, this reduction affected both the extracellular and the intracellular volumes. Assuming that the total water volume was 0.93 ± 0.06 ml/heart and the ratio of extracellular to intracellular water volume was around 0.7:1 (see Chapter 2), the extracellular space would decrease by 0.014 ml/heart and the intracellular space by 0.019 ml/heart. Such a small change in the intracellular water volume could not be picked up with taurine ADC measurements, as demonstrated in Fig. 7.8.

7.5. Conclusion

In conclusion, perfused KCl-arrested rat hearts were swollen with an average myocyte diameter of 40 ± 6 μm. At the end of 32 min total global ischaemia, the myocyte diameter had decreased to 27 ± 5 μm due to the cessation of the buffer flow to the heart and the consequent reduction of the perfusion pressure to zero. However, over a perfusion pressure range from 100 mmHg to 50 mmHg, the taurine ADC remained constant, and there was only a 4% decrease of the cross-sectional area of the heart in the FLASH

images. Hence the taurine ADC measurements were not sensitive enough to detect such a small change.

Chapter 8

Water ADC during ischaemia in the isolated rat heart

Abstract

The aim of the work in this chapter was to determine whether the water ADC could be used for the detection of ischaemic damage in the isolated, KCl-arrested rat heart. The non water-suppressed slice-selective STEAM sequence was used to obtain ADC values with a time resolution of 2 min. Signal amplitude loss as a function of increasing *b*-value was found to be biexponential and was attributed to two compartments in the myocardial slice. Using published ADC values, the compartment with an ADC of $(3.02 \pm 0.13) \times 10^{-3}$ mm^2/s was assigned to freely diffusing water in the bath around the heart and in the extracellular spaces (V_o). The compartment with an ADC of $(1.06 \pm 0.07) \times 10^{-3}$ mm^2/s was assigned to the intracellular space (V_i). Both V_o and V_i water ADCs remained constant throughout total global ischaemia and reperfusion either because swelling did not occur or water molecules freely traversed the membranes. Irrespective of the mechanism, it can be concluded that the measurement of the water ADC holds little potential for the detection of ischaemic damage in the isolated rat heart.

8.1. Introduction

In previous chapters experiments were described in which the ADCs of taurine and total creatine were measured in the isolated rat heart during perfusion, total global ischaemia and reperfusion. These metabolites were located intracellularly (see Chapter 5), and their ADCs reveal only cytoplasmic information. However, in clinical studies, the water ADC is measured because the pulse sequences are simple and the ADC can be obtained rapidly due to a high SNR (Doran et al. 1990; Jones et al. 1998a; Miranda et al. 1998). As water is present throughout the tissue, the water ADC provides information about the combined intracellular and the extracellular spaces, thereby making interpretation of the diffusion data difficult (Niendorf et al. 1996; Norris et al. 1994; Pfeuffer et al. 1998; van der Toorn et al. 1996a).

Nevertheless, the water ADC is useful clinically in that cerebral ischaemia can be detected using diffusion-weighted imaging much earlier than with conventional T_2-weighted imaging (MacFall et al. 1991; Moseley et al. 1990a; Moseley et al. 1990b). In animals, the water ADC decreased rapidly during cerebral ischaemia (Moseley et al. 1990b; van Gelderen et al. 1994a), seizure (Zhong et al. 1991), excitotoxic injury (Benveniste et al. 1992) or spinal cord trauma (Ford et al. 1994). Yet the pathophysiological mechanisms for the decreased water ADC in brain ischaemia are unknown. The currently favoured hypothesis is the formation of cytotoxic oedema with the net movement of water from the extracellular into the intracellular spaces where diffusion would be slower due to the presence of cell organelles and macromolecules (Moseley et al. 1990b; van der Toorn et al. 1996a; van Gelderen et al. 1994a). Other possible mechanisms involve changes in membrane permeability during cerebral ischaemia (Helpern et al. 1992), increased tortuosity of the extracellular space due to cell swelling (Niendorf et al. 1996; Norris et al. 1994; van der Toorn et al. 1995), or the

reduction of the intracellular water ADC due to the loss of cytoplasmic macromolecular motion or increased viscosity (Duong et al. 1998; Hazlewood et al. 1991; Neil et al. 1996). Nonetheless, the ADC decrease has been linked to the depletion of cellular energy stores and inhibited ion pumps (Busza et al. 1992; Moseley et al. 1990b; Norris et al. 1994; van der Toorn et al. 1996b). As the same processes also occur in the ischaemic rat heart (Cross et al. 1995b), it was assumed that the water ADC in heart would decrease during ischaemia. Therefore the aim of the work in this chapter was to determine whether changes in the water ADC occur in the totally ischaemic, isolated rat heart, making the ADC an early indicator of ischaemic damage. In order to match the NMR methods to those used to measure metabolite ADCs in previous chapters, the water ADC in the perfused rat heart was measured spectroscopically during perfusion, ischaemia and reperfusion, using the non water-suppressed slice-selective STEAM sequence (Chapter 3).

8.2. Methods

Hearts from male Wistar rats with a mean body weight of 369 ± 31 g (n = 4) were excised and perfused according to the methods described in Chapter 2. The intervention consisted of 20 min perfusion, 32 min total global ischaemia and 20 min reperfusion. Coronary flow was monitored during perfusion and at 5 min intervals during the reperfusion period. The non water-suppressed slice-selective STEAM sequence was used with a TR of 1.88 s, a TE of 20 ms and a TM of 40 ms. Choosing the same TM as used for metabolite ADC measurements (Chapter 6) allowed the direct comparison of water and metabolite ADCs. Diffusion gradients were applied in the x-direction with values of 1-16 G/cm in 1 G/cm steps corresponding to *b*-values ranging from 9 s/mm^2 to 2221 s/mm^2. With four averages acquired for each *b*-value, the water ADC time resolution was 2 min. Thus 10, 16, and 10

ADC values could be acquired during perfusion, ischaemia and reperfusion. The FIDs were line-broadened by 5 Hz and zero-filled once prior to FT. The loss of signal amplitude as a function of increasing *b*-value was fitted best by a biexponential function using the Origin fitting programme (Microcal Software, Inc., Northampton, MA, USA).

8.3. Results

The coronary flow rate during perfusion was 20 ± 2 ml/min, not significantly different from the flow rate during reperfusion. Water spectra acquired from a perfused KCl-arrested rat heart with increasing gradient strengths from 1 G/cm (first spectrum) to 16 G/cm (last spectrum) are shown in Fig. 8.1.

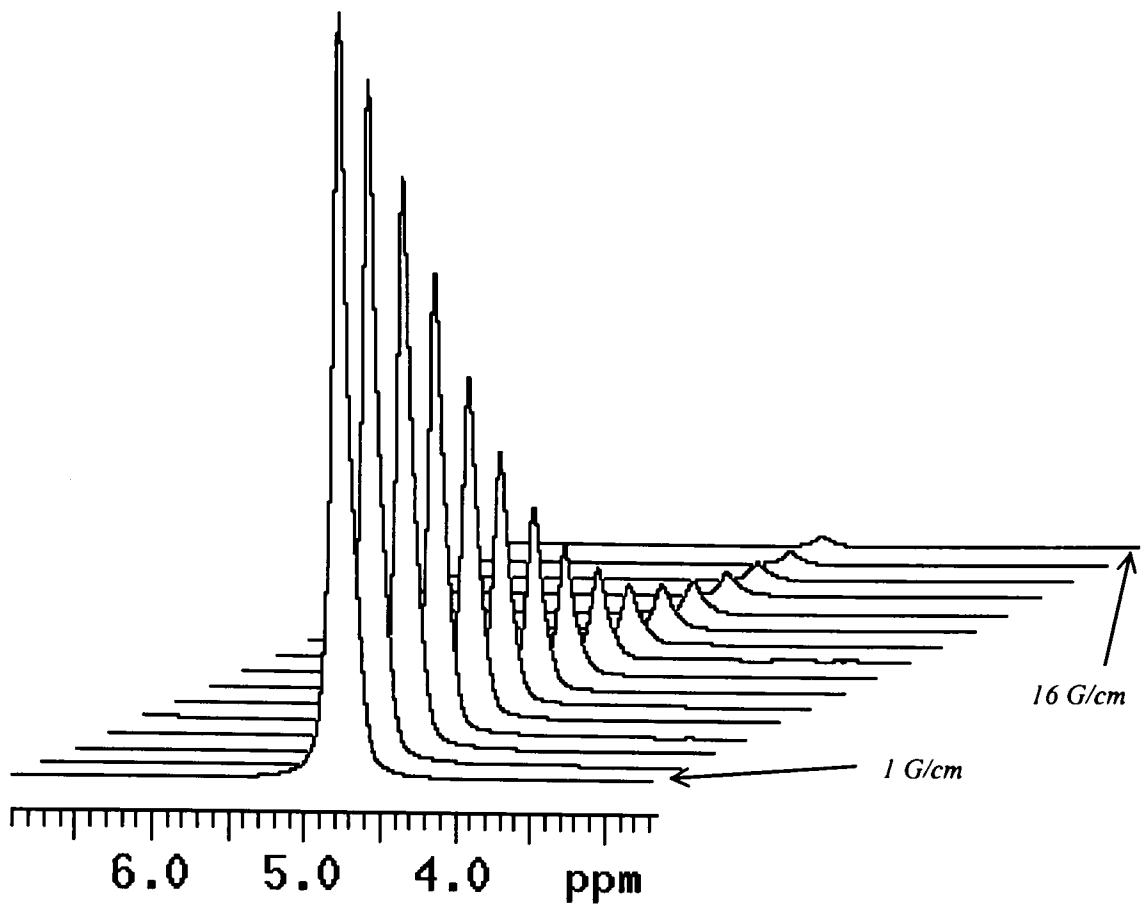

Fig. 8.1: Water signal from a perfused rat heart acquired at increasing b-values. As the pulse sequence was slice-selective, the signal contained contributions from the buffer in the bath around the heart, the ventricles, the vasculature and the interstitial and intracellular spaces.

The decrease in the signal intensity was biphasic, initially rapid then slower at higher gradient strengths. The corresponding semi-logarithmic plot of signal intensity as a function of the applied *b*-value was non-linear, suggesting the presence of more than one compartment (Fig. 8.2).

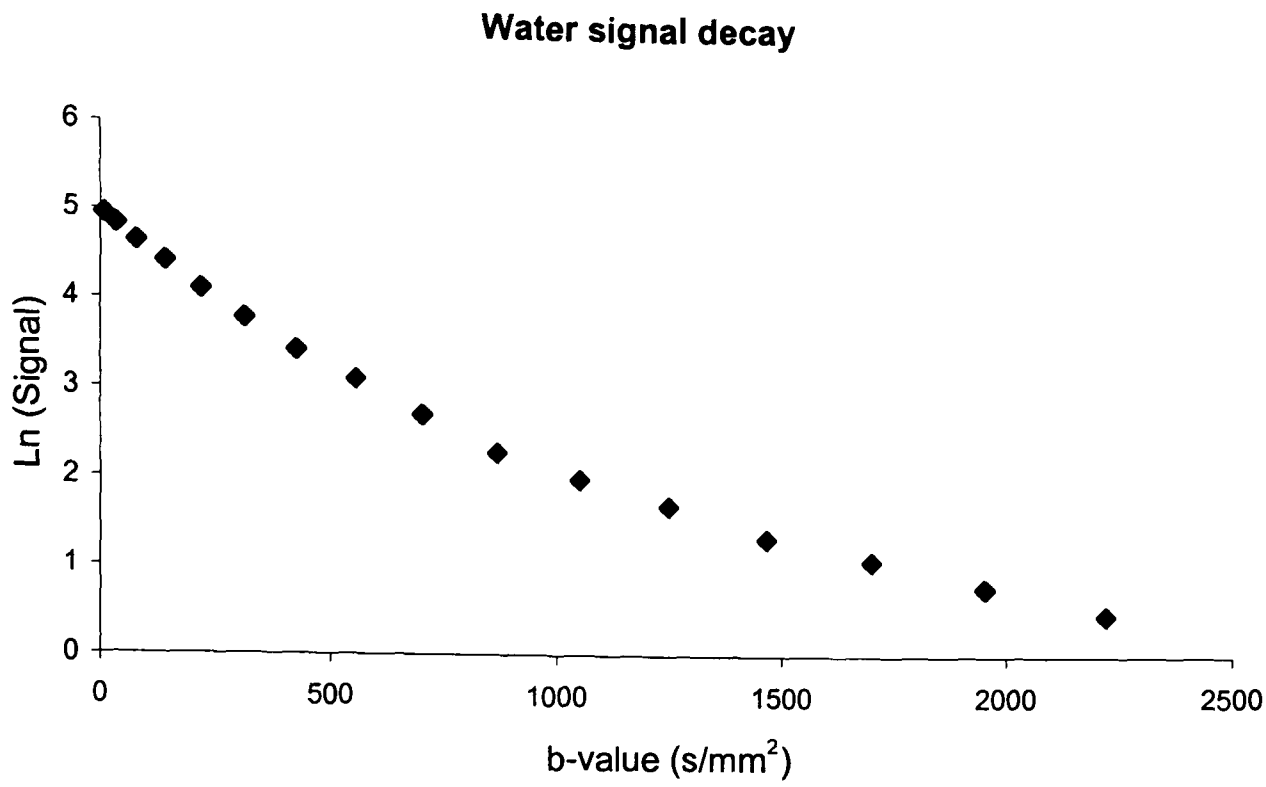

Fig. 8.2: Semi-logarithmic plot of the water signal as a function of increasing b-value in a slice through a perfused KCl-arrested rat heart. The non-linearity suggests the presence of more than one compartment.

The signal loss as a function of the *b*-value was best fit by a biexponential equation, suggesting two compartments (see also Fig. 5.2). The ADC of the first compartment of 3.02×10^{-3} mm^2/s was identical to that of 3.05×10^{-3} mm^2/s for free water at 37°C (Mills 1973), and so the first compartment was assigned to water in the bath around the heart and in the extracellular spaces (V_o). The ADC of the second compartment of 1.06×10^{-3} mm^2/s was close to that of 0.9×10^{-3} mm^2/s (Reese et al. 1995) and 1.2×10^{-3} mm^2/s (Edelman et al. 1994) previously found in heart, and so the second compartment was assigned to the intracellular water, V_i.

ADC values for water in V_o and V_i during perfusion, total global ischaemia and reperfusion were calculated and plotted (Fig. 8.3). The water ADCs from both compartments in the slice remained constant during perfusion, ischaemia and reperfusion,

with average values of (3.02 ± 0.13) × 10^{-3} mm^2/s and (1.06 ± 0.07) × 10^{-3} mm^2/s, respectively (Table 8.1).

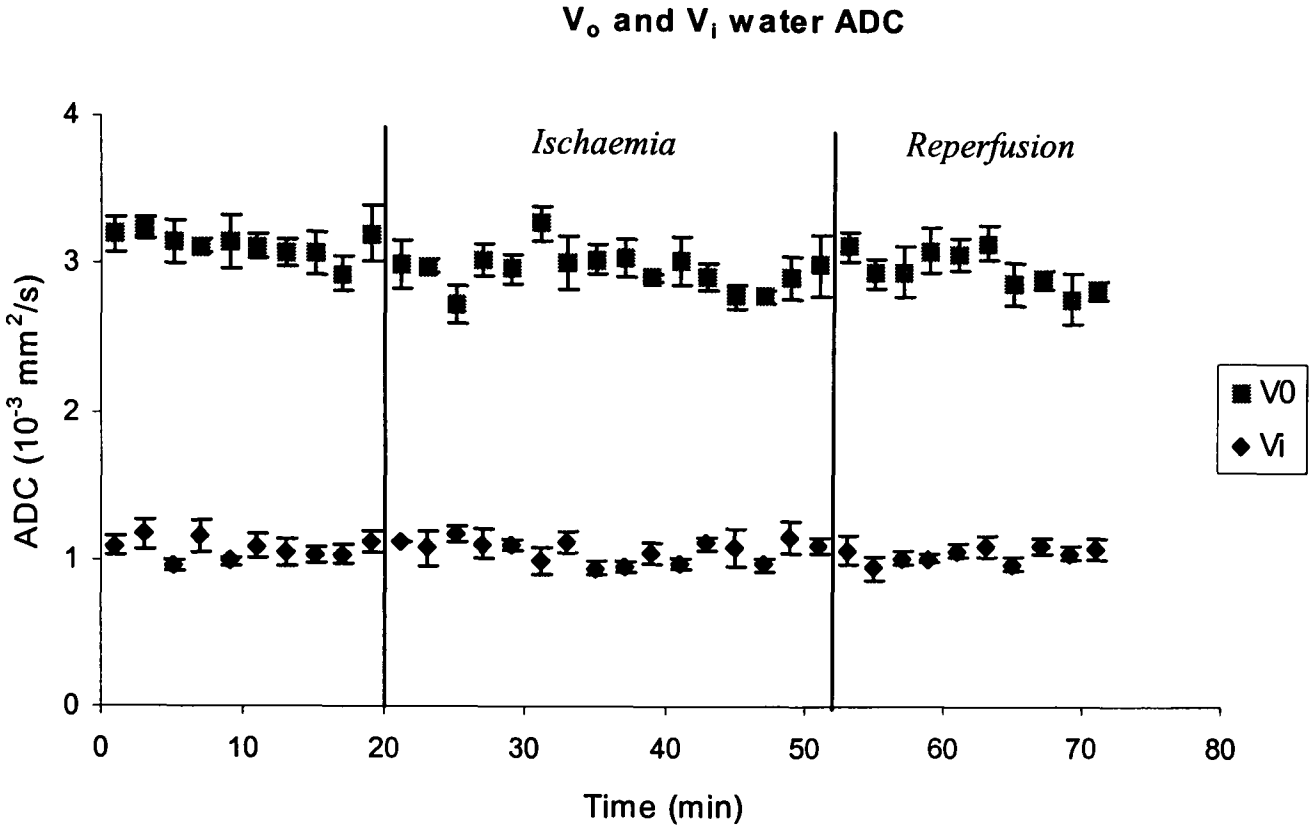

Fig. 8.3: The ADC of water in the heart spaces, V_o and V_i, remained constant during perfusion, total global ischaemia and reperfusion. Data are means ± SEM (n = 4).

Table 8.1: V_o and V_i water ADCs during perfusion, total global ischaemia and reperfusion in isolated rat hearts (n = 4). There were no significant differences between values during the protocol. Data are means ± SEM.

	V_o water ADC (10^{-3} mm^2/s)	V_i water ADC (10^{-3} mm^2/s)
Perfusion	3.13 ± 0.08	1.07 ± 0.07
Ischaemia	2.98 ± 0.13	1.07 ± 0.07
Reperfusion	2.99 ± 0.13	1.05 ± 0.05
Overall	***3.02 ± 0.13***	***1.06 ± 0.07***

8.4. Discussion

8.4.1. V_o and V_i compartments

The plot of the signal loss as a function of the *b*-value was fitted best by a biexponential equation, suggesting two compartments (Norris et al. 1994). Fitting a triexponential function, in an attempt to subdivide V_o and V_i further, gave no significant improvement in the fit (data not shown). The assignment of the two compartments was based on their ADC values of 3.02×10^{-3} mm^2/s and 1.06×10^{-3} mm^2/s.

The V_o water ADC reflected 'free' diffusion, hence the Stokes-Einstein formula (eq 1.5) would be applicable, such that V_o water ADC changes reveal temperature changes. The constant V_o water ADC during ischaemia therefore shows that the buffer temperature remained at 37°C when the flow was cut off.

The V_i water ADC of 1.06×10^{-3} mm^2/s was roughly one-third that of free water, thus it was assumed that the diffusion process was influenced by physical barriers, higher

viscosities and/or binding (see Chapter 4). Others have reported similar values of (0.82 ± 0.06) × 10^{-3} mm^2/s in the perfused rabbit heart (Hsu et al. 1995), and (0.9 ± 0.1) × 10^{-3} mm^2/s (Reese et al. 1995) and (1.2 ± 0.2) × 10^{-3} mm^2/s (Edelman et al. 1994) in the human heart. In diffusion imaging experiments in the perfused rat heart, water ADC values ranged from (0.77 ± 0.58) × 10^{-3} mm^2/s to (3.29 ± 0.57) × 10^{-3} mm^2/s, depending on the direction of the applied diffusion gradient (Garrido et al. 1994). The larger values were attributed to unrestricted diffusion along the direction of the fibre axes, whereas smaller values reflected restricted diffusion perpendicular to the fibre axes (Garrido et al. 1994). As the data from the present study were acquired from a large volume with a variety of fibre orientations (see Chapter 4), restriction effects would be more pronounced, giving a lower ADC of (1.06 ± 0.07) × 10^{-3} mm^2/s.

The V_i water ADC found in this study was slightly higher than those reported for brain at similar diffusion times, with the latter ranging from (0.62 ± 0.05) × 10^{-3} mm^2/s to (0.79 ± 0.05) × 10^{-3} mm^2/s (Duong et al. 1998; Merboldt et al. 1993; van der Toorn et al. 1996b; van Gelderen et al. 1994a). This is similar to the higher taurine and total creatine ADCs in heart (Chapter 5) than in brain, presumably due to intracellular oedema and the higher water content of the perfused heart.

8.4.2. V_i water ADC during myocardial ischaemia

The V_i water ADC stayed constant throughout ischaemia and reperfusion, demonstrating that it may not be a good marker of ischaemic damage in the perfused rat heart. This is in contrast to brain studies, in which a 20% decrease in the water ADC occurred after 10 min of ischaemia (van der Toorn et al. 1994). In support of the ADC differences, the water ADC in rat muscle remained constant *post mortem*, but decreased in brain in the same animal by about 30% (MacFall et al. 1991). The water ADC in the ischaemic region

of isolated rabbit hearts after ligation of the left anterior descending coronary artery remained constant for 60 min, and gradually decreased by 20% over the following 100 min of ischaemia (Hsu et al. 1998), attributed to the regulation of cell volume until the onset of irreversible injury after 60 min of ischaemia. Although Hsu and colleagues (1998) provided no cell volume data to support their hypothesis, the findings were consistent with the present results of a constant V_i water ADC during 32 min of total global ischaemia.

8.4.3. Membrane permeability to water

In order to compare the water ADC with the metabolite ADC acquired in other experiments (Chapter 6), the same diffusion time was used in both experiments. The ADC, and hence the average diffusion pathlength (eq 1.4), of water is higher than that of metabolites (see Chapter 3). At a diffusion time of 50 ms and an ADC of $(1.06 \pm 0.07) \times 10^{-3}$ mm^2/s, the average pathlength for a water molecule is 10.3 μm, about twice that of a larger taurine molecule at the same diffusion time. This suggests that the average distance was such that water molecules should have encountered cell membranes during the diffusion time. When the perfusion pressure was reduced to zero, loss of oedema and cell shrinking increased restriction of intracellular metabolites (Chapter 7). However, cell shrinking did not alter the water ADC, suggesting that water molecules did not experience the same degree of restriction. Instead, as water is in thermodynamic equilibrium across cell membranes (Leaf 1959; Mild and Lovtrup 1985; Safford et al. 1978), water molecules could have traversed the membranes, rather than being repelled (van Gelderen et al. 1994a). Hence, the water ADC remained constant irrespective of cell size. This is supported by reports of constant water ADCs for diffusion times larger than 20 ms in brain (Moonen et al. 1991; Norris and Niendorf 1995), and for diffusion times between 2

ms and 60 ms in heart (Cooper et al. 1974). Hence it can be concluded that cell membranes caused no water restriction and that water ADC measurements provide no evidence for cell swelling during ischaemia.

Chapter 9

Summary

The apparent diffusion coefficient (ADC) of a molecule provides information about its size, the environment through which it diffuses and the interaction between the molecule and its environment (Einstein 1906; Le Bihan 1991; Stilbs 1987). In tissue, the ADC of a molecule depends on the viscosity, on hindrance caused by macromolecular structures, on restriction caused by cell membranes and on fibre architecture (Le Bihan 1991; Moseley et al. 1990a; van der Toorn et al. 1996a). Consequently, it is difficult to attribute the ADC of water or metabolites in a biological system to a single factor. However, changes in the ADC are useful indicators of pathology (Davis et al. 1994; Decanniere et al. 1995; Neil et al. 1996; Wick et al. 1995). For example, changes in diffusion-weighted images have been used extensively to detect stroke at an early stage, earlier than conventional T_2-weighted images (Carano et al. 1998; Le Bihan 1991; Moseley et al. 1990b). Although the cellular mechanisms underlying the ADC changes are not understood, the ADC is used routinely as a clinical tool in brain examinations (Doran et al. 1990; Jones et al. 1998a; Miranda et al. 1998; Werring et al. 1998).

As opposed to work in brain, little is known of water or metabolite ADCs in the heart. Published cardiac water ADC studies demonstrated diffusion anisotropy caused by the fibre orientation (Edelman et al. 1994; Garrido et al. 1994; Scollan et al. 1998; Tseng et al. 1997), and a decreased water ADC during prolonged localised ischaemia in the isolated rabbit heart (Hsu et al. 1998). Such changes in the water ADC could result from changes in the intracellular and/or the extracellular spaces. This work is the first attempt to measure intracellular metabolite ADCs in the perfused heart, thus avoiding the problems associated with water ADCs due to the contribution from the extracellular space. The aim of the work was to determine whether the ADCs of intracellular taurine and creatine indicate swelling or damage during ischaemia in the isolated, KCl-arrested rat heart. ADCs were monitored during perfusion, total global ischaemia and reperfusion.

As it has been hypothesised by others that the extent of cardiomyocyte swelling correlates with the severity of ischaemia (Jennings et al. 1975; Powers et al. 1984; Sarkadi and Parker 1991), the ADC was used to estimate the ventricular cell diameter. Finally, the water ADC was determined in the rat heart during total global ischaemia and reperfusion.

In Chapter 2 energetics and extra- and intracellular heart volumes were measured during perfusion and low-flow ischaemia in the isolated rat heart using ^{31}P-NMR spectroscopy with phosphonate volume markers (Clarke et al. 1994; Clarke et al. 1990; Cross et al. 1995a). The severity of ischaemia was made mild or severe in different groups of hearts, using the presence/absence of glucose in the perfusion buffer. However, no cell swelling was detected in any heart due either to low sensitivity of the method or lack of cell swelling. The changes in energetics were used to show the extent of ischaemic damage in hearts in later experiments.

In Chapter 3 the slice-selective STEAM pulse sequence was developed and tested on solutions. Diffusion coefficients and tensors of water and metabolite solutions were 1.93 $\times$ 10^{-3} mm^2/s for water, and around 0.8 $\times$ 10^{-3} mm^2/s for metabolites, the same as published values (Mills 1973; van der Toorn et al. 1996a).

The work described in Chapter 4 established the experimental methods using the water-suppressed slice-selective STEAM sequence in the perfused heart. The perfusion buffer composition was investigated for spurious ^{1}H-NMR peaks interfering with heart metabolite resonances, leading to the use of a pyruvate-lactate-acetate substrate combination. T_1 relaxation times of the heart metabolites taurine, creatine, and a composite peak of choline-containing compounds, carnitine and taurine were of sufficient length for measurement of metabolite ADCs in heart at long diffusion times. In addition, the reproducibility of the measurement of metabolite ADCs was found to be within

published values (Dreher and Leibfritz 1998; van der Toorn et al. 1996a). ADC values were found to be 0.29×10^{-3} mm^2/s for taurine, 0.26×10^{-3} mm^2/s for total creatine and 0.32×10^{-3} mm^2/s for the Cho/Car/Tau mixture.

In Chapter 5 it was shown that the scalar ADC measurement gave identical values as the time-consuming diffusion tensor measurement (Basser et al. 1994a; Basser et al. 1994b; Basser and Pierpaoli 1996; Mattiello et al. 1994), with the effects due to the fibre orientation averaged out in the selected spectroscopy slice. It was also shown that artefacts in the ADC measurements occurred as a consequence of changes in perfusion pressure during ischaemia and reperfusion. A correction method was devised and applied in the later experiments. In addition, it was demonstrated that there was no release of taurine or creatine compounds during ischaemia.

In Chapter 6 the ADCs of taurine and total creatine were monitored during perfusion, total global ischaemia and reperfusion. The taurine ADC remained unchanged, probably due to the absence of cell swelling or the balancing of cell and organelle swelling (Greve et al. 1990). The ADC of total creatine increased during ischaemia, which was attributed to the hydrolysis of PCr to creatine.

In Chapter 7 it was demonstrated that intracellular taurine diffusion was restricted by sarcolemmal membranes at long diffusion times. The taurine ADC, as a function of the diffusion time, gave an average ventricular cardiomyocyte diameter during perfusion and total global ischaemia of 40 ± 6 μm and 27 ± 5 μm, respectively. Thus cardiomyocytes were swollen during perfusion but, during ischaemia, returned to sizes comparable to the *in vivo* cell size.

In Chapter 8 the water ADC was constant throughout ischaemia and so was not useful in demonstrating damage. This agreed with a recent study in isolated dextrose-perfused rabbit hearts, in which the water ADC remained constant for 60 min of local ischaemia

(Hsu et al. 1998). The constant ADC was either because the ischaemia was mild, or because of the ease at which water molecules traverse membranes.

The overall aim of this work was to design NMR methods to measure water and metabolite ADCs during perfusion, total global ischaemia and reperfusion in the isolated, KCl-arrested rat heart. The metabolite ADC was also used to determine the changes in the ventricular cell diameter during total global ischaemia. The water and metabolite ADC measurements failed to show myocardial damage, either due to the lack of severity of the ischaemic insult or the ability of water molecules to traverse sarcolemmal membranes. Hence the applicability of the water and metabolite ADC measurement for cardiac *in vivo* studies may be limited, especially with the additional difficulties caused by cardiac motion. This is the first time metabolite ADCs have been measured in the perfused heart and that the cardiomyocyte diameter has been determined using localised NMR diffusion spectroscopy.

Appendix A: Buffer compositions

Table A1: Composition of the basic Krebs-Henseleit buffer and the KCl-arrest Krebs-Henseleit buffer containing 20 mM KCl. The Na^+ concentration was lowered to keep a constant osmolarity.

Component	Basic Krebs-Henseleit *Concentration (mM)*	KCl-arrest Krebs-Henseleit *Concentration (mM)*
NaCl	118	102.7
KCl	4.7	20
$MgSO_4.7H_2O$	1.2	1.2
$CaCl_2.2H_2O$	1.75	1.75
Na_2-EDTA	0.5	0.5
$NaHCO_3$	25	25
KH_2PO_4	1.2	1.2

Table A2: Substrates and substances used in addition to the basic and the KCl-arrest Krebs-Henseleit perfusion buffer in the various chapters. "/" indicates that two experiments were conducted with two different concentrations of the indicated buffer component.

Component	Chapter 2 Volume experiments *Concentration (mM)*	Chapter 4 Buffer experiments *Concentration (mM)*	Chapters 5-8 All experiments *Concentration (mM)*
DMMP	10		
PPA	5		
NaOH	8.4		
Glucose	11 / 0	11 / 0	
Na-pyruvate	1 / 0	0 / 1.8	1.8
Na-lactate		0 / 0.2	0.2
Na-acetate		0 / 5	5

Appendix B: **b**-matrix calculations using the Mathematica programme

This Mathematica document calculates the **b**-matrices for the slice-selective STEAM pulse sequence. The calculation is carried out for a diffusion gradient of 1 G/cm applied in the x-direction. The b-matrix is calculated according to the equation:

$$\mathbf{b} = \gamma^2 \int_0^{TE} \left[\vec{F}(t') - 2H\left(t' - \frac{TE}{2}\right)\vec{f} \right] * \left[\vec{F}(t') - 2H\left(t' - \frac{TE}{2}\right)\vec{f} \right]^T dt' \qquad \text{(B.1)}$$

where H is the Heaviside function and the second term is a transposed vector (see Chapter 1). The vector function $\vec{F}$ is given by:

$$\vec{F}(t) := \int_0^t \vec{G}(t')dt' = \int_0^t \begin{pmatrix} G_x(t') \\ G_y(t') \\ G_z(t') \end{pmatrix} dt' \qquad \text{(B.2)}$$

The b-matrices are calculated according to the schematic diagram of the STEAM pulse sequence shown in Fig. B1.

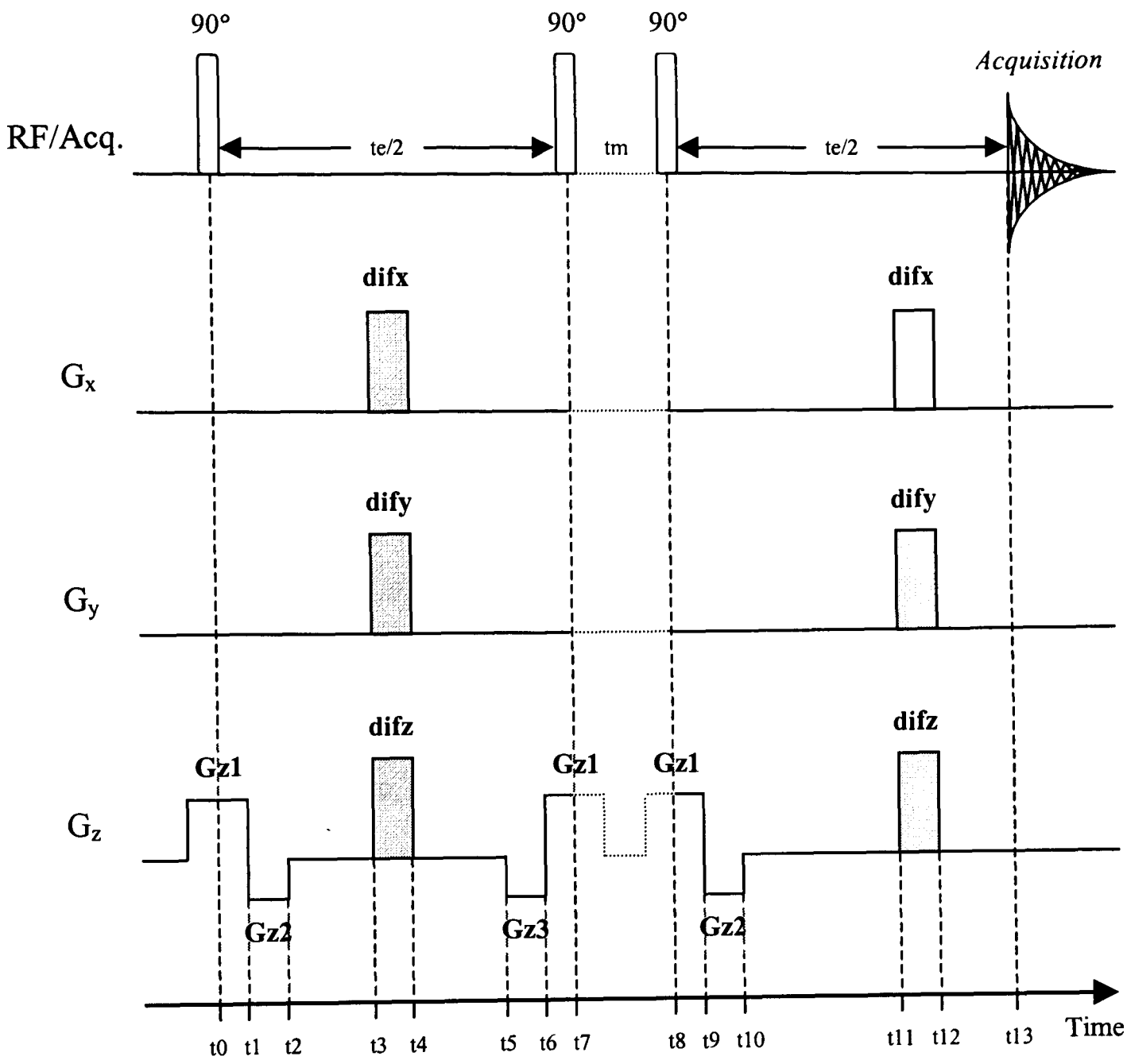

Fig. B1: Schematic of the slice-selective STEAM pulse sequence used in the Mathematica program to calculate the b-matrices. Gradients during the TM period are not drawn because they do not enter the calculation.

Input values

Enter TE, TM, δ, and the components of the diffusion gradient, difx, dify and difz. The factor *gcon* converts the gradient strength from units of G/cm into Hz/mm;

```
gcon = 428.63
428.63
te = 0.02
0.02
tm = 0.04
0.04
tdelta = 0.005
0.005
difx = gcon*1
428.63
dify = gcon*0
0
difz = gcon*0
0
```

Calculation of the correction terms in the first and second TE/2-, and the TM- period:

```
tau1 = te/2-(tdelta+0.00452)
0.00048
tau2 = tm-0.03608
0.00392
tau3 = te/2-(tdelta+0.00301)
0.00199
```

Definition of the pulse sequence timing:

```
t1 = 0.00051
0.00051
t2 = t1+0.001
0.00151
t3 = t2+0.0005+tau1
0.00249
t4 = t3+tdelta
0.00749
t5 = t4+0.0005
0.00799
t6 = t5+0.001
0.00899
t7 = t6+0.00101
0.01
t8 = t7+tm
0.05
t9 = t8+0.00051
0.05051
t10 = t9+0.001
0.05151
t11 = t10+0.0005
0.05201
t12 = t11+tdelta
0.05701
t13 = t12+0.001+tau3
```

```
0.06
```

Calculation of Δ:

```
DELTA = t11 - t3
0.04952
```

Specification of the slice-selection gradient strengths:

```
Gz1 = -gcon * 4.66558
-1999.81
Gz2 = gcon * 2.62002
1123.02
Gz3 = gcon * 4.47165
1916.68
```

The vector function $\vec{F}\left(TE/2\right)$ is defined component-wise and is specific for each gradient switching pattern in a pulse sequence. In the case of the slice-selective STEAM pulse sequence it is given by:

```
fx = difx * (t4 - t3)
2.14315
fy = dify * (t4 - t3)
0
fz = Gz1 * t1 + Gz2 * (t2 - t1) + difz * (t4 - t3) +
   Gz3 * (t6 - t5) + Gz1 * (t7 - t6)
-4.97211×10^-6
```

Together this then defines the vector function $\vec{F}$ at TE/2:

```
f = ⎛ fx ⎞
    ⎜ fy ⎟
    ⎝ fz ⎠
{{2.14315}, {0}, {-4.97211×10^-6}}
```

Time-dependent definition of the function $\vec{F}$:

<u>1.) 0 < t < t1</u>

```
Fx1[t_] := 0
Fy1[t_] := 0
Fz1[t_] := Gz1 * t
```

where these components are basically the area of all gradients up to that point in the timing of the pulse sequence;

$$\mathbf{F1[t\_]} = \begin{pmatrix} \mathbf{Fx1[t]} \\ \mathbf{Fy1[t]} \\ \mathbf{Fz1[t]} \end{pmatrix}$$

```
{{0}, {0}, {-1999.81 t}}
```

Calculate the first factor in the basic b-matrix equation:

```
H1[t_] := F1[t]
```

This term needs to be multiplied with its transposed:

```
J1[t_] := H1[t] . Transpose[H1[t]]
```

Integration of every single element of the matrix:

$$\mathbf{K1[t\_]} = \int_0^{t1} \mathbf{J1[t]}\, \mathbf{dt}$$

```
{{0, 0, 0}, {0, 0, 0}, {0, 0, 0.000176834}}
```

In future omit all comments and just perform calculation.

2.) t1 < t < t2

```
Fx2[t_] := 0
Fy2[t_] := 0
Fz2[t_] := Gz1 * t1 + Gz2 * (t - t1)
```

$$\mathbf{F2[t\_]} := \begin{pmatrix} \mathbf{Fx2[t]} \\ \mathbf{Fy2[t]} \\ \mathbf{Fz2[t]} \end{pmatrix}$$

```
H2[t_] := F2[t]
```

$$\mathbf{K2[t\_]} := \int_{t1}^{t2} (\mathbf{H2[t]} . \mathbf{Transpose[H2[t]]})\, \mathbf{dt}$$

3.) t2 < t < t3

$$Fx3[t\_] := 0$$
$$Fy3[t\_] := 0$$
$$Fz3[t\_] := Gz1 * t1 + Gz2 * (t2 - t1)$$
$$F3[t\_] := \begin{pmatrix} Fx3[t] \\ Fy3[t] \\ Fz3[t] \end{pmatrix}$$
$$H3[t\_] := F3[t]$$
$$K3[t\_] := \int_{t2}^{t3} (H3[t] \cdot Transpose[H3[t]])\, dt$$

4.) t3 < t < t4

$$Fx4[t\_] := difx * (t - t3)$$
$$Fy4[t\_] := dify * (t - t3)$$
$$Fz4[t\_] := Gz1 * t1 + Gz2 * (t2 - t1) + difz * (t - t3)$$
$$F4[t\_] := \begin{pmatrix} Fx4[t] \\ Fy4[t] \\ Fz4[t] \end{pmatrix}$$
$$H4[t\_] := F4[t]$$
$$K4[t\_] := \int_{t3}^{t4} (H4[t] \cdot Transpose[H4[t]])\, dt$$

5.) t4 < t < t5

$$Fx5[t\_] := difx * (t4 - t3)$$
$$Fy5[t\_] := dify * (t4 - t3)$$
$$Fz5[t\_] := Gz1 * t1 + Gz2 * (t2 - t1) + difz * (t4 - t3)$$
$$F5[t\_] := \begin{pmatrix} Fx5[t] \\ Fy5[t] \\ Fz5[t] \end{pmatrix}$$
$$H5[t\_] := F5[t]$$
$$K5[t\_] := \int_{t4}^{t5} (H5[t] \cdot Transpose[H5[t]])\, dt$$

6.) t5 < t <t6

$$Fx6[t\_] := difx * (t4 - t3)$$
$$Fy6[t\_] := dify * (t4 - t3)$$
$$Fz6[t\_] := Gz1 * t1 + Gz2 * (t2 - t1) + difz * (t4 - t3) + Gz3 * (t - t5$$
$$F6[t\_] := \begin{pmatrix} Fx6[t] \\ Fy6[t] \\ Fz6[t] \end{pmatrix}$$
$$H6[t\_] := F6[t]$$
$$K6[t\_] := \int_{t5}^{t6} (H6[t] \cdot Transpose[H6[t]])\, dt$$

7.) t6 < t < t7

$$Fx7[t\_] := difx * (t4 - t3)$$
$$Fy7[t\_] := dify * (t4 - t3)$$
$$Fz7[t\_] := Gz1 * t1 + Gz2 * (t2 - t1) + difz * (t4 - t3) + Gz3 * (t6 - t5) + Gz1 * (t - t6)$$
$$F7[t\_] := \begin{pmatrix} Fx7[t] \\ Fy7[t] \\ Fz7[t] \end{pmatrix}$$
$$H7[t\_] := F7[t]$$
$$K7[t\_] := \int_{t6}^{t7} (H7[t] \cdot Transpose[H7[t]])\, dt$$

8.) t7 < t < t8

From now on the Heaviside function, Hi[t_], equals 1;

$$Fx8[t\_] := difx * (t4 - t3)$$
$$Fy8[t\_] := dify * (t4 - t3)$$
$$Fz8[t\_] := Gz1 * t1 + Gz2 * (t2 - t1) + difz * (t4 - t3) + Gz3 * (t6 - t5) + Gz1 * (t7 - t6)$$
$$F8[t\_] := \begin{pmatrix} Fx8[t] \\ Fy8[t] \\ Fz8[t] \end{pmatrix}$$
$$H8[t\_] := F8[t] - 2 * f$$
$$K8[t\_] := \int_{t7}^{t0} (H8[t] \cdot Transpose[H8[t]])\, dt$$

9.) t8 < t <t9

$$Fx9[t\_] := difx * (t4 - t3)$$
$$Fy9[t\_] := dify * (t4 - t3)$$
$$Fz9[t\_] := Gz1 * t1 + Gz2 * (t2 - t1) + difz * (t4 - t3) + Gz3 * (t6 - t5) + Gz1 * (t7 - t6) + Gz1 * (t - t8)$$
$$F9[t\_] := \begin{pmatrix} Fx9[t] \\ Fy9[t] \\ Fz9[t] \end{pmatrix}$$
$$H9[t\_] := F9[t] - 2 * f$$
$$K9[t\_] := \int_{t0}^{t9} (H9[t] \,.\, Transpose[H9[t]])\, dt$$

10.) t9 < t < t10

$$Fxa[t\_] := difx * (t4 - t3)$$
$$Fya[t\_] := dify * (t4 - t3)$$
$$Fza[t\_] := Gz1 * t1 + Gz2 * (t2 - t1) + difz * (t4 - t3) + Gz3 * (t6 - t5) + Gz1 * (t7 - t6) + Gz1 * (t9 - t8) + Gz2 *$$
$$F10[t\_] := \begin{pmatrix} Fxa[t] \\ Fya[t] \\ Fza[t] \end{pmatrix}$$
$$H10[t\_] := F10[t] - 2 * f$$
$$K10[t\_] := \int_{t0}^{t10} (H10[t] \,.\, Transpose[H10[t]])\, dt$$

11.) t10 < t < t11

$$Fxb[t\_] := difx * (t4 - t3)$$
$$Fyb[t\_] := dify * (t4 - t3)$$
$$Fzb[t\_] :=$$
$$Gz1 * t1 + Gz2 * (t2 - t1) + difz * (t4 - t3) + Gz3 * (t6 - t$$
$$Gz1 * (t7 - t6) + Gz1 * (t9 - t8) + Gz2 * (t10 - t9)$$
$$F11[t\_] := \begin{pmatrix} Fxb[t] \\ Fyb[t] \\ Fzb[t] \end{pmatrix}$$
$$H11[t\_] := F11[t] - 2 * f$$
$$K11[t\_] := \int_{t10}^{t11} (H11[t] \,.\, Transpose[H11[t]])\, dt$$

12.) t11 < t < t12

```
Fxc[t_] := difx * (t4 - t3) + difx * (t - t11)
Fyc[t_] := dify * (t4 - t3) + dify * (t - t11)
Fzc[t_] := Gz1 * t1 + Gz2 * (t2 - t1) +
  difz * (t4 - t3) + Gz3 * (t6 - t5) + Gz1 * (t7 - t6) +
  Gz1 * (t9 - t8) + Gz2 * (t10 - t9) + difz * (t - t11)
```

$$F12[t\_] := \begin{pmatrix} Fxc[t] \\ Fyc[t] \\ Fzc[t] \end{pmatrix}$$

```
H12[t_] := F12[t] - 2 * f
```

$$K12[t\_] := \int_{t11}^{t12} (H12[t] \cdot Transpose[H12[t]])\, dt$$

13.) t12 < t < t13

```
Fxd[t_] := difx * (t4 - t3) + difx * (t12 - t11)
Fyd[t_] := dify * (t4 - t3) + dify * (t12 - t11)
Fzd[t_] := Gz1 * t1 + Gz2 * (t2 - t1) +
  difz * (t4 - t3) + Gz3 * (t6 - t5) + Gz1 * (t7 - t6) +
  Gz1 * (t9 - t8) + Gz2 * (t10 - t9) + difz * (t12 - t11)
```

$$F13[t\_] := \begin{pmatrix} Fxd[t] \\ Fyd[t] \\ Fzd[t] \end{pmatrix}$$

```
H13[t_] := F13[t] - 2 * f
```

$$K13[t\_] := \int_{t12}^{t13} (H13[t] \cdot Transpose[H13[t]])\, dt$$

Add up all the Ki[t]. Multiply final **b**-matrix by $4\pi^2$ to take account of the unit conversion of the gradient strength from G/cm into Hz/mm;

```
b = 4 π^2 * (K1[t] + K2[t] + K3[t] + K4[t] + K5[t] + K6[t] +
      K7[t] + K8[t] + K9[t] + K10[t] + K11[t] + K12[t] + K
{{8.67715, 0., 0.236878}, {0., 0., 0.},
 {0.236878, 0., 0.155923}}
```

Appendix C: Simulation to estimate ADC changes during ischaemia and reperfusion caused by signal changes due to shrinking and swelling.

In this work, ADCs were generally obtained over a series of five experiments with increasing *b*-values ranging from 9 s/mm^2 to 1466 s/mm^2; using the water-suppressed slice-selective STEAM sequence, a typical ADC value would be around 0.3×10^{-3} mm^2/s. The semi-logarithmic signal attenuation of such a measurement was simulated using these parameters, and is shown in Fig. C1*a*, representing, for instance, taurine diffusion in the perfused rat heart. If the heart is made ischaemic, the resulting shrinkage causes an increase in the signal S_0, and the diffusion-mediated signal attenuation would be negated by an increased number of myocytes in the selected slice. In Fig. C1*b* it has been assumed that S_0 increased in 5% steps from one measurement to the next; this assumption is realistic as demonstrated in Chapter 5. This would lead to an underestimation of the ADC by about 40%. Similarly, the signal decreases during the initial period of reperfusion due to the swelling of the heart, accelerating the signal losses that occur due to diffusion effects. Assuming a progressive 5% decrease of the signal, this will lead to an overestimation of the ADC values by about 45% (Fig. C1*c*).

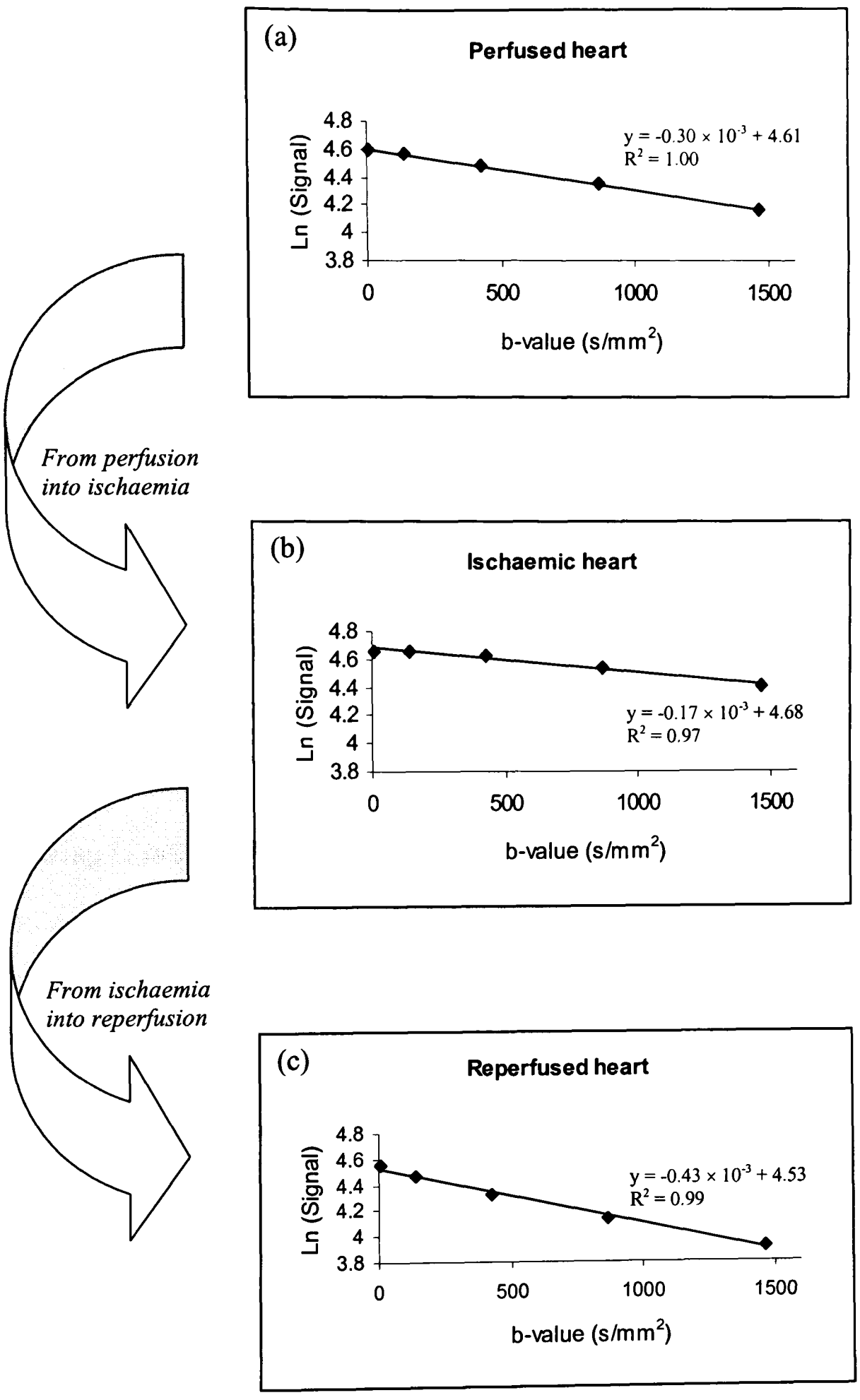

Fig. C1a-c: The artificial decrease and increase of the ADC as measured with the slice-selective STEAM sequence during the transition phase between perfusion, ischaemia and reperfusion. Substantial under- and overestimation of the ADC could be caused by a change in the number of myocytes in the selected slice. For details see text.

Appendix D: Simulation of the expected ADC variations due to S_0 changes during ischaemia and reperfusion

For this simulation it was assumed that the ADCs were measured using five *b*-values and by obtaining the best linear fit of a semi-logarithmic plot of the signal intensities *vs.* their respective *b*-values. It was further assumed that the 'ideal' signal amplitudes measured for each *b*-value yielded an ADC of 0.3×10^{-3} mm^2/s. To investigate what effect the shrinking process had on the measurement of the ADC, each 'ideal' signal was multiplied by the degree of shrinkage experienced by the heart at that particular time point. Eq 5.1 and the fitted rate of shrinking, k_{isch}, were used to calculate this correction. The best linear fit was then obtained through these values and the slope was the ADC measured when shrinking is present. For the swelling process, the same method was applied, this time employing the swelling equation (eq 5.2) and its respective fitted parameters (Table 5.5). Fig. D1 shows the relative values of the measured ADC, taking into account the signal changes due to shrinking and swelling, divided by the expected ADC during the intervention (i.e. by 0.3×10^{-3} mm^2/s) . The ADC would be underestimated by around 23% at the beginning of the ischaemic period due to the shrinking process, and overestimated by 26% upon reperfusion due to the swelling process.

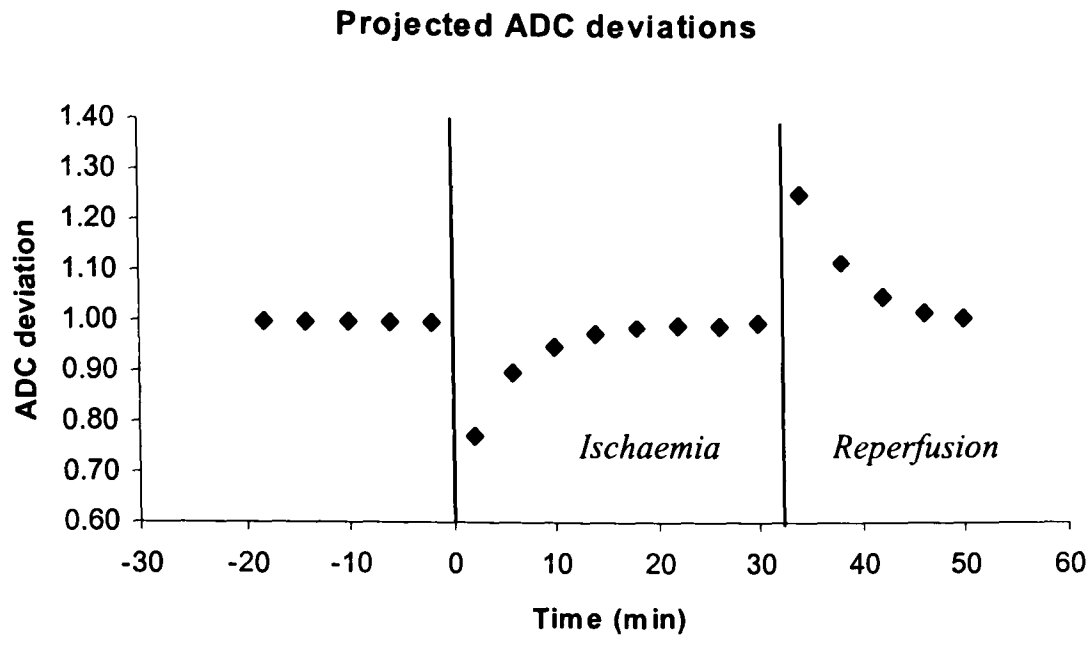

Fig. D1: Graph displaying the relative error in the ADC estimation due to the shrinking and swelling process during ischaemia and reperfusion.

Appendix E: S_0 corrections of ADC data during ischaemia and reperfusion

As pointed out in Chapter 5, errors in the estimation of the metabolite ADCs acquired from a perfused heart using the slice-selective STEAM sequence occur due to the effects of changes in the perfusion pressure during ischaemia and reperfusion, respectively. Fig. E1 illustrates the uncorrected and corrected taurine ADC data acquired in Chapter 6 from hearts during perfusion, ischaemia and reperfusion. S_0 corrections were carried out for each spectrum according to the data acquired in Chapter 5. The height of the taurine peak in each acquired spectrum was multiplied by a factor reflecting the change in the heart size caused by the change in the perfusion pressure. ADCs were then calculated from the corrected data as usual, using a linear best fit of the semi-logarithmic peak heights. Gaussian error progression was used to calculate the errors of the corrected data.

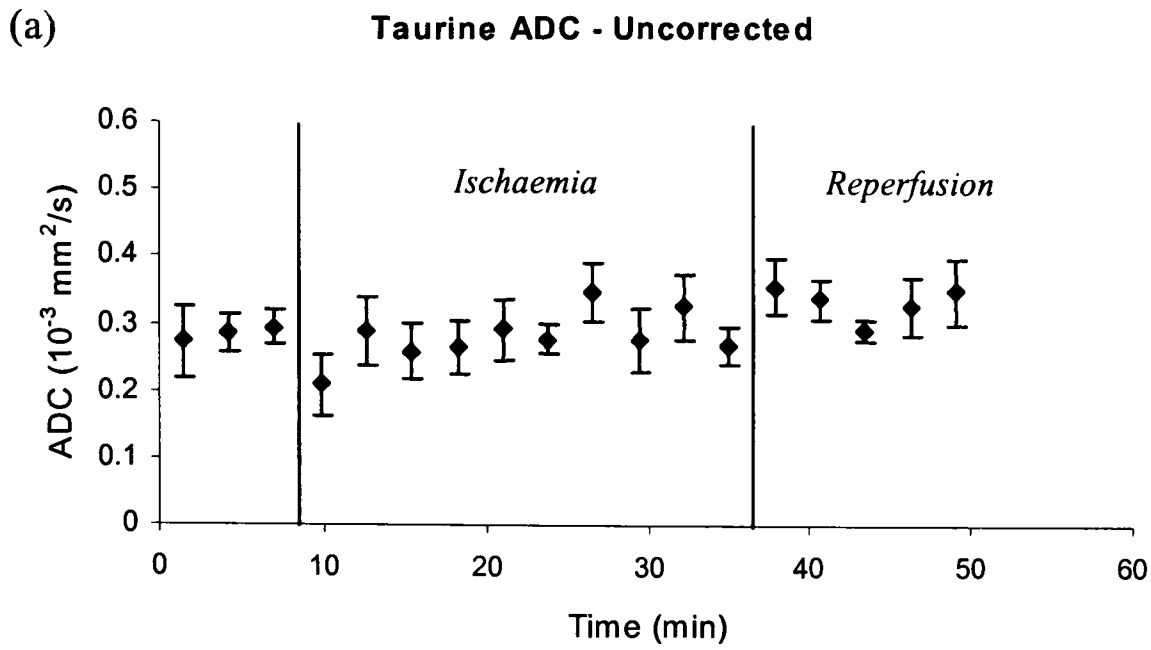

Fig. E1: Taurine ADC during perfusion, total global ischaemia and reperfusion from all hearts (n = 4). (a) uncorrected, (b), corrected for artefacts caused by the effects of the changes in the perfusion pressure during ischaemia and reperfusion (obtained from Chapter 5).

The changes were most obvious during the transition from perfusion to ischaemia, where the uncorrected ADC was lifted to a level identical to that throughout ischaemia.

A similar correction can be seen for the first ischaemia ADC for the total creatine peak in Fig. E2. Here changes in the available magnetisation detected in Chapter 5 resulted in a

considerable overestimation of the total creatine ADC during the transition phase from perfusion into ischaemia. S_0 corrections were taken from Fig. 5.5.

(a)

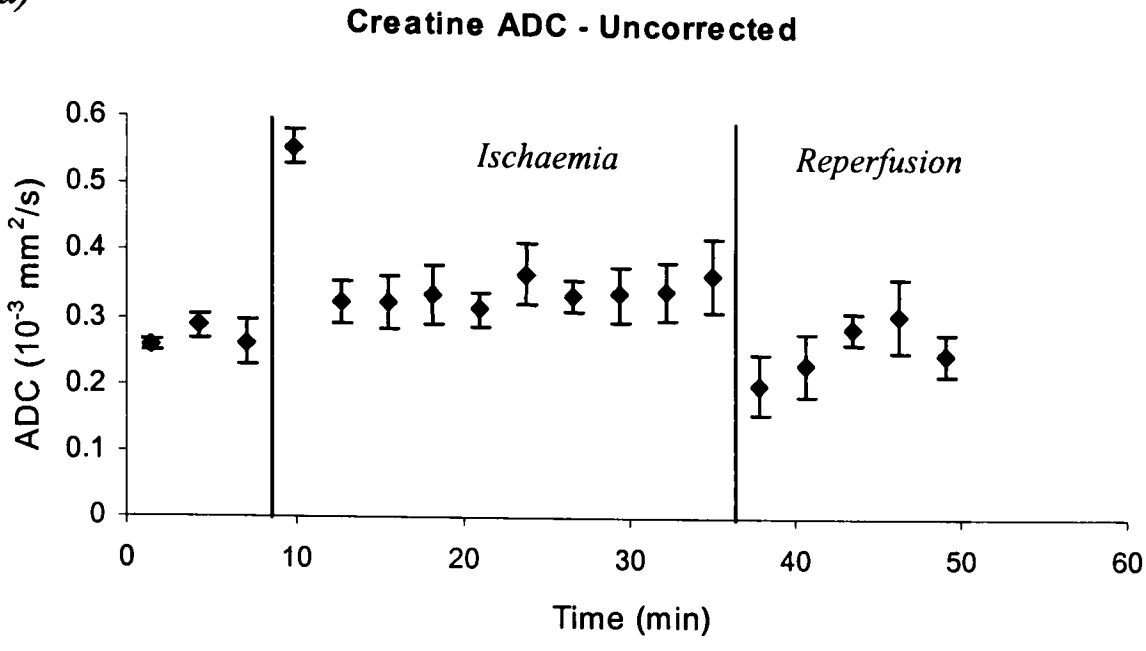

(b)

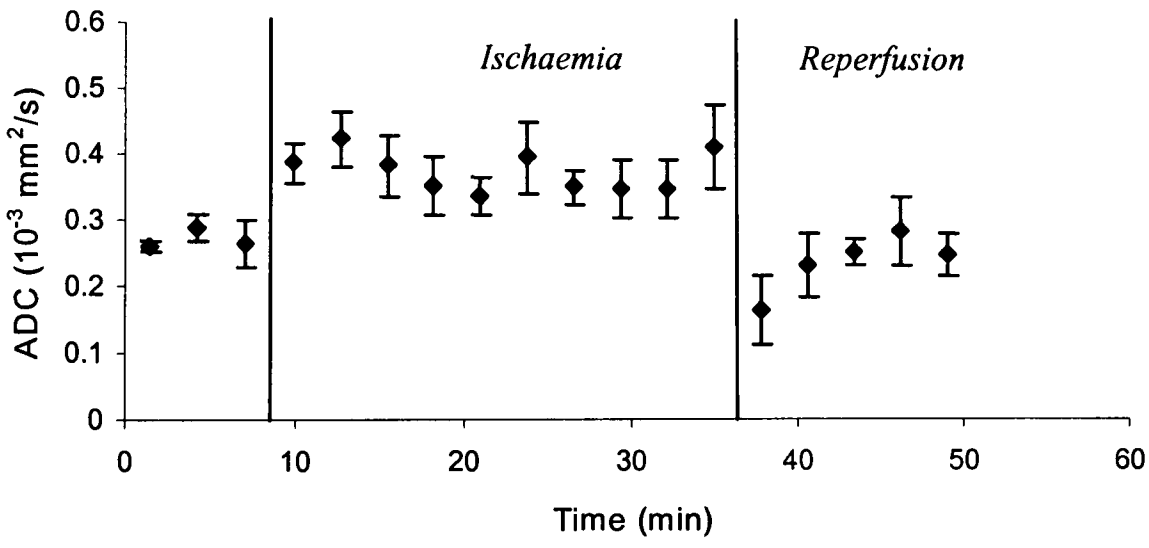

Fig. E2: Total creatine ADC during the protocol. (a), uncorrected; (b), corrected for the apparent ADC changes induced by changes in the perfusion pressure during ischaemia and reperfusion. Note that the initial sharp increase of the ADC upon induction of ischaemia was an artefact caused by those effects.

Appendix F: Estimated change in the total creatine ADC based on the conversion from PCr to creatine during the ischaemic period

The expected ADC change of the total creatine peak is calculated, based on the complete hydrolysis of PCr to creatine. The following assumptions are made:

a.) PCr and creatine are in fast exchange during the perfusion period

b.) The Stokes-Einstein equation applies

c.) The sum of the PCr and the creatine content is constant at all times

d.) The PCr concentration declined rapidly to zero during the ischaemic period

It then follows from assumptions *(a)* and *(b)* that the ADC during the perfusion period, ADC_{normal}, can be expressed as:

$$ADC_{normal} = \frac{[PCr]}{[PCr]+[Cr]} \cdot \frac{kT}{6\pi\eta_{normal} R_{H,PCr}} + \frac{[Cr]}{[PCr]+[Cr]} \cdot \frac{kT}{6\pi\eta_{normal} R_{H,Cr}} \qquad \text{(F.1)}$$

where *[PCr]* and *[Cr]* refer to the PCr and creatine content, k is the Boltzmann constant, T the absolute temperature, η the viscosity during perfusion and ischaemia, and R_H the hydrodynamic radius of PCr and creatine.

During ischaemia, with the PCr hydrolysed to creatine, the ADC is given by:

$$ADC_{isch} = \frac{kT}{6\pi\eta_{isch} R_{H,Cr}} \qquad \text{(F.2)}$$

Rearranging eq F.2 yields the ratio of the ADC during ischaemia to that during the perfusion period of

$$\frac{ADC_{isch}}{ADC_{normal}} = \frac{\eta_{normal}}{\eta_{isch}} \cdot \frac{1+x}{1+\frac{R_{H,Cr}}{R_{H,PCr}}x} \qquad \text{(F.3)}$$

where $x = [PCr]/[Cr]$. For instance, with an initial PCr concentration 2.3 ± 0.2 times higher than the initial creatine concentration as obtained in Chapter 2, the above ratio is 1.22 ± 0.02, provided the viscosity does not change in ischaemia. In other words, when all the PCr is converted to creatine the total creatine ADC should have increased by 22 ± 2%. However, because the Stokes-Einstein equation is strictly applicable only in infinite solutions, the viscosities in eq F.3 represent an overall hindrance factor to the molecular motion, including the 'true' viscosity as well as the effects of obstacles such as cell organelles. It can be assumed that this 'apparent viscosity' remains constant due to either the balance between organellar and cellular swelling or the absence of cell swelling during ischaemia, as shown by the constancy of the taurine ADC during the ischaemic period (Chapter 6). In that case, the maximum increase in the ADC of the total creatine peak is given by

$$\left.\frac{ADC_{isch}}{ADC_{normal}}\right|_{x\to\infty} = \frac{R_{H,PCr}}{R_{H,Cr}} = 1.34 \pm 0.03 \qquad \text{(F.4)}$$

In other words, if all the creatine exists as PCr during the perfusion period, PCr hydrolysis causes an increase in the total creatine ADC of 34 ± 3%, which is equal to the ratio of the hydrodynamic radii of the two compounds.

References

Agutter, P. S., Malone, P. C., and Wheatley, D. N. (1995). "Intracellular transport mechanisms: A critique of diffusion theory." *J. Theor. Biol.*, 176, 261-272.

Arnold, G., Kosche, F., Miessner, E., Neitzert, A., and Lochner, W. (1968). "The importance of the perfusion pressure in the coronary arteries for the contractility and the oxygen consumption of the heart." *Pflügers Archive*, 299, 339-356.

Arrio-Dupont, M., Cribier, S., Foucault, G., Devaux, P. E., and d'Albis, A. (1996). "Diffusion of fluorescently labeled macromolecules in cultured muscle cells." *Biophys. J.*, 70, 2327-2332.

Assaf, Y., and Cohen, Y. (1998). "Non-mono-exponential attenuation of water and N-acetyl aspartate signals due to diffusion in brain tissue." *J. Magn. Reson.*, 131, 69-85.

Baker, H., Lindsey, J., and Weisbroth, S. (1980). "The laboratory rat." , Academic Press, New York, 257-258.

Balinov, B., Jönsson, B., Linse, P., and Söderman, O. (1993). "The NMR self-diffusion method applied to restricted diffusion. Simulation of echo attenuation from molecules in spheres and between planes." *J. Magn. Reson. Ser. A*, 104, 17-25.

Barry, J. A., McGovern, K. A., Lien, Y.-H. H., Ashmore, B., and Gillies, R. J. (1993). "Dimethyl methylphosphonate (DMMP): A ^{31}P nuclear magnetic resonance spectroscopic probe of intracellular volume in mammalian cell cultures." *Biochemistry*, 32, 4665-4670.

Barth, E., Stämmler, G., Speiser, B., and Schaper, J. (1992). "Ultrastructural quantitation of mitochondria and myofilaments in cardiac muscle from 10 different animal species including man." *J. Mol. Cell. Cardiol.*, 24, 669-681.

Basser, P. J. (1995). "Inferring microstructural features and the physiological state of tissues from diffusion-weighted images." *NMR Biomed.*, 8, 333-344.

Basser, P. J., and Le Bihan, D. (1992). "Fibre orientation mapping in an anisotropic medium with NMR diffusion spectroscopy." *Proc. Soc. Magn. Reson. Med. 11th Sci. Meeting*, 1221.

Basser, P. J., Mattiello, J., and Le Bihan, D. (1992). "Diagonal and off-diagonal components of the self-diffusion tensor: their relation to and estimation from the NMR spin-echo signal." *Proc. Soc. Magn. Reson. Med. 11th Sci. Meeting*, 1222.

Basser, P. J., Mattiello, J., and Le Bihan, D. (1994a). "Estimation of the effective self-diffusion tensor from the NMR spin echo." *J. Magn. Reson., Ser. B*, 103, 247-254.

Basser, P. J., Mattiello, J., and Le Bihan, D. (1994b). "MR diffusion tensor spectroscopy and imaging." *Biophys. J.*, 66, 259-267.

Basser, P. J., and Pierpaoli, C. (1996). "Microstructural and physiological features of tissues elucidated by quantitative-diffusion-tensor MRI." *J. Magn. Reson., Ser. B*, 111, 209-219.

Basser, P. J., and Pierpaoli, C. (1998). "A simplified method to measure the diffusion tensor from seven MR images." *Magn. Reson. Med.*, 39, 928-934.

Benveniste, H., Hedlund, L. W., and Johnson, G. A. (1992). "Mechanism of detection of acute cerebral ischaemia in rats by diffusion-weighted magnetic resonance microscopy." *Stroke*, 23, 746-754.

Bottomley, P. A., Foster, T. H., Argersinger, R. E., and Pfeifer, L. M. (1984). "A review of normal tissue hydrogen NMR relaxation times and relaxation mechanisms from 1-100 MHz: Dependence on tissue type, NMR frequency, temperature, species, excision, and age." *Med. Phys.*, 11(4), 425-448.

Boyett, M. R., and Kirby, M. S. (1989). "Changes in the length, width and volume of isolated rat ventricular myocytes during an unloaded twitch contraction." *J. Physiol.*, 416, 40P.

Busza, A. L., Allen, K. L., King, M. D., van Bruggen, N., Williams, S. R., and Gadian, D. G. (1992). "Diffusion-weighted imaging studies of cerebral ischaemia in gerbils." *Stroke*, 23, 1602-1612.

Caillé, J. P., and Hinke, J. A. M. (1974). "The volume available to diffusion in the muscle fibre." *Can. J. Physiol. Pharmacol.*, 52, 814-828.

Callaghan, P. T. (1995). "Pulsed-gradient spin-echo NMR for planar, cylindrical, and spherical pores under conditions of wall relaxation." *J. Magn. Reson., Ser. A*, 113, 53-59.

Callaghan, P. T., Jolley, K. W., and Trotter, C. M. (1980). "Stable and accurate spin echoes in pulsed field gradient NMR." *J. Magn. Reson.*, 39, 525-527.

Carano, R. A. D., Li, F., Irie, K., Fisher, M., and Sotak, C. H. (1998). "The temporal evolution of diffusion anisotropy in the ischaemic rat brain." *Proc. Int. Soc. Magn. Reson. Med. 6th Sci. Meeting*, 530.

Chadwick, R. S. (1982). "Mechanics of the left ventricle." *Biophys. J.*, 39, 279-288.

Chanin, M., Roberts, E., and Goldman, A. (1956). "Influence of experimental myocardial infarction on free amino acids of dog heart." *Circ. Res.*, 6, 713-717.

Chapman, R. A., Suleiman, M.-S., and Earm, Y. E. (1993). "Taurine and the heart." *Cardiovasc. Res.*, 27, 358-363.

Choy, P. C., Chan, M., Hatch, G., and Man, R. Y. K. (1992). "Phosphatidylcholine metabolism in ischemic and hypoxic hearts." *Mol. Cell. Biochem.*, 116, 53-58.

Clark, J. F. (1997). "Creatine and phosphocreatine: A review of their use in exercise and sport." *J. Athletic Training*, 32, 45-51.

Clarke, K., Anderson, R. E., Nedelec, J.-F., Foster, D. O., and Ally, A. (1994). "Intracellular and extracellular spaces and the direct quantification of molar intracellular concentrations of phosphorus metabolites in the isolated rat heart using ^{31}P NMR spectroscopy and phosphonate markers." *Magn. Reson. Med.*, 32, 181-188.

Clarke, K., Nedelec, J.-F., Mills, P. A., and Ingwall, J. S. (1990). "Intra- and extracellular volumes during myocardial ischemia and reperfusion: Use of ^{31}P NMR spectroscopy and phosphonates in the isovolumic rat heart." *Proc. Soc. Magn. Reson. Med. 9th Sci. Meeting*, 177.

Clarke, K., Stewart, L. C., Neubauer, S., Balschi, J. A., Smith, T. W., Ingwall, J. S., Nedelec, J.-F., Humphrey, S. M., Kleber, A. G., and Springer, C. S. (1993). "Extracellular volume and transsarcolemmal proton movement during ischaemia and reperfusion: a ^{31}P NMR spectroscopic study of the isovolumic rat heart." *NMR Biomed.*, 6, 278-286.

Clarke, K., and Willis, R. J. (1987). "Energy metabolism and contractile function in rat heart during graded, isovolumic perfusion using ^{31}P nuclear magnetic resonance spectroscopy." *J. Mol. Cell. Cardiol.*, 19, 1153-1160.

Clegg, J. S. (1984). "Properties and metabolism of the aequeous cytoplasm and its boundaries." *Am. J. Physiol.*, 246, R133-R151.

Cleveland, G. G., Chang, D. C., Hazlewood, C. F., and Rorschach, H. E. (1976). "Nuclear magnetic resonance measurement of skeletal muscle. Anisotropy of the diffusion coefficient of the intracellular water." *Biophys. J.*, 16, 1043-1053.

Cooper, R. L., Chang, D. B., Young, A. C., Martin, C. J., and Ancker-Johnson, B. (1974). "Restricted diffusion in biophysical systems." *Biophys. J.*, 14, 161-177.

Coremans, J., Luypaert, R., Verhelle, F., Stadnik, T., and Osteaux, M. (1994). "A method for myelin fiber orientation mapping using diffusion-weighted MR Images." *Magn. Reson. Imag.*, 12(3), 443-454.

Crass, M. F., III, and Lombardini, J. B. (1978). "Release of tissue taurine from the oxygen-deficient perfused rat heart." *Proc. Soc. Exp. Biol. Med.*, 157(3), 486-488.

Cross, H. R., Clarke, K., Opie, L. H., and Radda, G. K. (1995a). "Is lactate-induced myocardial ischaemic injury mediated by decreased pH or increased intracellular lactate?" *J. Mol. Cell. Cardiol.*, 27, 1369-1381.

Cross, H. R., Radda, G. K., and Clarke, K. (1995b). "The role of Na^+/K^+ ATPase activity during low flow ischemia in preventing myocardial injury: A ^{31}P, ^{23}Na and ^{87}Rb NMR spectroscopic study." *Magn. Reson. Med.*, 34, 673-685.

Davis, D., Ulatowski, J., Eleff, S., Izuta, M., Mori, S., Shungu, D., and van Zijl, P. C. M. (1994). "Rapid monitoring of changes in water diffusion coefficients during reversible ischemia in cat and rat brain." *Magn. Reson. Med.*, 31, 454-460.

de Graaf, R. A., van Kranenburg, A., and Nicolay, K. (1998). "*In vivo* ^{31}P NMR diffusion spectroscopy of phosphocreatine and ATP in rat skeletal muscle." *Proc. Int. Soc. Magn. Reson. Med. 6th Sci. Meeting.*

Decanniere, C., Eleff, S., Davis, D., and van Zijl, P. C. M. (1995). "Correlation of rapid changes in the average water diffusion constant and the concentrations of lactate and ATP breakdown products during global ischemia in cat brain." *Magn. Reson. Med.*, 34, 343-352.

Doran, M., Hajnal, J. V., van Bruggen, N., King, M. D., Young, I. R., and Bydder, G. M. (1990). "Normal and abnormal white matter tracts shown by MR imaging using directional diffusion weighted sequences." *J. Comp. Assist. Tomogr.*, 14, 865-873.

Dreher, W., and Leibfritz, D. (1998). "Apparent diffusion coefficient of metabolites with uncoupled and coupled resonances measured in the healthy rat brain by diffusion weighted ^{1}H-CT-PRESS." *Proc. Int. Soc. Magn. Reson. Med. 6th Sci. Meeting*, 343.

Drewnowska, K., and Baumgarten, C. M. (1991). "Regulation of cellular volume in rabbit ventricular myocytes: bumetanide, chlorothiazide, and ouabain." *Am. J. Physiol.*, 260, C122-C131.

Drewnowska, K., Clemo, H. F., and Baumgarten, C. M. (1991). "Prevention of myocardial intracellular edema induced by St. Thomas Hospital cardioplegic solution." *J. Mol. Cell. Cardiol.*, 23, 1215-1221.

Duong, T. Q., Ackerman, J. J. H., Yablonskiy, D., and Neil, J. J. (1998). "Extracellular and intracellular apparent diffusion in normal and focally-ischemic rat brain via ^{1}H MRS." *Proc. Int. Soc. Magn. Reson. Med. 6th Sci. Meeting*, 342.

Edelman, R. R., Gaa, J., Wedeen, V. J., Loh, E., Hare, J. M., Prasad, P., and Li, W. (1994). "*In vivo* measurement of water diffusion in the human heart." *Magn. Reson. Med.*, 32, 423-428.

Edoute, Y., van der Merwe, E., Sanan, D., Kotzé, J. C. N., Steinmann, C., and Lochner, A. (1983). "Normothermic ischemic cardiac arrest of the isolated working rat heart - Effects of time and reperfusion on myocardial ultrastructure, mitochondrial oxidative function, and mechanical recovery." *Circ. Res.*, 53, 663-678.

Einstein, A. (1906). "Eine neue Bestimmung der Molekueldimensionen." *Ann. Phys.*, 19, 289-306.

Fieno, D. S., and Judd, R. M. (1998). "Physiologic basis for potassium (^{39}K) MRI of the heart." *Proc. Int. Soc. Magn. Reson. Med. 6th Sci. Meeting*, 556.

Flaherty, J. T., Weisfeldt, M. L., Bulkley, B. H., Gardner, T. J., Gott, V. L., and Jacobus, W. E. (1982). "Mechanisms of ischemic myocardial cell damage assessed by phosphorus-31 nuclear magnetic resonance." *Circulation*, 65(3), 561-570.

Ford, J. C., Hackney, D. B., Alsop, D. C., Jara, H., Joseph, P. M., Hand, C. M., and Black, P. (1994). "MRI characterization of diffusion-coefficients in a rat spinal cord injury model." *Magn. Reson. Med.*, 31, 488-494.

Frahm, J., Haase, A., Matthaei, D., Merboldt, K.-D., and Hänicke, W. (1985). "Rapid NMR imaging using stimulated echoes." *J. Magn. Reson.*, 65, 130-135.

From, A. H. L., Petein, M. A., Michurski, S. P., Zimmer, S. D., and Ugurbil, K. (1986). "^{31}P-NMR studies of respiratory regulation in the intact myocardium." *FEBS*, 206(2), 257-261.

From, A. H. L., Zimmer, S. D., Michurski, S. P., Mohanakrishnan, P., Ulstad, V. K., Thoma, W. J., and Ugurbil, K. (1990). "Regulation of the oxidative phophorylation rate in the intact cell." *Biochemistry*, 29, 3731-3743.

Fujimori, H., Michaelis, T., Wick, M., and Frahm, J. (1998). "Proton T_2 relaxation of cerebral metabolites during transient global ischemia in rat brain." *Magn. Reson. Med.*, 39, 647-650.

Fushimi, K., and Verkman, A. S. (1991). "Low viscosity in the aqueous domain of cell cytoplasm measured by picosecond polarization microfluorimetry." *J. Cell. Biol.*, 112(4), 719-725.

Gadian, D. G. (1996). *NMR and its applications to living systems*, Academic Press, Oxford.

Gard, J. K., Kichura, G. M., Ackerman, J. J. H., Eisenberg, J. D., Billadello, J. J., Sobel, B. E., and Gross, R. W. (1985). "Quantitative ^{31}P nuclear magnetic resonance analysis of metabolite concentrations in Langendorff-perfused rabbit hearts." *Biophys. J.*, 48, 803-813.

Garlick, P. B., and Humphrey, S. M. (1989). "Ischemia affects the NMR-invisibility of ATP, PCr and Pi in the perfused rat heart." *Circulation abstracts*, I-693, 2760.

Garlick, P. B., and Townsend, R. M. (1992). "NMR visibility of Pi in perfused rat hearts is affected by changes in substrate and contractility." *Am. J. Physiol.*, 263, H497-H502.

Garrido, L., Wedeen, V. J., Kwong, K. K., Spencer, U. M., and Kantor, H. L. (1994). "Anisotropy of water diffusion in the myocardium of the rat." *Circ. Res.*, 74(5), 789-793.

Gershon, N. D., Porter, K. R., and Trus, B. L. (1985). "The cytoplasmic matrix: Its volume and surface area and the diffusion of molecules through it." *Proc. Natl. Acad. Sci. USA*, 82, 5030-5034.

Greve, G., and Grong, K. (1991). "Ultrastructural changes at the border of the ischaemic zone within one hour of coronary artery occlusion." *Acta Physiol. Scand.*, S599, 109-116.

Greve, G., Rotevatn, S., Svendby, K., and Grong, K. (1990). "Early morphologic changes in cat heart muscle cells after acute coronary artery occlusion." *Am. J. Pathol.*, 136, 273-283.

Haase, A., Frahm, J., Matthaei, D., Hänicke, W., Bomsdorf, H., Kunz, D., and Tischler, R. (1986). "MR imaging using stimulated echoes (STEAM)." *Radiology*, 160(3), 787-790.

Hahn, E. L. (1950). "Spin echoes." *Phys. Rev.*, 80(4), 580-594.

Hansen, J. R. (1971). "Pulsed NMR study of water mobility in muscle and brain tissue." *Biochim. Biophys. Acta*, 230, 482-486.

Harris, K. R., Mills, R., Back, P. J., and Webster, D. S. (1978). "An improved NMR spin-echo apparatus for the measurement of self-diffusion coefficients: The diffusion of water in aqueous electrolyte solutions." *J. Magn. Reson.*, 29, 473-482.

Hazlewood, C. F., Rorschach, H. E., and Lin, C. (1991). "Diffusion of water in tissues and MRI." *Magn. Reson. Med.*, 19, 214-216.

Helpern, J. A., Ordidge, R. J., and Knight, R. A. (1992). "The effect of cell membrane water permeability on the apparent diffusion coefficient of water." *Proc. Soc. Magn. Reson. Med. 11th Sci. Meeting*, 1201.

Henriksen, O., Rosenbaum, S., Sperling, B., and Boysen, G. (1995). "Increased NAA diffusion in ischemic human brain tissue." *Proc. Int. Soc. Magn. Reson. Med. 3rd Sci. Meeting*, 137.

Hsu, E. W., Atalay, M. K., Mori, S., and Forder, J. R. (1995). "Reduction of water apparent diffusion coefficient in regional myocardial ischaemia." *Proc. Int. Soc. Magn. Reson. Med. 3rd Sci. Meeting*, 1406.

Hsu, E. W., and Mori, S. (1995). "Analytical expressions for the NMR apparent diffusion coefficients in an anisotropic system and a simplified method for determining fiber orientation." *Magn. Reson. Med.*, 34, 194-200.

Hsu, E. W., Xue, R., Holmes, A., and Forder, J. R. (1998). "Delayed reduction of tissue water diffusion after myocardial ischemia." *Am. J. Physiol.*, 275, H697-H702.

Humphrey, S. M., and Garlick, P. B. (1991). "NMR-visible ATP and Pi in normoxic and reperfused rat hearts: a quantitative study." *Am. J. Physiol.*, 260, H6-H12.

Huxtable, R. J. (1978). "Regulation of taurine in the heart." Taurine and Neurological Disorders, A. Barbeau and R. J. Huxtable, eds., Raven Press, New York, 5-17.

Huxtable, R. J. (1992). "Physiological actions of taurine." *Physiol. Rev.*, 72(1), 101-161.

Idell-Wenger, J. A., Grotyohann, L. W., and Neely, J. R. (1978). "Coenzyme A and carnitine distribution in normal and ischemic hearts." *J. Biol. Chem.*, 253(12), 4310-4318.

Ingwall, J. S., Clarke, K., Stewart, L. C., and Bernard, M. (1996). "Cation movements across cell walls of intact tissues using MRS." *Encyclopaedia of NMR*, 1189-1196.

Jeffrey, F. M., Storey, C. J., Nunnally, R. L., and Malloy, C. R. (1989). "Effect of ischemia on NMR detection of phosphorylated metabolites in the intact rat heart." *Biochemistry*, 28, 5323-5326.

Jennings, R. B., Ganote, C. E., and Reimer, K. A. (1975). "Ischemic tissue injury." *Am. J. Pathol.*, 81, 179-198.

Jennings, R. B., Reimer, K. A., and Steenbergen, C. (1986). "Myocardial ischaemia revisited. The osmolar load, membrane damage, and reperfusion." *J. Mol. Cell. Cardiol.*, 18, 769-780.

Jennings, R. B., Scharper, J., Hill, M. L., Steenbergen, C., Jr., and Reimer, K. (1985). "Effect of reperfusion late in the phase of reversible ischemic injury. Changes in cell volume, electrolytes, metabolites, and ultrastructure." *Circ. Res.*, 56, 262-278.

Jones, D. K., Markus, H. S., Lythgoe, D., Williams, S. C. R., Simmons, A., and Horsfield, M. A. (1998a). "Characterisation of the nature of ischaemic damage in leukoaraiosis with diffusion tensor imaging." *Proc. Int. Soc. Magn. Reson. Med. 6th Sci. Meeting*, 194.

Jones, D. K., Simmons, A., Williams, S. C. R., and Horsfield, M. A. (1998b). "Non-invasive assessment of structural connectivity in white matter by diffusion tensor MRI." *Proc. Int. Soc. Magn. Reson. Med. 6th Sci. Meeting*, 531.

Kao, H. P., Abney, J. R., and Verkman, A. S. (1993). "Determinants of the translational mobility of a small solute in cell cytoplasm." *J. Cell Biol.*, 120(1), 175-184.

Kinsey, S. T., Locke, B. R., Penke, B., and Moerland, T. S. (1999). "Diffusional anisotropy is induced by subcellular barriers in skeletal muscle." *NMR Biomed.*, 12, 1-7.

Kirk, K. (1997). "Swelling-activated organic osmolyte channels." *J. Membrane Biol.*, 158, 1-16.

Kirk, K., and Kuchel, P. W. (1985). "Red cell volume changes monitored using a new ^{31}P NMR procedure." *J. Magn. Reson.*, 62, 568-572.

Knopf, H., Theising, R., Moon, C. H., and Hirche, H. (1990). "Continuous determination of extracellular space and changes of K^+, Na^+, Ca^{2+}, and H^+ during global ischaemia in isolated rat hearts." *J. Mol. Cell. Cardiol.*, 22, 1259-1272.

Kupriyanov, V. V., Jean, M. S., Xiang, B., Butler, K. W., and Deslauriers, R. (1995). "Contractile dysfunction caused by normothermic ischaemia and KCl arrest in the isolated pig heart: A ^{31}P NMR study." *J. Mol. Cell. Cardiol.*, 27, 1715-1730.

Kwong, K. K., McKinstry, R. C., Chien, D., Crawley, A. P., Pearlman, J. D., and Rosen, B. R. (1991). "CSF-suppressed quantitative single-shot diffusion imaging." *Magn. Reson. Med.*, 21, 157-163.

Lang, F., Ritter, R., Völkl, H., and Häussinger, D. (1993). "The biological significance of cell volume." *Renal Physiol. Biochem.*, 16, 48-65.

Latour, L. L., Mitra, P. P., Kleinberg, R. L., and Sotak, C. H. (1993). "Time-dependent diffusion coefficient of fluids in porous media as a probe of surface-to-volume ratio." *J. Magn. Reson., Ser. A*, 101, 342-346.

Le Bihan, D. (1991). "Molecular diffusion nuclear magnetic resonance imaging." *Magn. Reson. Q.*, 7(1), 1-30.

Le Bihan, D. (1995). "Molecular diffusion, tissue microdynamics and microstructure." *NMR Biomed.*, 8, 375-386.

Le Bihan, D., Breton, E., Lallemand, D., Grenier, P., Cabanis, E. A., and Lavel-Jeantet, M. (1986). "MR imaging of intravoxel incoherent motions: application to diffusion and perfusion in neurologic disorders." *Radiology*, 161, 401-407.

Leaf, A. (1959). "Maintenance of concentration gradients and regulation of cell volume." *Ann. N.Y. Acad. Sci.*, 72, 396-404.

Lee, Y. C. P., and Visscher, M. B. (1961). "On the state of creatine in heart muscle." *Proc. Natl. Acad. Sci. USA*, 47, 1510-1515.

Leem, C. H., Ho, W.-K., and Earm, Y. E. (1996). "The effect of taurine on the activation osmolality of the osmosensitive current in single ventricular myocytes of rabbits." *Exp. Physiol.*, 81, 189-202.

Liess, C., Duckworth, J., Clarke, K., Cross, H. R., Styles, P., and Radda, G. K. (1996). "^{1}H STEAM and ^{31}P NMR detection and quantification of osmolyte changes in ischaemic rat hearts." *Proc. Int. Soc. Magn. Reson. Med. 4th Sci. Meeting*, 1018.

Lochner, A., and de Villiers, M. (1989). "Phosphatidylcholine biosynthesis in myocardial ischemia." *J. Mol. Cell. Cardiol.*, 21, 151-163.

Luby-Phelps, K. (1994). "Physical properties of cytoplasm." *Current Opinion in Cell Biology*, 6, 3-9.

Luby-Phelps, K., Castle, P. E., Taylor, D. L., and Lanni, F. (1987). "Hindered diffusion of inert tracer particles in the cytoplasm of mouse 3T3 cells." *Proc. Natl. Acad. Sci. USA*, 84, 4910-4913.

Luby-Phelps, K., Mujumdar, S., Mujumdar, R. B., Ernst, L. A., Galbraith, W., and Waggoner, A. S. (1993). "A novel fluorescence ratiometric method confirms the low solvent viscosity of the cytoplasm." *Biophys. J.*, 65, 236-242.

MacFall, J. R., Maki, J. H., Johnson, G. A., Hedlund, L. W., and Cofer, G. P. (1991). "Pre- and postmortem diffusion coefficients in rat neural and muscle tissues." *Magn. Reson. Med.*, 20, 89-99.

Madden, M. C., van Winkle, W. B., Vaughn, J. M., Pohost, G. M., and Wolkowicz, P. E. (1993). "Morphometric analysis demonstrates that metabolically active cardiac triglycerides are ^{1}H NMR visible." *J. Mol. Cell. Cardiol.*, 25, 587-597.

Mansfield, P., and Chapman, B. (1986). "Active magnetic screening of coils for static and

time-dependent magnetic field generation in NMR imaging." *J. Phys. E: Sci. Instrum.*, 19, 540-545.

Mastro, A. M., Babich, M. A., Taylor, W. D., and Keith, A. D. (1984). "Diffusion of a small molecule in the cytoplasm of mammalian cells." *Proc. Natl. Acad. Sci. USA*, 81, 3414-3418.

Mastro, A. M., and Keith, A. D. (1984). "Diffusion in the aqueous compartment." *J. Cell. Biol.*, 99(1), 180s-187s.

Matthaei, D., Haase, A., Frahm, J., Bomsdorf, H., and Vollmann, W. (1986). "Multiple chemical shift selective (CHESS) MR imaging using stimulated echoes." *Radiology*, 160(3), 791-794.

Matthews, P. M., Bland, J. L., Gadian, D. G., and Radda, G. K. (1982). "A ^{31}P-NMR saturation transfer study of the regulation of creatine kinase in the rat heart." *Biochim. Biophys. Acta*, 721, 312-320.

Mattiello, J., Basser, P. J., and Le Bihan, D. (1994). "Analytical expressions for the b matrix in NMR diffusion imaging and spectroscopy." *J. Magn. Reson., Ser. A*, 108, 131-141.

Merboldt, K., Hänicke, W., and Frahm, J. (1985). "Self-diffusion NMR imaging using stimulated echoes." *J. Magn. Reson.*, 64, 479-486.

Merboldt, K.-D., Hoerstermann, D., Haenicke, W., Bruhn, H., and Frahm, J. (1993). "Molecular self-diffusion of intracellular metabolites in rat brain *in vivo* investigated by localized proton NMR diffusion spectroscopy." *Magn. Reson. Med.*, 29, 125-129.

Mild, K. H., and Lovtrup, S. (1985). "Movement and structure of water in animal cells. Ideas and experiments." *Biochim. Biophys. Acta*, 822, 155-167.

Mills, R. (1973). "Self-diffusion in normal and heavy water in the range 1-45°." *J. Phys. Chem.*, 77(5), 685-688.

Miranda, M. J., Born, P., and Wiegell, M. R. (1998). "White matter visualisation in infants by diffusion tensor MRI." *Proc. Int. Soc. Magn. Reson. Med. 6th Sci. Meeting*, 528.

Mitra, P. P., and Sen, P. N. (1992). "Effects of microgeometry and surface relaxation on NMR pulsed-field-gradient experiments: Simple pore geometries." *Phys. Rev. B*, 45(1), 143-156.

Mitra, P. P., Sen, P. N., Schwartz, L. M., and Le Doussal, P. (1992). "Diffusion propagator as a probe of the structure of porous media." *Phys. Rev. Letters*, 68(24), 3555-3558.

Moonen, C. T. W., Pekar, J., de Vleeschouwer, M. H. M., van Gelderen, P., van Zijl, P. C. M., and DesPres, D. (1991). "Restricted and anisotropic displacement of water in healthy cat brain and in stroke studied by NMR diffusion imaging." *Magn. Reson. Med.*, 19, 327-332.

Moonen, C. T. W., van Zijl, P. C. M., Le Bihan, D., and DesPres, D. (1990). "*In vivo* NMR diffusion spectroscopy: ^{31}P Application to phosphorus metabolites in muscle." *Magn. Reson. Med.*, 13, 467-477.

Moseley, M. E., Cohen, Y., Kucharczyk, J., Mintorovitch, J., Asgari, H. S., Wendland, M. F., Tsuruda, J., and Norman, D. (1990a). "Diffusion-weighted MR imaging of anisotropic water diffusion in cat central nervous system." *Radiology*, 176, 439-445.

Moseley, M. E., Cohen, Y., Mintorovitch, J., Chileuitt, L., Shimiyu, H., Kucharczyk, J., Wendland, M. F., and Weinstein, P. R. (1990b). "Early detection of regional cerebal ischemia in cats: Comparison of diffusion- and T_2-weighted MRI and spectroscopy." *Magn. Reson. Med.*, 14, 330-346.

Murday, J. S., and Cotts, R. M. (1968). "Self-diffusion coefficient of liquid lithium." *J. Chem. Phys.*, 48(11), 4938-4945.

Murphy, E., LeFurgey, A., and Lieberman, M. (1987). "Biochemical and structural changes in cultured heart cells induced by metabolic inhibition." *Am. J. Physiol.*, 253, C700-C706.

Nakada, T., and Kwee, I. L. (1991). "Maturational changes in intracellular high energy phosphate transport in rat brain." *Neuro Report*, 2, 777-780.

Nakada, T., Kwee, I. L., and Igarashi, H. (1994). "Brain maturation and high-energy phosphate diffusivity: alteration in cytosolic microenvironment and effective viscosity." *Developmental Brain Res.*, 80, 121-126.

Nash, G. B., Tatham, P. E. R., Powell, T., Twist, V. W., Speller, R. D., and Loverock, L. T. (1979). "Size measurements on isolated rat heart cells using Coulter analysis and light scatter flow cytometry." *Bioch. Biophys. Acta*, 587, 99-111.

Nedelec, J.-F., Ally, A., Foster, D. O., Anderson, R. E., and Clarke, K. (1991). "Quantification of ^{31}P NMR spectra of pig heart: use of phosphonates *in vivo*." *Circulation*, 84, II-380.

Nedelec, J.-F., Saunders, J. K., Morris, P., and Clarke, K. (1992). "Changes in probe sensitivity during NMR spectroscopic studies of the perfused rat heart: a warning." *Magn. Reson. Med.*, 27, 343-348.

Neeman, M., Freyer, J. P., and Sillerud, L. O. (1990). "Pulsed-gradient spin-echo diffusion studies in NMR imaging. Effects of the imaging gradients on the determination of diffusion coefficients." *J. Magn. Reson.*, 90, 303-312.

Neil, J. J., Duong, T. Q., and Ackerman, J. J. H. (1996). "Evaluation of intracellular diffusion in normal and globally-ischemic rat brain via ^{133}Cs NMR." *Magn. Reson. Med.*, 35, 329-335.

Nicholson, C., and Phillips, J. M. (1981). "Ion diffusion modified by tortuosity and volume fraction in the extracellular microenvironment of the rat cerebellum." *J. Physiol.*, 321, 225-257.

Nicolay, K., van der Toorn, A., and Dijkhuizen, R. M. (1995). "*In vivo* diffusion spectroscopy. An overview." *NMR Biomed.*, 8, 365-374.

Niendorf, T., Dijkhusen, R. M., Norris, D. G., van Lookeren Campagne, M., and Nicolay, K. (1996). "Biexponential diffusion attenuation in various states of brain tissue: Implications for diffusion-weighted imaging." *Magn. Reson. Med.*, 36, 847-857.

Nilsson, P. G., and Lindman, B. (1983). "Water self-diffusion in nonionic surfactant solutions. Hydration and obstruction effects." *J. Phys. Chem.*, 87, 4756-4761.

Nishiki, K., Erecinska, M., and Wilson, D. F. (1978). "Energy relationships between cytosolic metabolism and mitochondrial respiration in rat heart." *Am. J. Physiol.*, 234(3), C73-C81.

Norris, D. G., and Niendorf, T. (1995). "Interpretation of DW-NMR data: Dependence on experimental conditions." *NMR Biomed.*, 8, 280-288.

Norris, D. G., Niendorf, T., and Leibfritz, D. (1994). "Healthy and infarcted brain tissues studied at short diffusion times: the origins of apparent restriction and the reduction in apparent diffusion coefficient." *NMR Biomed.*, 7, 304-310.

Opie, L. H. (1998). "Chapter 3: Heart Cells and Organelles." The Heart. Physiology, from cell to circulation, Lippincroft-Raven, Philadelphia PA, USA, 43-68.

Parker, J. C. (1993). "In defense of cell volume?" *Am. J. Physiol.*, 265, C1191-C1200.

Patt, S. L., and Sykes, B. D. (1972). "Water eliminated Fourier transform N.M.R. spectroscopy." *J. Chem. Phys.*, 56(6), 3182-3184.

Pattany, P. M., Puckett, W. R., Klose, K. J., Quencer, R. M., Bunge, R. P., Kasuboski, L., and Weaver, R. G. (1997). "High resolution diffusion-weighted MR imaging of fresh and fixed cat spinal cords: evaluation of diffusion coefficients and anisotropy." *Proc. Int. Soc. Magn. Reson. Med. 5th Sci. Meeting*, 1718.

Periasamy, N., Kao, H. P., Fushimi, K., and Verkman, A. S. (1992). "Organic osmolytes increase cytoplasmic viscosity in kidney cells." *Am. J. Physiol.*, 263, C901-C907.

Pfeuffer, J., Floegel, U., and Leibfritz, D. (1998). "Monitoring of cell volume and water exchange time in perfused cells by diffusion-weighted ^{1}H NMR spectroscopy." *NMR Biomed.*, 11, 11-18.

Polimeni, P. I., and Buraczewski, S. I. (1988). "Expansion of extracellular tracer spaces in the isolated heart perfused with crystalloid solutions: expansion of extracellular space, trans-sarcolemmal leakage, or both?" *J. Mol. Cell. Cardiol.*, 20, 15-22.

Powell, T., Steen, E. M., Twist, V. W., and Woolf, N. (1978). "Surface characteristics of cells isolated from adult rat myocardium." *J. Mol. Cell. Cardiol.*, 10, 287-292.

Powers, E. R., DiBona, D. R., and Powell, W. J., Jr. (1984). "Myocardial cell volume and coronary resistance during diminished coronary perfusion." *Am. J. Physiol.*, 247, H467-H477.

Price, W. S., and Kuchel, P. W. (1991). "Effect of nonrectangular field gradient pulses in the Stejskal and Tanner (diffusion) pulse sequence." *J. Magn. Reson.*, 94, 133-139.

Rabkin, S. W. (1993). "Effect of exogenous CDP-choline on choline metabolism in isolated adult rat ventricular myocytes under normoxic and hypoxic conditions." *Cell Biochem. Funct.*, 11, 137-143.

Reese, T. G., Weisskoff, R. M., Smith, R. N., Rosen, B. R., Dinsmore, R. E., and Wedeen, V. J. (1995). "Imaging myocardial fiber architecture *in vivo* with magnetic resonance." *Magn. Reson. Med.*, 34, 786-791.

Roos, K. P. (1986). "Length, width, and volume changes in osmotically stressed myocytes." *Am. J. Physiol.*, 251, H1373-H1378.

Safford, R. E., Bassingthwaighte, E. A., and Bassingthwaighte, J. B. (1978). "Diffusion of water in cat ventricular myocardium." *J. Gen. Physiol.*, 72, 513-538.

Sako, E. Y., Kingsley-Hickman, P. B., From, A. H. L., Ugurbil, K., and Foker, J. E. (1988). "Substrate effects in the post-ischemic myocardium." *J. Surg. Res.*, 44, 430-435.

Saks, V. A., Khuchua, Z. A., Vasilyeva, E. V., Belikova, O. Y., and Kuznetsov, A. V. (1994). "III-1 Metabolic compartmentation and substrate channelling in muscle cells. Role of coupled creatine kinases in *in vivo* regulation of cellular respiration - a synthesis." *Mol. Cell. Biochem.*, 133/134, 155-192.

Sarkadi, B., and Parker, J. C. (1991). "Activation of ion transport pathways by changes in cell volume." *Biochim. Biophys. Acta*, 1071, 407-427.

Sato, K., Kashiwaya, Y., Keon, C. A., Tsuchiya, N., King, M. T., Radda, G. K., Chance, B., Clarke, K., and Veech, R. L. (1995). "Insulin, ketone bodies, and mitochondrial energy transduction." *FASEB J.*, 9, 651-658.

Sattin, W., Mareci, T. H., and Scott, K. N. (1985). "Exploiting the stimulated echo in nuclear magnetic resonance imaging. I. Method." *J. Magn. Reson.*, 64, 177-182.

Saunders, J. K., Foster, D. O., Nedelec, J.-F., Anderson, R. E., and Clarke, K. (1990). "Quantification of brain metabolites *in vivo* using ^{31}P NMR spectroscopy and dimethyl methylphosphonate as an internal standard." *Proc. Soc. Magn. Reson. Med. 9th Sci. Meeting*, 1144.

Savabi, F. (1988). "Free creatine available to the creatine phosphate energy shuttle in isolated rat atria." *Proc. Natl. Acad. Sci. USA*, 85, 7476-7480.

Schaper, J., Hein, S., Brand, T., and Schaper, W. (1989). "Contractile proteins and the cytoskeleton in isolated rat myocytes." *J. Appl. Cardiol.*, 4, 423-429.

Schaper, J., Meiser, E., and Stämmler, G. (1985). "Ultrastructural morphometric analysis of myocardium from dogs, rats, hamsters, mice, and from human hearts." *Circ. Res.*, 56, 377-391.

Schneider, J., Weisser, A., Neubauer, S., Haase, A., and von Kienlin, M. (1998). "A method for determination of the total creatine content in perfused rat hearts by ^{1}H-MRS." *Proc. Int. Soc. Magn. Reson. Med. 6th Sci. Meeting*, 1835.

Schwartz, A., Wood, J. M., Allen, J. C., Bornet, E. P., Entman, M. L., Goldstein, M. A., Sordahl, L. A., Suzuki, M., and Lewis, R. M. (1973). "Biochemical and morphologic correlates of cardiac ischaemia." *Am. J. Cardiol.*, 32, 46-61.

Scollan, D. F., Holmes, A., Winslow, R., and Forder, J. (1998). "Histological validation of myocardial microstructure obtained from diffusion tensor magnetic resonance imaging." *Am. J. Physiol.*, 275, H2308-H2318.

Shug, A. L., Thomsen, J. H., Folts, J. D., Bittar, N., Klein, M. I., Koke, J. R., and Huth, P. J. (1978). "Changes in tissue levels of carnitine and other metabolites during myocardial ischemia and anoxia." *Arch. Biochem. Biophys.*, 187(1), 25-33.

Söderman, O., and Jönsson, B. (1995). "Restricted diffusion in cylindrical geometry." *J. Magn. Reson., Ser. A*, 117, 94-97.

Sorenson, A. L., Tepper, D., Sonnenblick, E. H., Robinson, T. F., and Capasso, J. M. (1985). "Size and shape of enzymatically isolated ventricular myocytes from rats and cardiomyopathic hamsters." *Cardiovasc. Res.*, 19, 793-799.

Stanisz, G. J., Szafer, A., Wright, G. A., and Henkelman, R. M. (1997). "An analytical model of restricted diffusion in bovine optic nerve." *Magn. Reson. Med.*, 37, 103-111.

Steenbergen, C., Hill, M. L., and Jennings, R. B. (1985). "Volume regulation and plasma membrane injury in aerobic, anaerobic, and ischemic myocardium *in vitro*. Effects of osmotic cell swelling on plasma membrane integrity." *Circ. Res.*, 57, 864-875.

Stejskal, E. O. (1965). "Use of spin echoes in a pulsed magnetic-field gradient to study anisotropic, restricted diffusion and flow." *J. Chem. Phys.*, 43(10), 3597-3603.

Stejskal, E. O., and Tanner, J. E. (1965). "Spin diffusion measurements: Spin echoes in the presence of a time-dependent field gradient." *J. Chem. Phys.*, 42(1), 288-292.

Stilbs, P. (1987). "Fourier transform pulsed-gradient spin-echo studies of molecular diffusion." *Progr. NMR Spectr.*, 19, 1-45.

Strange, K. (1994). "Are all cell volume changes the same?" *NIPS*, 9, 223-228.

Suleiman, M.-S., and Chapman, R. A. (1993). "Changes in the principal free intracellular amino acids in the Langendorf perfused guinea pig heart during arrest with calcium-free or high potassium media." *Cardiovasc. Res.*, 27, 1810-1814.

Suleiman, M.-S., Rodrigo, G. C., and Chapman, R. A. (1992). "Interdependence of intracellular taurine and sodium in guinea pig heart." *Cardiovasc. Res.*, 26, 897-905.

Takami, H., Furuya, E., Tagawa, K., Seo, Y., Murakami, M., Watari, H., Matsuda, H., Hirose, H., and Kawashima, Y. (1988). "NMR-invisible ATP in rat heart and its change in ischemia." *J. Biochem.*, 104, 35-39.

Tanner, J. E. (1978). "Transient diffusion in a system partitioned by permeable barriers. Application to NMR measurements with a pulsed field gradient." *J. Chem. Phys.*, 69(4), 1748-1754.

Tanner, J. E. (1979). "Self diffusion of water in frog muscle." *Biophys. J.*, 28, 107-116.

Tanner, J. E., and Stejskal, E. O. (1968). "Restricted self-diffusion of protons in colloidal systems by the pulsed-gradient, spin-echo method." *J. Chem. Phys.*, 49(4), 1768-1777.

Thurston, J. H., Hauhart, R. E., and Naccarato, E. F. (1981). "Taurine: Possible role in osmotic regulation of mammalian heart." *Science*, 214, 1373-1374.

Torrey, H. C. (1956). "Bloch equations with diffusion terms." *Phys. Rev.*, 104(3), 563-565.

Tranum-Jensen, J., Janse, M. J., Foilet, J. W. T., Krieger, W. J. G., Naumann D'Alnoncourt, C., and Durrer, D. (1981). "Tissue osmolality, cell swelling and reperfusion in acute regional myocardial ischemia in the isolated porcine heart." *Circ. Res.*, 49(2), 364-381.

Tseng, G.-N. (1992). "Cell swelling increases membrane conductance of canine cardiac cells: evidence for a volume-sensitive Cl channel." *Am. J. Physiol.*, 262, C1056-C1068.

Tseng, W.-Y. I., Reese, T. G., Dinsmore, R. E., Weisskoff, R. M., and Wedeen, V. J. (1997). "Progress in MRI of myocardial structure and function using diffusion and strain." *Proc. Int. Soc. Magn. Reson. Med. 5th Sci. Meeting*, 228.

Turner, C. J., and Garlick, P. B. (1984). "One- and two-dimensional ^{31}P spin-echo studies of myocardial ATP and phosphocreatine." *J. Magn. Reson.*, 57, 221-227.

Ugurbil, K., Petein, M., Maidan, R., Michurski, S., Cohn, J. N., and From, A. F. (1984). "High resolution proton NMR studies of perfused rat hearts." *FEBS*, 167(1), 73-78.

Unitt, J. F., Schrader, J., Brunotte, F., Radda, G. K., and Seymour, A.-M. L. (1992). "Determination of free creatine and phosphocreatine concentrations in the isolated perfused rat heart by ^{1}H- and ^{31}P-NMR." *Biochim. Biophys. Acta*, 1133, 115-120.

van der Toorn, A., Dijkhuizen, R. M., Tulleken, C. A. F., and Nicolay, K. (1995). "T_1 and T_2 relaxation times of the major ^{1}H-containing metabolites in rat brain after focal ischaemia." *NMR Biomed.*, 8, 245-252.

van der Toorn, A., Dijkhuizen, R. M., Tulleken, C. A. F., and Nicolay, K. (1996a). "Diffusion of metabolites in normal and ischaemic rat brain measured by localized ^{1}H MRS." *Magn. Reson. Med.*, 36, 914-922.

van der Toorn, A., Sykova, E., Dijkhuizen, R. M., Vorisek, I., Vargova, l., Skobisova, E., van Lookeren Campagne, M., Reese, T., and Nicolay, K. (1996b). "Dynamic changes in water ADC, energy metabolism, extracellular space volume, and tortuosity in neonatal rat brain during global ischemia." *Magn. Reson. Med.*, 36, 52-60.

van der Toorn, A., Verheul, H. B., Berkelbach van der Sprenkel, J.-W., Tulleken, C. A. F., and Nicolay, K. (1994). "Changes in metabolites and tissue water status after focal ischemia in cat brain assessed with localized proton MR spectroscopy." *Magn. Reson. Med.*, 32, 685-691.

van Gelderen, P., de Vleeschouwer, M. H. M., DesPres, D., Pekar, J., van Zijl, P. C. M., and Moonen, C. T. W. (1994a). "Water diffusion in acute stroke." *Magn. Reson. Med.*, 31, 154-163.

van Gelderen, P., DesPres, D., van Zijl, P. C. M., and Moonen, C. T. W. (1994b). "Evaluation of restricted diffusion in cylinders. Phosphocreatine in rabbit leg muscle." *J. Magn. Reson., Ser. B*, 103, 255-260.

Vandenberg, J. I., Rees, S. A., Wright, A. R., and Powell, T. (1996). "Cell swelling and ion transport pathways in cardiac myocytes." *Cardiovasc. Res.*, 32, 85-97.

Vandenberg, J. I., Yoshida, S., Kirk, K., and Powell, T. (1994). "Swelling-activated and isoprenaline-activated chloride currents in guinea pig cardiac myocytes have distinct electrophysiology and pharmacology." *J. Gen. Physiol.*, 104, 997-1017.

Varian. (1995). "Unity INOVA acceptance tests specifications." Pub. No. 87-195329-00, Rev. B0795, Palo Alto, California, USA.

Wallimann, T., Wyss, M., Brdiczka, D., Nicolay, K., and Eppenberger, H. M. (1992). "Intracellular compartmentation, structure and function of creatine kinase isoenzymes in tissues with high and fluctuating energy demands: the 'phosphocreatine circuit' for cellular energy homeostasis." *Biochem. J.*, 281, 21-40.

Werring, D. J., Clark, C. A., Barker, G. J., Symms, M. R., Franconi, F., Thompson, A. J., and Miller, D. H. (1998). "The structural properties of multiple sclerosis (MS) lesions demonstrated by diffusion tensor imaging." *Proc. Int. Soc. Magn. Reson. Med. 6th Sci. Meeting*, 119.

Whitmer, J. T., Idell-Wenger, J. A., Rovetto, M. J., and Neely, J. R. (1978). "Control of fatty acid metabolism in ischemic and hypoxic hearts." *J. Biol. Chem.*, 253(12), 4305-4309.

Wick, M., Nagatomo, Y., Prielmeier, F., and Frahm, J. (1995). "Alteration of intracellular metabolite diffusion in rat brain *in vivo* during ischemia and reperfusion." *Stroke*, 26, 1930-1934.

Woessner, D. E. (1963). "N.M.R. spin-echo self-diffusion measurements on fluids undergoing restricted diffusion." *J. Phys. Chem.*, 67, 1365-1367.

Wright, A. R., Rees, S. A., Vandenberg, J. I., Twist, V. W., and Powell, T. (1995). "Extracellular osmotic pressure modulates sodium-calcium exchange in isolated guinea-pig ventricular myocytes." *J. Physiol.*, 488(2), 293-301.

Yoshizaki, K., Watari, H., and Radda, G. K. (1990). "Role of phosphocreatine in energy transport in skeletal muscle of bullfrog studied by ^{31}P-NMR." *Biochim. Biophys. Acta*, 1051, 144-150.

Zhong, J., Kennan, R. P., and Gore, J. C. (1991). "Effects of susceptibility variations on NMR measurements of diffusion." *J. Magn. Reson.*, 95, 267-280.

Zweier, J. L., and Jacobus, W. E. (1987). "Substrate-induced alterations of high energy phosphate metabolism and contractile function in the perfused heart." *J. Biol. Chem.*, 262(17), 8015-8021.